

DTIC FILE COPY

(4)

GL-TR-89-0124(II)
Report PSI-9032/TR-901

CANOE II: DYNAMICS OF ATMOSPHERIC INFRARED
THERMOCHEMICAL EXCITATION

W.T. Rawlins
L.G. Piper
M.E. Fraser
H.C. Murphy
T.R. Tucker
A. Gelb

Physical Sciences Inc.
Research Park
P.O. Box 3100
Andover, MA 01810

March 1989

Final Report
24 March 1985 - 24 May 1989

DTIC
ELECTE
OCT 10 1989
S E D

APPROVED FOR PUBLIC RELEASE; DISTRIBUTION UNLIMITED

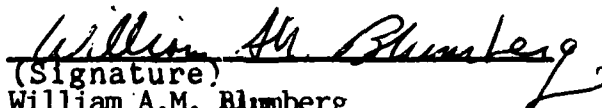
GEOFYSICS LABORATORY
AIR FORCE SYSTEMS COMMAND
UNITED STATES AIR FORCE
HANS COM AIR FORCE BASE, MA 01731-5000

89 10 10157

"This technical report has been reviewed and is approved for publication"



(Signature)
STEVEN M. MILLER
Contract Manager



(Signature)
William A.M. Blumberg
Branch Chief, Acting

FOR THE COMMANDER



(Signature)
R. EARL GOOD
Director

This report has been reviewed by the ESD Public Affairs Office (PA) and is releasable to the National Technical Information Service (NTIS).

Qualified requestors may obtain additional copies from the Defense Technical Information Center. All others should apply to the National Technical Information Service.

If your address has changed, or if you wish to be removed from the mailing list, or if the addressee is no longer employed by your organization, please notify AFGL/DAA, Hanscom AFB, MA 01731. This will assist us in maintaining a current mailing list.

Do not return copies of this report unless contractual obligations or notices on a specific document requires that it be returned.

UNCLASSIFIED

SECURITY CLASSIFICATION OF THIS PAGE

REPORT DOCUMENTATION PAGE

1a. REPORT SECURITY CLASSIFICATION UNCLASSIFIED			1b. RESTRICTIVE MARKINGS N/A since unclassified		
2a. SECURITY CLASSIFICATION AUTHORITY N/A since unclassified			3. DISTRIBUTION / AVAILABILITY OF REPORT Approved for public release; distribution unlimited		
2b. DECLASSIFICATION / DOWNGRADING SCHEDULE N/A since unclassified					
4. PERFORMING ORGANIZATION REPORT NUMBER(S) PSI-9032/TR-901 (Volume II)			5. MONITORING ORGANIZATION REPORT NUMBER(S) GL-TR-89-0124 (II)		
6a. NAME OF PERFORMING ORGANIZATION Physical Sciences Inc.		6b. OFFICE SYMBOL (If applicable)	7a. NAME OF MONITORING ORGANIZATION Geophysics Laboratory		
6c. ADDRESS (City, State, and ZIP Code) Research Park, P.O. Box 3100 Andover, MA 01810			7b. ADDRESS (City, State, and ZIP Code) Hanscom Air Force Base, MA 01731-5000		
8a. NAME OF FUNDING / SPONSORING ORGANIZATION GL		8b. OFFICE SYMBOL (If applicable)	9. PROCUREMENT INSTRUMENT IDENTIFICATION NUMBER F19628-85-C-0032		
8c. ADDRESS (City, State, and ZIP Code) Hanscom Air Force Base, MA 01731-5000			10. SOURCE OF FUNDING NUMBERS		
			PROGRAM ELEMENT NO. 61102F	PROJECT NO. 2310	TASK NO. G4
			WORK UNIT ACCESSION NO. BJ		
11. TITLE (Include Security Classification) CANOES II: Dynamics of Atmospheric Infrared Thermochemical Excitation					
12. PERSONAL AUTHOR(S) Rawlins, Wilson T.; Piper, Lawrence G.; Fraser, Mark E.; Murphy, Henry C.; Tucker, Thomas P.; and Gelb, A.					
13a. TYPE OF REPORT Final		13b. TIME COVERED FROM 850324 TO 890524		14. DATE OF REPORT (Year, Month, Day) 1989 March	
15. PAGE COUNT 284					
16. SUPPLEMENTARY NOTATION Volume I: pages 1-92; Volume II: pages 93-372; Volume III: pages 373-624; Volume IV: pages 625-362 <i>Capitals > 1000 (1.5)</i>					
17. COSATI CODES			18. SUBJECT TERMS (Continue on reverse if necessary and identify by block number)		
FIELD	GROUP	SUB-GROUP	Infrared emission; Oxygen, Nitrogen, Nitric oxide, Ozone, Molecular dynamics, Vibrational excitation, Atmospheric background, Reaction Kinetics, Coefficients, Reaction flows		
19. ABSTRACT (Continue on reverse if necessary and identify by block number) <i>Oxygen, Nitric oxide</i> In the electron disturbed upper atmosphere, electronically excited metastable forms of oxygen and nitrogen are formed by electron impact processes. These species dissipate their energy into the atmosphere largely by collisional quenching and chemical reaction. Specific species and reactions of interest include: (1) electronically and/or vibrationally excited nitrogen, N_2^* , its spectroscopy, energy pooling and interactions with O , O_2 and trace, infrared-active atmospheric species such as CO , CO_2 , and N_2O ; (2) metastable atomic nitrogen, $N(^2D, ^2P)$, reaction kinetics and product branching ratios in interactions with the above atmospheric species; (3) various metastable states of O_2 , O_2^* , and their potential as auroral precursors of infrared radiation.					
20. DISTRIBUTION / AVAILABILITY OF ABSTRACT <input checked="" type="checkbox"/> UNCLASSIFIED/UNLIMITED <input type="checkbox"/> SAME AS RPT <input type="checkbox"/> DTIC USERS			21. ABSTRACT SECURITY CLASSIFICATION UNCLASSIFIED/UNLIMITED		
22a. NAME OF RESPONSIBLE INDIVIDUAL Steven Miller			22b. TELEPHONE (Include Area Code)		22c. OFFICE SYMBOL GL/OPI

DO FORM 1473, 84 MAR

83 APR edition may be used until exhausted.

All other editions are obsolete.

UNCLASSIFIED

UNCLASSIFIED

SECURITY CLASSIFICATION OF THIS PAGE

19. ABSTRACT (Continued)

from other atmospheric species; and (4) the role of metastable-metastable O_2/N_2 interactions as potential sources for non-linear infrared effects which might occur in strong aurorae. This document reports on the results from a four-year coupled experimental program using the COCHISE and FAKIR facilities to investigate these issues in fundamental detail.

UNCLASSIFIED

SECURITY CLASSIFICATION OF THIS PAGE

CONTENTS

<u>Section</u>	<u>Page</u>
APPENDICES	
A. COCHISE INVESTIGATIONS OF UPPER ATMOSPHERIC INFRARED BACKGROUNDS	93
B. RATE COEFFICIENTS FOR $N(^2D)$ REACTIONS	121
C. THE RATE COEFFICIENTS FOR QUENCHING $N(^2D)$ BY $O(^3P)$	153
D. EXPERIMENTAL DETERMINATION OF THE RATIO A_{00}/A_{01} FOR THE INFRARED ATMOSPHERIC BANDS OF MOLECULAR OXYGEN	179
E. EINSTEIN COEFFICIENTS AND TRANSITION MOMENT VARIATION FOR THE $NO(A^2\Sigma^+-X^2\Pi)$ TRANSITION	195
F. STATE-TO-STATE EXCITATION OF $NO(A^2\Sigma^+, v'=0,1,2)$ BY $N_2(A^3\Sigma_u^+, v'=0,1,2)$	213
G. STATE-TO-STATE $N_2(A^3\Sigma_u^+)$ ENERGY-POOLING REACTIONS: I. THE FORMATION OF $N_2(C^3\Pi_u)$ AND THE HERMAN INFRARED SYSTEM	253
H. STATE-TO-STATE $N_2(A^3\Sigma_u^+)$ ENERGY-POOLING REACTIONS: I. THE FORMATION OF $N_2(C^3\Pi_u)$ AND THE HERMAN INFRARED SYSTEM	
I. THE EXCITATION OF $N(^2P)$ BY $N_2(A^3\Sigma_u^+, v'=0,1)$	335

APPENDIX A

(SR-348 reproduced in its entirety)

Proc. IRIS Specialty Group on Targets,
Backgrounds and Discrimination (1988)

Accession For	
NTIS GRA&I	<input checked="checked" type="checkbox"/>
DTIC TAB	<input type="checkbox"/>
Unannounced	<input type="checkbox"/>
Justification	
By	
Distribution/	
Availability Codes	
Dist	Avail and/or Special
A-1	

COCHISE INVESTIGATIONS OF UPPER ATMOSPHERIC
INFRARED BACKGROUNDS

3 February 1988

S.M. Miller
Air Force Geophysics Laboratory
Hanscom Air Force Base, MA 01731

W.T. Rawlins, M.E. Fraser
T.R. Tucker, and L.G. Piper
Physical Sciences Inc.
Research Park, P.O. Box 3100
Andover, MA 01810

Proc. IRIS Specialty Group on Targets,
Background, and Discrimination
Monterey, CA
(9-11 February 1988)

COCHISE INVESTIGATIONS OF UPPER ATMOSPHERIC
INFRARED BACKGROUNDS

3 February 1988

S.M. Miller
Air Force Geophysics Laboratory
Hanscom Air Force Base, MA 01731

W.T. Rawlins, M.E. Fraser
T.R. Tucker, and L.G. Piper
Physical Sciences Inc.
Research Park, P.O. Box 3100
Andover, MA 01810

ABSTRACT

Experiments have been performed using the AFGL COCHISE facility to investigate chemiluminescent reactions of atmospherically important radiators which could significantly contribute to emissions in several important infrared wavelength window regions under atmospherically disturbed conditions. The first of these radiators, N_2O , is not currently considered to be important at high altitudes. However, observations of its production from ongoing experiments involving metastable nitrogen-metastable oxygen reactions indicate that significant amounts of N_2O could be present under highly disturbed conditions. These results indicate that significant radiation in the 4 to 5, 7 to 9, and/or 17 to 24μ regions could be produced and that the magnitude of these emissions depends on the type and amount of vibrational excitation given N_2O by these metastable nitrogen/oxygen reactions. The impact of N_2O production processes on nuclear code predictions of IR backgrounds in the disturbed atmosphere is discussed. A second major result of our COCHISE experiments is the observation of additional radiation from NO and CO which is attributed to rotationally "hot" states of these molecules. This "hot" NO radiation, previously observed in the upper atmosphere, is expected to radiate in the 6 to 9μ region and thus act as a window fill. While CO is not a major high altitude radiator in the natural atmosphere, it may be a significant 4.3μ radiator when produced by the dissociation of CO_2 in the nuclear heated aura region. These experiments have provided evidence for radiation from rotationally excited bands of NO and CO, yet these emissions are not fully explained by theory, especially for the higher vibration and rotation states. This calls into question the ability of present models to accurately predict NO radiance levels. Several mechanisms have been proposed for the production of this "hot" NO and CO, and experiments are currently in progress to determine the production mechanism. These COCHISE and related laboratory measurements provide important new data for the production of N_2O and the presence of NO/CO "hot band" emissions which require further detailed investigations if present nuclear models are to accurately account for IR radiation in the 4.3 and 7.0μ radiance windows.

1.0 INTRODUCTION

The infrared emission spectrum of the quiescent upper mesosphere and lower thermosphere is primarily due to radiative and collisional up-pumping of infrared-active trace species, most notably CO_2 (ν_3 , 4.3 μm ; ν_2 , 15 μm), O_3 (ν_3 , 10 μm), and NO ($\nu=1$, 5.2 μm). However, in the electron-disturbed upper atmosphere, the creation of energetic metastable species can lead to additional IR radiation from chemiluminescent processes or from thermal excitation of species formed during the bombardment. This is of particular interest to systems applications when the bombardment-induced radiation occurs in unexpected bandpasses due to the non-equilibrium nature of the excitation processes. Direct auroral observations have provided a wealth of data on the more direct excitation phenomena, such as excitation of $\text{CO}_2(\nu_3)$ and $\text{NO}(\nu)$; however, many excitation mechanisms involving two or more aurorally created precursor species may be undetectable in a moderate aurora but dominant in an intense dosing. Observations of Class III to IV auroras, such as that encountered by the HIRIS mission¹ in 1976, would provide a valuable data base for the study of these types of processes; however, the determination of relationships for scaling intensities and spectral distributions with dosing and atmospheric conditions can only be accomplished through detailed understanding of the elementary reaction mechanisms for the excitation processes. We report here the results of experimental investigations of mechanisms for excitation of IR emission from N_2O , NO , and CO which could impact nuclear code predictions for radiation in the MWIR (4 to 8 μm) and LWIR (8 to 20 μm).

Our experimental approach employs complementary measurements of

- (1) microwave discharge-induced infrared fluorescence/chemiluminescence in the cryogenic (20 K) COCHISE reactor/spectrometer facility, at AFGL, and
- (2) metastable quenching and product formation kinetics in a discharge-flow

1. Stair, A.T., Jr., Pritchard, J., Coleman, I., Bohne, C., Williamson, W., Rogers, J., and Rawlins, W.T., "The Rocketborne Cryogenic (10 K) High Resolution Interferometer Spectrometer Flight-HIRIS: Atmospheric and Auroral Infrared Emission Spectra," *Appl. Opt.* 22, 1056 (1983).

reactor at PSI. In the COCHISE experiments, the IR radiation is observed from a low-pressure (3 mtorr, near single collision conditions) interaction region where flows of discharge-excited gas mixtures (excited in fast-flow sidearms at 1 torr with a 2 ms residence time) meet opposing counterflows of reagent gases.² An example of a spectrum obtained for discharge-excited air diluted in argon is shown in Figure 1. Prominent features in this spectrum include emission from vibrationally excited N₂O, 4.4 to 5.0 μ m, and NO, 5.2 to 6.0+ μ m. Additional spectra, obtained by chopping the discharges and using asynchronous detection, show that the N₂O emission is out of phase with the NO emission, as shown in Figure 2; this suggests a complex discharge excitation mechanism. Also contributing to these spectra are electronic transitions of N₂(W³ $\Delta_u \rightarrow$ B³ Π_g)³ at 4.0 μ m (4,2), 6.5 μ m (1,0), and 7.8 μ m (2,1), and O₃($\nu_1 + \nu_3$) at 4.7 μ m. Observations such as those shown in Figures 1 and 2 have motivated detailed experimental investigations directed at achieving a mechanistic understanding of the discharge excitation processes, in order to assess their relevance to the nuclear scenario.

2.0 EVIDENCE FOR N₂O PRODUCTION

The potential for chemical generation of N₂O in the upper atmosphere has been the subject of continuing debate for some years.⁴⁻¹³ However, reactions of atmospheric species which can result in N₂O formation at low pressures have yet to be conclusively identified. The possible reactions would require at least one excited-state reactant species, and thus may occur most prominently

2. Rawlins, W.T., Murphy, H.C., Caledonia, G.E., Kennealy, J.P., and Robert, F.X., Corman, A., and Armstrong, R.A., "COCHISE: Laboratory Studies of Atmospheric Infrared Chemiluminescence in a Cryogenic Environment," Appl. Opt. 23, 3316 (1984).
3. Fraser, M.E., Rawlins, W.T., and Miller, S.M., "Infrared (2 to 8 μ m) Fluorescence of the W³ $\Delta_u \rightarrow$ B³ Π_g and w¹ $\Delta_u \rightarrow$ a¹ Π_g Systems of Nitrogen," J. Chem. Phys. 88, 538 (1988).
4. Zipf, E.C., "A Laboratory Study on the Formation of Nitrous Oxide by the Reaction N₂(A³ Σ_u^+) + O₂ \rightarrow N₂O + O," Nature 287, 523 (1980) and "Production of Nitrous Oxide in the Auroral and D and E Regions," Nature 287, 525 (1980).

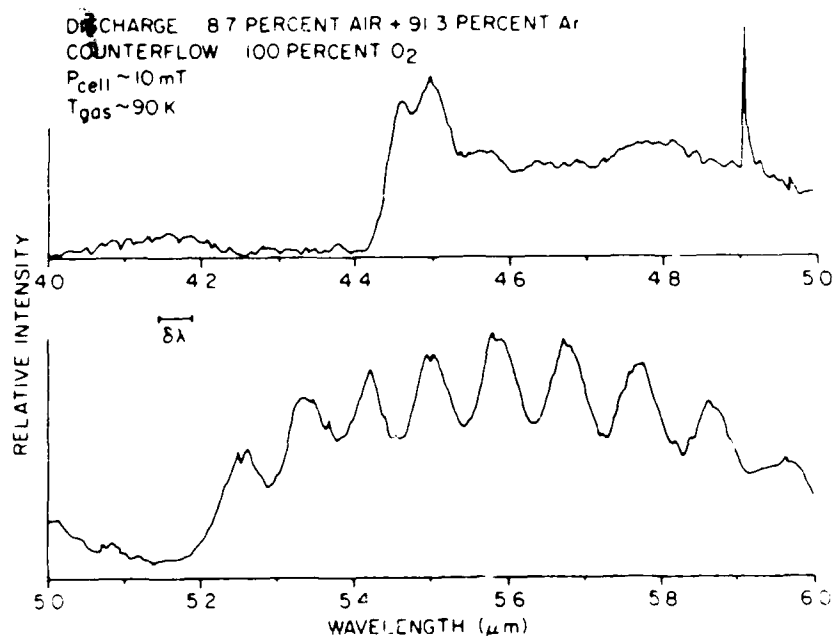


FIGURE 1. MWIR SPECTRUM (UNCORRECTED) FOR DISCHARGED AIR/ARGON. THE SPECTRAL RESOLUTION IS $0.27 \mu\text{m}$

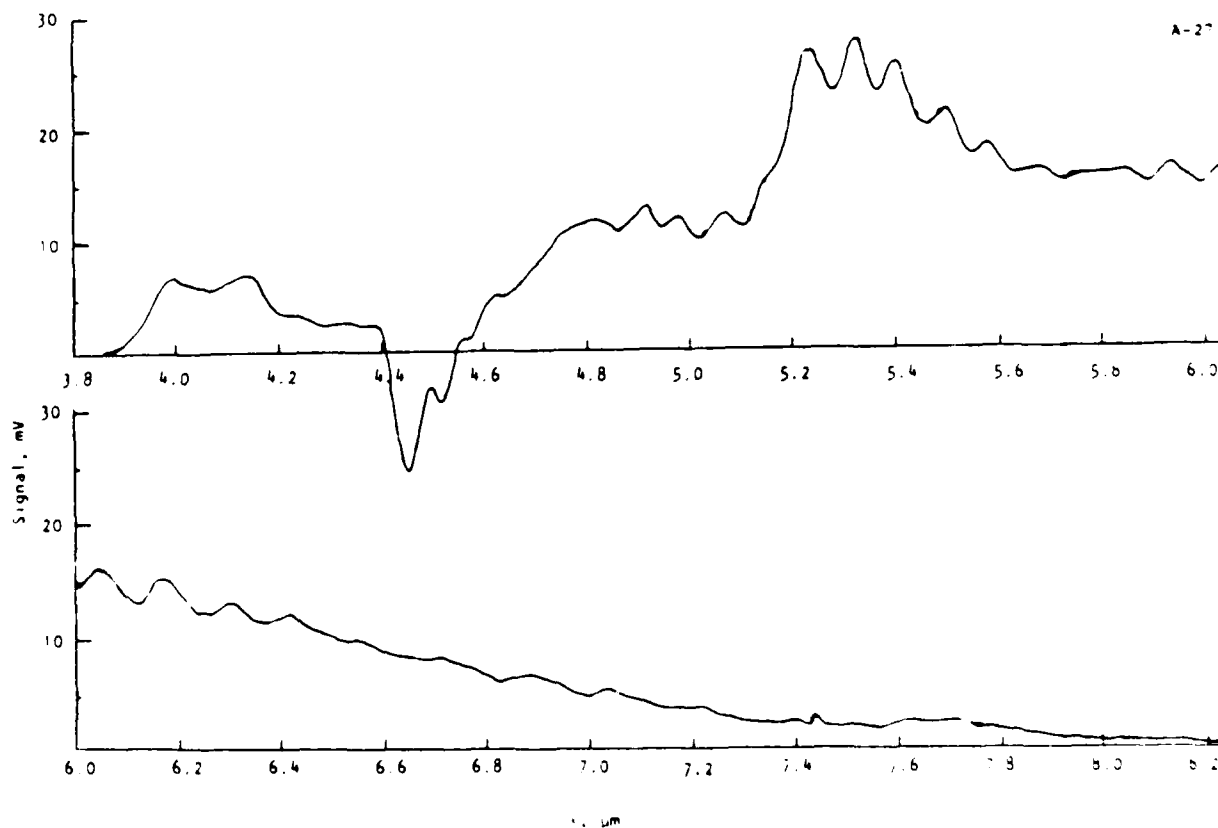


FIGURE 2. MWIR SIGNATURE FOR DISCHARGED N₂/O₂/Ar MIXTURE, EXCESS N₂. EXPERIMENTAL CONDITIONS ARE AS FOLLOWS: N₂/O₂/Ar = 0.2/0.010/3.7 std l/min, T = 80 K, P = 1.3 torr, RESOLUTION = $0.04 \mu\text{m}$

in laboratory discharges or intense atmospheric dosings. These reactions would be sufficiently exoergic to produce vibrationally excited N_2O , resulting in IR chemiluminescence near 4.5 (ν_3), 7.8 (ν_1), and 17 (ν_2) μm . The COCHISE experiments with discharge-excited N_2/O_2 mixtures, typified by Figures 1 and 2, indicate the formation of N_2O in at least four and possibly up to nine vibrational levels of the ν_3 mode. Thus the formation process must be a highly exoergic (1 to 2 eV) reaction involving discharge-created metastable species. Other COCHISE measurements of the interactions of discharged O_2/Ar with N_2 and of discharged N_2/Ar with O_2 give no measurable formation of $N_2O(v)$. These results contraindicate the formation of $N_2O(v)$ from the reactions of $O_3(v)$ with N_2 , metastable O_2 with N_2 , and metastable N_2 with O_2 .

5. Iannuzzi, M.P., Jeffries, J.B., and Kaufman, F., "Product Channels of the $N_2(A^3\Sigma_u^+) + O_2$ Interaction," Chem. Phys. Lett. 87, 570 (1982).
6. Black, G., Hill, R.M., Sharpless, R.L., and Slanger, T.G., "Laboratory Studies on N_2O Relevant to Stratospheric Processes," J. Photochem. 22, 369 (1983).
7. Zipf, E.C. and Prasad, S.S., "Nitrous Oxide Formation by Metastable $N_2(A^3\Sigma_u^+)$ Chemistry: A New Perspective on Its Prospects," Preprint, 1984.
8. De Souza, A.R., Touseau, M., and Petitdidier, M., "Quenching Reactions of Metastable $N_2(A^3\Sigma, v=0,1,2)$ Molecules by O_2 ," Chem. Phys. Lett. 121, 423 (1985).
9. Eliasson, B. and Kogelschatz, U., " N_2O Formation in Ozonizers," J. Chim. Phys. 83, 279 (1986).
10. Zipf, E.C. and Prasad, S.S., "A Mesospheric Source of Nitrous Oxide," Nature 295, 133 (1982).
11. Hill, R.D., Rinker, R.G., and Coucouvinos, A., "Nitrous Oxide Production by Lightning," J. Geophys. Res. 89, 1411 (1984).
12. Levine, J.S., Hughes, R.E., Chameides, W.L., and Howell, W.E., " N_2O and CO Production by Electric Discharge: Atmospheric Implications," Geophys. Res. Lett. 6, 557 (1979).
13. Prasad, S.S. and Zipf, E.C., "Atmospheric Nitrous Oxide Produced by Solar Protons and Relativistic Electrons," Nature 291, 564 (1981).

Furthermore, recent careful experiments at PSI¹⁴ have conclusively ruled out the possibility for N₂O formation from the reaction



This reaction has long been invoked^{2,5} as a source of N₂O in discharged air, but its acceptance has been based on misinterpretation of complex experiments in which a variety of excited state species were present in addition to N₂(A). Based on the present results, we postulate that excited and/or metastable forms of both N₂ and O₂ are required in the critical reaction(s). This could entail reactions of one of the forms of N₂^{*} (electronic or vibrational excitation) with O₂^{*} or perhaps O₃(v). We have investigated this possibility using a discharge flow reactor at PSI.

The experiments were performed in a discharge-flow apparatus with cryogenic (liquid nitrogen) trapping of the gaseous products followed by GCMS analysis. The experimental conditions are listed in Table 1, and the observed N₂O production rates are listed in Table 2. Most of the discharge configurations failed to produce N₂O in excess of background levels ($\approx 10^{15}$ molecules for a 10 min trapping time). However, in keeping with the COCHISE results, co-discharged (microwave, 2450 MHz) N₂/O₂ mixtures with excess nitrogen produced high N₂O yields ($\approx 10^{18}$ molecules). Under these conditions, roughly 1 percent the initial O₂ was converted to N₂O. Discharging the nitrogen and oxygen separately with subsequent mixing downstream produced similar N₂O yields, especially considering the increased surface quenching of excited state precursors for this configuration. Discharged nitrogen with "cold" oxygen added downstream produced measurable amounts of N₂O but at greatly reduced yields; discharged oxygen with "cold" nitrogen added downstream produced negligible amounts of N₂O.

14. Fraser, M.E. and Piper, L.G., "N₂O, O(³P), AND O₂(B³Σ_u⁻) Product Branching Ratios from the N₂(A³Σ_u⁺ + O₂ Reaction," J. Phys. Chem. 92, XXXX (1988).

TABLE 1. TYPICAL EXPERIMENTAL CONDITIONS FOR N₂O FORMATION

Total flow rate	1900 μ mole/s
N ₂ flow	0 to 200 μ mole/s (typically 100 μ mole/s)
O ₂ flow	2 to 56 μ mole/s (typically 2 μ mole/s)
Pressure	2.6 torr
Linear flow velocity	670 cm/s
Trapping time	5 min
Discharge	Microwave (2450 MHz, <50W)

TABLE 2. RESULTS FOR N₂O FORMATION

Experiment	N ₂ O Formation Rate (μ mole/s)
Co-discharged Ar/N ₂ /O ₂	0.053 \pm 0.012
MW Ar/N ₂ + MW Ar/O ₂	0.022 \pm 0.003
MW Ar/N ₂ + MW Ar/O ₂ + w/Ni screen	0.0103 \pm 0.003
MW Ar/N ₂ w/glass wool + MW Ar/O ₂	0.0056 \pm 0.0013
MW Ar/N ₂ w/glass wool + MW Ar/O ₂ w/Ni screen	0.0027 \pm 0.00065
MW Ar/N ₂ + O ₂	0.0019 \pm 0.0004
MW Ar/N ₂ w/glass wool + O ₂	0.00056 \pm 0.00011
Ar metastables + N ₂ /O ₂	<10 ⁻⁵
MW Ar/O ₂ + N ₂	0.0
MW = microwave discharge	

In an attempt to isolate the excited state species contributing to N_2O formation, experiments were conducted with modified discharge conditions. Glass wool was placed downstream of the Ar/N_2 discharge to remove discharge-excited electronic states of N_2 . This has the additional effect of reducing the discharge-excited $N_2(v)$ number densities, completely eliminating metastable N^* , and reducing the ground-state N-atom number density. Metastable electronic states formed downstream by N recombination, e.g., $N_2(A^3\Sigma_u^+, A'^5\Sigma_g^+)$, would also be reduced by this procedure. As shown in Table 2, the addition of glass wool to the N_2/Ar discharge caused a reduction in the N_2O yield of about a factor of 4. This is commensurate with the reduction that might be expected for $N_2(v)$ under these conditions. Similarly, a nickel screen was placed downstream of the O_2/Ar discharge; this screen quenches discharge-produced metastables and catalytically recombines some of the atomic oxygen to form electronically excited O_2 , e.g., $O_2(A^3\Sigma_u^+, b^1\Sigma_g^+, a^1\Delta_g)$. This procedure caused only a factor of 2 decrease in the N_2O yield, implying that electronic metastables of O_2 are involved in the production mechanism.

Estimates of the effluent number densities at the mixing point of the N_2/Ar and O_2/Ar discharges are listed in Table 3. For the conditions we have employed, steady-state NO number densities formed in the flow tube are too small to permit observable formation of N_2O by either gas phase ($N + NO_2$) or heterogeneous processes. Similarly, ozone formed by three-body recombination of O and O_2 cannot reach sufficient number densities to account for the observed results. It can be seen from Table 3 that number densities of $N_2(A)$ and other electronically excited forms of N_2^* are too small to account for the copious N_2O production we observe. A possible exception to this is $N_2(A')$, which is believed to be formed by N recombination but whose kinetic behavior is not known well enough to estimate its abundance. Thus the most likely nitrogenous N_2O precursors appear to be $N_2(v)$ and possibly $N_2(A')$. The most abundant molecular effluents of the O_2/Ar discharge are expected to be $O_2(a,b)$; $O_2(A,A',c)$ are probably significantly less abundant and are therefore unlikely to be involved, but we cannot completely rule them out based on these

TABLE 3. DISCHARGE EFFLUENTS

Species	Approximate Concentration (molecules/cm ³)	τ_{rad}	Flow Rate ($\mu\text{mole/s}$)
N ₂	4.8×10^{15}	--	100
O ₂	9.6×10^{13}	--	2
N(⁴ S)	$10^{13} - 10^{14}$	--	0.1 - 1
O(³ P)	$\sim 3 \times 10^{13}$	--	0.65
N ₂ (v ≥ 7)*	$\sim 5 \times 10^{14}$	--	10
N ₂ (v ≥ 15)*	$\sim 5 \times 10^{13}$	--	1.0
O ₂ (a ¹ Δ)	10^{13}	65 min	0.22
O ₂ (b ¹ Σ)	10^{12}	12s	2.2×10^{-2}
N(² D)	$\sim 4 \times 10^{10}$	12 hr	8.6×10^{-4}
N(² P)	$\sim 4 \times 10^9$	12	8.6×10^{-5}
N ₂ (A)	10^9	1-3s	2.2×10^{-5}
Other N ₂ electronically excited species	$<10^9$	$<<1\text{s}$	$<10^{-5}$
<p>*Assuming a Treanor distribution</p> <p>The concentrations shown in this table are rough estimates for the effluents of the discharged Ar/N₂ and Ar/O₂ prior to mixing.</p>			

preliminary results. The observation of slight N_2O formation when the O_2 is not discharged suggests a serial process in which the O_2 must first be excited by collisions with N_2^* before it can react to form N_2O .

We therefore conclude that N_2O is indeed formed in discharge-excited nitrogen/oxygen mixtures at low pressures, and that the most likely reaction(s) involve vibrationally excited $N_2(X)$ or $N_2(A')$ and electronically excited $O_2(a$ or $b)$. In order for the spin-allowed reaction



to be exoergic, $N_2(v \geq 15)$ is required. The further implication from COCHISE that the product N_2O is vibrationally excited requires $N_2(v \geq 20)$. The occurrence of a spin-forbidden reaction path forming $O(^3P)$ or the involvement of $O_2(b)$ lowers this energetic requirement by seven or two quanta, respectively. For our present results to be accounted for by Reaction (2) requires a lower bound to its rate coefficient on the order of $10^{-14} \text{ cm}^3\text{s}^{-1}$. The actual rate coefficient could well be much larger owing to precursor quenching effects and competitive reactions which we have not yet evaluated, as well as to participation of higher energy states which would be at lower number densities in our apparatus.

The occurrence of a reaction of the form



has significant implications for predictions of radiation signatures in the nuclear-disturbed upper atmosphere. Owing to the requirement that both reactants must be excited, this reaction would be unobservable in even strong auroral events, and its rate would scale steeply with dosing strength so that the reaction could become a prolific source of N_2O in the 80 to 110 km region during a nuclear bombardment. The N_2O thus formed can be expected to be efficiently excited through the usual radiative and thermal (collisional)

up-pumping processes, resulting in IR radiation near 4.5, 7.8, and 17 μm corresponding to the ν_3 , ν_1 , and ν_2 vibrational modes, respectively. The further possibility that N_2O is formed vibrationally excited means that the vibrational band signatures could be redshifted and that the detailed band-shapes may depend upon collisional and radiative relaxation effects which have yet to be evaluated. Finally, reliable estimates of the rate of Reaction (3) in a nuclear scenario would require accurate modeling of the evolution of excited states of N_2 and O_2 during electron bombardment.

3.0 ROVIBRATIONAL EXCITATION OF NO AND CO

The reaction



gives rise to vibrational chemiluminescence from $\text{NO}(\nu)$ over at least 14 observable vibrational levels.¹⁵ This reaction determines both the NO vibrational distribution and the total NO production rate in the aurorally dosed atmosphere¹⁶ and is critically important for interpreting auroral infrared spectral distributions in the vicinities of the fundamental (5 to 7 μm) vibration-rotation bands.¹⁷ Furthermore, $(\Delta\nu=2)/(\Delta\nu=1)$ branching ratios of the overtone and fundamental band transition probabilities are required to interpret high-altitude observations near 2.7 μm . Although these values have

15. Kennealy, J.P., DelGreco, F.P., Caledonia, G.E., and Green, B.D., "Nitric Oxide Chemiexcitation Occurring in the Reaction Between Metastable Nitrogen Atoms and Oxygen Molecules," J. Chem. Phys. 69(4), 1574 (1978).
16. Caledonia, G.E. and Kennealy, J.P., "NO Infrared Radiation in the Upper Atmosphere," Planet. Spa. Sci. 30, 1043 (1982).
17. Rawlins, W.T., Caledonia, G.E., Gibson, J.J., and Stair, A.T., Jr., "Infrared Emission from $\text{NO}(\Delta\nu=1)$ in an Aurora: Spectral Analysis and Kinetic Interpretation of HIRIS Measurements," J. Geophys. Res. 86, 1313 (1981).

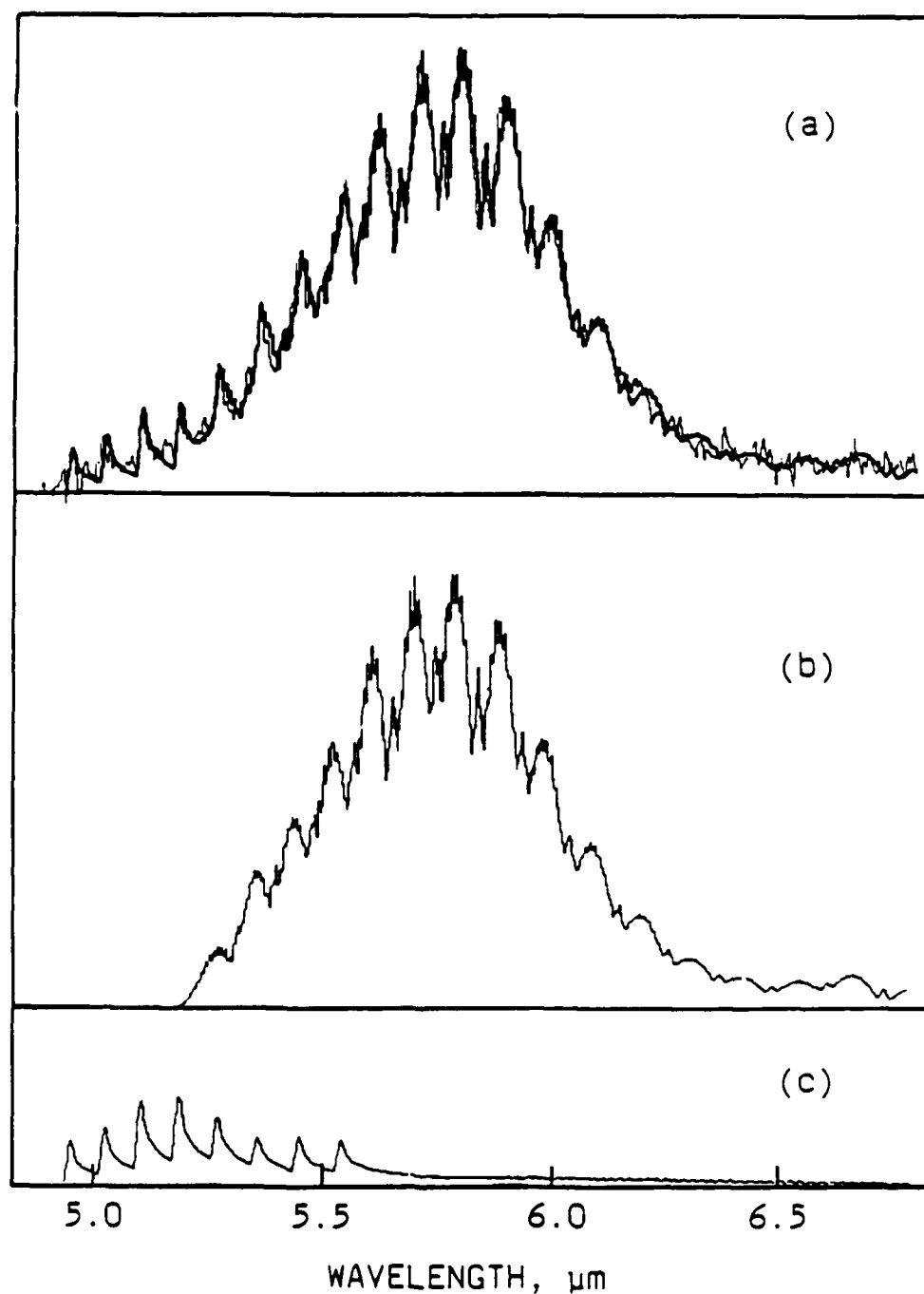
been predicted theoretically¹⁸ and have been determined experimentally for some vibrational levels¹⁹ considerable uncertainty still exists, most notably for $v'=2,3$ and $v'>7$.

We have used the cryogenic COCHISE reactor/spectrometer facility at AFGL² to study systematically the reaction of microwave-discharge-excited N_2/Ar mixtures (1 to 10 percent N_2) with O_2 at 80 K and 3 to 5 mtorr in order to (1) identify all the excitation mechanisms; (2) remove uncertainties due to underlying spectral features; and (3) determine the overtone/fundamental branching ratios. Most of the observed fluorescence was due to the $N(^2D) + O_2$ reaction as reported in Ref. 15; strong bands of the $N_2(W^3\Delta_u - B^3\Pi_g)$ system³ were also observed in the vicinity of the NO overtone band and in the 6 to 8 μm region of the fundamental band. However, a heretofore unidentified band system comprising ~8 sharp features was clearly observed to the blue and slightly overlapping with the NO fundamental band near 5 μm . The features of this progression do not correspond to known or extrapolated positions of vibrational bands of NO^+ or N_2O , or with electronic transitions of N_2 or O_2 .

We have assigned these features as high-J rotational bandheads for the vibrational levels 1 through 8. To obtain the observed intensity distribution in these features, we require significant population of levels $J' \sim 80$ to 100, corresponding to Maxwellian rotational "temperatures" of $\sim 10^4$ K. This is in striking contrast to the ~ 120 K rotational temperatures determined for the remainder of the NO spectrum. A comparison of computed and observed fundamental band spectra is shown in Figure 3; the corresponding vibrational state number densities are shown in Figure 4. The presence of rotational bandheads in the overtone spectrum has a serious impact on the determination of overtone transition intensities, since the overlap with low v' transitions is much

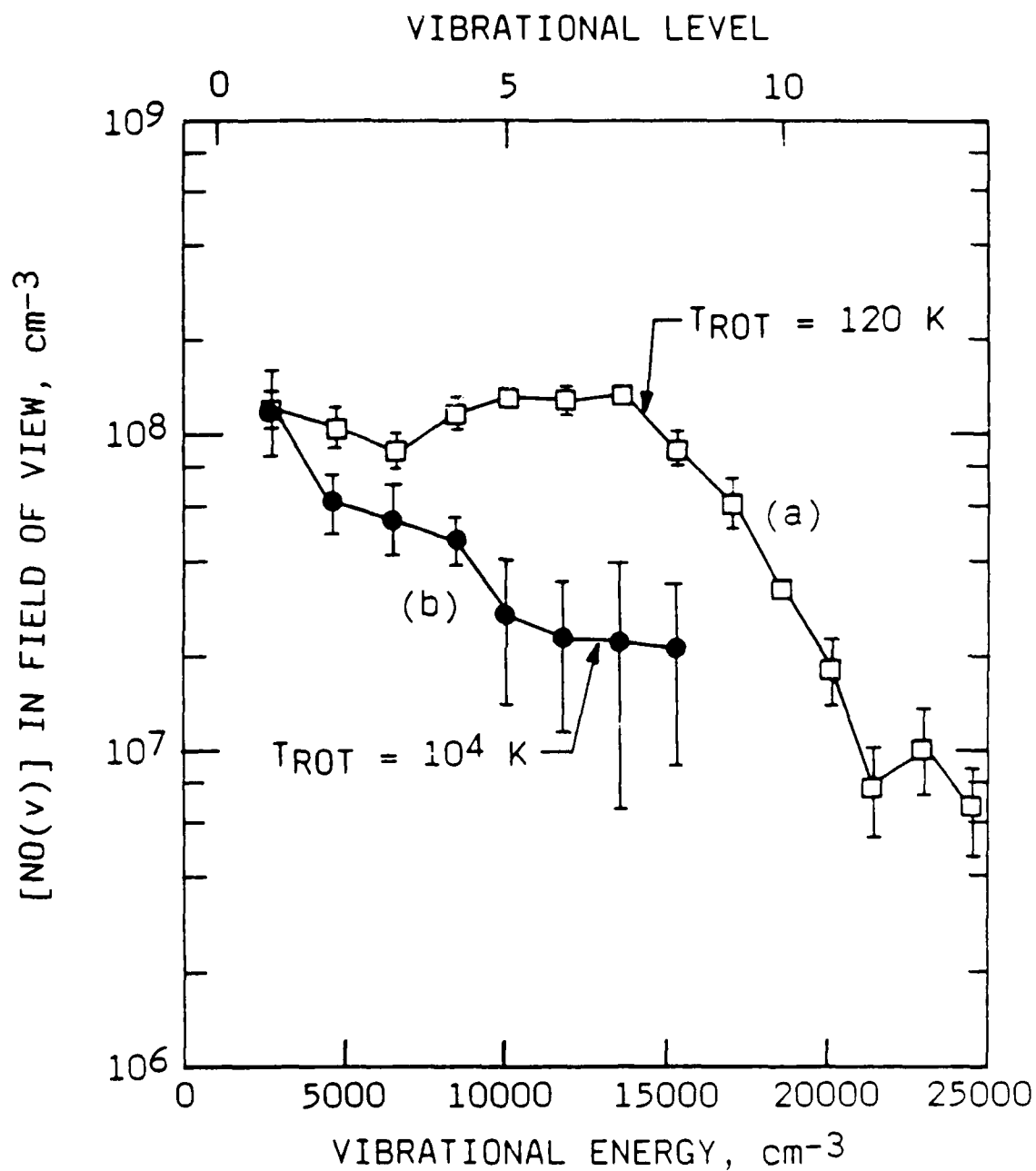
18. Billingsley, F.P., II, "Calculated Vibration-Rotation Intensities for $NO(X^2\Pi)$," J. Mol. Spec. 61, 53 (1976).

19. Green, B.D., Caledonia, G.E., and Murphy, R.E., "A Determination of the Nitric Oxide Einstein Coefficient Ratios," J. Quant. Spectrosc. Radiat. Transfer 26(3) (1982).



A-6944

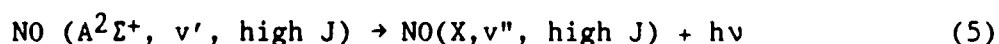
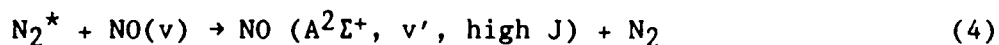
FIGURE 3. COMPARISON OF COMPUTED AND OBSERVED $\text{NO}(v)$ SPECTRA. Discharge: 12% N_2 in Ar; counterflow: O_2 ; gas temperature: 80 K; spectral resolution: 0.0013 μm FWHM; corrected for background emission from the discharges. (a) Comparison of calculated (heavy line) and observed (light line) spectra. (b) Contribution to computed spectrum from rotationally "cold" component, $T_{\text{ROT}} = 120$ K, $v=1-14$. (c) Contribution to computed spectrum from rotationally "hot" component, $T_{\text{ROT}} = 10,000$, $v=1-8$. The sharp features between 4.9 and 5.6 μm are the R-branch bandheads for $v=1-8$.



A-6946

FIGURE 4. AVERAGE VIBRATIONAL POPULATION DISTRIBUTIONS FOR (a) ROTATIONALLY THERMAL AND (b) ROTATIONALLY "HOT" PORTIONS OF THE NO CHEMILUMINESCENCE

more extensive than in the fundamental band. Spectral observations were made as functions of mole fraction of N_2 and O_2 in an attempt to isolate the excitation mechanism for rotationally "hot" NO. Candidate processes include reaction of $N(^2P)$ or excited state with O_2 , and the excitation of NO by energy transfer from N_2 :



where reaction (5) is essentially instantaneous ultraviolet fluorescence in the well-known γ -band system of NO. Reactions (4) and (5) are consistent with our recent data on the excitation of NO by $N_2(A^3E_u^+)$,²⁰ showing excess rotational energy in low-pressure NO(A) fluorescence spectra. This process, unlike reaction (1), would scale nonlinearly with auroral dosing, and may be expected to become significant in fairly strong dosings. However, $N_2(A)$ has insufficient energy to excite NO(A) with 1 eV of rotational energy, and the NO number density in the COCHISE experiments is too small to permit significant collisional excitation during the residence time. Similar arguments rule out excitation of NO(v, J) by collisional $V \rightarrow R$ transfer or hot-atom $T \rightarrow R$ transfer, and the reaction of N_2^* with O_2 is unlikely because it requires a metathetic four-center exchange.

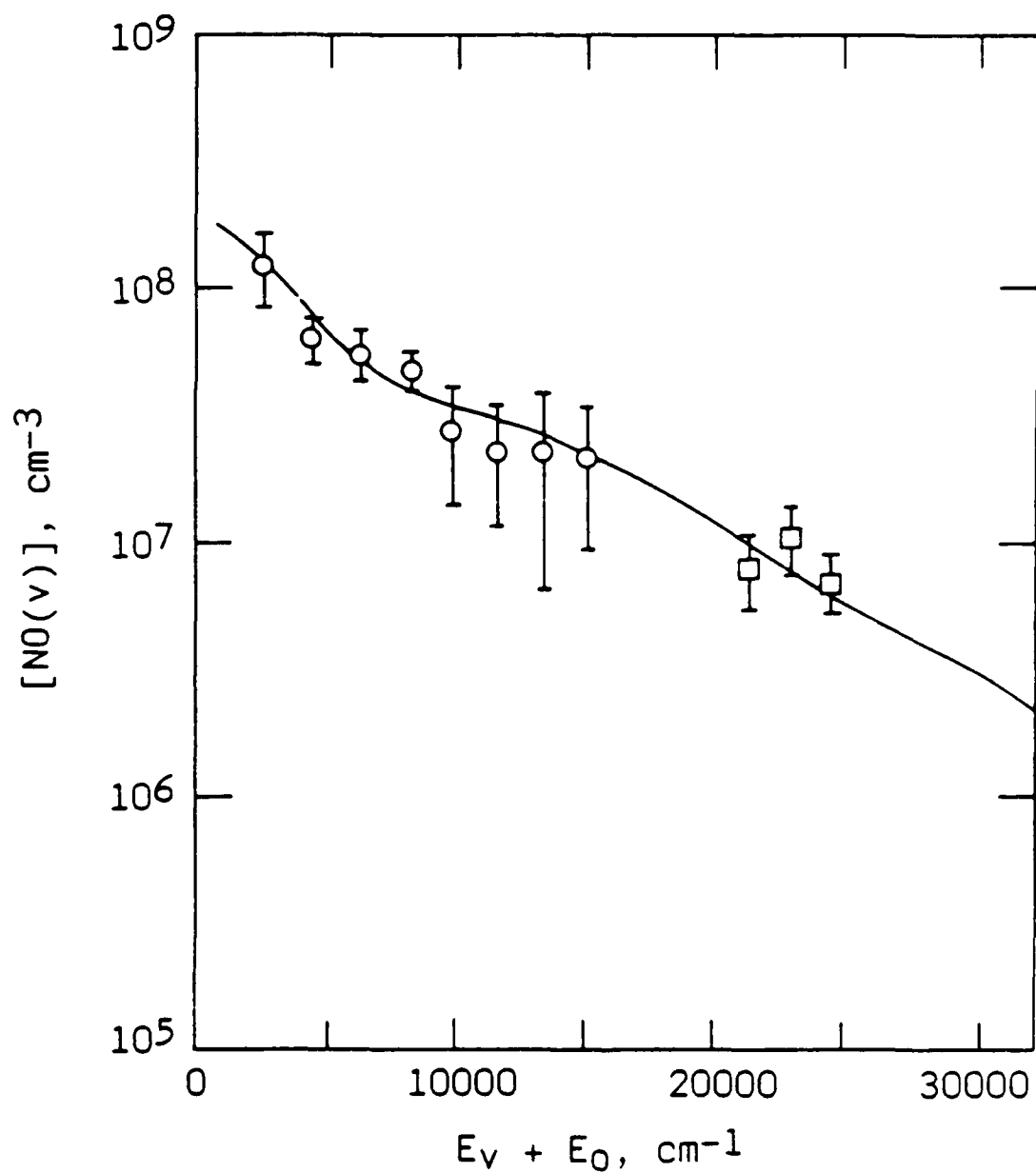
We conclude that the rotationally excited component of NO(v) arises from the reaction of $N(^2P)$ with O_2 . While this reaction does not have an adiabatic path for the formation of ground-state O, there are adiabatic paths for the formation of O(1D , 1S), and curve crossing to give O(3P) as a product would not be surprising for this system. We report detailed nascent vibrational distributions and reaction branching ratios, as inferred from surprisal

20. Piper, L.G., Cowles, L.M., and Rawlins, W.T., "State-to-State Excitation of $NO(A^2E^+, v'=0,1,2)$ by $N_2(A^3E_u^+, v'=0,1,2)$," J. Chem. Phys. 85, 3369 (1986).

analysis, in a separate publication.²¹ The identification of the rotational bandheads forces a substantial re-interpretation of previous results¹⁵ for this system. The final inferred vibrational state distributions for the reactions of $N(^2D, ^2P)$ with O_2 are shown in Figures 5 and 6. The $N(^2D)$ reaction forms NO preferentially in $v=7$, with no substantial excess rotational energy, characteristic of an abstraction reaction with a short-lived reaction complex. In contrast, the $N(^2P)$ reaction gives essentially statistical product distributions with a great deal of excess rotational energy, signifying an insertion reaction with a long-lived complex. This type of reaction can be expected to violate the relatively weak rules of orbital angular momentum conservation which forbid the $O(^3P)$ product route, giving significant production of $NO(v=14-26)$, and would thus be the major source of $NO(\text{high } v)$ in the disturbed atmosphere. The excess rotational energy leads not only to the formation of the distinctive R-branch bandheads near $5 \mu\text{m}$, but also to the corresponding P-branches which spread throughout the 6 to $8 \mu\text{m}$ region. The COCHISE results indicate that these P-branches from the lower vibrational levels are the dominant sources of radiation in this spectral region, being significantly brighter than emission from $NO(\text{high } v)$ for collisional conditions corresponding to altitudes above 100 km. These results permit extensive re-evaluation of previous interpretations of the radiation signatures of $NO(v)$ in the disturbed upper atmosphere. The observation of statistical product branching ratios for the $N(^2P) + O_2$ reaction leads to the further speculation that the product channel forming $NO(a^4\pi)$, which ought to radiate near $10 \mu\text{m}$, may also occur; we plan to investigate this possibility in COCHISE in the near future.

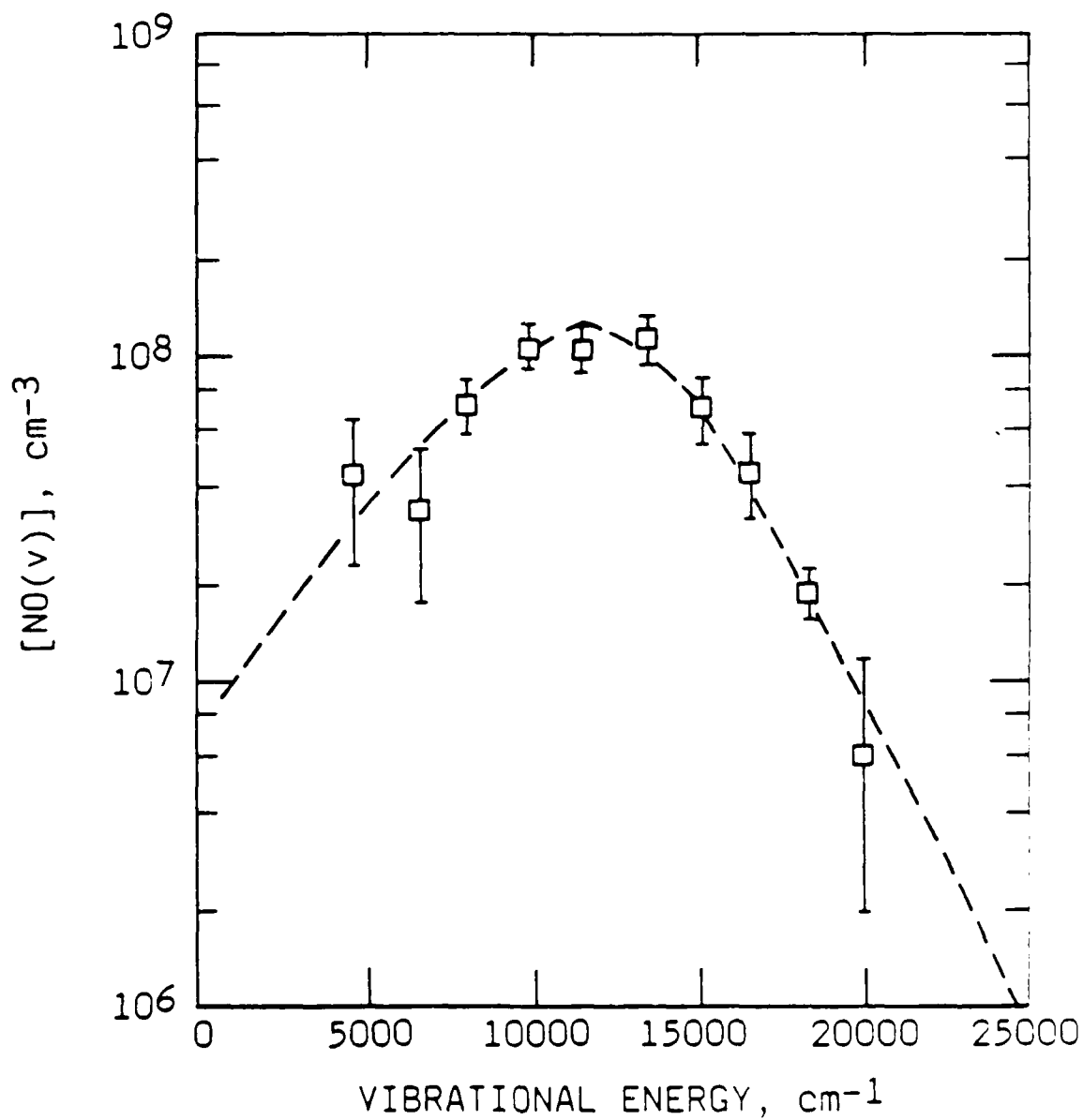
We have also observed rotational excitation effects in COCHISE studies of the interaction of discharge-excited N_2/Ar mixtures with CO. These results

21. Rawlins, W.T., Fraser, M.E., and Miller, S.M., "Rovibrational Excitation of Nitric Oxide in the Reaction of O_2 with Metastable Atomic Nitrogen," J. Phys. Chem., Submitted, 1987.



A-6949

FIGURE 5. COMPARISON OF ROTATIONALLY "HOT" POPULATIONS FOR $v=1-8$ AND ROTATIONALLY "THERMAL" POPULATIONS FOR $v=12-14$ TO COMPOSITE PRIOR DISTRIBUTION FOR THE $N(^2P) + O_2$ REACTION (CURVE)



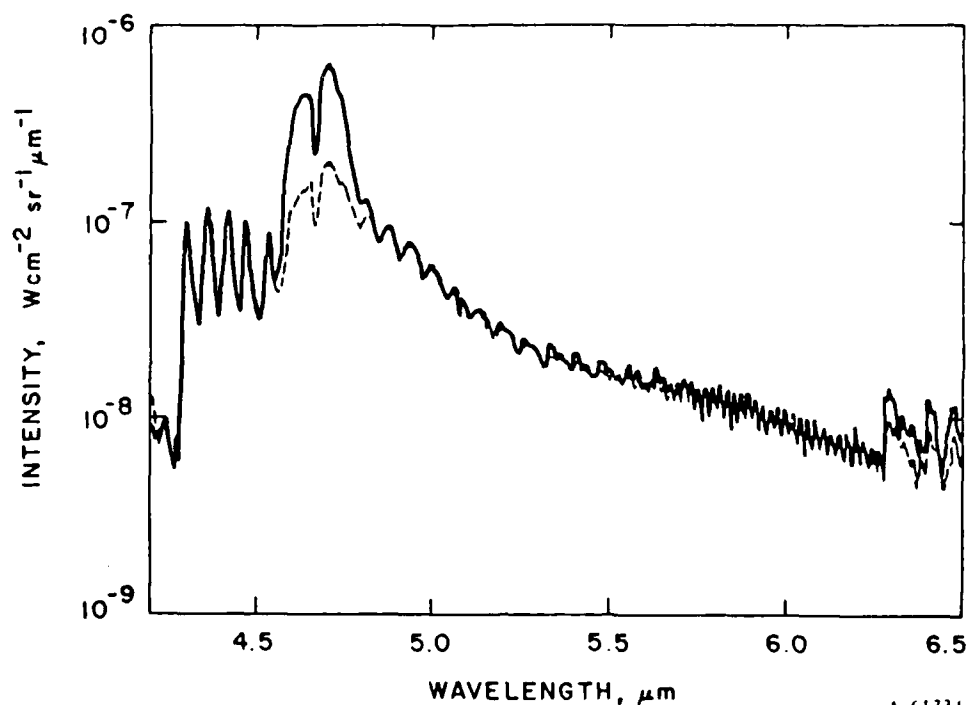
A-6951

FIGURE 6. ROTATIONALLY THERMAL POPULATIONS, CORRECTED FOR THERMALIZED HIGH-J COMPONENT. THE DASHED CURVE REPRESENTS POPULATIONS DETERMINED FROM THE SURPRISAL ANALYSIS

are also reported in detail elsewhere.²² A typical CO(v) excitation spectrum and the resulting vibrational population distributions are shown in Figures 7 and 8. As was the case with NO, 3 to 4 eV of excess rotational energy, sufficient to cause formation of R-branch bandheads to the blue of the thermal CO spectrum, is evident. When corrected for contributions by the well-known near resonant V-V transfer from N₂(v=1,2) to CO(v=1,2), the similarity in vibrational distribution of the rotationally cold and hot spectral components suggests a single excitation process; we expect sufficient collisional thermalization of the initially excited rotational states to account for the relative contribution of the cold component. However, in contrast to the NO results, this excitation must be due to an energy transfer between metastable nitrogen and CO. The atomic metastables can be ruled out rather easily; N(²D) has insufficient energy to account for the levels of vibrational and rotational excitation we observe, and N(²P) (which satisfies the energetic requirements quite nicely) is quenched far too slowly by CO to account for the observed excitation rates. N(²D) probably contributes to excitation of CO(v=1-8), but the rate of this process is evidently much slower than the one we observe.

The remaining electronic metastables, N₂(A³Σ_u⁺, a'¹Σ_u⁻), are known to efficiently excite CO to its a³Π and A¹Π states, respectively, with insufficient excess energy available for 3 eV of rotational excitation, so these states appear not to be likely precursors for CO(v,J) excitation. Surprisal analysis indicates that the net energy transferred to CO(X) is approximately 3.5 eV, corresponding to N₂(X,v≥13). We anticipate that substantial N₂(high v) is produced in our discharge conditions, and are continuing to investigate the possibility that this is the precursor to the observed CO excitation. In addition, the metastable N₂(A') cannot be ruled out as a possible agent for excitation of CO(v,J); however, the kinetics of this little-known state of N₂ are completely unknown. Finally, there are

22. Fraser, M.E., Rawlins, W.T., and Miller, S.M.. "Rovibrational Excitation of CO by Energy Transfer from Excited Nitrogen." J. Phys. Chem., to be submitted, 1988.



A-61331

FIGURE 7. CO(v,J) EXCITATION SPECTRA. The dark line shows a typical spectrum obtained under conditions of 12% discharged N₂/Ar reacting with a counterflow of 33% CO/Ar. The light line shows data taken at 3.17% N₂/Ar and identical counterflow conditions.

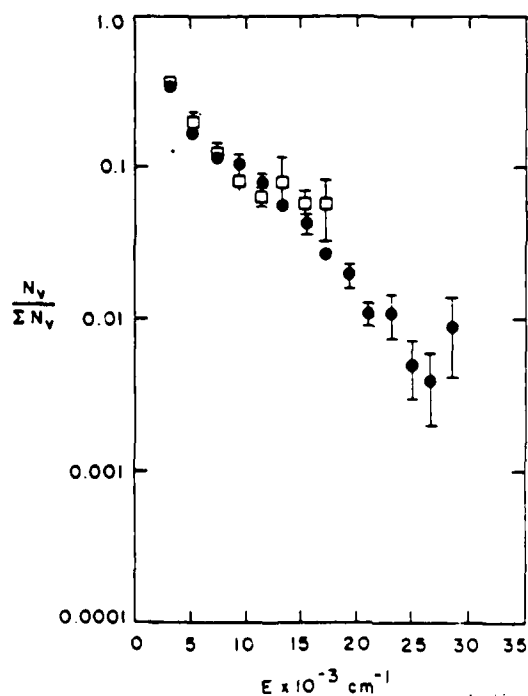
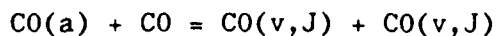
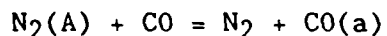


FIGURE 8. AVERAGED RELATIVE POPULATION DISTRIBUTIONS FOR 11 DATA FILES, CORRECTED FOR N₂-CO V-V component at V=1-2. Both thermalized (circles) CO and the bandheads (squares) are shown but have been normalized independently. The error bars represent one standard deviation.

sufficient collisions in the interaction region (10 to 30) to permit the rapid sequential process



We are continuing to investigate the mechanisms for excitation of CO in these experiments.

If CO(v,J) is indeed excited by direct energy transfer from vibrationally or electronically excited N₂, these results have some significance for the modeling of MWIR signatures in nuclear scenarios, since CO₂ dissociation is expected to be significant for those conditions. The R-branch rotational bandheads extend to 4.3 μm, and the corresponding P-branches extend into the 6 to 7 μm region as noted above for NO. Moreover, these results serve to verify the effects on a molecular infrared signature due to extensive rotational excitation. Such rotational excitation is possible for other IR radiating species which might be excited by metastable energy transfer or chemiluminescent processes.

4.0 CONCLUSIONS

In the nuclear-disturbed upper atmosphere, the local number densities of excited metastable energy carriers, such as N₂(A,a',A'), N₂(high v), N(²D, ²P), and O₂(a,b, etc.), can build up to substantially larger values than are encountered in the moderate auroral dosings that comprise most of the data base on IR signatures of the disturbed upper atmosphere. The abundance of such energetic, highly labile species can lead to chemical product formation and species excitation which are not encountered in conventional upper atmospheric experiments, and which are often not adequately represented in the modeling of high altitude nuclear effects. We have presented the results of recent laboratory investigations of three such processes which provide new

information impacting MWIR and LWIR modeling. First, it is likely that vibrationally excited N_2O is efficiently formed in electron-bombarded air by reaction(s) of metastable forms of N_2 and O_2 , providing a hitherto unrecognized source of radiation near 4.5, 7.8, and 17 μm . Second, the reaction of $N(^2P)$ with O_2 , once believed not to occur, appears to be an efficient source of vibrationally and highly rotationally excited NO , with the resultant rotational excitation dominating the NO spectral signature in the 4.9 to 5.2 and 6.5 to 8.0 μm bandpasses. Third, CO , which is likely to be present in the nuclear-disturbed upper atmosphere due to CO_2 dissociation, is efficiently vibrationally and rotationally excited by either direct or indirect energy transfer from metastable forms of N_2 , with the resultant rotational/vibrational excitation providing radiation from 4.3 to 7 μm .

The results of these experiments have a common significance: in a sufficiently intense electron dosing of the upper atmosphere, energetic metastable species are created whose subsequent chemistry can lead to the formation of new classes of IR radiators, containing large amounts of vibrational, rotational, or perhaps even electronic energy, which can exhibit complex IR signatures in the 80 to 120 km region. Verification of the effects of these types of processes on predictions of atmospheric IR backgrounds requires reliable modeling of the excitation of atmospheric metastables at high altitudes, and continued laboratory studies of metastable reaction dynamics.

ACKNOWLEDGEMENTS

The authors benefitted from numerous discussions and suggestions by many scientific colleagues, especially B.D. Green (PSI), G.E. Caledonia (PSI), and W.A.M. Blumberg (AFGL). This work was performed under Contract F19628-85-C-0032 with the Air Force Geophysics Laboratory, and was sponsored by the U.S. Air Force Office of Scientific Research under Task 2310G4 and by the Defense Nuclear Agency under Project 5A, Task 5A, Work Unit 115.

APPENDIX B

(SR-257 reproduced in its entirety)

J. Phys. Chem. 91, 3883 (1987)

RATE COEFFICIENTS FOR $N(^2D)$ REACTIONS

Lawrence G. Piper, Megan E. Donahue,* and Wilson T. Rawlins

Physical Sciences Inc

Research Park, P.O. Box 3100

Andover, MA 01810

J. Phys. Chem. 91, 3883 (1987)

*Present address, Department of Astrophysics, University of Colorado
Boulder, Colorado

ABSTRACT

We have measured rate coefficients for the reactions of $N(^2D)$ with O_2 , CO_2 , N_2O , CO and H_2 in a discharge-flow reactor. A resonance-fluorescence diagnostic having an ultimate sensitivity of better than 1×10^8 atoms cm^{-3} monitors the number density of $N(^2D)$. The extreme sensitivity of the diagnostic allows kinetic measurements to be made in regions of the flow reactor far downstream from the source of the metastables. This feature removes fluid dynamic complications which plague most flow reactor studies of metastable kinetics. The diagnostic sensitivity also affords over two orders of magnitude in $N(^2D)$ number density decays, thereby ensuring the accurate determination of kinetic decay rates. A movable injector for the reactants allows measurements at a variety of reaction times, thereby eliminating uncertainties caused by imperfect mixing in the reactor.

I. INTRODUCTION

Metastable atomic nitrogen, $N(^2D, ^2P)$, plays an important role in the chemistry of the non-equilibrium upper atmosphere and of systems employing nitrogen or air discharge plasmas. $N(^2D)$, through its chemiluminescent reaction with molecular oxygen,



controls the production of NO in the thermosphere, and provides a key source of vibrationally excited NO (and perhaps electronically excited O) in electron-irradiated air.^{1,2} Similarly, quenching of $N(^2D)$ by other common atmospheric species such as CO_2 , N_2O , CO, H_2 or H_2O may proceed by chemical or energy transfer reactions to form internally excited molecular products.

Several investigators³⁻⁸ have studied the quenching kinetics of $N(^2D)$ using either discharge-flow or flash photolysis techniques. Most of these studies employed relatively insensitive and error-prone techniques for detecting the commonly-obtained, low concentrations of $N(^2D)$, viz. resonance absorption,^{4,5,8} electron-spin resonance (ESR) spectroscopy,⁶ and tracer fluorescence.⁷ Since the maximum obtainable $N(^2D)$ number densities are typically only slightly above the detection limits of techniques such as resonance absorption or ESR, it is difficult to obtain the factor of 10 to 100 first-order $N(^2D)$ decays which are required not only for precise rate-coefficient determinations but also to rule out interference from secondary reactions. The limitation in dynamic range imposes additional uncertainties on the flow reactor studies,^{4,6,8} where the measurements must be made at fairly short flow distances under conditions of poorly characterized flow development. As a

result, $N(^2D)$ quenching rate coefficients available in the literature still exhibit considerable disparity, often as much as a factor of 3.

The diagnostic technique of $N(^2D)$ atomic resonance fluorescence, first described briefly by Iannuzzi and Kaufman,³ provides the high sensitivity and correspondingly large dynamic range required to overcome the above difficulties. However, the use of this technique requires careful correction for spectroscopic interference from other species as well as considerable optimization of the light source and detection system. We describe here the use of $N(^2D)$ resonance fluorescence, coupled with proper delineation of fluid dynamic conditions in a discharge-flow reactor, to obtain unequivocal rate coefficients for quenching of $N(^2D)$ by several atmospherically important molecular species.

II. EXPERIMENTAL

A. APPARATUS

The apparatus is a modification of one we have used previously in a number of other studies.⁹⁻¹³ It consists of a two-inch flow tube pumped by a Leybold-Heraeus Roots blower/forepump combination capable of producing linear velocities up to 5×10^3 cm s⁻¹ at pressures of one torr. The flow-tube design is modular (see Figure 1), with separate source, reaction, and detection sections which clamp together with O-ring joints. The detection region is a rectangular stainless-steel block bored out internally to a two-inch circular cross section and coated with Teflon® (Dupont Poly TFE #852-201) to retard surface recombination of atoms.¹⁴ The surface was primed with black primer prior to the Teflon® coating to reduce scattered light inside the block. Two sets of viewing positions consisting of circular ports on each of the four faces of the block are separated by a distance of 7.5 cm. The circular ports, all of which contain MgF₂ windows, accommodate vacuum ultraviolet resonance lamps, VUV and visible monochromator interfaces, laser delivery side-arms and a spatially filtered photomultiplier/interference filter combination.

The upstream observation position is fitted with two microwave-discharge resonance lamps placed normal to each other, and a 0.2m vacuum ultraviolet monochromator (Minuteman 302 VM) diametrically opposite one of the resonance lamps. The lamp which is viewed by the monochromator is used in absorption studies while the lamp normal to the monochromator's optical axis is used to excite resonance fluorescence of atomic species formed in the flow reactor. The lamps and the monochromator are separated from the flow tube by 25 mm diameter MgF₂ windows which have a short-wavelength cutoff of 115 nm.

A schematic showing the resonance lamps and detection cell is given in Figure 2. The lamps are constructed from 13 mm (o.d.), medium-wall Pyrex® tubing. He or Ar flow through each lamp at rates of $\sim 150 \mu\text{mol s}^{-1}$ and total pressures of ~ 1.5 torr. The discharge plasmas are excited by Evenson¹⁵ cavities powered by 2.45 GHz supplies (Raytheon PGM-10) operating at a power of about 20W for the absorption lamp and 50W for the resonance-fluorescence lamp. The gas flow enters the lamp near the window and passes from front to back. This procedure inhibits the buildup of pockets of absorbing atoms between the emitting region and the exit window. Controlled amounts of air can be added to the lamp to enhance nitrogen emissions, but usually the impurity level of N_2 (i.e., a few ppm) in the He or Ar bath gases is sufficient to give intense but optically thin multiplets at 149 and 174 nm. Instability in the emission intensity, due to long-term variations in the lamp cooling rate and thereby in the steady-state operating temperature of the lamp (typically 500-600 K), is minimized by regulating the flow of cooling air to the cavity. In practice, He bath gas was commonly used in the lamps. We have observed previously¹⁰ that excitation by metastable argon gives excessive non-thermal line broadening of the NI emission.

Atomic nitrogen metastables are made in the flow tube by discharging mixtures of nitrogen and either argon or helium in a McCarroll¹⁶ cavity powered by another Raytheon 2.45 GHz supply. Molecular nitrogen is moderately efficient at quenching the atomic metastables ($k_{\text{N}(2\text{D}) + \text{N}_2} = 1.6 \times 10^{-14} \text{ cm}^3 \text{ molecule}^{-1} \text{ s}^{-1}$),^{4,5} so that the best metastable yields come from airily dilute mixtures of N_2 in the Ar or He, typically $< 1\% \text{ N}_2$.

Quenching reagents enter the flow reactor through a movable injector which consists of a 0.25 in. diameter length of stainless steel tubing with a teflon loop epoxied into its downstream end. The loop is slightly more than an inch in diameter and is set on the stainless steel tube so that it is concentric with the flow reactor. A number of small holes have been drilled around both the inside and outside of the loop to allow reagent gas to escape into the gas stream. The quality of mixing was checked by observing the air afterglow when NO was added through the loop injector to a flow containing O-atoms. The 0.25 in. stainless tube slides along the bottom of the flow reactor, and exits it through a Swagelok® fitting in the end flange of the flow reactor. The Swagelok® fitting has been slightly modified for this purpose by boring it out completely to accept the tube, using a double O-ring seal in place of the front ferrule, and by reversing the rear ferrule. The zero of the scale relating the distance between the injector and the detection region was calibrated by measuring the point at which the scattered light from the resonance fluorescence lamp suddenly increased as the injector was moved into the detection region.

Mass-flow meters monitor the flow rates of all gases. All flow meters were calibrated by measuring rates of increase of pressure with time into 6.5 or 12 l flasks, using appropriate differential pressure transducers (Validyne DP-15) which had themselves been calibrated with silicon oil or mercury manometers. Typically the flow rates for argon or helium, nitrogen, and quencher were 2000-5000, 50, and 0-120 $\mu\text{mole s}^{-1}$, respectively. The total pressure was generally 1-3 torr, and the flow velocity was 1000-3500 cm s^{-1} .

The argon or helium and the nitrogen flow through molecular-sieve traps to remove water and carbon dioxide prior to entry into the flow reactor. In

most experiments the quenchers flowed straight from their cylinders into the reactor without further purification.

A MgF_2 lens collected vacuum ultraviolet fluorescence from the flow tube and focused the light on the entrance slit of a 0.2 m monochromator which employed a concave grating. A turbomolecular pump maintained a pressure $<1 \times 10^{-6}$ torr in the monochromator. A solar blind photomultiplier with KI photocathode detected photons exiting the monochromator, with the aid of a photon-counting rate meter. In some cases, a scaler counted individual photons. Since the dark count of the VUV solar blind PMT was about 0.4 Hz, count rates on the order of 1 Hz could be determined with reasonable precision. When pulse counting, the procedure generally was to average 4-10 sets of 10 second counts. A laboratory personal computer and data-acquisition system read photon-counter and mass-flow-meter outputs and stored them on floppy disks for subsequent analysis. The data were reduced and analyzed with the aid of LOTUS 123® spread sheets which we designed to average the raw signals, convert them to appropriate engineering units and to perform the requisite least-squares fitting and plotting of the data.

B. Resonance-Fluorescence Diagnostic

A resonance fluorescence diagnostic monitors the number density of the $\text{N}(^2\text{D})$. While this technique is straightforward for most systems,¹⁷⁻¹⁹ several interferences make it more difficult to apply to $\text{N}(^2\text{D})$ studies. The observed signal consisted of four components: the resonance-fluorescence signal of interest ($0 < I_f < 2000$ Hz); Lyman-Birge-Hopfield (LBH, $\text{N}_2(a^1\Pi_g - x^1\Sigma_g^+)$) and a small amount of Ogawa-Tanaka-Wilkinson-Mulliken (OTWM, $\text{N}_2(a^1\Sigma_u^- - x^1\Sigma_g^+)$) emission from the gas stream ($0 < I_{\text{LBH}} < 100$ Hz); scattered light from the excitation

source ($I_{sc} \sim 3-6$ Hz); and dark counts from the photomultiplier ($I_{dk} \approx 0.4$ Hz). Separating these phenomena required four sets of measurements: 1) metastables and lamp on, $I_1 = I_f + I_{LBH} + I_{sc} + I_{dk}$; 2) metastables on, lamp off, $I_2 = I_{LBH} + I_{dk}$; 3) metastables off, lamp on, $I_3 = I_{sc} + I_{dk}$; and 4) metastables and lamp off, $I_4 = I_{dk}$. The desired signal then was $I_f = I_1 - I_2 - I_3 + I_4$. The LBH emission is excited primarily in collisions between buffer gas and $N_2(a'^1\Sigma_u^-)$.^{20,21} Because most gases rapidly quench $N_2(a'^1\Sigma_u^-)$,²¹ I_{LBH} varies with number density of added reagents. This variation must be determined. Generally the scattered light and dark counts remained constant with quencher flow, but did vary from day to day. In the case of the reaction with carbon monoxide, both I_{LBH} and I_{sc} increased with added quencher. This was because of CO fourth-positive ($A'^1\Pi-X'^1\Sigma^+$) excitation by $N_2(a'^1\Sigma_u^-)$ ²¹ in the gas stream and some CO fourth-positive resonance fluorescence excited by impurity emissions in the lamp. Figures 3 and 4 illustrate the emissions observed in the reactor with the resonance-fluorescence lamp on and off, respectively.

At sufficiently high number densities, the observed resonance-fluorescence intensity varies non-linearly with the number density of the species being monitored because the resonance fluorescence is absorbed by metastables between the excitation region and the monochromator. This non-linearity complicates the interpretation of kinetic measurements.²² In order to determine the safe region for operation, we measured the resonance-fluorescence intensity, and under identical conditions determined the $N(^2D)$ number density via resonance absorption. Figure 5 shows a plot of the data. Above about 1.5 kHz the resonance-fluorescence signal falls off from linearity under the observation conditions employed. When the abscissa of the plot is

placed on an absolute basis,²³ we find a signal of 1 Hz corresponds to a number density of $<10^8$ atoms cm^{-3} . Enhancements in sensitivity over the conditions of Figure 5 result from using larger slits and monitoring the 149 nm fluorescence rather than that at 174 nm.

The final and most nagging problem in applying resonance-fluorescence to the detection of $\text{N}(^2\text{D})$ lies in separating its resonance-fluorescence signal from that of accompanying $\text{N}(^2\text{P})$ metastables. The two metastable nitrogen atoms, $\text{N}(^2\text{D})$ and $\text{N}(^2\text{P})$, have a common upper state for their resonance lines so that one of the lines must be filtered from the lamp to discriminate between the two levels. A laser reflector centered at about 175 nm on a MgF_2 substrate discriminates moderately well against the 174 nm line which is absorbed by $\text{N}(^2\text{P})$ while passing the 149 nm multiplet which is absorbed by $\text{N}(^2\text{D})$. We found that commercially available reflectors were imperfect, however, giving a transmission ratio, T_{149}/T_{174} of about 8:1. Some further discrimination which enhances resonance fluorescence from $\text{N}(^2\text{D})$ pumping over that from $\text{N}(^2\text{P})$ pumping results from a greater intensity in the 149 nm multiplet, a slightly larger oscillator strength for 149 nm absorption,²⁴ and by the fact that $\text{N}(^2\text{D})$ outnumbered $\text{N}(^2\text{P})$ in the flow reactor. Absorption measurements on the ratio of $[\text{N}(^2\text{D})]$ to $[\text{N}(^2\text{P})]$ showed a variation of greater than 7:1 in argon to as little as 2.5:1 in the helium. The lower $\text{N}(^2\text{P})$ number density in an argon carrier results from an enhanced quenching of $\text{N}(^2\text{P})$ relative to $\text{N}(^2\text{D})$ by argon. The fraction of the initial resonance fluorescence observed in argon which could be attributed to $\text{N}(^2\text{P})$ pumped by leakage through the lamp filter was only about one percent, but was as much as three to five percent in helium buffer. This leakage causes severe problems in getting reliable kinetic data

because the $N(^2P)$ is much less readily quenched by most gases than is $N(^2D)$ -- generally by one to two orders of magnitude -- so that after only one e-fold in measured resonance-fluorescence decay, as much as 15 percent of the residual resonance-fluorescence signal comes from unquenched $N(^2P)$. Thus, decay plots in helium can become severely non-linear over less than an order of magnitude decay. Such non-linearity is unacceptable for obtaining reliable quenching measurements. One would like two orders of magnitude of linear decay if possible, and given the low background counts in our system, several orders of magnitude in resonance fluorescence decay as a function of added quencher is certainly attainable.

We overcame the problems of residual $N(^2P)$ resonance fluorescence interference by using two filters back-to-back to discriminate against the 174 nm line from the lamp, and by making most measurements at moderately high pressures of argon buffer. With this procedure we could obtain linear decays over more than two orders of magnitude.

A final complication to using a resonance-fluorescence diagnostic is the possible absorption of the resonance radiation by the quencher. This problem will be most evident in studies with relatively inefficient quenchers for which larger number densities of reactant must be added to the reactor. For the species studied here, only CO_2 is a potential problem. We were careful to keep CO_2 number densities low enough to avoid significant absorption, and worked at longer decay times to obtain adequate decays. Finally, the CO_2 results were carefully cross checked using a resonance-absorption diagnostic, which gave similar results to the resonance-fluorescence runs.

III. RESULTS

Rate coefficients are determined from measurements of the change in the natural log of the metastable nitrogen number density as a function of number density of added quenching reagent with fixed reaction distance z :

$$-\frac{d \ln[N(^2D)]}{d[Q]} = 0.62 k_Q z / \bar{v} = \Gamma(z) \quad , \quad (2)$$

where k_Q is the reaction rate coefficient, z the distance between the injector and observation region, \bar{v} the bulk flow velocity, and the factor of 0.62 corrects for the coupling of a radial density gradient in $N(^2D)$ with a parabolic velocity profile of the gas stream.²⁵⁻²⁸ This analysis requires corrections to the reaction distance, z , to account for imperfect mixing at the injector. Thus, one must measure decays at several different distances with all other conditions fixed, and then determine the reaction-rate coefficient from a plot of Γ versus z .

The slopes of lines in Figure 6 are the decay coefficients, $\Gamma(z)$, as defined by Eq. (2). The slope of a plot of Γ versus effective reaction time, \bar{z}/v , determines the reaction rate coefficient. Figure 7 illustrates this for the data of Figure 6. Note the non-zero intercept indicating a finite mixing time for the experimental conditions employed. The first column of Table 1 lists our results. The error bars on our measurements are a root-mean-square weighting of the statistical uncertainties as reflected in reproducibility of results from one experiment to another, and the systematic uncertainties involved in measuring temperature, pressure, flow rates, reaction distances,

etc. As a cross check on our results, we also measured $N(^2D)$ decays via resonance absorption for quenching by O_2 , CO , N_2O and CO_2 . Although an inherently much less sensitive diagnostic technique (see below), the absorption measurements agreed excellently with the more comprehensive set of resonance-fluorescence kinetic runs.

Table 1 also compares our results with other measurements in the literature. The flash photolysis measurements of Husain et al.⁵ agree well with our determinations except for the rate coefficient for quenching by CO_2 . Iannuzzi and Kaufman's³ measurement on the total rate coefficient for reaction with O_2 also agrees well. Most of the other measurements are substantially larger than our result. The flow reactor measurements of Lin and Kaufman⁴ and Fell et al.⁶ suffer greatly from overall lack of sensitivity as well as from uncertainties in the development of their flow profile. We discuss these problems in some detail below. The photolysis studies of Black et al.^{7,8} monitored temporal decays of emission between 300 and 400 nm in mixtures of N_2O and reactant. Their analysis is based on the assumption that $N(^2D)$ is produced in the photolysis and that it reacts with N_2O to give $NO(B^2\Pi - X^2\Pi)$ emission. The NO emission is then a tracer of their $N(^2D)$ number density. Kinetic measurements employing tracers is often somewhat dangerous unless one can be absolutely certain of the identity of the precursor to the tracer.⁹ Black et al.'s measurements also lacked sensitivity, having a dynamic range of less than a factor of ten.

The experimental approach described above, together with the extreme sensitivity of the resonance fluorescence diagnostic, eliminates most large systematic errors inherent in flow-reactor studies of metastable kinetics. A major potential source of error lies in correcting for the coupling between the

radial density gradient of the metastables and the parabolic velocity profile of the bulk gas. Under conditions such that laminar flow is fully developed, the rate coefficient as determined under the assumption of plug flow must be multiplied by a factor of 1.6 to correct for these fluid dynamic effects.²⁵⁻²⁸ The formula commonly given for the entry length, i.e., the distance the gas must flow down the tube before laminar flow is fully developed, is generally written in terms of the product of the flow reactor radius and the Reynolds number.²⁹ Because at constant gas flow rate, the Reynolds number varies inversely with flow tube radius, the entry length in reality has no dependence on the reactor diameter. Only the molar flow rate of the gas, its molecular weight, and its viscosity affect the entry length. Thus, we find the entry length, l_e , is best expressed as

$$l_e = 7.23 \times 10^{-8} \frac{f M}{\eta} \quad (3)$$

where f is the flow rate in $\mu\text{mol s}^{-1}$ and M is the gram molecular weight of the gas, and η is the viscosity in Poise. Under typical conditions in our studies, $f \sim 2500 \mu\text{mol s}^{-1}$, $M = 40$, $\eta \sim 2.22 \times 10^{-4}$, we find the entry length is 32 cm. In order to ensure fully developed flow in our system, therefore, our detection region is generally >60 cm downstream from the entrance of the flow reactor, and our measurements cover reaction distances no closer than 25 cm from the upstream end of the reactor.

Another potentially large source of error lies in correcting for imperfect mixing at the injector. Figure 7 shows that under our conditions the effective mixing correction for O_2 is 2 ms. This value is a function of pressure, flow velocity, bath gas species, reactant species, and injector design. The mixing correction must be determined, therefore, for each set of conditions. Clearly, under the conditions of Figure 7, a fixed point determination

at a reaction time of 24 ms would produce a reasonably accurate result even if the mixing correction were ignored. If sensitivity constraints confine one to short reaction times (<10 ms), however, then neglect of the mixing correction will produce results substantially in error.

Allowing adequate flow time to eliminate uncertainties in the fluid dynamic or mixing corrections requires an extremely sensitive diagnostic. In most systems absorption measurements become impractical for fractional absorptions below 0.01 to 0.02. Under the conditions employed in producing Figure 2, the resonance fluorescence intensity is several hundred Hertz for a fractional absorption of 0.01. Thus, the resonance-fluorescence system still has more than two orders of magnitude of dynamic range left after an absorption diagnostic has become useless. This dynamic range is important in kinetic measurements because one cannot ensure linear semi-log decay plots, indicative of freedom from competing processes, with less than one order of magnitude decay.

IV. SUMMARY AND DISCUSSION

We have developed a flow reactor technique for measuring metastable reaction kinetics accurate to 15 percent. The current studies involve monitoring $N(^2D)$ number densities with a resonance-fluorescence diagnostic which has an ultimate sensitivity $\sim 10^8$ atoms cm^{-3} . This sensitivity allows long enough flow times in the reactor to eliminate uncertainties in fluid dynamic and mixing corrections, and further gives large enough dynamic range in decay measurements to allow accurate determination of decay rates.

The quenching rate coefficients obtained here are consistent with those of previous investigators, especially in view of the uncertainties inherent in the earlier work, but offer significantly improved absolute accuracy and relative precision. For most of the quenchants tested, the observed rate coefficients correspond to cross sections on the order of 1/100 of the gas kinetic value, with the value for CO_2 being another order of magnitude smaller. Thus, the rate coefficients may have a significant temperature dependence (e.g., see Ref. 8). Furthermore, the quenching may occur through formation of reactive complexes, with energy barriers in the exit channels such that vibrationally excited molecular products are formed. The work of Lin and Kaufman⁴ seemed to indicate that quenching of $N(^2D)$ by O_2 , N_2O , and CO_2 proceeds primarily by chemical reaction. More recent observations of NO vibrational luminescence from the O_2 reaction^{2,30} appear to be quantitatively consistent with this view. Similarly, efficient vibrational luminescence has been observed from $\text{NH}(v)$ formed from $N(^2D) + \text{H}_2$,³¹ and from $\text{CO}(v)$ excited by energy transfer from $N(^2D)$.³⁰ In continuing investigations, we hope to determine product branching ratios for reactions of $N(^2D)$ and $N(^2P)$.

ACKNOWLEDGMENTS

This work was supported by the Infrared Technology Division of the Air Force Geophysics Laboratory, the Air Force Office of Scientific Research, and the Defense Nuclear Agency. The comments and advice of Dave Green and George Caledonia and the experimental expertise of Henry Murphy greatly benefitted our efforts.

REFERENCES

1. C.E. Caledonia, and J.P. Kennealy, Planet Sp. Sci. 30, 1043 (1982).
2. J.P. Kennealy, F.P. DelGreco, G.E. Caledonia, and B.D. Green, J. Chem. Phys. 69, 1574 (1978).
3. M.P. Iannuzzi and F. Kaufman, J. Chem. Phys. 73, 4701 (1980).
4. C.L. Lin and F. Kaufman, J. Chem. Phys. 55, 3760 (1971).
5. D. Husain, S.K. Mitra, and A.N. Young, JCS Faraday II 70, 1721 (1974).
6. B. Fell, I.V. Rivas, and D.L. McFadden, J. Phys. Chem. 85, 224 (1981).
7. G. Black, T.G. Slanger, G.A. St.John, and R.A. Young, J. Chem. Phys. 51, 116 (1969).
8. T.G. Slanger, B.J. Wood, and G. Black, J. Geophys. Res. 76, 8430 (1971).
9. L.G. Piper, G.E. Caledonia, and J.P. Kennealy, J. Chem. Phys. 74, 2888 (1981).
10. W.T. Rawlins and L.G. Piper, Proc. Soc. Photo.-Opt. Instrum. Eng. 279, 58 (1981).
11. L.G. Piper, W.J. Marinelli, W.T. Rawlins, and B.D. Green, J. Chem. Phys. 83, 5602 (1985).
12. L.G. Piper and W.T. Rawlins, J. Phys. Chem. 90, 320 (1986).
13. L.G. Piper, L.M. Cowles, and W.T. Rawlins, J. Chem. Phys. 85, 3369 (1986).
14. H.C. Berg and D. Kleppner, Rev. Sci. Instrum. 33, 248 (1962).
15. F.C. Fehsenfeld, K.M. Evenson, and H.A. Broida, Rev. Sci. Instr. 36, 294 (1965).
16. B. McCarroll, Rev. Sci. Instr. 41, 279 (1970).
17. P.P. Bemand and M.A.A. Clyne, JCS Faraday II 69, 1643 (1973).

18. M.A.A. Clyne and H.W. Cruse, JCS Faraday II 68, 1281 (1972).
19. M.A.A. Clyne and Y. Ono, Chem. Phys. 69, 381 (1982).
20. M.P. Cassasa and M.F. Golde, Chem. Phys. Lett. 60, 281 (1979).
21. L.G. Piper and M.A. DeFaccio, J. Chem. Phys. submitted (1986).
22. M.J. Linevsky and N. DeHaas, J. Chem. Phys. 77, 6060 (1982).
23. L.G. Piper, H.C. Murphy, and W.T. Rawlins, Physical Sciences Inc. TR-292 under Air Force Contract No. F19628-80-C-0174, AFGL-TR-81-0318 (1981).
24. G.M. Lawrence and B.D. Savage, Phys. Rev. 141, 67 (1966).
25. E.E. Ferguson, F.C. Fehsenfeld, and A.L. Schmeltekopf, Advances in Atomic and Molecular Physics V, edited by D.R. Bates, New York, Academic Press, (1970).
26. R.C. Bolden, R.S. Hemsworth, M.J. Shaw, and N.D. Twiddy, J. Phys. B 3, 45 (1970).
27. G.W. Huggins and J.H. Cahn, J. Appl. Phys. 38, 180 (1967).
28. J.H. Kolts and D.W. Setser, J. Chem. Phys. 68, 4848 (1978).
29. S. Dushman, and L.M. Lafferty, Scientific Foundations of Vacuum Technique, 2nd ed., New York: J. Wiley (1962).
30. B.D. Green, G.E. Caledonia, W.A.M. Blumberg, and F.H. Cook, J. Chem. Phys. 80, 773 (1984).
31. G.E. Caledonia and B.D. Green, J. Chem. Phys. 77, 3821 (1982).
32. W.T. Rawlins, H.C. Murphy, G.E. Caledonia, J.P. Kennealy, F.X. Robert, A. Corman, and R.A. Armstrong, Appl. Opt. 23, 3316 (1984).

Table 1. $N(^2D)$ Removal Rate Coefficients^a

Reactant	Group				
	PSI ^b	Cambridge U. ¹¹	U. of Pittsburgh ^{1,10}	Boston College ¹⁶	SRI ^{17,18}
O ₂	4.6±0.5	5.2±0.4	6±2 5.3±0.5	6.1±1.8	7.0±1.8
N ₂ O	2.2±0.3	1.6±0.1	3.5±1.2	3±1	3.0±0.8
CO ₂	0.35±0.03	0.18±0.02	0.5±0.2	0.7±0.2	0.60±0.15
CO	1.7±0.4	2.1±0.2			6.0±1.5
H ₂	2.3±0.5	2.1±0.3		3.5±1	5.0±1.2
^a Units are 10 ⁻¹² cm ³ molecule ⁻¹ s ⁻¹ , T=300 K ^b Present results					

Figure 1. Apparatus for N^* (2D , 2P) studies

Figure 2. Cross section view of the absorption/fluorescence cell showing the placement of the lamps. The direction of the flow in the reactor is perpendicular to the figure.

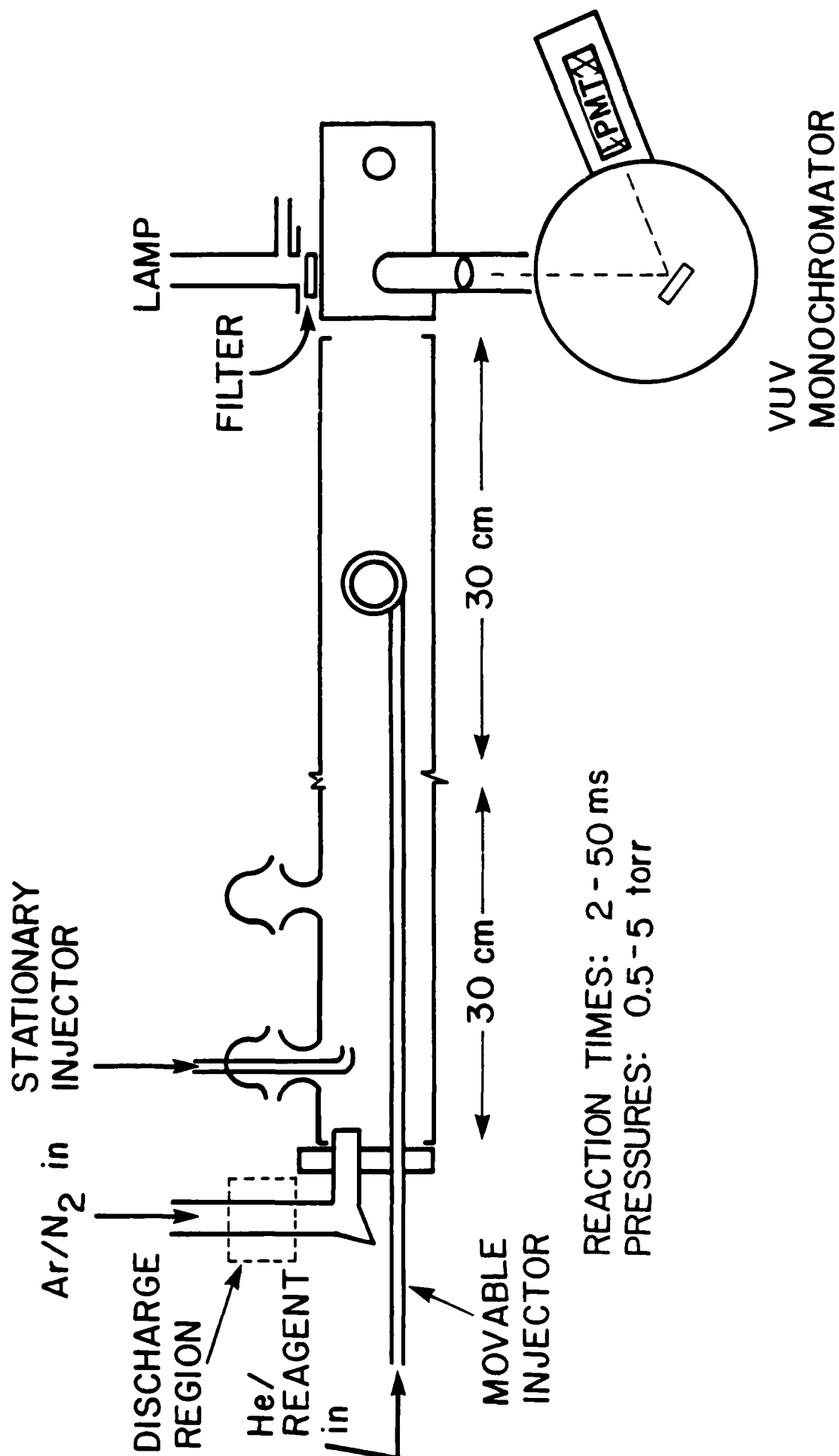
Figure 3. Resonance fluorescence spectrum from $N(^2D)$ 18 ms downstream from an Ar/ N_2 discharge, $X_{N_2} \approx 0.01$

Figure 4. Background spectrum of Ar/ N_2 discharge effluent 18 ms downstream from the discharge with the $N(^2D)$ resonance-fluorescence lamp off

Figure 5. Variation of $N(^2D)$ resonance fluorescence intensity at 174 nm as a function of relative $N(^2D)$ number density. Ar buffer: 250 μm slits.

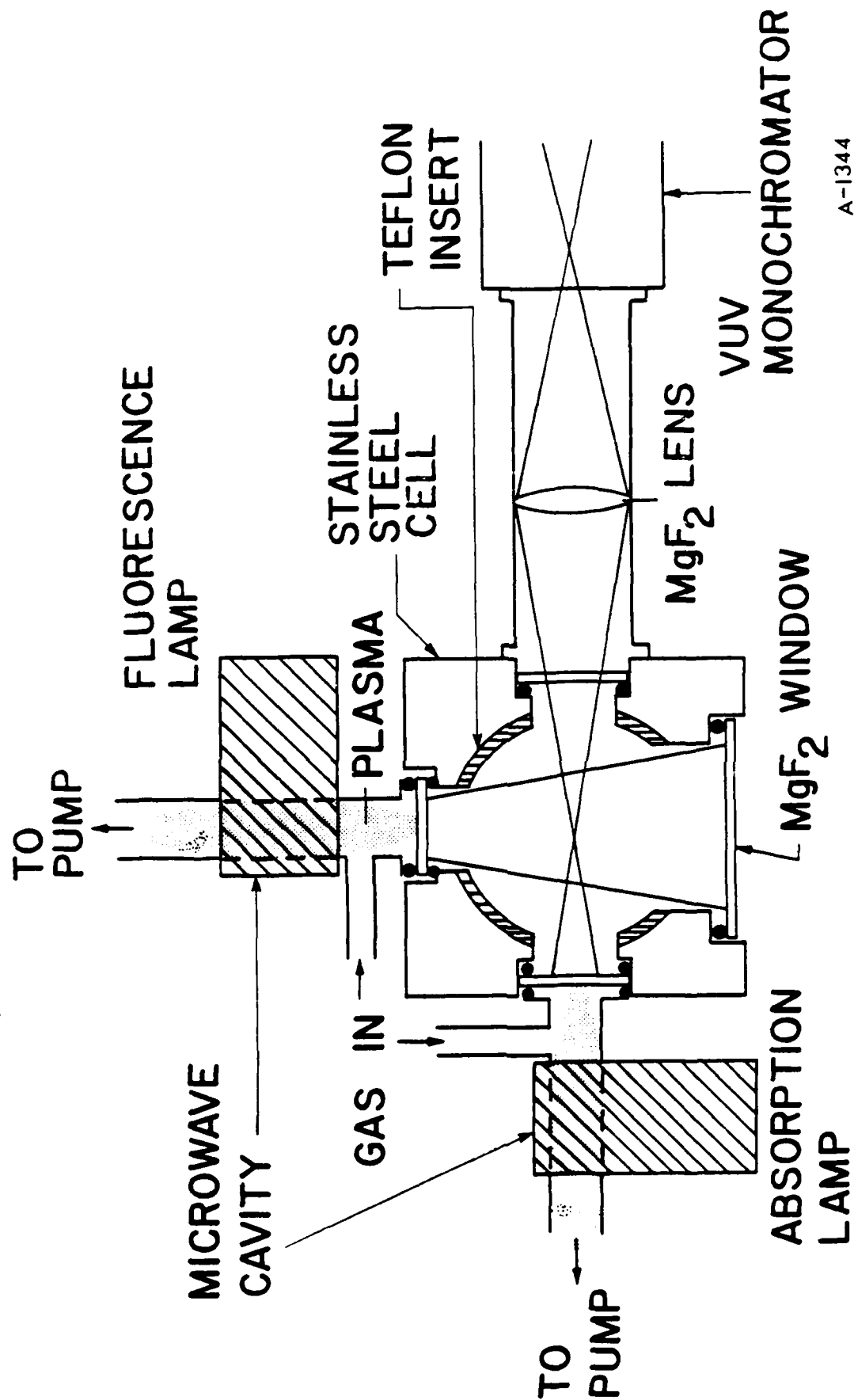
Figure 6. Decay of the log of $[N(^2D)]$ as a function of $[O_2]$ at five different reaction distances.

Figure 7. Variation in decay coefficient with reaction time for $N(^2D) + O_2$ reaction. The ordinates of the data points are determined from the slopes of the lines in Figure 6.



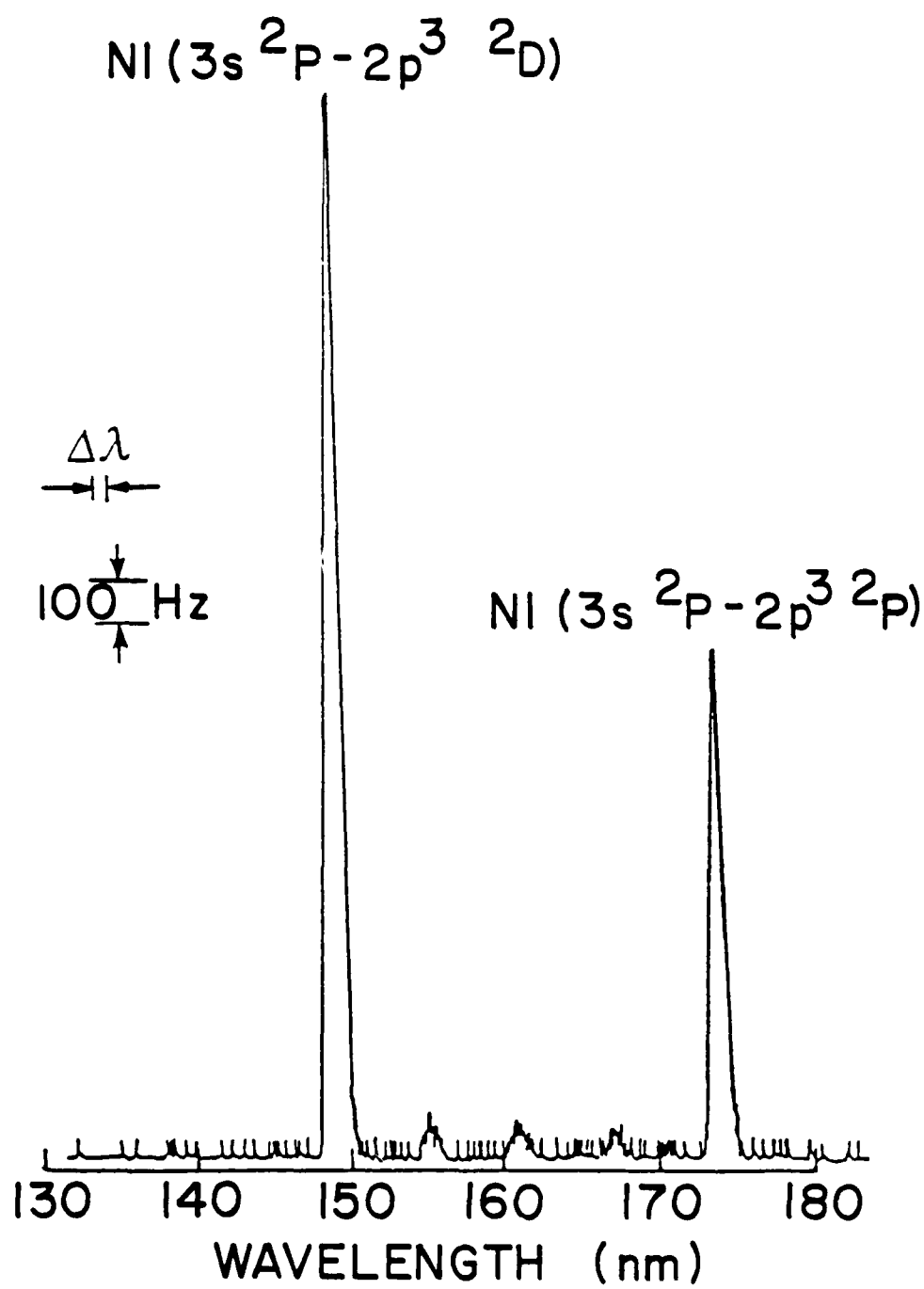
A-3168

FIGURE 1



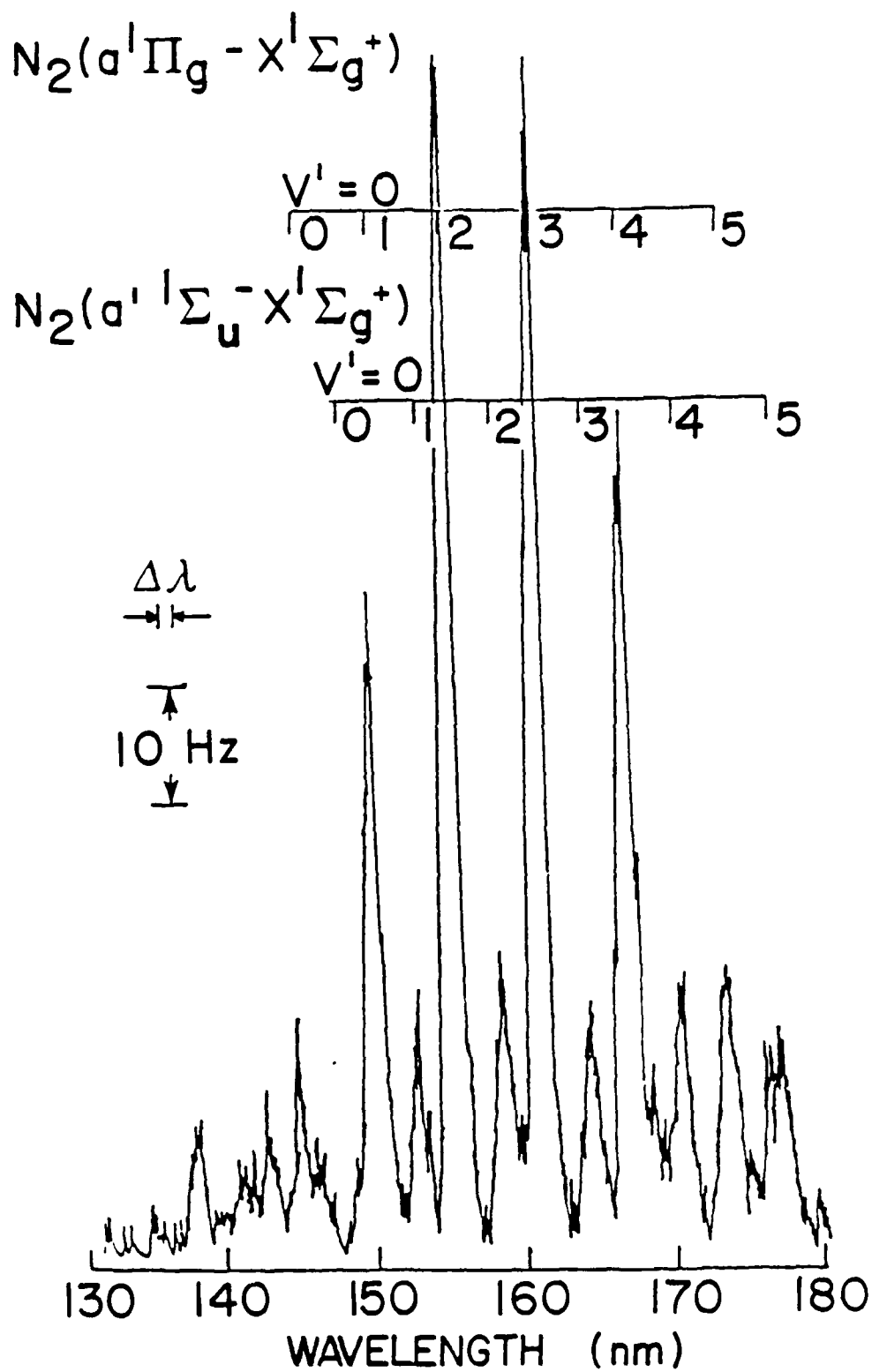
A-1344

FIGURE 2



A-3166

FIGURE 3



A-3167

FIGURE 4

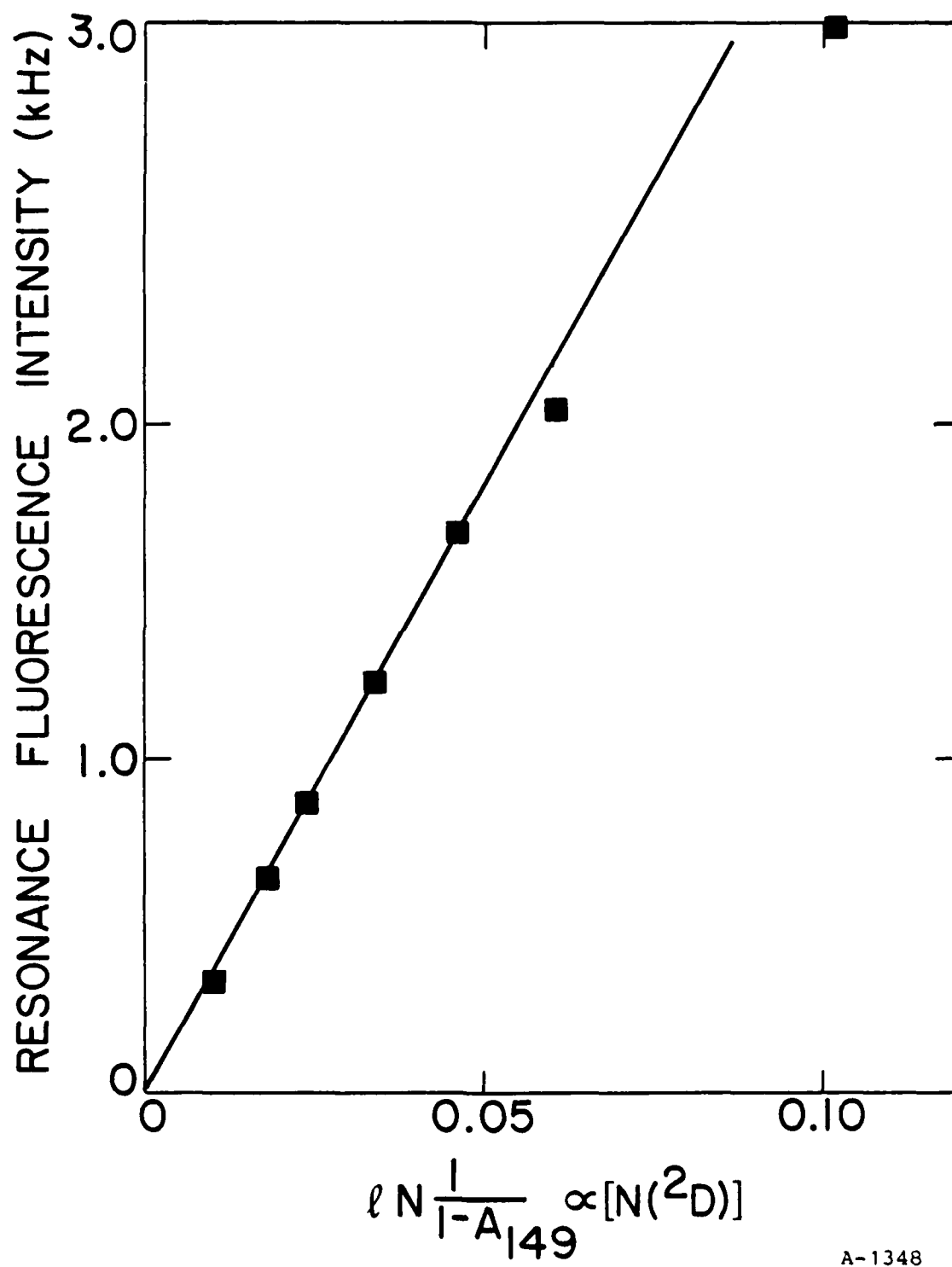
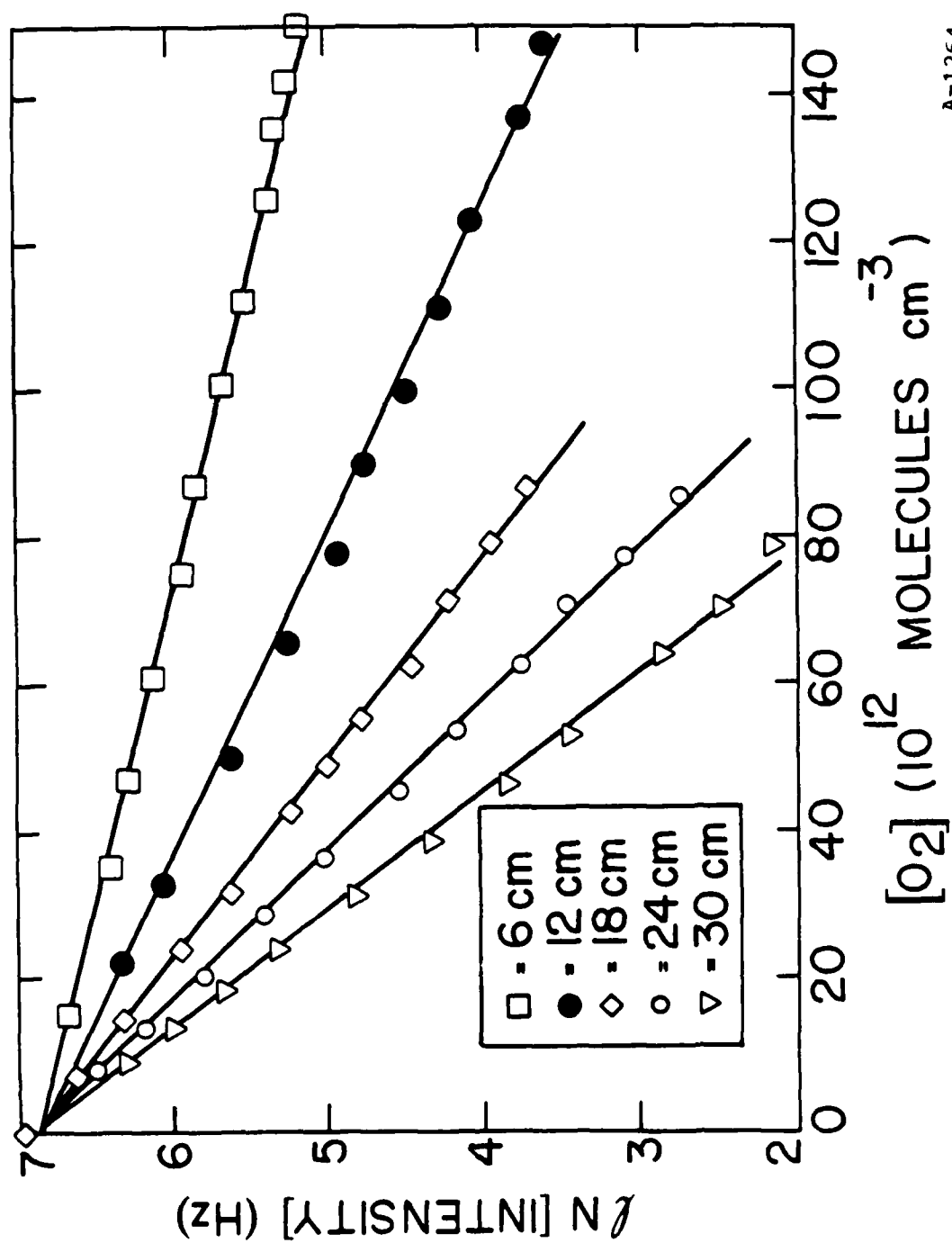
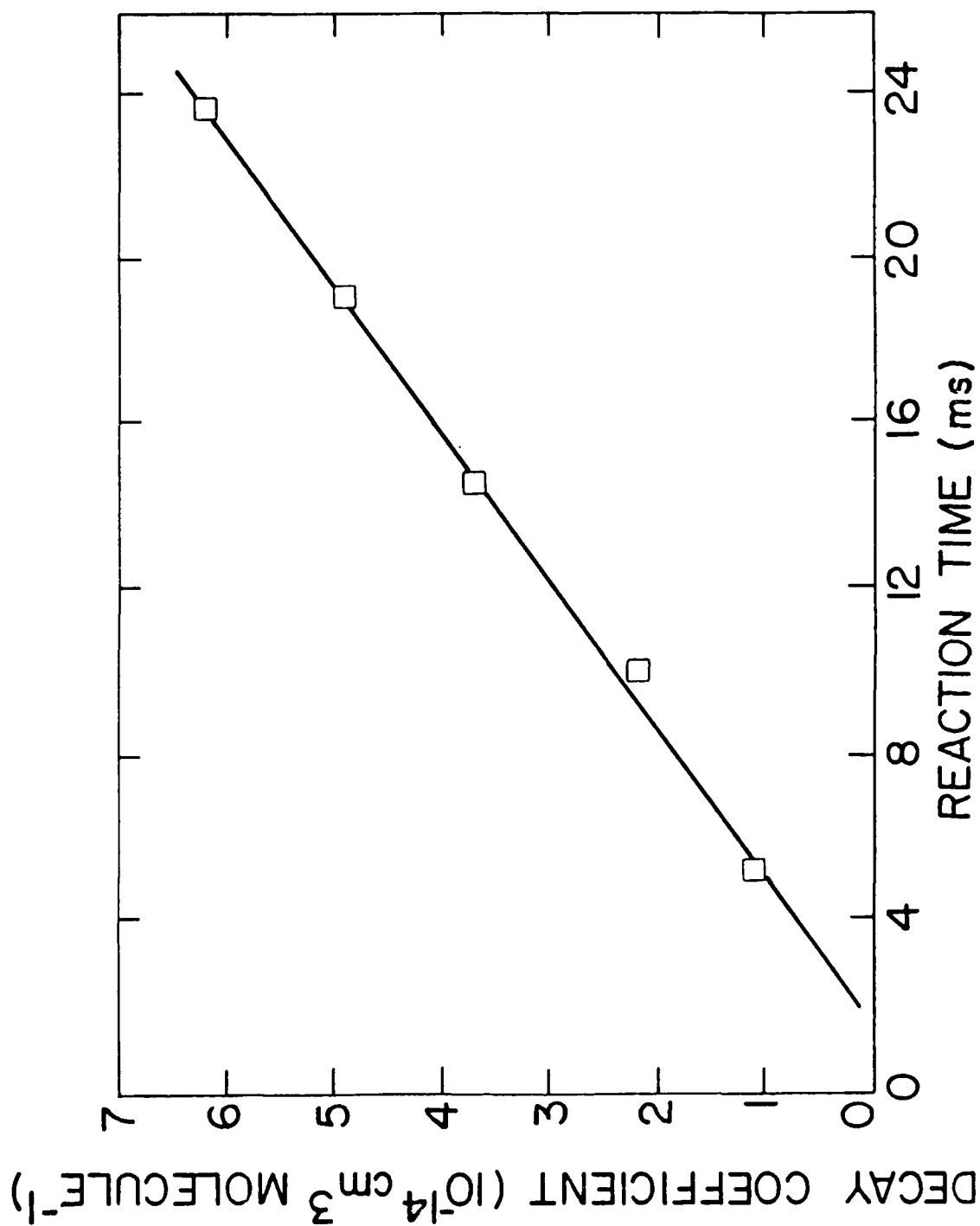


FIGURE 5



A-1264

FIGURE 6



A-1265

FIGURE 7

ACKNOWLEDGEMENTS

This work was performed under Contract F19628-85-C-0032 with the Air Force Geophysics Laboratory and sponsored by the Defense Nuclear Agency under Project SA, Task SA, Work Unit 00115 and by The Air Force Office of Scientific Research under Task 2310G4. The comments and advice of Dave Green, George Caledonia, Hart Legner, and Peter Wu, and the experimental expertise of Henry Murphy greatly benefitted our efforts.

APPENDIX C

(SR-390 reproduced in its entirety)

J. Chem. Phys. 91, XXXX (1989)

THE RATE COEFFICIENT FOR QUENCHING $N(^2D)$ BY $O(^3P)$

Lawrence G. Piper

Physical Sciences Inc.

Research Park, P.O. Box 3100

Andover, MA, 01810-7100

J. Chem. Phys. 91, XXXX (1989)

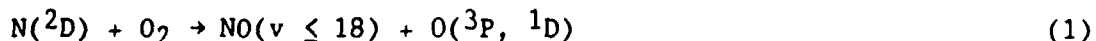
December 1988

ABSTRACT

We have studied the quenching of $N(^2D)$ by atomic oxygen in a discharge-flow reactor. Vacuum ultraviolet resonance fluorescence is used to detect the metastables. Three different discharge-based sources provide the atomic oxygen: discharged O_2/Ar , discharged N_2O/Ar , and the reaction of N with NO . Results from the three different approaches are congruent and indicate that the rate coefficient at 300 K is $(1.06 \pm 0.26) \times 10^{-12} \text{ cm}^3 \text{ molecule}^{-1} \text{ s}^{-1}$.

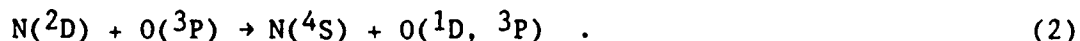
1. INTRODUCTION

The reaction of $N(^2D)$ with O_2 ,



is the major source of NO in the upper atmosphere.¹ Radiation from vibrationally excited NO is one of the primary pathways for cooling the upper atmosphere. Collisions with translationally hot O-atoms and absorption of earthine radiation are the primary mechanisms for exciting $NO(v)$ in the quiescent atmosphere, whereas reaction 1 is the primary source of $NO(v)$ under auroral conditions. Because $N(^2D)$ controls NO production rates in the upper atmosphere, understanding $N(^2D)$ chemistry is essential to understanding upper atmospheric radiative transport.

Caledonia and Kennealy have shown that one of the controlling factors of $N(^2D)$ number densities in the upper atmosphere is the quenching of $N(^2D)$ by atomic oxygen:



Efficient quenching by O will reduce $N(^2D)$ number densities and thereby those of NO. Conversely, inefficient quenching will result ultimately in increased NO production. Reaction (2) also affects the total atmospheric NO in that efficient quenching of $N(^2D)$ by O not only reduces the total NO by moderating its production via reaction (1), but also it generates² $N(^4S)$ which is a sink for atmospheric NO via reaction (3),



The magnitude of the rate coefficient for reaction (2) has been the subject of considerable controversy over a number of years, and is considered to be uncertain to within at least a factor of three. This uncertainty in the

quenching rate coefficient, therefore, lends considerable uncertainty to efforts to model NO in the upper atmosphere as well as radiative cooling of the atmosphere.

In 1976 Davenport et al.³ used vacuum ultraviolet (VUV) resonance absorption to monitor $N(^2D)$ number densities in a discharge-flow reactor to determine a ratio $k_1/k_2 = 3.0 \pm 0.5$. Assuming a value for k_1 of $5.5 \times 10^{-12} \text{ cm}^3 \text{ molecule}^{-1} \text{ s}^{-1}$, they reported $k_2 = (1.8 \pm 0.6) \times 10^{-12} \text{ cm}^3 \text{ molecule}^{-1} \text{ s}^{-1}$. Several years later, Iannuzzi and Kaufman⁴ monitored $N(^2D)$ in the presence of atomic oxygen with a VUV resonance-fluorescence diagnostic and reported an upper limit to reaction (2) which agreed with the value given by Davenport et al.

Modeling studies, on the other hand, generally have favored values for k_2 which are factors of two or more lower than those proposed by Davenport et al. and by Iannuzzi and Kaufman. Frederick and Rusch⁵, for example, modeled $N(^2D)$ profiles from airglow measurements taken by Atmospheric Explorer C and D and concluded that k_2 must be $4 \times 10^{-13} \text{ cm}^3 \text{ molecule}^{-1} \text{ s}^{-1}$. A similar modeling effort by Richards et al.² concluded that Frederick and Rusch underestimated $N(^2D)$ production rates and revised their value upwards slightly to $6 \times 10^{-13} \text{ cm}^3 \text{ molecule}^{-1} \text{ s}^{-1}$. Cravens et al.⁶ and Strobel et al.⁷ modeled NO profiles in the upper atmosphere and concluded that $k_2 = 1 \times 10^{-12} \text{ cm}^3 \text{ molecule}^{-1} \text{ s}^{-1}$, whereas similar modeling efforts by Oran et al.⁸ concluded $k_2 < 10^{-14} \text{ cm}^3 \text{ molecule}^{-1} \text{ s}^{-1}$.

Recently Jusinski et al.⁹ reported a laboratory measurement of $(2.1 \pm 0.8) \times 10^{-11} \text{ cm}^3 \text{ molecule}^{-1} \text{ s}^{-1}$ for this reaction at room temperature. This value is an order of magnitude greater than previous laboratory measurements, and even more discordant with the estimates derived from atmospheric modeling.

The discrepancies between the various laboratory and aeronomic results are such that additional laboratory investigations of this reaction were

imperative. We have studied this reaction in a discharge-flow reactor using a sensitive resonance-fluorescence diagnostic for the $N(^2D)$ atoms. We used three different sources for the atomic oxygen to try to reduce systematic errors. In each of these sources the atomic oxygen is prepared separately from the $N(^2D)$ and then mixed only subsequently. The three different sets of experiments give consistent results and indicate that the two old laboratory measurements of the rate coefficient are about a factor of two too large.

2. EXPERIMENTAL

A. Apparatus

The experiments were carried out in the discharge-flow reactor shown schematically in Fig. 1. The $N(^2D)$ was generated at the upstream end of the reactor in a 70 W microwave discharge of 1 to 2 percent nitrogen in argon. Further downstream, a flow of atomic oxygen enters the reactor through a hook-shaped injector. At the extreme down-stream end of the reactor, $N(^2D)$ number densities are monitored by vacuum-ultraviolet resonance fluorescence. We have detailed our general procedures for monitoring $N(^2D)$ and measuring its kinetics previously.¹⁰

The three different sources of atomic oxygen are all microwave-discharge based, the discharge being upstream in the hook-shaped injector. One source consists of discharging mixtures of argon and molecular oxygen. In some cases small amounts of SF_6 were added to the discharge to enhance the oxygen dissociation. Adding SF_6 to the discharge in the absence of oxygen had no effect on the $N(^2D)$ number densities. The principal effluents of this discharge will be O , $O_2(X^3\Sigma_g^-)$, and $O_2(a^1\Delta_g)$. We describe tests for the effects of $O_2(a)$ below.

The second source of atomic oxygen was a microwave discharge through a mixture of argon and nitrous oxide, or in some instances argon, nitrogen, and nitrous oxide. We have shown previously¹¹ that, at low mole fractions of

nitrous oxide, this discharge produces oxygen and nitrogen atoms, with the oxygen generally being at least an order of magnitude or more abundant than the nitrogen. The small N-atom flows do not affect our kinetic measurements because atomic nitrogen is not a significant quencher of $N(^2D)$. At higher mole fractions of nitrous oxide, nitric oxide accompanies the atomic oxygen out of the discharge. Since NO reacts readily with $N(^2D)$,^{12,13} such conditions are to be avoided. Adding molecular nitrogen to the discharge defers the production of nitric oxide to larger nitrous oxide mole fractions. Undissociated N_2O , and perhaps O_2 or $O_2(a)$, which might be produced by recombination in the active discharge are also effluents of this discharge source.

Our third source of atomic oxygen was to titrate N atoms with NO in the injector, upstream from its opening into the main flow tube. In this case we discharged mixtures of N_2 and SF_6 in Ar. The SF_6 greatly enhanced N_2 dissociation.¹⁴ For some experiments we placed a glass wool-plug downstream from the discharge but upstream from the NO injector to ensure removal of excited states of atomic and molecular nitrogen produced in the discharge.¹⁵ The presence of the glass-wool plug had no effect on results.

Turning on the secondary discharge, to make the atomic nitrogen, increased the resonance fluorescence signals between 5 and 30 percent, depending upon conditions. This additional contribution to the resonance fluorescence signal varied with the amount of NO added to the injector flow, and had to be subtracted, therefore, from the signal due to metastables produced in the primary discharge.

Atomic oxygen number densities were monitored by measuring the O/NO air-afterglow when nitric oxide was added to the flow reactor with the $N(^2D)$ discharge off. A photometer consisting of an interference filter centered at 580 nm with a full width at half maximum of 10 nm and an HTV R-955 photomultiplier detected the air-afterglow fluorescence. O-atom number densities were determined for each flow rate of O_2 or N_2O , and the photometer calibration was checked after each run under the identical flow and pressure conditions of the run. Previous reports detail our procedures for measuring

O-atom number densities from air-afterglow observations as well as our photometer-calibration procedures.^{11,16}

Typical conditions in the reactor include main argon and nitrogen flow rates of 1500 to 4000 $\mu\text{mol s}^{-1}$ and 25 to 75 $\mu\text{mol s}^{-1}$ respectively, argon and nitrogen flows through the injector discharge of 200 to 700 $\mu\text{mol s}^{-1}$ and 15 to 100 $\mu\text{mol s}^{-1}$, respectively, reagent O_2 , N_2O or NO flows of 0 to 8, 0 to 20 and 0 to 6 $\mu\text{mol s}^{-1}$, respectively, SF_6 flow rates less than or equal to 0.05 $\mu\text{mol s}^{-1}$, and total pressures between 0.8 and 3 torr.

B. Experimental Technique

In addition to reactions (1) and (2), important processes for removing $\text{N}(^2\text{D})$ in our reactor are



and



For the case of using O_2 as a source of atomic oxygen, the differential equation describing the rate of change in the $\text{N}(^2\text{D})$ number density with time is

$$\frac{d[\text{N}(^2\text{D})]}{dt} = -\left\{k_5 + k_1[\text{O}_2]\right\} [\text{N}(^2\text{D})] \quad (6)$$

For the case where the injector discharge is off, and

$$\frac{d[\text{N}(^2\text{D})]}{dt} = -\left\{k_5 + k_2[\text{O}] + k_1[\text{O}_2]\right\} [\text{N}(^2\text{D})] \quad (7)$$

when the injector discharge is on. Because the number density of $N(^2D)$ is much smaller than that of either O or O_2 , these two differential equations are effectively first-order and can be solved analytically. The resulting solutions become

$$\ln \left\{ \frac{[N(^2D)](t)}{[N(^2D)](t=0)} \right\} = - \left\{ k_5 + k_1 [O_2] \right\} t , \quad (8)$$

with the discharge off, and

$$\ln \left\{ \frac{[N(^2D)](t)}{[N(^2D)](t=0)} \right\} = - \left\{ k_5 + k_1 [O] + k_1 [O_2] \right\} t , \quad (9)$$

with the discharge on. The decay coefficient, Γ , is the variation in the $N(^2D)$ number density as a function of molecular oxygen number density at a fixed time. This quantity is proportional to the quenching rate coefficient.

With the discharge off, we have

$$\Gamma_{\text{off}} = - \frac{d \ln I_{\text{off}}}{d[O_2]} = k_1 t \quad (10)$$

where we have exploited the fact that the $N(^2D)$ number density is directly proportional to the resonance-fluorescence intensity, I .¹⁰

When the discharge is on, some of the molecular oxygen is dissociated to make atomic oxygen. The relationship between the number densities of the two species is

$$[O] = 2 \alpha [O_2]_0 \quad (11)$$

and

$$[O_2] = (1-\alpha) [O_2]_0 \quad , \quad (12)$$

where the subscript 0 indicates the number density which would have obtained in the absence of dissociation, i.e. the number density with the discharge off, and α is the fractional dissociation. In terms of experimentally measured quantities

$$\alpha = \frac{[O]}{2[O_2]_0} \quad . \quad (13)$$

When the molecular-oxygen mole fraction in the discharge region is on the order of a per cent or less, α is invariant to changes in oxygen flow rate. This allows the decay coefficient with the discharge on to be expressed as

$$\Gamma_{on} = - \frac{d \ln I_{on}}{d[O_2]_0} = \left\{ 2 \alpha k_2 + (1-\alpha)k_1 \right\} t \quad . \quad (14)$$

The basic experimental approach is to determine decay coefficients with the discharge on and with it off. Any differences between the two measurements result from differences between the rate coefficients for reactions 1 and 2. Ratioing equations 14 and 10 gives

$$\frac{\Gamma_{on}}{\Gamma_{off}} = 2 \alpha \frac{k_2}{k_1} + 1 - \alpha \quad . \quad (15)$$

Equation 15 can be solved to give the ratio of the rate coefficients k_2 to k_1 in terms of the experimentally measured quantities α and the ratio of the decay coefficient with the discharge on to that with it off. Since we have previously established¹⁰ that the rate coefficient for reaction (1) is $(4.6 \pm 0.5) \times 10^{-12} \text{ cm}^3 \text{ molecule}^{-1} \text{ s}^{-1}$, k_2 can be determined unambiguously.

This approach to determining k_2 has the added advantage that by determining it from the ratio of two rate coefficients, one of which is already well established, uncertainties introduced by poor mixing or incompletely developed laminar flow conditions are eliminated. This is an important point because hook-shaped injectors generally do not give the good mixing that results from using loop injectors. Furthermore mixing corrections cannot be explored easily using a fixed injector. We have shown previously that such corrections can at times be considerable in studies of metastable kinetics.¹⁰

A similar approach results from using discharged N_2O as the atomic-oxygen source. In this case the relevant data-analysis equation is

$$\frac{\Gamma_{on}}{\Gamma_{off}} = \alpha \frac{k_2}{k_4} + 1 - \alpha, \quad (16)$$

where we have assumed that undissociated nitrous oxide is the primary effluent, in addition to atomic oxygen, exiting the discharge. If instead of N_2O , the other effluent from the discharge is molecular oxygen, the analysis equation becomes

$$\frac{\Gamma_{on}}{\Gamma_{off}} = \frac{1}{k_4} \left\{ \alpha k_2 + \frac{1-\alpha}{2} k_1 \right\}. \quad (17)$$

Given that the ratio of the rate coefficients $k_1/k_4 = 2.1 \pm 0.3$, Eq. (17) will give similar results to those derived using Eq. (16). Here again we determine k_2 from the ratio of two rate coefficients. We have shown previously¹⁰ that $k_4 = (2.2 \pm 0.3) \times 10^{-12} \text{ cm}^3 \text{ molecule}^{-1} \text{ s}^{-1}$.

Generating O atoms from the reaction between N and NO results in a much simpler analysis. The basic measurement is of the decay coefficient, determined similarly to Eq. (10), but as a function of added nitric oxide number density (that is the number density of nitric oxide which would obtain in the absence of reaction (3)). This analysis relies on the fact that reaction (3) is stoichiometric.¹⁷ In addition, we assume that none of the atomic oxygen

recombines on the injector walls prior to injection into the flow reactor. Given that the injector was teflon coated, this is a reasonable assumption. In order to avoid the uncertainties of mixing and flow development, we divided the decay coefficients we obtained by decay coefficients for molecular oxygen removal of $N(^2D)$ measured under identical conditions. This result again gives the ratio of rate coefficients k_2/k_1 .

3. RESULTS

Figures 2 and 3 show examples of data taken using O_2 and N_2O , respectively, as atomic-oxygen sources. These figures show clearly that the effect of turning on the discharge is to reduce the effective decay coefficient. This can only be so if some discharge-produced species has a smaller rate coefficient than does either O_2 or N_2O . Since the major discharge-produced species in both cases is atomic oxygen, it follows that k_2 will be less than either k_1 or k_4 .

Another significant discharge effluent from both sources, but especially from the molecular oxygen source, is electronically excited $O_2(a^1\Delta_g)$. In several experiments we tried to enhance the production of $O_2(a)$ by placing a nickel screen downstream from the discharge in the injector. The screen recombines some of the atoms into molecular electronic states which readily quench to $O_2(a^1\Delta)$ in the presence of O_2 .¹⁸ The rate coefficients obtained for O-atom quenching agreed within experimental error to those obtained without the presence of the screen but under otherwise similar conditions. This suggests that $O_2(^1\Delta)$ quenching of $N(^2D)$ is similar to $O_2(X)$ quenching.

Figure 4 shows the results of two different experiments using the reaction between N and NO as the O-atom source. In both cases the decay is relatively slow, but as the lower curve shows conclusively, the decay rate increases dramatically past the N-atom titration end point when NO is allowed to enter the flow reactor. Clearly the NO reacts much more rapidly with the $N(^2D)$ than does the atomic oxygen. The much greater number densities of

ground-state nitrogen atoms than $N(^2D)$ in the flow reactor do not remove the NO by reaction (3) fast enough to protect $N(^2D)$ from NO quenching. One must be careful, therefore, to prepare the atomic oxygen reagent in the injector, removed from the $N(^2D)$ reactant.

Table 1 summarizes our results for the various experimental runs. The error bars represent 1σ standard deviations. The error bars on the weighted averages include the uncertainties in the reference rate coefficients, and the weighted average of the three sets of data include an additional 10 percent uncertainty to account for possible determinate errors. At the 95 percent confidence level, 2σ , our experiments indicate that k_2 is $(1.06 \pm 0.26) \times 10^{-12}$ $\text{cm}^3 \text{ molecule}^{-1} \text{ s}^{-1}$.

4. DISCUSSION

Our results are somewhat lower than the two earlier experimental studies^{3,4} but do agree with them within the limits of experimental error. Agreement with the aeronomically derived values of Cravens et al.⁶ and of Strobel et al.⁷ is very good, and agreement with Richards et al.'s² model-derived value is acceptable.

The major disagreement with the recent results of Jusinski et al.⁹ indicates the likelihood of a large systematic error in those experiments. The basis of their experiment was to add NO directly to the flowing stream of active nitrogen, and to rely on the much greater number density of ground-state nitrogen atoms than of metastable-nitrogen atoms to convert the NO to atomic oxygen before the NO had a chance to diminish the $N(^2D)$ number density significantly. In principle, this approach should work provided that the difference in number densities between $N(^4S)$ and $N(^2D)$ is sufficiently great and provided that mixing is instantaneous and uniform. In practice, the approach does not work. Figure 4, as well as the results of similar experiments by Ianuzzi and Kaufman,⁴ shows that adding NO to a stream of active nitrogen greatly enhances the rate of removal of $N(^2D)$ over that due to atomic oxygen.

Very recently, Miller et al.¹⁹ have investigated the quenching of $N(^2D)$ in a flow of active nitrogen upon adding NO. In some of their experiments they tried to reproduce the operating conditions of Jusiniski et al. using resonance-enhanced multiphoton ionization to detect both $N(^2D)$ and NO, Miller et al. found that NO persisted in the afterglow for times much greater than they would expect based upon the rate of consumption of NO by $N(^4S)$ that they calculated to be appropriate to their experimental conditions. They attributed this discrepancy to be due to slow mixing of the NO into the main flow. They noted that the $N(^2D)$ number-density decay was effectively first order in added NO, but that the effective rate coefficient for $N(^2D)$ quenching was significantly faster under conditions where significant NO remained at the detection region compared to conditions under which the NO was completely consumed. Their analysis of mixing effects allowed them to uncouple the effects of NO quenching of $N(^2D)$ from those of O quenching. Their data imply a rate coefficient for reaction 2 of $(1.0 \pm 0.3) \times 10^{-12} \text{ cm}^3 \text{ molecule}^{-1} \text{ s}^{-1}$, in excellent agreement with our results.

The doublet potential curves which asymptotically correlate to an $N(^2D)$ and an $O(^3P)$ atom have myriad crossings with lower potential curves whose asymptotic limits correlate to $N(^4S)$ and either $O(^3P)$ or $O(^1D)$ atoms. On the basis of spin conservation, one would expect that the favored product would be $O(^3P)$ atoms. Oran et al.,⁸ on the other hand, speculated that the one-electron spin-orbit matrix elements will couple the incoming doublet states with the quartet states correlating to the production of an $O(^1D)$ atom as facilely as to the doublet states correlating to $O(^3P)$ atoms as a product. Davenport et al.,³ however, report that unpublished calculations by Olson and Smith show the channel leading to $O(^3P)$ production will be favored.

Sivjee et al.²⁰ report anomalies, noted in auroras over J. Algard, in the ratio of emission of the two components of the $N(^2D_{5/2,3/2} - ^4S_{3/2})$ doublet at 520 nm. They suggest that these differences might result from the need of reaction (2) to conserve total angular momentum. The $J=5/2$ sublevel, therefore, could react only with the $J=1,0$ sublevels of atomic oxygen, producing

the $J=2,1$ sublevels. The $J=3/2$ sublevel of $N(^2D)$, on the other hand, can react with all three sublevels of $O(^3P)$. Thus, under certain conditions, they would expect to see a depletion in the emission from $N(^2D_{3/2})$. The relatively high pressure in our reactor ensures that the two sublevels of $N(^2D)$ will be in equilibrium. Our measurements, therefore, will be an average of the reactivities of the two sublevels, and cannot be used to test Sivjee et al.'s hypothesis.

One cannot use the criterion of conserving total angular momentum as an argument against the production of $O(^1D)$ in reaction (2). Both sublevels of $N(^2D)$ can interact with one of the sublevels of $O(^3P)$ to produce $O(^1D_2)$. All that can be argued on this basis, therefore, is that with fewer channels available, $O(^1D)$ production would be expected to be less efficient than that of $O(^3P)$.

In the event that $O(^3P)$ is the favored product, reaction (2) will proceed with the release of 2.38 eV of translational energy. This reaction, therefore, could be a source of translationally hot O and N atoms in the upper atmosphere. The reactions of these hot atoms could be somewhat different from those of thermal atoms. For example, the production of NO from the reaction of $N(^4S)$ with O_2 could be much more efficient if the nitrogen atoms are translationally hot.

5. SUMMARY AND CONCLUSIONS

We have shown that the rate coefficient for quenching $N(^2D)$ by atomic oxygen is $(1.06 \pm 0.26) \times 10^{-12} \text{ cm}^3 \text{ molecule}^{-1} \text{ s}^{-1}$ at 300 K. This value is consistent with many of the aeronomically derived quenching rate coefficients. In particular, very recent modeling results of Geraru et al.²¹ favor a value of $1 \times 10^{-12} \text{ cm}^3 \text{ molecule}^{-1} \text{ s}^{-1}$ for k_2 . The atmospheric chemistry of $N(^2D)$ as well as of NO appears to be reasonably well understood.

The slightly smaller value for k_2 favored in some modeling studies might indicate a temperature dependence for k_2 . This is an issue we intend to investigate in the future.

Agreement with earlier laboratory studies is within experimental error. The discrepancies with the most recent laboratory study, however, indicates a large systematic uncertainty in that experiment.

ACKNOWLEDGMENTS

We appreciate the financial support of the Air Force Office of Scientific Research (Task 2310G4) and the Defense Nuclear Agency (project SA, Task SA/SDI, work unit 00175) through Air Force Geophysics Laboratory contract F19628-85-C-0032. Discussions with PSI colleagues Terry Rawlins and Dave Green, and Chris Fenn, Steve Miller and Bill Blumberg of the Air Force Geophysics Laboratory were most fruitful. Tom Tucker and Bill Cummings aided the experimental and analytical efforts.

REFERENCES

1. Caledonia, G.E. and Kennealy, J.P., "NO Infrared Radiation in the Upper Atmosphere," *Planet. Space Sci.* 30, 1043 (1982).
2. Richards, P.G., Torr, D.G., and Torr, M.R., "Photodissociation of N_2 : A Significant Source of Thermospheric Atomic Nitrogen," *J. Geophys. Res.* 86, 1495 (1981).
3. Davenport, J.E., Slinger, T.G., and Black, G., "The Quenching of $N(^2D)$ by $O(^3P)$," *J. Geophys. Res.* 81, 12 (1976).
4. Ianuzzi, M.P. and Kaufman, F., "Rates of Some Reactions of $N(^2D)$ and 2P Near 300 K," *J. Chem. Phys.* 73, 4701 (1980).
5. Frederick, J.E. and Rusch, D.W., "On the Chemistry of Metastable Atomic Nitrogen in the F Region Deduced From Simultaneous Satellite Measurements of the 5200-Å Airglow and Atmospheric Composition," *J. Geophys. Res.* 82, 3509 (1977).
6. Cravens, T.E., Gerard, J.C., Stewart, A.I. and Rusch, D.W., "The Latitudinal Gradient of Nitric Oxide in the Thermosphere," *J. Geophys. Res.* 84, 2675 (1979).
7. Strobel, D.F., Young, T.R., Meier, R.R., Coffey, T.P., and Ali, A.W., "The Nighttime Ionosphere: E Region and Lower F Region," *J. Geophys. Res.* 79, 3171 (1974).
8. Oran, E.S., Julianne, P.S., and Strobel, D.F., "The Aeronomy of Odd Nitrogen in the Thermosphere," *J. Geophys. Res.* 80, 3068 (1975).
9. Jusiniski, L.E., Black, G., and Slinger, T.G., "Resonance-Enhanced Multiphoton Ionization Measurements of $N(^2D)$ Quenching by $O(^3P)$," *J. Phys. Chem.* 92, 5977 (1988).
10. Piper, L.G., Donahue, M.E., and Rawlins, W.T., "Rate Coefficients for $N(^2D)$ Reactions," *J. Phys. Chem.* 91, 3883 (1987).
11. Piper, L.G. and Rawlins, W.T., "O-Atom Yields From Microwave Discharges in N_2O/Ar Mixtures," *J. Phys. Chem.* 90, 320 (1986).
12. Husain, D., Mitra, S.K., and Young, A.N., "Kinetic Study of Electronically Excited Nitrogen Atoms, $N(^2D_J, ^2P_J)$ by Attenuation of Atomic Resonance Radiation in the Vacuum Ultraviolet," *JCS Faraday 2* 70, 1721 (1974).
13. Black, G., Slinger, T.G., St. John, G.A., and Young, R.A., "Vacuum-Ultraviolet Photolysis of N_2O . IV. Deactivation of $N(^2D)$," *J. Chem. Phys.* 51, 116 (1969).

REFERENCES (CONTINUED)

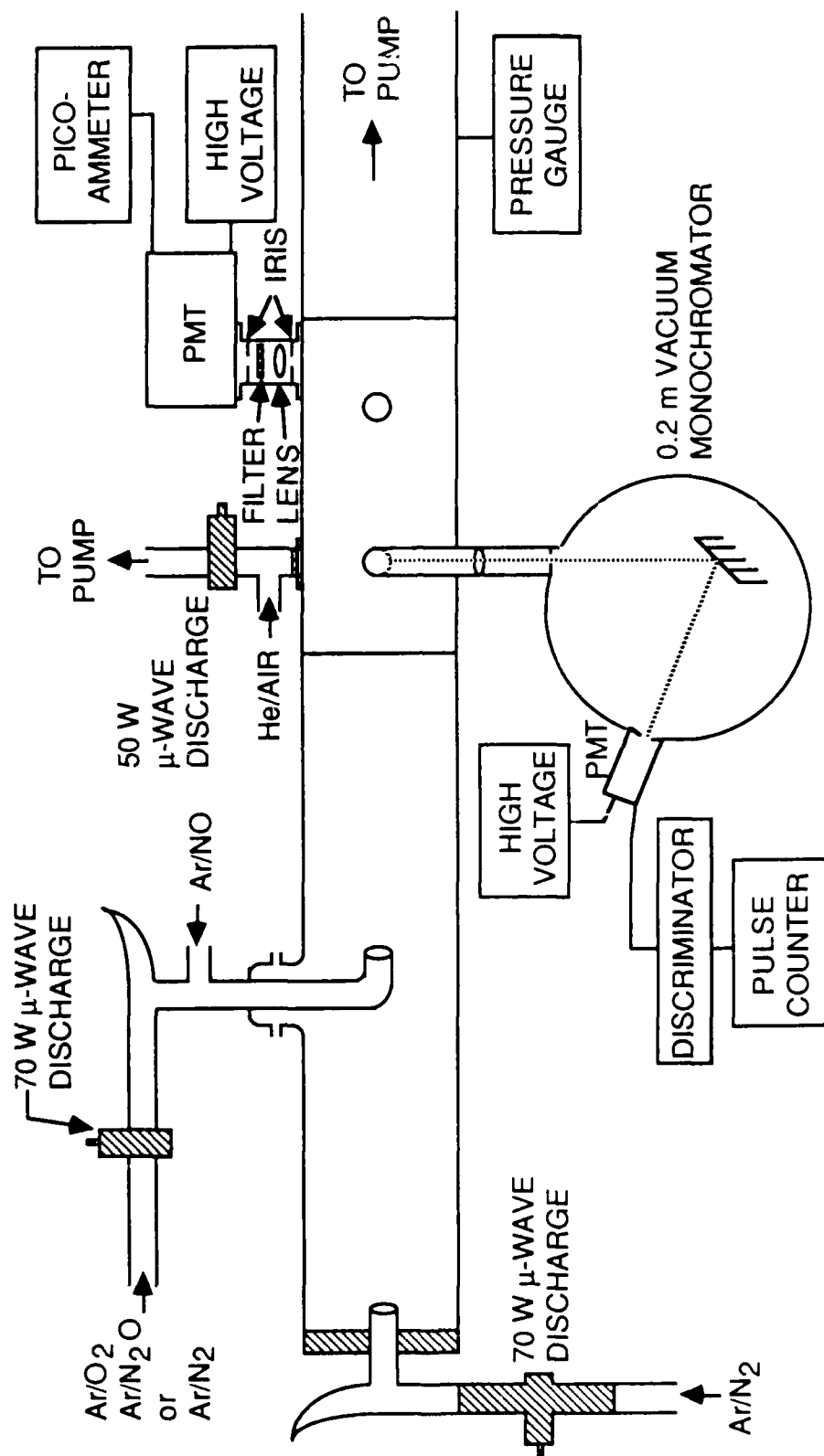
14. Young, R.A., Sharpless, R.L., and Stringham, R., "Catalyzed Dissociation of N_2 in Microwave Discharges. I," J. Chem. Phys. 40, 117 (1964).
15. Morgan, J.E. and Schiff, H.I., "The Study of Vibrationally Excited N_2 Molecules with the Aid of an Isothermal Calorimeter," Can. J. Chem. 41, 903 (1963).
16. Piper, L.G., Caledonia, G.E., and Kennealy, J.P., "Rate Constants for Deactivation of $N_2(A^3\Sigma_u^+, v'=0,1)$ by O", J. Chem. Phys. 75, 2847 (1981).
17. Brocklehurst, B. and Jennings, K.R., "Reactions of Nitrogen Atoms in the Gas Phase," Prog. React. Kinet. 4, 1 (1967).
18. a. Kenner, R.D. and Ogryzlo, E.A., "Quenching of $O_2(c^1\Sigma_u^-)$ $v=0$ by $O(^3P)$, $O_2(a^1\Delta)$, and Other Gases," Can. J. Chem. 61, 921 (1983).
 b. Ali, A.A., Ogryzlo, E.A., Shen, Y.Q., and Wassell, P.T., "The Formation of $O_2(a^1\Delta_g)$ in Homogeneous and Heterogeneous Atom Recombination," Can. J. Phys. 64, 1614 (1986).
19. Miller, S.M., Fell, C.P. and Steinfeld, J.I., EOS 69, 1347 (1988).
20. Sivjee, G.G., Deehr, C.S., and Henriksen, K., "Difference in Quenching of $N(^2D_{3/2}^0)$ and $N(^2D_{5/2}^0)$ by Atomic Oxygen," J. Geophys. Res. 86, 1581 (1981).
21. Gerard, J.C., Fesen, C.G., and Rusch, D.W., EOS 69, 1346 (1988).

TABLE 1. RESULTS OF N(²D) + O STUDIES

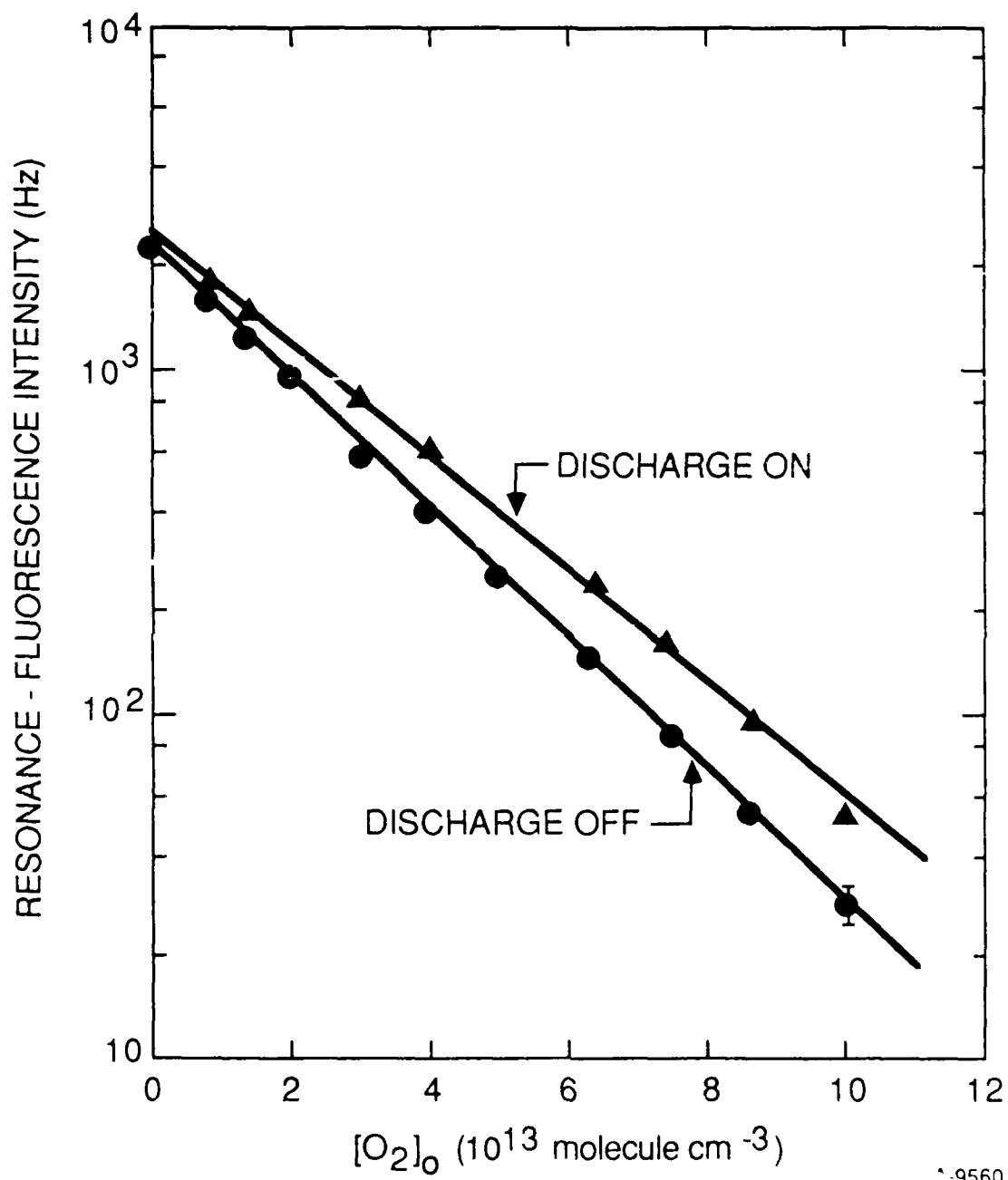
O-Atom Source	Run number	α	$k_2(10^{-12} \text{ cm}^3 \text{ molecule}^{-1} \text{ s}^{-1})$	Weighted Average ^a $k_2(10^{-12} \text{ cm}^3 \text{ molecule}^{-1} \text{ s}^{-1})$
O ₂	1	0.16	1.56 ± 0.78	1.21 ± 0.18
	2	0.30	1.61 ± 0.69	
	3	0.61	1.06 ± 0.32	
	4	0.57	0.92 ± 0.32	
	5	0.34	0.55 ± 0.46	
	6	0.37	1.43 ± 0.18	
	7	0.15	0.92 ± 0.67	
N ₂ O	1	0.34	0.88 ± 0.13	0.90 ± 0.13
	2	0.27	0.68 ± 0.12	
	3	0.26	0.77 ± 0.17	
	4	0.46	1.19 ± 0.25	
	5	0.40	1.32 ± 0.11	
	6	0.41	0.70 ± 0.11	
N + NO	1		1.10 ± 0.064	1.15 ± 0.13
	2		1.19 ± 0.064	
	3		1.17 ± 0.074	
				<hr/> 1.06 ± 0.13 ^b
a. Includes uncertainties in reference rate coefficients b. Includes estimated 10 percent uncertainty for systematic errors				

FIGURE CAPTIONS

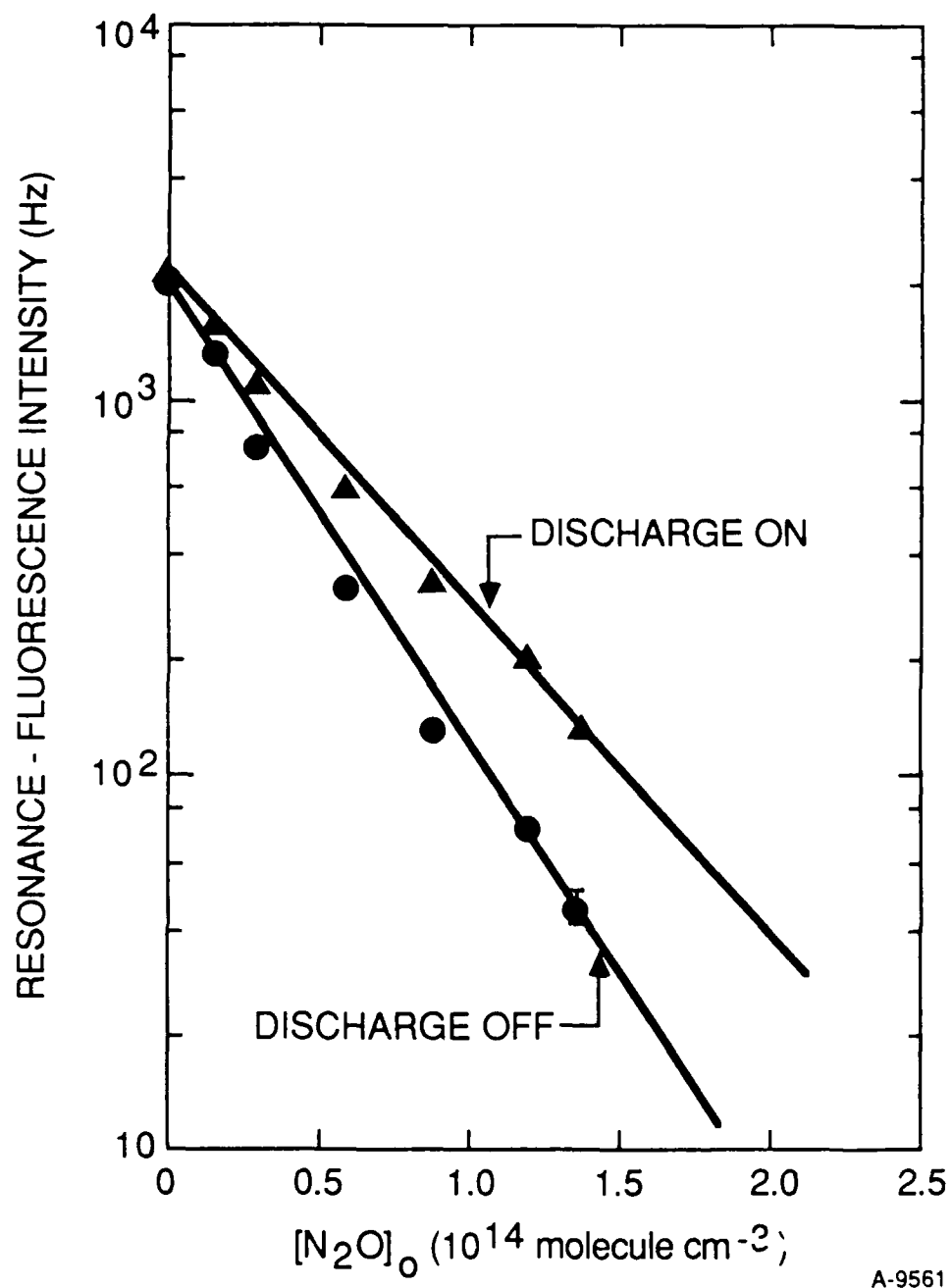
1. Apparatus for studying the kinetics of $N(^2D)$ with $O(^3P)$.
2. Decay of $N(^2D)$ resonance-fluorescence intensity as a function of number density of discharged and un-discharged O_2 .
3. Decay of $N(^2D)$ resonance-fluorescence intensity as a function of number density of discharged and un-discharged N_2O .
4. Decay of $N(^2D)$ resonance-fluorescence intensity as a function of atomic-oxygen number density.



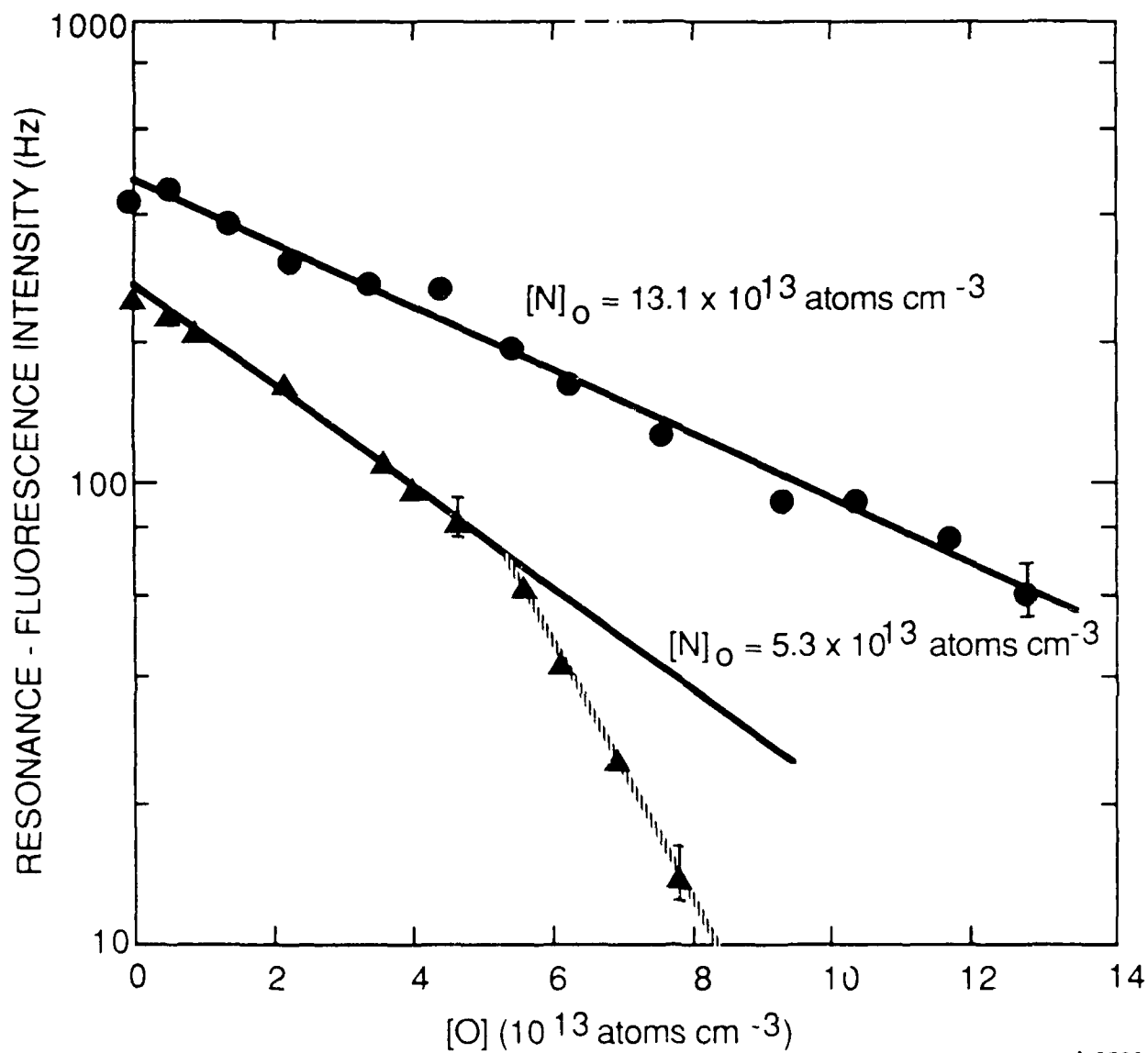
A-9559



^9560



L. Piper
J. Chem. Phy.
Fig. 3



A-9562

L. Piper
J. Chem. Phys.
Fig. 4

PENDIX D

(SR-400 reproduced in its entirety)

To be submitted to J. Geophys. Res. (1989)

PSI-9032/
SR-400

EXPERIMENTAL DETERMINATION OF THE RATIO A_{00}/A_{01} FOR THE INFRARED
ATMOSPHERIC BANDS OF MOLECULAR OXYGEN

Lawrence G. Piper

Physical Sciences Inc.
Dascomb Research Park
P.O. Box 3100
Andover, MA, 01810-7100

J. Geophys. Res., submitted (1989)

EXPERIMENTAL DETERMINATION OF THE RATIO A_{00}/A_{01} FOR THE INFRARED
ATMOSPHERIC BANDS OF MOLECULAR OXYGEN

Lawrence G. Piper

Physical Sciences Inc.
Dascomb Research Park
P.O. Box 3100
Andover, MA, 01810-7100

ABSTRACT

We have re-examined the ratio of the Einstein coefficients of the 0-0 to 0-1 transitions of the infrared atmospheric bands of molecular oxygen. Our measurements involve scanning the spectrum of an afterglow of an oxygen discharge between 1000 and 1600 nm. We calibrated the relative spectral response of our detection system by scanning spectral output of three different standard radiation sources. Our measurements indicate that the ratio A_{00}/A_{01} is 85 ± 8 . Since the accepted value for A_{00} is $2.6 (\pm 15\%) \times 10^{-4} \text{ s}^{-1}$, A_{01} will be $3.0 (\pm 18\%) \times 10^{-6} \text{ s}^{-1}$.

1. INTRODUCTION

The infrared atmospheric bands of molecular oxygen at 1270 nm, $O_2(a^1\Delta_g \rightarrow X^3\Sigma_g^-)$, are a prominent feature of the dayglow. They are produced from solar photolysis of ozone and from homogeneous recombination of oxygen atoms. Observations of $O_2(a)$ emission routinely is combined with photochemical models to monitor ozone concentrations in the upper atmosphere.¹ Ground-based monitoring at 1270 nm introduces the substantial uncertainty in model calculations of accounting for reabsorption of the radiation by molecular oxygen in the atmosphere. A better approach for ground-based monitoring of $O_2(a)$ emission rates, therefore, is to monitor the 0-1 band at 1580 nm. This emission is optically thin under all atmospheric conditions.

The complication introduced in monitoring $O_2(a)$ at 1580 nm is that the Einstein coefficient for this emission band is not well determined. Haslet and Fehsenfeld² generated $O_2(a)$ in a discharge-flow reactor and simultaneously monitored emissions at 1270 and 1580 nm using photometers consisting of interference filters placed in front of photomultipliers. Their data suggested a value of 80 ± 20 for the ratio A_{00}/A_{01} . Pick et al.'s³ observations of the dayglow resulted in a similar value, 80 ± 15 . They used a scanning infrared spectrometer suspended from a balloon at 40 km above the earth to make these observations.

Discharge-flow observations by Findlay,⁴ who used a scanning monochromator, and Becker et al.,⁵ who used a circular variable filter spectrometer, obtained somewhat lower values, however, for the ratio A_{00}/A_{01} : 46.0 ± 0.7 and 49.5 ± 4 , respectively. More recently, Winick et al.¹ deduced a value of

52 ± 25 based upon observations of the dayglow at 1580 nm and a photochemical model. Their observations were made by a circular variable filter spectrometer mounted on a rocket. It viewed the earth's limb from a height of about 250 km. The experimental values divide rather neatly into two camps. Apparently, A_{00}/A_{01} for $O_2(a - X)$ is either about 50 or else about 80. Given the disparity between these results, new measurements seemed to be warranted.

2. EXPERIMENTAL

We generated $O_2(a^1\Delta_g)$ by discharging a flow of oxygen in the sidearm of a vacuum ultraviolet discharge lamp. A scanning monochromator viewed the afterglow fluorescence, through a quartz window, down the axis of the body of the discharge lamp. A number of scans were taken with varying spectral resolution (8 to 34 nm). Figure 1 shows the apparatus schematically.

The monochromator used in these studies was a 0.5 m Minuteman instrument outfitted with a 300 l/mm grating which was blazed at 1000 nm. Light from the afterglow was restricted to wavelengths longer than 1000 nm by placing an RG-1000 cut-off filter in front of the monochromator entrance slit. A mechanical chopper modulated the light prior to its entering the monochromator. A liquid nitrogen cooled intrinsic Ge detector coupled to a lock-in amplifier detected the light as it exited the monochromator.

The wavelength of the monochromator was calibrated by measuring the positions of a number of atomic argon lines excited in a discharge lamp. The relative response of the detection system was calibrated by scanning the spectra of three different radiation sources. We used two different

quartz-halogen lamps and a 1250 K black body. The emission from each source was reflected into the monochromator off a BaSO_4 screen to ensure filling the optics. All calibrations agreed to within 5 percent between 1000 and 1600 nm.

3. RESULTS

Figure 2 shows a typical spectrum of the oxygen afterglow generated in our apparatus. The amplifier sensitivity changes by a factor of 40 at 1350 nm so that the 0-1 band can be observed at 1580 nm. The areas under the two peaks were integrated and corrected for variations in monochromator response. The Einstein coefficient ratio will then be the ratio of the corrected integrated intensities of the two transitions. Our data result in a value of 85 ± 8 for A_{00}/A_{01} . The error bars include not only statistical variations between the various sets of data, but also estimated uncertainties in the response function.

4. DISCUSSION

4.1 Comparison with Other Data

Table 1 lists our result and compares it with other published values. Our measurement supports a value of 80 for the Einstein coefficient ratio as opposed to the value of 50 proposed some groups.^{1,4,5} We are hard pressed to explain the reason for the data's falling into two groupings. Our spectrum indicates the presence of radiation underlying the 1580 nm transition. Measurements with a wide spectral resolution might miss the underlying radiation and, as a result, not correct for it. In this case, one would report a ratio that was too small.

Table 1. A_{00}/A_{01} for $O_2(a^1\Delta_g \rightarrow X^3\Sigma_g^-)$

A_{00}/A_{01}	$\Delta\lambda$ (nm)	Reference
80 ± 20	?	Haslett and Fehsenfeld (1963)
46.0 ± 0.7	6	Findlay (1969)
80 ± 15	20	Pick et al. (1971)
49.5 ± 4	61-72	Becker et al. (1971)
52 ± 25	140	Winick et al. (1985)
85 ± 8	8-34	Present results

This rationalization might explain the low results of Becker et al.⁵ and of Winick et al.¹ who had spectral resolutions of 61-72 and 140 nm, respectively, compared to the 8-34 nm resolution in the present study and the 20 nm resolution of Pick et al.³ Haslett and Fehsenfeld² do not give their spectral resolution. Unfortunately, this rationalization breaks down in explaining disagreement with Findlay⁴ who had the best spectral resolution of all, 6 nm. We can only speculate that he may have made an error in his response function calibration.

If the electronic transition moment were constant with internuclear distance, the intensity ratio would just be given by the ratio of the product of the Franck-Condon factor times the cube of the transition frequency for the two emissions. In this case one would expect a ratio of 146.

No reason exists to suspect that the transition moment is invariant with internuclear separation. Klotz and Peyerimhoff⁷ calculated transition moment

variations for a number of forbidden transitions in molecular oxygen between the $A^3\Sigma_u^+$, $A'^3\Delta_u$, and $c^1\Sigma_u^-$ states and the $X^3\Sigma_g^-$, $a^1\Delta_g$, and $b^1\Sigma_g^+$ states. In general, their calculations indicated quite strong variations. Unfortunately, they did not calculate the transition moment function for the $a - X$ transition,⁸ but variations of 20 - 50 percent over the range of internuclear separations appropriate to the 0-0 and 0-1 transitions would certainly be in keeping with their results on the other transitions.

4.2 Absolute Einstein Coefficients

The generally accepted value for the Einstein coefficient for the 0,0 transition of the infrared atmospheric oxygen system is $2.6 \times 10^{-4} \text{ s}^{-1}$. This value is based upon low pressure, long pathlength absorption measurements by Badger et al. They stated their experimental uncertainty was $\pm 15\%$. Using this value and the Einstein coefficient ratio that we measured, we find that A_{01} is $3.0 (\pm 18\%) \times 10^{-6} \text{ s}^{-1}$.

No other group has attempted a direct experimental verification of Badger et al.'s absorption coefficient. Indirect experimental evidence, however, supports Badger et al.'s measurement. Lilienfeld et al.¹⁰ reported that the ratio of the Einstein coefficients of the $O_2(a-X)$ to the $I(^2P_{1/2} - ^2P_{3/2})$ emissions at 1270 nm and 1315 nm, respectively, was 3.5×10^{-5} . They made this measurement in a discharge-flow reactor in which they had established chemical equilibrium between $O_2(a)$, $O_2(X)$, $I(^2P_{1/2})$ and $I(^2P_{3/2})$. They monitored the relative intensities of the two emissions, and used electron paramagnetic resonance measurements to determine the ratios of the number densities of excited to unexcited oxygen and iodine. Given an Einstein coefficient of

7.9 s^{-1} for the iodine transition, the Einstein coefficient for the a-X transition of O_2 becomes $2.8 \times 10^{-4} \text{ s}^{-1}$.

The Einstein coefficient of the iodine transition appears to be fairly well established. Garstang¹¹ calculated a value of 7.8 s^{-1} . His numerous calculations on forbidden atomic transition probabilities generally have been shown to be correct by more modern calculational techniques as well as by experimental tests. Lilenfeld et al.¹² measured the g-values of the $^2\text{P}_{1/2}$ state of iodine. From this measurement they calculated an Einstein coefficient of 7.9 s^{-1} . Finally, Engleman et al.¹³ determined a value of 8.0 s^{-1} from laser-based absorption measurements.

Theoretical calculations also agree moderately well with Badger et al.'s Einstein coefficient for the 0,0 transition of $\text{O}_2(\text{a-X})$. Zhu et al.¹⁴ calculated a value of $2.5 \times 10^{-4} \text{ s}^{-1}$. This excellent agreement with Badger et al.'s value must be considered fortuitous, however, because Zhu et al. used the same computational approach to calculate an Einstein coefficient for the $\text{O}_2(\text{b}^1\Sigma_g^+ \rightarrow \text{X}^3\Sigma_g^-)$ transition which is more than a factor of five smaller than the currently accepted value^{15,16} of 0.08 s^{-1} . Klotz et al.⁸ have calculated an Einstein coefficient of $1.9 \times 10^{-4} \text{ s}^{-1}$ for the $\text{O}_2(\text{a-X})$ transition. Their computational methods appear to be somewhat more reliable than those of Zhu et al. because their Einstein coefficient for the b-X transition is 0.086 s^{-1} .

5. SUMMARY

We have determined that the ratio of the Einstein coefficients for the 0,0 to 0,1 transitions of the atmospheric oxygen bands is 85 ± 8 . This value along with the previously established absolute value for the 0,0 Einstein coefficient implies that A_{01} is $3.0 (\pm 18\%) \times 10^{-6} \text{ s}^{-1}$.

Aknowledgements

We appreciate financial support from the Air Force Geophysics Laboratory under contract F19628-85-C-0032. They were sponsored by the U.S. Air Force Office of Scientific Research under Task 2310G4 and by the Defense Nuclear Agency under Project SA/SDI, Task SA, Work Unit 115. Advice and comments from Steve Davis and Terry Rawlins of PSI and Jeremy Winick of AFGL were most beneficial.

Reference

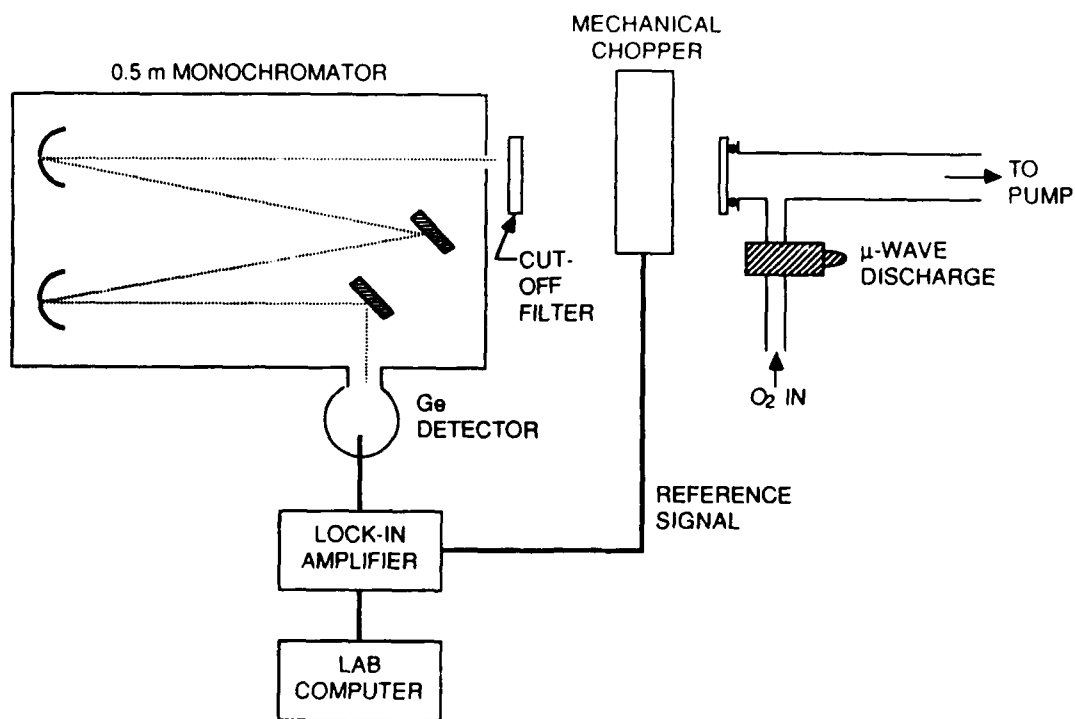
1. Winick, J.R., Picard, R.H., Sharma, R.D., and Nadile, R.M., "Oxygen Singlet Delta 1.58-Micrometer (0-1) Limb Radiance in the Upper Stratosphere and Lower Mesosphere," J. Geophys. Res. 90, 9804 (1985).
2. Haslett, J.C. and Fehsenfeld, F.C., "Ratio of the $O_2(^1\Delta_g \rightarrow ^3\Sigma_g^-)$ (0-0), (0,1) Transitions," J. Geophys. Res. 74, 1878 (1969).
3. Pick, D.R., Llewellyn, E.J., and Vallance Jones, A., "Twilight Airglow Measurements of the OH and O_2 Bands by Means of Balloon-Borne Instruments," Can. J. Phys. 49, 897 (1971).
4. Findlay, F.D., "Relative Band Intensities in the Atmospheric and Infrared Atmosphere Systems of Molecular Oxygen," Can. J. Phys. 47, 687 (1969).
5. Becker, R.H., Groth, W., and Schurath, U., "The Ratio of the Franck-Condon Factors $q(0,0)/q(0,1)$ of the Infrared Atmospheric Band System of Oxygen," Planet. Space Sci. 19, 1009 (1971).
6. Krupenie, P.H., "The Spectrum of Molecular Oxygen," J. Phys. Chem. Ref. Data 1, 423 (1972).
7. Klotz, R. and Peyerimhoff, S.D., "Theoretical Study of the Intensity of the Spin- or dipole- forbidden transitions between the $c^1\Sigma_u^-$, $A'^3\Delta_u$, $A^3\Sigma_u^+$ and $X^3\Sigma_g^-$, $a^1\Delta_g$, $b^1\Sigma_g^+$ States in O_2 ," Mol. Phys. 57, 573 (1986).
8. Klotz, R., Marian, C.M., Peyerimhoff, S.D., Hess, B.A., and Buenker, R.J., "Calculation of Spin-Forbidden Radiative Transitions Using Correlated Wavefunctions: Lifetimes of $b^1\Sigma^+$, $a^1\Delta$ States in O_2 , S_2 and SO ," Chem. Phys. 89, 223, (1984).
9. Badger, R.M., Wright, A.C., and Whitlock, R.F., "Absolute Intensities of the Discrete and Continuous Absorption Bands of Oxygen Gas at 1.26 and 1.065 μ and the Radiative Lifetime of the $^1\Delta_g$ State of Oxygen," J. Chem. Phys. 43, 4345 (1965).
10. Lilienfeld, H.V., Carr, P.A.G., and Hovis, F.E., "Investigation of the Temperature Dependence of the Excitation Mechanism of the Oxygen-Iodine Chemical Laser," Chem. Phys. Lett. 93, 38 (1982).
11. Garstang, R.H., "Transition Probabilities of Forbidden Lines," J. Res. Nat. Bur. Stand. A 68, 61 (1964).
12. Lilienfeld, H.V., Richardson, R.J., and Hovis, F.E., "The Electron Spin Resonance Spectrum of the $^2P_{1/2}$ State of Atomic Iodine," J. Chem. Phys. 74, 2129 (1981).

References (Continued)

13. Engleman, Jr., R., Palmer, B.A., and Davis, S.J., "Transition Probability and Collision Broadening of the 1.3 μm Transition of Atomic Iodine," J. Op. Soc. of Amer. 73, 1585 (1983).
14. Zhu, Ji-Kang, Li, Junqing, and Pan, Yuh-Kang, "Radiative Lifetimes of the Singlet Oxygen Molecule," Chem. Phys. Lett. 78, 129 (1981).
15. Miller, J.H., Boese, R.W., and Giver, L.P., "Intensity Measurements and Rotational Intensity Distribution for the Oxygen A-Band," J. Quant. Spectrosc. Radiat. Transfer. 9, 1507 (1969).
16. Grossmann, B.E., Cahen, C., Lesne, J.L., Benard, J., and Leboudec, G., "Intensities and Atmospheric Broadening Coefficients Measured for O_2 and H_2O absorption Lines Selected for DIAL Monitoring of Both Temperature and Humidity. 1: O_2 ," Appl. Opt. 25, 4261 (1986).

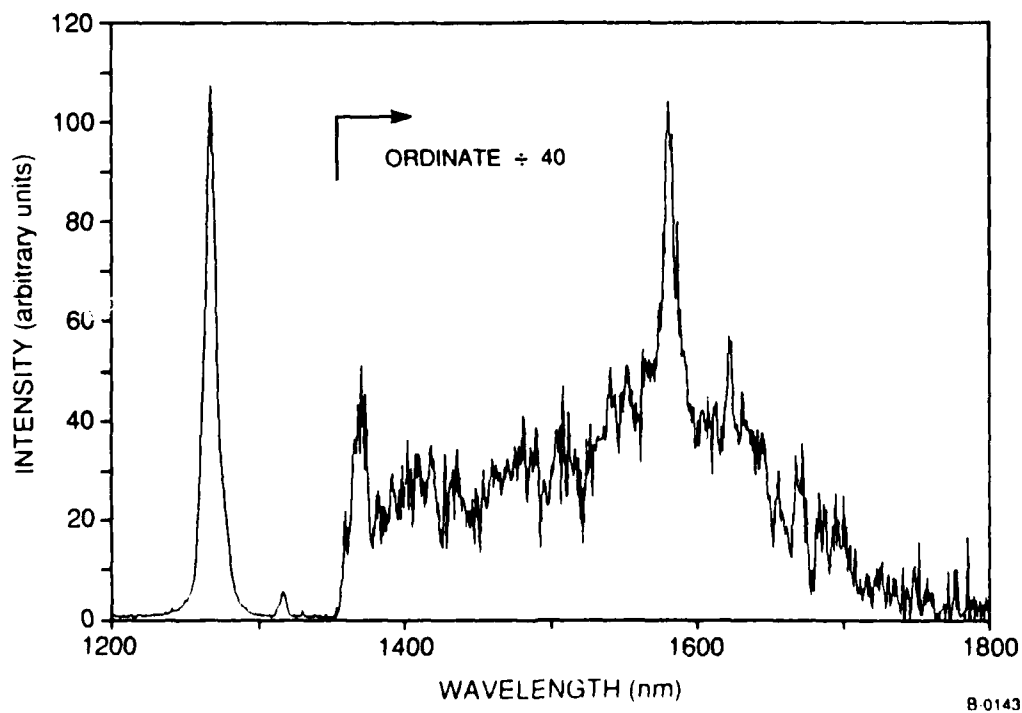
Figure Captions

1. Schematic of discharge-flow apparatus for generating $O_2(a^1\Delta_g)$.
2. Spectrum of oxygen infrared atmospheric bands.



G 0144

Figure 1. Schematic of discharge-flow apparatus for generating $O_2(a^1\Delta_g)$.



B 0143

Figure 2. Spectrum of oxygen infrared atmospheric bands.

APPENDIX E

(SR-240 reproduced in its entirety)

J. Chem. Phys. 85, 2419 (1986)

EINSTEIN COEFFICIENTS AND TRANSITION MOMENT
VARIATION FOR THE $\text{NO}(A^2\Sigma^+-X^2\Pi)$ TRANSITION

Lawrence G. Piper and Lauren M. Cowles*

Physical Sciences Inc.
Research Park, P.O. Box 3100
Andover, MA 01810

J. Chem. Phys. 85, 2419 (1986)

*Present address: Department of Physics, Brandeis University, Waltham, MA

ABSTRACT

Branching ratio measurements for the NO γ -bands excited by energy transfer from metastable nitrogen molecules show that the electronic transition moment for the NO($A^2\Sigma^+-X^2\Pi$) transition varies by about 40 percent over the r-centroid range of 1.13 to 0.97Å. Combining this transition-moment variation with radiative lifetime measurements provides a complete set of Einstein coefficients for NO(A-X) transitions from $v'=0-2$.

I. INTRODUCTION

The issue of whether or not the $\text{NO}(A^2\Sigma^+-X^2\Pi)$ electronic transition moment varies significantly with r -centroid has been the subject of a number of papers over the last several decades.¹⁻¹² While a number of papers have shown evidence of a significant transition-moment variation,¹⁻⁶ several groups have disputed this contention.⁷⁻¹² References 6 and 10 review most of the relevant literature. The general consensus in the scientific community seems to be that no significant transition-moment variation occurs for the NO γ -bands. Recently, while studying the electronic energy transfer between $\text{N}_2(A^3\Sigma_u^+)$ and NO,^{13,14} we found inconsistencies in $\text{NO}(A^2\Sigma^+)$ excitation rates measured using different bands originating from $v'=0$ if we invoked a constant transition moment. The excitation of the NO γ -bands by $\text{N}_2(A^3\Sigma_u^+)$ energy transfer to $\text{NO}(X^2\Pi)$ provides a source of γ -band emission which is free from other significant overlapping band systems in the spectral region. We find that our observed branching ratios for transitions from a common vibrational level in the upper state cannot be explained by variations in the Franck-Condon factors. Our observations show variations in the electronic transition moment of more than 40 percent over the r -centroid range 1.13 to 0.97Å.

Correct transition probabilities for the $\text{NO}(A-X)$ system bear directly upon atmospheric science through such processes as the measurement of NO column densities in the mesosphere¹⁵ or the interpretation of emissions in a strong aurora. In addition proper $\text{NO}(A-X)$ transition probabilities are needed to calculate the gain for various transitions in the optically pumped $\text{NO}(A-X)$ laser.¹⁶ Correct $\text{NO}(A-X)$ transition probabilities affect a wider range of studies, however. Because they are easy to excite, the NO γ -bands are often used to establish the relative spectral response of monochromators in the

ultraviolet.^{7,9} Using incorrect branching ratios for the A-X transition will of course result in an incorrect response function, and will thereby invalidate all other measurements which depend upon the spectral response determined from the γ -band branching ratio measurements. The technique of laser-induced fluorescence on NO(A-X) transitions has become an increasingly important tool for probing the vibrational distributions of ground electronic state NO produced in chemical or photolytic reactions.^{17,18} Incorrect values for the NO(A-X) transition probabilities invalidates the results of these measurements, and thereby casts doubt on the validity of dynamical interpretations of the results.

II. EXPERIMENTAL

The apparatus used in these studies has been described in detail in a number of other papers.^{13,14,19-23} Briefly, the experiment involved exciting the NO γ -bands in the energy-transfer reaction between $N_2(A^3\Sigma_u^+)$ and NO in a discharge-flow apparatus. Adding nitrogen molecules to a flow of metastable argon atoms produced $N_2(A)$ molecules in the absence of significant number densities of nitrogen atoms or $N_2(X,v)$.²⁴⁻²⁶ A low-power, dc discharge through a flow of argon atoms generated the argon metastables. NO was added to the flow downstream from nitrogen addition inlet and the resulting spectrum was recorded photoelectrically at moderate resolution ($\Delta\lambda = 0.33$ nm) between 200 and 400 nm. A least-squares spectral fitting procedure determined the intensities of each band.²² Standard quartz-halogen and D₂ lamps were used to determine the relative response of the spectral system as a function of wavelength. Excellent agreement between observed and calculated intensities of a number of bands of the $N_2(A^3\Sigma_u-X^1\Sigma_g^+)$ and $N_2(C^3\Pi_u-B^3\Pi_g^+)$ systems between 220 and 400 nm confirmed the reliability of the calibration.

III. RESULTS AND DISCUSSION

The intensity of emission from a given band is the product of the number density in the upper state and the Einstein coefficient for spontaneous radiation. The Einstein coefficient can be separated into a product of the Franck-Condon factor, the cube of the transition frequency, and the square of the electronic transition moment. Thus

$$I_{v'v''} = N_{v'} A_{v'v''} \propto N_{v'} q_{v'v''} \nu_{v'v''}^3 |R_e(\bar{r}_{v'v''})|^2 \quad (1)$$

The constant-moment population in the upper state is then determined from the ratio of the integrated band intensity to the product of the Franck-Condon factor and the cube of the transition frequency:

$$N_{v'v''}^* = \frac{I_{v'v''}}{q_{v'v''} \nu_{v'v''}^3} = N_{v'} |R_e(\bar{r}_{v'v''})|^2 \quad (2)$$

The ratios of these constant-moment populations to each other should be unity unless the transition moment varies with r-centroid. The relative variation in the transition moment with r-centroid results from the ratio of the various constant-moment populations to one reference population. Scaling the relative transition moments to experimentally determined lifetime or oscillator-strength data is then a relatively simple process.

We determined the constant-moment populations of the bands emanating from $v'=0$ and 1 using a spectral fitting routine for each Δv sequence from $\Delta v=1$ to $\Delta v=-8$. The fitting routine corrected for spectral overlap between the transitions for $v'=0$ and 1. The fit included the different effective rotational temperatures for the two vibrational levels.¹⁴ We ratioed each of these populations to the ones determined for the $\Delta v=-3$ sequence. This sequence is in the middle of the wavelength range for the band system and thus should minimize any systematic errors in the relative monochromator response function.

The Franck-Condon factors of both Nicholls²⁷ and Albritton et al.²⁸ gave similar results. Our final results incorporate the latter set.

Figure 1 shows the electronic transition moment relative to its value for the $\Delta v = -3$ sequence plotted against r -centroid. The variation is small, but consistent, up through the $\Delta v = -3$ sequence, but rises much more sharply for the $\Delta v < -3$ sequences. The diamonds in Figure 1 show our re-analysis of the branching-ratio measurements of McGee et al.¹¹ They excited NO(A, $v' = 0$) with a laser and reported relative band emission intensities. Their results agree excellently with ours. Finally, we have also plotted the transition moment variation given by Brzozowski et al.⁵ who observed γ -band emission in electron-beam excited NO during studies on NO predissociation.

We fit the results of the three experiments to a quadratic function of r -centroid:

$$|R_e(\bar{r}_{v',v''})|_{\text{rel}} = 33.08 - 58.77 \bar{r}_{v',v''} + 26.85 \bar{r}_{v',v''}^2 \quad (3)$$

Using this functional form for the relative transition moment, we determined a smoothed set of branching ratios for emission from a given upper state as being

$$B_{v',v''} = \frac{q_{v',v''} v_{v',v''}^3 |R_e(\bar{r}_{v',v''})|_{\text{rel}}^2}{\sum_{v''} q_{v',v''} v_{v',v''}^3 |R_e(\bar{r}_{v',v''})|_{\text{rel}}^2} \quad (4)$$

The Einstein coefficient for spontaneous radiation from each band is the product of the branching ratio for the given band and the reciprocal of the radiative lifetime of the upper state vibrational level. The average of nine apparently reliable determinations of the fluorescence lifetime of NO(A, $v' = 0$)

gives a value of (202 ± 14) ns.^{8,10,29-35} Eight different determinations for the $v'=1$ level give a value of (192 ± 14) ns.^{10,29,30,33,34,36-38} In both cases the error bars represent one standard deviation. Table 1 lists the Einstein coefficients for each band.

Equation 5 relates the Einstein coefficient for a given $v'v''$ transition to the absorption oscillator strength:

$$f_{v'v''}^{abs} = \frac{m_e c \lambda_o^2}{8\pi e} \frac{d_u}{d_l} A_{v'v''} \quad (5)$$

Here m_e is the electron mass, e its charge in esu, c the speed of light, λ_o the transition wavelength, and d_u and d_l are the electronic degeneracies of the upper and lower states, respectively. These last quantities are 1 and 2 for $A^2\Sigma^+$ and $X^2\Pi$, respectively. Applying our Einstein coefficients to Equation 5 gives absorption oscillator strengths for the 0,0 and 1,0 bands of $(3.9 \pm 0.3) \times 10^{-4}$ and $(8.2 \pm 0.6) \times 10^{-4}$, respectively. These values agree excellently with literature measurements of $(4.03 \pm 0.22) \times 10^{-4}$ for the 0,0 transition (five different experiments)³⁹⁻⁴³ and $(8.26 \pm 0.48) \times 10^{-4}$ for the 1,0 transition (three different measurements).^{40,42,43} Thus our transition moment function satisfies the important criterion that the lifetime and absorption measurements be consistent.

We have also calculated Einstein coefficients for $v'=2$ assuming the transition moment variation of Equation 3 and a radiative-decay lifetime for $v'=2$ of (182 ± 10) ns.^{10,29,30,33,34} Because the transition moment variation was extrapolated to regions outside the fit, the transition probabilities from $v'=2$ are less reliable. This may be reflected in the modest disagreement between the absorption oscillator strength of the 2,0 band calculated from the

transition probabilities given in Table 1 of $(8.1 \pm 0.4) \times 10^{-4}$ and the experimental value of $(6.8 \pm 0.2) \times 10^{-4}$.^{40,42,43} Better agreement with the 2,0 band absorption measurements results from having the transition moment become constant at r -centroid values greater than 1.11\AA but with the same transition moment variation shown in Figure 1 for smaller r -centroid values. This adjustment degrades the agreement with the 0,0 and 1,0 oscillator strengths slightly, however. We do not feel the accuracy of the oscillator strength measurements, probably about 20 percent for any individual measurement, justifies making such an adjustment for an apparent 16 percent discrepancy.

An apparent transition-moment variation could also be the result of our having an incorrect relative monochromator response function. In that case our analysis for the transition moment function would also be invalid. This does not appear to be a significant problem in our work, however, because we very accurately fit the Vegard-Kaplan ($A^3\Sigma_u^+ - X^1\Sigma_g^+$) and second-positive ($C^3\Pi_u - B^3\Pi_g$) bands of nitrogen over the same wavelength region. In addition, the good agreement between our own results and those of the two other groups alluded to previously^{5,11} confirms that our wavelength response function is accurate. Recently McGee et al.⁴⁴ published branching ratios for $\text{NO}(A, v'=1)$ transitions. These measurements also agree quite well with the results presented here when properly analyzed to show the transition-moment variation.

ACKNOWLEDGEMENTS

We appreciate partial support for this work from the Air Force Geophysics Laboratories under Contract No. F19628-82-C-0050 and from the Air Force Weapons Laboratories under Contract No. F29601-84-C-0076. L. G. Piper thanks Don Setser (Kansas State University) for sending the Franck-Condon factors, and George Caledonia, Dave Green, and Terry Rawlins, all from PSI, for comments and suggestions.

REFERENCES

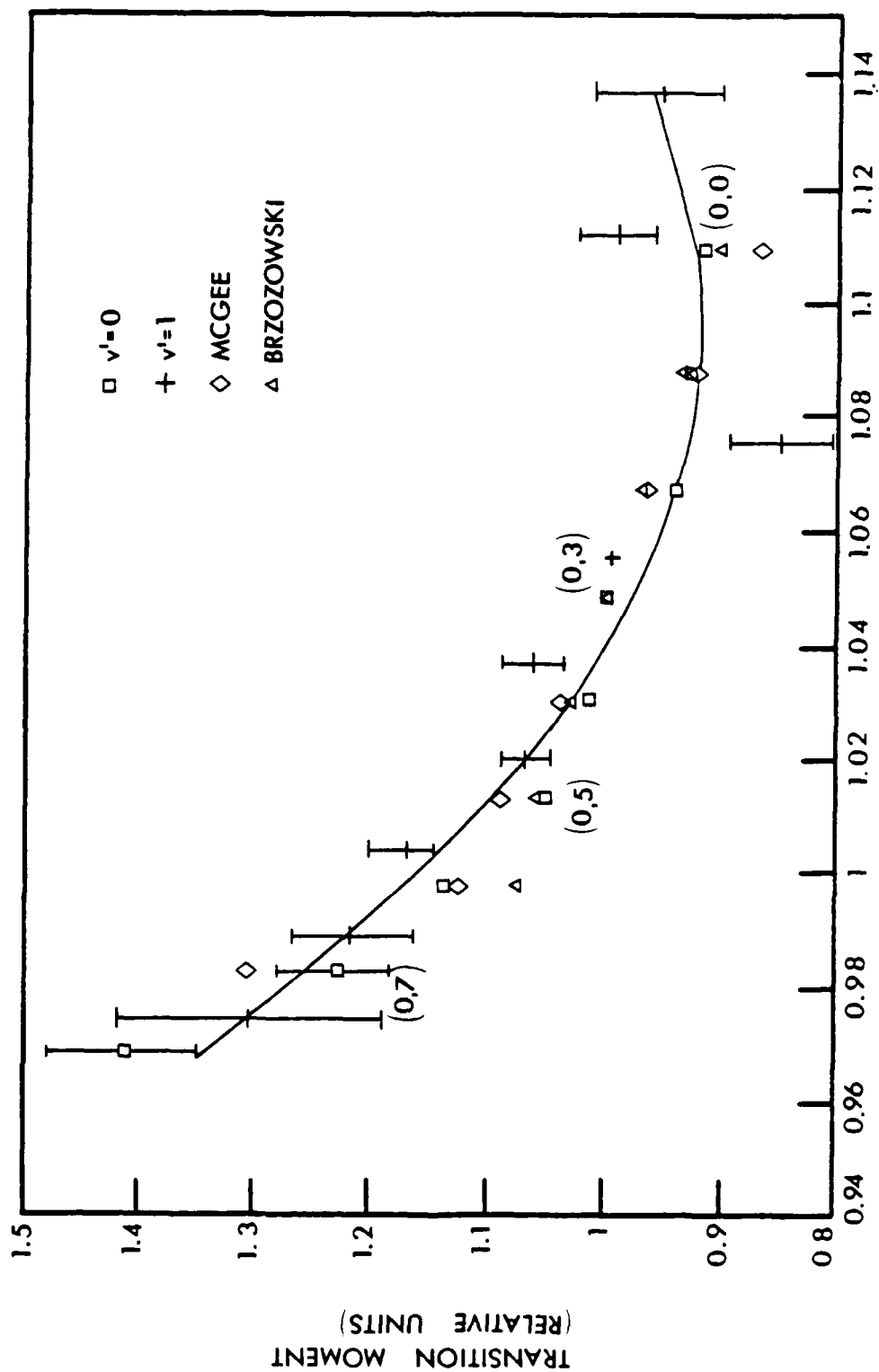
1. D. Robinson and R.W. Nicholls, Proc. Phys. Soc. LXXI, 957 (1958).
2. J.C. Keck, R. A. Allen, and R.L. Taylor, J. Quant. Spectrosc. Radiat. Transfer 3, 335 (1963).
3. A.B. Callear, M.J. Pilling, and I.W.M. Smith, Trans. Faraday Soc. 62, 2997 (1966).
4. H. Bubert, J. Chem. Phys. 56, 1113 (1972).
5. J. Brzozowski, P. Erman, and M. Lyyra, Physica Scripta 14, 290 (1976).
6. N.E. Kuz'menko, L.A. Kuznetsova, A.P. Monyakin, and Yu. Ya. Kuzyakov, J. Quant. Spectrosc. Radiat. Transfer 24, 219 (1980).
7. H.M. Poland and H.P. Broida, J. Quant. Spectrosc. Radiat. Transfer 11, 1863 (1971).
8. M. Jeunehomme, J. Chem. Phys. 45, 4433 (1966).
9. M.J. Mumma, J. Opt. Soc. Amer. 62, 1459 (1972).
10. G.R. Mohlmann, H.A. Van Sprang, E. Bloemen, and F.J. De Heer, Chem. Phys. 32, 239 (1978).
11. T.J. McGee, G.E. Miller, J. Burris, Jr. and T.J. McIlrath, J. Quant. Spectrosc. Radiat. Transfer 29, 333 (1983).
12. B.S. Navati and V.N. Korwar, Physica 124C, 421 (1984).
13. L.G. Piper, PSI-07C/TR-518, prepared for the Air Force Weapons Laboratories under Contract No. F29601-84-C-0076 (1985). Available from the authors upon request.
14. L.G. Piper, L.M. Cowles, and W.T. Rawlins, J. Chem. Phys. 85, xxxx (1986).
15. G. Witt, J. Dye, and N. Wilhelm, J. Atmos. Terr. Phys. 38, 223 (1976).
16. M.D. Burrows, Appl. Phys. Lett. 46, 22 (1985).
17. T.G. Slinger, W.K. Bischel, and M.J. Dyer, J. Chem. Phys. 79, 2231 (1983).
18. R.R. Herm, B.J. Sullivan, and M.E. Whitson, J. Chem. Phys. 79, 2221 (1983).
19. W.T. Rawlins, L.G. Piper, G.E. Caledonia, and B.D. Green, Physical Sciences Inc. Technical Report TR-293 (1981). Available from the authors upon request.

20. L.G. Piper, G.E. Caledonia, and J.P. Kennealy, J. Chem. Phys. 74, 2888 (1981).
21. W.T. Rawlins and L.G. Piper, Proc. Soc. Photo. Opt. Instr. Eng. 279, 58 (1981).
22. L.G. Piper, W.J. Marinelli, W.T. Rawlins, and B.D. Green, J. Chem. Phys. 83, 5602 (1985).
23. L.G. Piper and W.T. Rawlins, J. Phys. Chem. 90, 320 (1986).
24. D.W. Setser, D.H. Stedman, and J.A. Coxon, J. Chem. Phys. 53, 1004 (1970).
25. D.H. Stedman and D.W. Setser, Chem. Phys. Lett. 2, 542 (1968).
26. N. Sadeghi and D.W. Setser, Chem. Phys. Lett. 82, 44 (1981).
27. R.W. Nicholls, J. Res. NBS 68A, 535 (1964).
28. D.L. Albritton, A.L. Schmeltekopf, and R.N. Zare, private communication via D.W. Setser (1985).
29. H. Zacharias, J.B. Halpern, and K.H. Welge, Chem. Phys. Lett. 43, 41 (1976).
30. A.J. Smith and F.H. Read, J. Phys. B: Atom. Molec. Phys. 11, 3263 (1978).
31. I.S. McDermid and J.B. Laudenslager, J. Quant. Spectrosc. Radiat. Transfer 27, 483 (1982).
32. D.R. Crosley and R.N. Zare, J. Chem. Phys. 49, 4231 (1968).
33. J. Brozozowski, N. Elander, and P. Erman, Phys. Scr. 9, 99 (1974).
34. O. Benoist D'Azy, R. Lopez-Delgado, and A. Tramer, Chem. Phys. 9, 327 (1975).
35. J. Hesser, J. Chem. Phys. 48, 2518 (1968).
36. H. Bubert and F. W. Froben, Chem. Phys. Lett. 8, 242 (1971).
37. K.R. German, R. N. Zare and D.R. Crosley, J. Chem. Phys. 54, 4039 (1971).
38. E.M. Weinstock and R. N. Zare, J. Chem. Phys. 56, 3456-3462 (1972).

39. V. Hasson, A.J.D. Farmer, R.W. Nicholls, J. and Anketell, J. Phys. B: Atom. Molec. Phys. 5, 1248 (1972).
40. A.J.D. Farmer, V. Hasson, and R.W. Nicholls, J. Quant. Spectrosc. Radiat. Transfer 12, 627 (1972).
41. A. Pery-Thorne and F.P. Banfield, J. Phys. B: Atom. Molec. Phys. 3, 1011 (1970).
42. D. Weber and S.S. Penner, J. Chem. Phys. 26 860 (1957).
43. G.W. Bethke, J. Chem. Phys. 31, 662 (1959).
44. T.J. McGee, J. Burris, Jr., and J. Barnes, J. Quant. Spectrosc. Radiat. Transfer 34, 81 (1985).

Table 1. Einstein Coefficients for NO($A^2\Sigma^+-X^2\Pi$)

$v'=0$	v''	Wavelength (nm)	$Q_{v',v''}$	$\bar{r}_{(v',v'')}(\text{\AA})$	$R_e(r)$	Branching Ratio	$A_{v',v''} (s^{-1})$
	0	226.548	0.16697	1.1091	0.921429	0.202462	1.002E+06
	1	236.604	0.26345	1.0873	0.917005	0.277740	1.375E+06
	2	247.421	0.23646	1.067	0.935830	0.227041	1.124E+06
	3	259.087	0.15962	1.0481	0.973248	0.144364	7.147E+05
	4	271.700	0.090505	1.0303	1.026027	0.078883	3.905E+05
	5	385.377	0.045696	1.0135	1.091448	0.038094	1.925E+05
	6	300.252	0.021285	0.9977	1.166803	0.017777	8.801E+04
	7	316.482	0.009363	0.9827	1.250746	0.007673	3.799E+04
	8	334.256	0.003954	0.9684	1.342021	0.003166	1.568E+04
	9	353.794	0.001622	0.9548	1.439015	0.001259	6.235E+03
	10	375.362	0.000652	0.9419	1.540195	0.000485	2.405E+03
	11	399.283	0.000259	0.9295	1.645876	0.000183	9.061E+02
	12	425.947	0.000102	0.9177	1.754110	0.000067	3.339E+02
$v'=1$	v''	Wavelength (nm)	$Q_{v',v''}$	$\bar{r}_{(v',v'')}(\text{\AA})$	$R_e(r)$	Branching Ratio	$A_{v',v''} (s^{-1})$
	0	215.134	0.33353	1.1364	0.962957	0.451795	2.353E+06
	1	224.182	0.10295	1.1108	0.922847	0.113188	5.895E+05
	2	233.870	0.00097	1.0920	0.915801	0.000925	4.818E+03
	3	244.266	0.07231	1.0754	0.925357	0.061794	3.218E+05
	4	255.446	0.13381	1.0551	0.957153	0.106972	5.572E+05
	5	267.499	0.13257	1.0368	1.004782	0.101704	5.297E+05
	6	280.526	0.097792	1.0198	1.065139	0.073099	3.807E+05
	7	294.644	0.060554	1.0039	1.135635	0.044406	2.313E+05
	8	309.990	0.033426	0.9888	1.215151	0.024100	1.255E+05
	9	326.723	0.017042	0.9745	1.301742	0.012043	6.273E+04
	10	345.032	0.008212	0.9609	1.394282	0.005653	2.944E+04
	11	365.139	0.003800	0.9480	1.491236	0.002524	1.315E+04
	12	387.312	0.00171	0.9357	1.592003	0.001084	5.651E+03
	13	411.871	0.000753	0.9238	1.697225	0.000451	2.352E+03
	14	439.206	0.000327	0.9126	1.803203	0.000182	9.507E+02
	15	469.796	0.000141	0.9017	1.912810	0.000072	3.769E+02
$v'=2$	v''	Wavelength (nm)	$Q_{v',v''}$	$\bar{r}_{(v',v'')}(\text{\AA})$	$R_e(r)$	Branching Ratio	$A_{v',v''} (s^{-1})$
	0	204.952	0.29246	1.1654	1.050907	0.468229	2.573E+06
	1	213.147	0.017314	1.1516	1.003423	0.022467	1.234E+05
	2	221.886	0.15606	1.1194	0.932396	0.154996	8.516E+05
	3	231.223	0.07289	1.0947	0.915646	0.061695	3.390E+05
	4	241.217	0.00038	1.0770	0.923791	0.000288	1.584E+03
	5	251.936	0.034722	1.0644	0.939840	0.023936	1.315E+05
	6	263.459	0.08771	1.0440	0.983897	0.057946	3.184E+05
	7	275.873	0.10421	1.0265	1.039499	0.066934	3.678E+05
	8	289.281	0.088733	1.0103	1.105627	0.055919	3.072E+05
	9	303.801	0.062245	0.9951	1.180487	0.038608	2.121E+05
	10	319.569	0.038476	0.9807	1.262851	0.023464	1.289E+05
	11	336.744	0.021789	0.9671	1.350863	0.012995	7.140E+04
	12	355.514	0.011589	0.9542	1.443523	0.006707	3.685E+04
	13	376.099	0.005891	0.9419	1.540195	0.003278	1.801E+04
	14	398.761	0.002897	0.9301	1.640572	0.001534	8.432E+03
	15	423.818	0.001392	0.9189	1.742761	0.000693	3.808E+03
	16	451.643	0.000688	0.9081	1.847680	0.000304	1.672E+03



R-CENTROID

A-1145

APPENDIX F

(SR-242 reproduced in its entirety)

J. Chem. Phys. 85, 3369 (1986)

STATE-TO-STATE EXCITATION OF $\text{NO}(A^2\Sigma^+, v'=0,1,2)$

BY $\text{N}_2(A^3\Sigma_u^+, v'=0,1,2)$

Lawrence G. Piper, Lauren M. Cowles*, and Wilson T. Rawlins

Physical Sciences Inc.
Research Park, P.O. Box 3100
Andover, MA 01810

J. Chem. Phys. 85, 3369 (1986)

*Present address: Department of Physics, Brandeis University, Waltham, MA

ABSTRACT

We have determined that the rate coefficient for quenching $N_2(A^3\Sigma_u^+, v'=0)$ by NO is $(6.6 \pm 1.0) \times 10^{-11} \text{ cm}^3 \text{ molecule}^{-1} \text{ s}^{-1}$. Higher levels of $N_2(A)$ appear to be quenched with a similar rate coefficient. Separate studies show that the rate coefficient for the excitation of $NO(A^2\Sigma^+, v'=0-2)$ by $N_2(A^3\Sigma_u^+, v'=0)$ is $(10 \pm 3) \times 10^{-11} \text{ cm}^3 \text{ molecule}^{-1} \text{ s}^{-1}$. The apparent discrepancy between the quenching and excitation rate coefficient measurements most likely results from an error in the accepted value of the lifetime $N_2(A)$. Our studies indicate that this lifetime is probably about 30 percent longer than currently believed. We also report rate coefficients for excitation of each of the vibrational levels 0-2 of $NO(A)$ by each of the vibrational levels 0-2 of $N_2(A)$ relative to the rate coefficient for excitation of $NO(A, v'=0)$ by $N_2(A, v'=0)$.

I. INTRODUCTION

The excitation of the NO γ -bands in the energy-transfer reaction between $N_2(A)$ and NO is now well established.¹⁻⁴ What is not well established is the fraction of total $N_2(A)$ quenching which results in NO(A) excitation. The published values of the rate coefficient for excitation of NO(A) by $N_2(A)$ ^{1,2} are both a factor of two greater than most of the measurements of the rate coefficient for the destruction of $N_2(A)$ by NO.^{2,3,5,6} The magnitude of this discrepancy demands further investigation. In addition, the state-to-state partitioning between vibrational levels of the $N_2(A)$ pumping reagent and the NO(A) is uncertain. Callear and Wood³ claim a strong difference in the ratio of NO(A) $v'=0$ to $v'=1$ excited by $N_2(A, v'=0)$ (9.8:1) compared to that excited by $N_2(A, v'=1)$ (1.9:1). Some preliminary results from a Physical Sciences Inc. (PSI) study a number of years ago aimed at using NO γ -bands as a monitor of system purity⁴ indicate a much smaller difference (7:1 and 4:1, respectively). It is also not clear if there is a strong difference in the quenching rate coefficients for the different $N_2(A)$ vibrational levels. Dreyer et al.⁶ found NO quenched $N_2(v'=1)$ almost 70 percent faster than $N_2(A, v'=0)$ while Clark and Setser¹ and Young and St. John² say both $N_2(A)$ levels are quenched by NO with equal efficiency. Consequently, we undertook a careful investigation which we report here.

II. EXPERIMENTAL

The apparatus is a 2-in. flow tube pumped by a Leybold-Heraeus Roots blower/forepump combination capable of producing linear velocities up to 5×10^3 cm s⁻¹ at pressures of 1 Torr. The flow tube design is modular (see Figure 1), with separate source, reaction, and detection sections which clamp together with O-ring joints. We have previously described this apparatus in

various configurations.⁷⁻¹⁰ The detection region is a rectangular stainless-steel block bored out internally to a 2-in. circular cross section and coated with Teflon® (Dupont Poly TFE #852-201) to retard surface recombination of atoms.¹¹⁻¹⁴ Use of a black primer prior to the Teflon® coating reduces scattered light inside the block dramatically. The block has two sets of viewing positions consisting of four circular ports each on the four faces of the block. These circular ports accommodate vacuum-ultraviolet resonance lamps, VUV and visible monochromator interfaces, laser delivery side-arms and a spatially filtered photomultiplier/interference filter combination.

In these experiments a suprasil lens collected light from the center of the flow tube and focussed it on the entrance slit of a 0.5m Minuteman monochromator which is outfitted with a 1200 groove mm^{-1} grating blazed at 250 nm. A thermoelectrically-cooled photomultiplier (HTV R943-02) detected photons with the aid of an SSR 1105 photon-counting rate meter. A laboratory computer system digitized the analog output from the rate meter and stored the information on floppy disks for further processing. The computer system comprises an IBM PC with 512K of RAM, two 360K diskette drives, a monochrome monitor, and a 160 cps dot-matrix printer with graphics capability. The data are acquired via a Data Translation I/O system (DT2801A), which features 16 channels of A/D inputs, two channels of D/A output, two 8-bit digital I/O ports, software programmable gain, single-ended or differential input, and data acquisition rates as fast as 14 kHz. The acquisition is interfaced to the computer by a Laboratory Technologies Inc. software package, "Real-time Laboratory Notebook," which organizes data in a form compatible for analysis using the "Lotus 123" business spreadsheet software or for sending to the PRIME 400 computer in PSI's computer center for analysis there. Much of the

analysis revolves around least-squares fitting of spectra. Our procedure⁹ is to generate basis functions consisting of a synthetic electronic spectrum for a unit population in each vibrational level of each electronic state appearing in the spectral region of interest. A linear least-squares routine then finds the populations of each vibronic band which, when multiplied by the appropriate basis function and summed with overlapping bands, gives a composite spectrum most nearly matching the experimental spectrum.

Standard quartz-halogen and D₂ lamps were used to calibrate the spectral system for relative response as a function of wavelength. Excellent agreement between observed and calculated intensities of a number of bands of the N₂(A³Σ_u⁺-X¹Σ_g⁺) system between 220 and 400 nm confirmed the reliability of the UV calibration.

The reaction between metastable Ar(³P_{0,2}) and molecular nitrogen produces the metastable nitrogen molecules, N₂(A³Σ_u⁺).^{15,16} This transfer excites N₂(C³Π_u)¹⁷ which quickly cascades radiatively to the metastable A³Σ_u⁺ state via the B(³Π_g) state. A hollow-cathode discharge source operating at 240 Vdc and 3 mA produces the argon metastables. The argon and nitrogen are purified by flowing them through traps filled with 5A molecular sieve.

Observations of strong Vegard-Kaplan, N₂(A³Σ_u⁺-X¹Σ_g⁺), emission downstream of the Ar/N₂ mixing zone confirms the production of the nitrogen metastables (Figure 2). Co-discharging the nitrogen with the argon increases the N₂(A) yield by a factor of about six¹⁸ but we have found that this procedure also produces some atomic nitrogen, vibrationally excited N₂ and metastable N₂(a¹Σ_u⁻).¹⁹ Unequivocal measurements on N₂(A³Σ_u⁺) reactions, therefore, demand that the nitrogen be added downstream from the discharge. In the absence of vibrational relaxation partners the initial N₂(A) vibrational distribution is a function of nitrogen mole fraction, total pressure, and

transit time between the discharge and the observation region. Under conditions of short transit time, low pressure and low nitrogen mole fraction, we have observed emission from levels as high as $v'=4$. More typically, because of vibrational relaxation by N_2 and Ar during the ≈ 25 ms transit time between the discharge and the observation region, we observe only levels 0-2 with a distribution of 1:0.7:0.2, respectively.

Nitric oxide enters the flow tube through a 1-in. diameter loop injector seated on the end of a 1/4-in. diameter tube which slides along the bottom of the flow tube and parallel to its axis. This allows a variety of reaction distances for accurate kinetic studies. Adding CH_4 , CF_3H , or CF_4 to the gas stream through a fixed, hook-shaped injector just downstream from where the $N_2(A)$ entered the flow reactor, relaxes $N_2(A)$ vibrational excitation without significant electronic quenching.^{9,20}

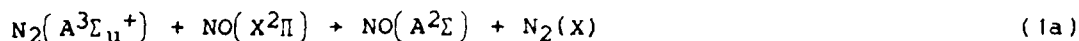
Mass-flow meters or rotameters monitor gas flow rates. All flow meters are calibrated by measuring rates of increase of pressure with time into 6.5 or 12l flasks, using appropriate differential pressure transducers (Validyne DP-15) which themselves have been calibrated with silicon oil or mercury manometers. Typical flow rates for argon, nitrogen, and helium through the injector are 2000-5000, 100-500 and 50 $\mu\text{mol s}^{-1}$, while the NO flow rate ranges between 0 and 1 or 0 and 0.01 $\mu\text{mol s}^{-1}$ for decay or excitation rate measurements, respectively. Total pressures, as measured by a Baratron® capacitance manometer, range from 0.3 to 10 Torr, and flow velocities vary from 500 to 5000 cm s^{-1} .

Nitric oxide is purified by slowly flowing it at atmospheric pressure through an Ascarite® trap and then through a cold finger surrounded by a methanol/ lN_2 slush bath (-100°C). The NO is then diluted in argon and the mixtures stored in 5-l Pyrex® flasks. Mixtures of 5 to 8 percent NO sufficed

for decay rate measurements while the excitation-rate determinations required NO mole fractions $\lesssim 10^{-3}$.

III. RESULTS

Complete characterization of the energy-transfer reaction between $N_2(A)$ and NO,



involves measuring both the rate coefficient for removal of $N_2(A)$ by NO and the rate coefficient for the excitation of the NO γ -bands in the energy transfer reaction. The rapid vibrational relaxation of $N_2(A)$ by molecules such as CF_4 , CF_3H , and CH_4 , with no accompanying electronic quenching^{9,20} allows us to alter the vibrational distribution of the $N_2(A)$. This makes state-to-state measurements possible.

A. The Quenching of $N_2(A^3\Sigma_u^+, v'=0)$ by NO

Measurements of the rate of removal of $N_2(A)$ by NO are not so straightforward as corresponding measurements of $N_2(A)$ quenching by other molecules. Ordinarily, one follows $N_2(A)$ number density decays by monitoring the Vegard-Kaplan emission.^{7,9,21} The extremely bright NO γ -band emission in the same region of the spectrum, however, masks the Vegard-Kaplan bands. Fortunately γ -band emission is a sensitive tracer of the $N_2(A)$ number density.

The differential equation describing the rate of change in the $NO(A^2\Sigma^+)$ number density with time is

$$\frac{d[NO(A)]}{dt} = k_1 [N_2(A)][NO(X)] - k_2 [NO(A)] \quad (3)$$

The $NO(A)$ is in steady state in the observation volume because the lifetime of $NO(A)$ is short compared to the time a molecule resides within the field of view of the detector. Thus the intensity of the γ -band emission is

$$I_{NO^*} = k_2[NO^*] = k_{1a}[N_2(A)][NO] \quad (4)$$

Upon rearranging this equation, we relate the number density of $N_2(A)$ in the observation volume to the ratio of the γ -band emission intensity and the NO number density:

$$[N_2(A)] = \frac{I_{NO^*}}{k_{1a}[NO]} \quad (5)$$

The differential equation describing the decay of $N_2(A)$ in the reactor is

$$\frac{d[N_2(A)]}{dt} = -(k_1[NO] + k_{wall})[N_2(A)] \quad (6)$$

where k_{wall} is the first-order (pressure dependent) rate coefficient for $N_2(A)$ quenching in wall collisions. Because the NO number density is typically several orders of magnitude greater than the $N_2(A)$ number density, we can assume that the NO number density is a constant (the pseudo-first-order approximation). This approximation leads to an analytical solution to Eq. (6), viz,

$$\ln \frac{[N_2(A)]}{[N_2(A)]^0} = -(k_1[NO] + k_{wall}) z/\bar{v} \quad (7)$$

We have replaced the reaction time by the ratio of the distance z , from flow tube injector to the observation point, to the bulk flow velocity in the reactor, \bar{v} . Inserting Eq. (5) into Eq. (7) gives

$$\ln \left\{ \frac{I_{NO^*}/[NO]}{I_{NO^*}^0/[NO]^0} \right\} = -k_1[NO] + k_{wall} z/\bar{v} \quad (8)$$

The above equation shows that measurements of the logarithm of the ratio of γ -band intensity to NO number density as a function of NO number density but with fixed reaction time will give a linear relationship with a slope of

$-k_1 z/\bar{v}$. Such measurements at several different reaction distances, under otherwise constant conditions of pressure, temperature, total flow rate, etc., will correct for non-instantaneous mixing at the injector. The results must further be corrected by a factor of $(0.62)^{-1}$ to correct for the coupling of a radial density gradient in $N_2(A)$ number density with a parabolic velocity profile.²²⁻²⁹

We have shown previously⁷ that rate coefficients measured using a tracer can be seriously in error if the tracer is sensitive to several different $N_2(A)$ vibrational levels each of which quenches at significantly different rates. For this reason we have relaxed the $N_2(A)$ vibrational distribution to only $v'=0$. CF_3H , CF_4 , and CH_4 all were used to relax $N_2(A)$ to $v'=0$. As expected, the results were invariant with relaxation partner.

Figure 3 shows a plot of the ratio of the natural log of the γ -band intensity to the NO number density as a function of the NO number density for several different distances between the injector and observation volume. The linearity of these plots is quite good, extending over more than two orders of magnitude. Figure 4 shows a plot of the slopes of the lines in Figure 3 and two other sets of data plotted as a function of the reaction time. The slope of this plot, when divided by the radial-profile correction factor, 0.62, gives the rate coefficient for quenching $N_2(A)$ by NO. Note the non-zero intercept, indicative of the finite time required for complete reagent mixing.

A number of experiments spanning a range in total gas pressures from 0.7 to 3.7 Torr and reaction times from 11 to 124 ms, and using several different NO/Ar gas mixtures all gave consistent results for the rate coefficient for $N_2(A, v'=0)$ quenching by NO of $(5.6 \pm 0.8) \times 10^{-11} \text{ cm}^3 \text{ molecule}^{-1} \text{ s}^{-1}$. The quoted error estimate is one standard deviation in the averaging process. The

total experimental uncertainty, including estimates in the uncertainties in the calibrations of the flow meters, pressure gauges, etc. is about 15 percent. A few decay measurements in which the $N_2(A)$ was not vibrationally relaxed gave decays only slightly larger ($\lesssim 5$ percent) than those measured for the relaxed $N_2(A)$. Thus we infer that NO quenches vibrationally excited $N_2(A)$ at a rate similar to that for quenching $v'=0$.

Our result disagrees markedly with Dreyer and Perner's reported value of $2.8 \times 10^{-11} \text{ cm}^3 \text{ molecule}^{-1} \text{ s}^{-1}$ for $v'=0$.⁶ We agree excellently with the recent result of Shibuya et al.,³⁰ $(6.9 \pm 0.7) \times 10^{-11} \text{ cm}^3 \text{ molecule}^{-1} \text{ s}^{-1}$, and also quite well with early measurements by Callear and Wood,³ 8.0×10^{-11} , Young and St. John,² 7.0×10^{-11} , Hill et al.,⁵ 7.5×10^{-11} , and Piper³¹ at 196 K $(9 \pm 2) \times 10^{-11}$. Mandel and Ewing's³² rate coefficient, 4.3×10^{-11} , appears to be discordant with the rest of the literature. All the above rate coefficients are in units of $\text{cm}^3 \text{ molecule}^{-1} \text{ s}^{-1}$. All measurements excepting Dreyer and Perner's used tracer techniques, and were not state specific. As we have pointed out, however, our measurements indicate that the quenching of $N_2(A)$ by NO does not appear to show a strong dependence on the $N_2(A)$ vibrational level. Callear and Wood³ also reached this conclusion when they attempted to relax $N_2(A)$ vibration with large additions of helium to their flash photolysis system.

B. The Excitation of $NO(A^2\Sigma^+, v'=0)$ by $N_2(A^3\Sigma_u^+, v'=0)$

We have determined the rate coefficient for excitation of $NO(A^2\Sigma^+, v'=0)$ by measuring the increase in the intensity of several bands originating from $NO(A, v'=0)$ as a function of added NO number density but for constant $N_2(A)$ number density. If we note that the $N_2(A)$ number density is the intensity of

the Vegard-Kaplan bands divided by the Einstein coefficient³³ for spontaneous radiation, we can rearrange Eq. (5) to give the working equation for our analysis

$$I_{\text{NO}^*} = k_{1a} \frac{I_{\text{VK}}}{A_{\text{VK}}} [\text{NO}] \quad (14)$$

One convenient feature of this analysis is that the absolute calibrations for photon-emission rate measurements of the two intensities cancel and only the relative spectral response is important. Thus the intensity measurements do not introduce significant potential sources of systematic error. In practice, we determined total Vegard-Kaplan intensity from a spectral fit to the whole band system. We then measured the change in the peak intensity of one of the bands of NO(A) as a function of added NO number density, being careful to keep added NO number densities below the range giving significant N₂(A) quenching. Multiplying the peak intensity by a correction factor gave the total integrated intensity under that specific band. Dividing the integrated intensity by the appropriate branching ratio which we reported elsewhere³⁴ determined the total emission from NO(A). We observed the 0,1, 0,4 and 0,5 γ -bands. Under our experimental resolution, the 1,5 and 1,6 bands overlap the 0,4 and 0,5 γ -bands and thus contribute to the observed emission intensity. We subtracted out this small contribution from our data. All three of the observed γ -bands gave excitation rate coefficients which were identical within experimental error.

Figure 5 shows that the intensity of the 0,1 band increases linearly with added NO number density in accord with Eq. (9). A number of such experiments yielded a rate coefficient for exciting NO(A, v'=0) by N₂(A, v'=0) of $(9.0 \pm 2.7) \times 10^{-11} \text{ cm}^3 \text{ molecule}^{-1} \text{ s}^{-1}$, where the error bars represent the

total estimated statistical and systematic error. The major contribution to the uncertainty is in the 20 percent uncertainty quoted for the $N_2(A)$ Einstein coefficient.³³ Variations of greater than a factor of five in pressure, and of more than an order of magnitude in $N_2(A)$ number density gave consistent results. We also varied the distance between the NO injector and the observation region to insure that the NO was fully mixed. In addition, using $Xe^* + N_2$ as the $N_2(A)$ source, and using several different NO/Ar gas mixtures did not change the results.

Relatively high resolution scans over the 0,6 and 1,7 bands as a function of pressure between 0.4 and 10 Torr showed that the ratio of $NO(A, v'=1)$ to $NO(A, v'=0)$ excitation by $N_2(A, v'=0)$ was 0.094 ± 0.006 , Figure 6, and that this ratio was independent of pressure. Spectral scans between 200 and 400 nm indicated that excitation of $NO(A, v'=2)$ and $NO(B, v'=0)$ were both $\lesssim 0.003$ as compared to $NO(A, v'=0)$. Thus the total rate coefficient for NO excitation by $N_2(A, v'=0)$ is $(10 \pm 3) \times 10^{-11} \text{ cm}^3 \text{ molecule}^{-1} \text{ s}^{-1}$.

C. State-to-State Excitation of $NO(A, v'=0,1,2)$ by $N_2(A, v'=0,1,2)$

We scanned a number of spectra of the NO γ -bands and N_2 Vegard-Kaplan bands with fixed NO number density but with varying CF_4 number density, and thus varying $N_2(A)$ vibrational distribution (Figures 7 and 8). The total $N_2(A)$ number density changed little over the series of experiments, but the vibrational distribution changed from one in which more than half of the $N_2(A)$ was vibrationally excited to one in which well over 80 percent of the $N_2(A)$ was in $v'=0$. These measurements therefore tracked how the $NO(A)$ vibrational distribution changed with changes in $N_2(A)$ vibrational distribution. We can express the observed intensity of a given $NO(A)$ vibrational level by Eq (10),

$$I_{NO^*v} = \{k_{0v} [N_2A]_0 + k_{1v} [N_2A]_1 + k_{2v} [N_2A]_2\} [NO], \quad (10)$$

where the subscripts on the k 's represent the vibrational level of the $N_2(A)$ and $NO(A)$ respectively. CF_4 vibrationally relaxes $N_2(A)$ in $\Delta v=1$ transitions, and relaxes $v' > 2$ much more efficiently than it does $v'=1$.²⁰ Thus for small CF_4 additions, the $v'=1$ number density stays relatively constant, and primarily $v' > 2$ is quenched. For example, while the fraction of total $N_2(A)$ in $v' > 2$ drops from 0.20 to <0.05 , the fraction in $v'=1$ changes from 0.34 to 0.31. For moderate to high amounts of vibrational relaxation, therefore, only $N_2(A)$ $v'=0$ and 1 remain in the reactor and further relaxation beyond that point changes only the ratio of $v'=1/v'=0$; thus Eq. (10) can be simplified and rearranged to give,

$$\frac{I_{NO^*v}}{[N_2A]_0} = \left\{ k_{0v} + k_{1v} \frac{[N_2A]_1}{[N_2A]_0} \right\} [NO] . \quad (11)$$

The ratio of the slope to intercept of the linear plot implied by Eq. (11) will give the ratio of the rate coefficients k_{1v}/k_{0v} . Figure 9 shows that this linear relationship does indeed obtain for $NO(A, v=0)$.

Using the results for $v'=1$ excitation derived from the moderate-to-high relaxation data, we can subtract out the contribution to observed excitation from $v'=1$ for the data showing little relaxation and thereby probe contributions from $v' > 2$. A small amount of $N_2(A)$, $v'=3$ was observed in our reactor in the absence of CF_4 ($<4\%$ of total $N_2(A)$), but we observed no emission from higher levels under the conditions of these experiments. With the addition of CF_4 , the ratio of $v'=3$ to $v'=2$ was less than 0.1. Thus the relatively unrelaxed measurements probe only $v'=2$. The working equation is

$$\frac{I_{NO^*v}}{[N_2A]_0} - k_{1v} \frac{[N_2A]_1}{[N_2A]_0} [NO] = \left\{ k_{0v} + k_{2v} \frac{[N_2A]_2}{[N_2A]_0} \right\} [NO] . \quad (12)$$

Figure 10 shows the linear relationship implied by this equation for NO(A, $v'=1$). The ratio of the slope to intercept from this plot and a similar one for NO(A, $v'=0$) gives the ratio k_{2v}/k_{0v} . Because excitation of NO(A, $v'=2$) and NO(B, $v'=0$) were such minor channels, we only estimated their contributions to the total excitation by measuring the integrated intensity under the 2,0 gamma band and the 0,7 beta band in several spectra in which the $N_2(A)$ was vibrationally excited and several more in which it was relaxed. Thus we report only an excitation rate coefficient for excited and unexcited $N_2(A)$ for these two states. Table 1 lists the relative excitation rate coefficients for the state-to-state excitation of NO(A, $v'=0,1,2$) and NO(B, $v'=0$) by $N_2(A, v'=0,1,2)$.

IV. DISCUSSION

If the energy transfer between $N_2(A)$ and NO proceeds only through exit channels of radiating NO states, then the rate coefficients for $N_2(A, v'=0)$ quenching by NO ($6.6 \pm 1.0 \times 10^{-11} \text{ cm}^3 \text{ molecule}^{-1} \text{ s}^{-1}$) and for NO(A,B) excitation by $N_2(A, v'=0)$ ($10 \pm 3 \times 10^{-11} \text{ cm}^3 \text{ molecule}^{-1} \text{ s}^{-1}$) ought to be the same. We are therefore somewhat disturbed by the lack of congruency between the two measurements, even though they do overlap slightly at the extreme limits of their respective error bars. We have cross checked our data very carefully, and varied the experimental conditions over a wide range, thereby hoping to find systematic trends which might explain the discrepancy. We have been unable to find any. Our conclusion, therefore, is that the Einstein coefficient for the $N_2(A-X)$ transition is in error by about 30 percent (it should be smaller).

The experimental determination of lifetimes on the order of 2 seconds is extremely difficult and fraught with manifold uncertainties. The accepted

value of the Einstein coefficient for the $N_2(A-X)$ transition rests upon absorption measurements by Shemansky in the vacuum ultraviolet³³ and his reanalysis³⁵ of Carleton and Oldenberg's absorption measurements of $N_2(A)$ in a discharge.³⁶ His analysis requires a long extrapolation of the transition-moment function with r -centroid from the region encompassed by his absorption measurements into the region of r -centroid sampled by the strong transitions from the $v'=0$ level. He tied this extrapolation to the lifetime for the $v'=0$ level derived from the Carleton and Oldenberg reanalysis. Carleton and Oldenberg³⁶ attempted to measure simultaneously the absolute photon-emission rate of the 0,6 Vegard-Kaplan band and the absolute number density $v'=0$ level of the A state via resonance absorption on the 1,0 transition of the first-positive system ($N_2 B-A$). Assuming that the experimental observations of Carleton and Oldenberg are accurate, and that Shemansky's re-analysis of their observations is correct, then their derived lifetime for $N_2(A, v'=0)$ depends directly upon the accuracy of the lifetime of the $v'=1$ level of $N_2(B)$. While the recent lifetime measurements of Eyler and Pipkin³⁷ on the radiative lifetimes of $N_2(B, v'=5-12)$ indicate that the transition probabilities of the first-positive system given by Shemansky³⁸ are essentially correct for $v' \gtrsim 3$, we do not feel confident that Shemansky's transition probabilities for the three lowest levels are necessarily accurate. The transition probabilities for these three levels depend predominantly upon an extrapolation of the electronic transition-moment function which Shemansky derived from relative intensity measurements of bands with r -centroid values between 1.35 and 1.6 Å out to r -centroid values as small as 1.0. This is generally a risky procedure. The recent ab initio calculations of the transition-moment function by Werner et al.,³⁹ Yeager and McKoy⁴⁰ and Weiner and Öhrn⁴¹ all show a much

slower increase in the transition moment to smaller r -centroid than is given by Shemansky's extrapolation. The lifetimes Werner et al.,³⁹ calculated from their transition-moment function, are consistently 16 percent larger than the lifetimes measured by Eyler and Pipkin,³⁷ but the relative variation of their calculated lifetimes with vibrational level matches that of Eyler and Pipkin quite well. They also match the relative variation in the lifetimes measured by Jeunehomme,⁴² and by Carlson et al.⁴³ and those calculated from Shemansky's transition probabilities for $v' > 4$. They deviate markedly from the experimental results, however, for the lowest vibrational levels, with the calculated lifetimes of Werner et al., being somewhat longer. If we reduce the calculated lifetimes of Werner et al., by 16 percent to make them coincide with Eyler and Pipkin's measurements for the high vibrational levels, we obtain a lifetime for $v'=1$ of $N_2(B)$ of $9.5 \mu s$ in contrast to the value of $7.8 \mu s$ which results from Shemansky's transition probabilities. This large a change in the lifetime of the B state will reduce the transition probability for $N_2(A, v'=0)$ from Carleton and Oldenberg's experiment by 20 percent. This reduction would then bring our quenching- and excitation-rate measurements into reasonable agreement. Taking the ab initio transition probabilities at face value would result in a Vegard-Kaplan transition probability about 40 percent smaller than the currently accepted values, and would bring our two measurements into almost perfect congruence. The other theoretical treatments agree with Werner et al.'s calculations. The lifetime of $N_2(B, v'=0)$ measured by Heidner et al.⁴⁴ via resonance fluorescence is also somewhat larger than given by Shemansky's extrapolation.

A reduction in the transition probability of the $N_2(A)$ state on the order of 20 to 30 percent would still give a variation in the absolute transition

moment of the A-X transition fully consistent with the absolute measurements of Shemansky that sampled smaller values of the r-centroid, and the relative transition-moment measurements of Broadfoot and Maran⁴⁵ which sampled larger r-centroid values, those sensitive to the Vegard-Kaplan transitions from $v'=0$. Clearly, this issue needs further investigation.

Our measurements on the vibrational-level dependence of NO excitation by $N_2(A)$ show that $N_2(A, v'=1)$ excites NO(A,B) about 25 percent more efficiently than does $N_2(A, v'=0)$. $N_2(A, v'=2)$ however, is somewhat less efficient at exciting NO transitions. The reduction in observed intensity of NO(A,B) from excitation by $N_2(A, v'=2)$ could result from one of three possibilities. First, the quenching efficiency could be smaller. Second, the more highly excited $N_2(A)$ can access higher lying levels of NO(A,B) which might be collisionally coupled into other states of NO which do not radiate or emit outside our spectral bandpass, such as the $b^4\Sigma^-$ or $a^4\Pi$ states. The third possibility is that some of the encounters between $N_2(A, v'=2)$ and NO end up dissociating the NO. Only vibrational levels of $N_2(A)$ greater than or equal to two have sufficient energy to dissociate the NO. We have not yet attempted to look for atom production from this interaction, but such measurements would confirm this possibility.

The difference between the excitation rates of $N_2(A, v'=1)$ and $N_2(A, v'=0)$ is not sufficiently great for us to observe significant changes in decay-rate measurements involving vibrationally excited and unexcited $N_2(A)$. Given a typical $v'=1/v'=0$ ratio of 0.6, we compute that the effective decay rate would increase by only 10 percent when both $N_2(A)$ vibrational levels were present. Within experiment error, this small enhancement is consistent with our observations.

In order to investigate more completely the energy disposal in the reaction, we scanned the 0,6 and 1,7 bands of NO(A-X) under moderate resolution ($\Delta\lambda \approx 0.20$ nm) at pressures between 0.4 and 9 torr. This resolution was adequate to resolve partially the rotational structure. We then adjusted rotational temperatures in our fitting program until we could match our observations. At 0.4 torr, Boltzmann rotational temperatures of 1400 K and 800 K fit the emission from $v'=0$ and 1 respectively quite well. At higher pressures, however, the band contours were decidedly non-Boltzmann. Collisions with the argon bath gas relaxed the lower rotational levels much more efficiently than they did the higher rotational levels. For example, at 4.0 torr a rotational temperature of 600 K fit region around the heads of the 0,6 band quite well, while the high rotational levels in which are prominent the short-wavelength tail of the band followed an 1100 K Boltzmann distribution. Assuming a hard-sphere model with a 40\AA^2 collision cross section, we calculate that an excited NO molecule will experience 1.5 collisions during a radiative lifetime at 1 torr. Thus at 0.4 torr most of the NO(A) molecules will not experience a collision prior to radiation, whereas at 4 torr they will experience an average of six collisions. Thus the rotational relaxation of NO(A) by Ar is a relatively efficient process, requiring only a few collisions to remove most of the rotational energy. The efficient rotational relaxation of low J levels of NO(A) by argon and the correspondingly much smaller efficiency for high-J level relaxation has been studied in some detail by Ebata et al.⁴⁶

The efficient transfer of vibronic energy from $N_2(A)$ to NO may occur by a Franck-Condon type of mechanism. Deperasinska et al.⁴⁷ have calculated Franck-Condon factors for the transitions relevant to the transfer of energy from $N_2(A, v'=0)$ to NO. The Franck-Condon factors for producing NO(A) are

three orders of magnitude greater than those for producing NO(B), which they claim is reflected in the much smaller efficiency for producing NO(B) relative to NO(A). Their calculated Franck-Condon factors, however, would predict roughly equal probabilities for producing vibrational levels $v'=0$ and 1 of NO(A). In contrast, our observations show that NO(A, $v'=0$) is produced ten times more efficiently than NO(A, $v'=1$). They have not performed the relevant Franck-Condon calculations for $N_2(A, v'=1, 2)$.

The kinetics of the $N_2(A) + NO$ energy transfer have been studied by several other investigators. Callear and Wood³ estimated rate coefficient ratios from their work of $k_{01}/k_{00} = 0.105$ in reasonable agreement with our value of 0.094 ± 0.006 and $k_{11}/k_{10} = 0.53$ in disagreement with our value of 0.20 ± 0.03 . Clark and Setser¹ determined a population ratio for NO(A, $v'=0, 1, 2$) of 1.0:0.15:0.014 respectively from excitation by $N_2(A)$ with the ratio $v'=1/v'=0$ of 0.61. With the same $N_2(A)$ vibrational distribution, we calculate an NO(A) vibrational distribution from our excitation rate coefficients of 1.0:0.14:0.011 respectively, in excellent agreement with Clark and Setser's observations. More recently Golde and Moyle⁴⁸ have measured vibrational distributions of NO(A) from $N_2(A)$ excitation of 1.00:0.083:0.002 for excitation by $N_2(A, v'=0)$ and 1.00:0.17:0.025 for excitation by $N_2(A)$ with a vibrational distribution of 1.00:0.48:0.19:0.14 for $v'=0-3$ respectively. Our rate coefficients would predict an NO(A) vibrational distribution of 1.00:0.19:0.013 given the same initial $N_2(A)$ vibrational distribution. In order to make this comparison, we assumed $v'=2$ and $v'=3$ had the same excitation rates. Golde and Moyle's data show a seven percent decrease in total NO(A) intensity for the vibrationally excited case whereas our results would indicate that the intensities of the NO(A) produced from vibrationally excited

and unexcited $N_2(A)$ would be within 2 percent of each other. Our error limits encompass a range from a six percent decrease in intensity to a three percent increase with some additional uncertainty added by our having treated $N_2(A)$ vibrational levels 2 and 3 the same. They are therefore fully consistent with Golde and Moyle's result.

ACKNOWLEDGEMENT

We appreciate partial support for this work from the Air Force Weapons Laboratories under Contract No. F29601-84-C-0076 and from the Air Force Geophysics Laboratories under Contract No. F19628-82-C-0050. The comments and advice of Dave Green and George Caledonia of PSI aided us greatly.

REFERENCES

1. W.G. Clark and D.W. Setser, J. Phys. Chem. 84, 2225 (1980).
2. R.A. Young and G.A. St. John, J. Chem. Phys. 48, 898 (1968).
3. A.B. Callear and P.M. Wood, Trans. Faraday Soc. 67, 272 (1971).
4. W.T. Rawlins, L.G. Piper, G.E. Caledonia, and B.D. Green, Physical Sciences Inc. Technical Report TR-298 (1981). Available from the authors upon request.
5. R.M. Hill, R.A. Gutcheck, D.L. Huestis, K. Mukherjee, and D.C. Lorents, SRI Report No. MP74-39 under ARPA Contract No. N00014-72-C-0478 (1974).
6. J.W. Dreyer, D. Perner, and C.R. Roy, J. Chem. Phys. 61, 3164 (1974).
7. L.G. Piper, G.E. Caledonia, and J.P. Kennealy, J. Chem. Phys. 74, 2888 (1981).
8. W.T. Rawlins, and L.G. Piper, Proc. Soc. Photo. Opt. Instr. Eng. 279, 58 (1981).
9. L.G. Piper, W.J. Marinelli, W.T. Rawlins, and B.D. Green, J. Chem. Phys. 83, 5602 (1985).
10. L.G. Piper and W.T. Rawlins, J. Phys. Chem. 90, 320 (1986).
11. R.H. Krech, G.J. Diebold, and D.L. McFadden, J. Am. Chem. Soc. 99, 4605 (1977).
12. R.H. Krech, Masters dissertation, Dept. of Chem., Boston College, 1976.
13. M. Kaufman and C.E. Kolb, NR 092-531, 8 (1971).
14. H.C. Berg and D. Kleppner, Rev. Sci. Instrum. 33, 248 (1962).
15. D.W. Setser, D.H. Stedman, and J.A. Coxon, J. Chem. Phys. 53, 1004 (1970).
16. Stedman, D. H. and Setser, D. W., Chem. Phys. Lett. 2, 542 (1968).
17. N. Sadeghi and D.W. Setser, Chem. Phys. Lett. 82, 44 (1981).
18. J.M. Thomas and F. Kaufman, Photochemistry Symposium, Harvard University, August (1984).
19. M.F. Golde, Chem. Phys. Lett. 31, 348 (1975).

20. J.M. Thomas, J.B. Jeffries, and F. Kaufman, Chem. Phys. Lett. 102, 50 (1983).
21. L.G. Piper, G.E. Caledonia, and J.P. Kennealy, J. Chem. Phys. 75, 2847 (1981).
22. E.E. Ferguson, F.C. Fehsenfeld, and A.L. Schmeltekopf, Advances in Atomic and Molecular Physics V, edited by D. R. Bates, New York, Academic Press, (1970).
23. R.C. Bolden, R.S. Hemsworth, M.J. Shaw, and N.D. Twiddy, J. Phys. B 3, 45 (1970).
24. A.L. Farragher, Trans. Faraday Soc. 66, 1411 (1970).
25. R.W. Huggins, and J.H. Cahn, J. Appl. Phys. 38, 180 (1967).
26. R.E. Walker, Phys. Fluids 4, 1211 (1961).
27. R.V. Poirier and R.W. Carr, J. Phys. Chem. 75, 1593 (1971).
28. M. Cher and C.S. Hollingsworth, Adv. Chem. Ser. 80, 118 (1969).
29. J.H. Kolts and D.W. Setser, J. Chem. Phys. 68, 4848 (1978).
30. K. Shibuya, T. Imajo, K. Obi, and I. Tanka, J. Phys. Chem. 88, 1457 (1984).
31. L.G. Piper, Kansas State Univ. (1972). The results are reported in W.G. Clark and D.W. Setser, J. Phys. Chem. 84, 2225 (1980).
32. A. Mandel and J.J. Ewing, J. Chem. Phys. 67, 3490 (1977).
33. D.E. Shemansky, J. Chem. Phys. 51, 689 (1969).
34. L.G. Piper and L.M. Cowles, J. Chem. Phys. 85, xxxx (1986).
35. D.E. Shemansky and N.P. Carleton, J. Chem. Phys. 51, 682 (1969).
36. N.P. Carleton and O. Oldenberg, J. Chem. Phys. 36, 3460 (1967).
37. E.E. Eyler and F.M. Pipkin, J. Chem. Phys. 79, 3654 (1983).
38. D.E. Shemansky and A.L. Broadfoot, J. Quant. Spectrosc. Radiat. Transfer 11, 1335 (1971).
39. H.J. Werner, J. Kalcher, and E.A. Reinsch, J. Chem. Phys. 81, 2420 (1984).
40. D.L. Yeager and V. McKoy, J. Chem. Phys. 67, 2473 (1977).

41. B. Weiner and Y. Öhrn, J. Chem. Phys. 80, 5866 (1984).
42. M. Jeunehomme, J. Chem. Phys. 45, 1805 (1966).
43. T.A. Carlson, N. Duric, P. Erman, and M. Larsson, Physica Scripta 19, 25 (1979).
44. R.F. Heidner III, D.G. Sutton, and S.N. Suchard, Chem. Phys. Lett. 37, 243 (1976).
45. A.L. Broadfoot and S.P. Maran, J. Chem. Phys. 51, 678 (1969).
46. T. Ebata, Y. Anezaki, M. Fujii, and N. Mikami, and M. Ito, Chem. Phys. 84, 151 (1984).
47. I. Deperasinka, J.A. Beswick, and A. Tramer, J. Chem. Phys. 71, 2477 (1979).
48. M.F. Golde and A.M. Moyle, Chem. Phys. Lett. 117, 375 (1985).

Table 1. State-to-State Relative Excitation-Rate Coefficients

N ₂ (A) v'	NO(A) v' =			NO(B, v' = 0)
	0	1	2	
0	1*	0.094 ± 0.006	0.003	0.0032 ± 0.0007
1	1.11 ± 0.07	0.22 ± 0.03	0.024	0.033 ± 0.007
2	0.29 ± 0.07	0.32 ± 0.03		
*1 = 9.0 x 10 ⁻¹¹ cm ³ molecule ⁻¹ s ⁻¹				

- Figure 1. Flow tube apparatus configured for $N_2(A)$ decay kinetics measurements.
- Figure 2. Vegard-Kaplan emission in flow reactor 9 ms downstream from the discharge.
- Figure 3. Decay in the natural log of the $N_2(A, v'=0)$ number density as a function of NO number density at three different reagent mixing distances.
- Figure 4. $N_2(A, v'=0)$ decay constants in NO as a function of reaction time.
- Figure 5. Variation in the peak intensity of the $NO(A-X, 0,1)$ band as a function of added NO number density.
- Figure 6. Ratio in the rate coefficients for exciting $NO(A, v'=1)$ to $NO(A, v'=0)$ by $N_2(A, v'=0)$ as a function of argon pressure.
- Figure 7. Spectrum of $NO(A-X)$ in the absence of CF_4 . The light line shows the experimental data, while the heavy line shows the synthetic best fit to the data.
- Figure 8. Spectrum of $NO(A-X)$ and $N_2(A-X)$ in presence of CF_4 which relaxes most of the $N_2(A)$ vibrational energy. The light line is the experimental data while the heavy line shows the synthetic best fit.
- Figure 9. Excitation of $NO(A, v'=0)$ as a function of the ratio of $N_2(A, v'=1)$ to $N_2(A, v'=0)$.
- Figure 10. Variation in the excitation of $NO(A, v'=1)$ as a function of the ratio of $N_2(a, v'=2)$ to $N_2(A, v'=0)$.

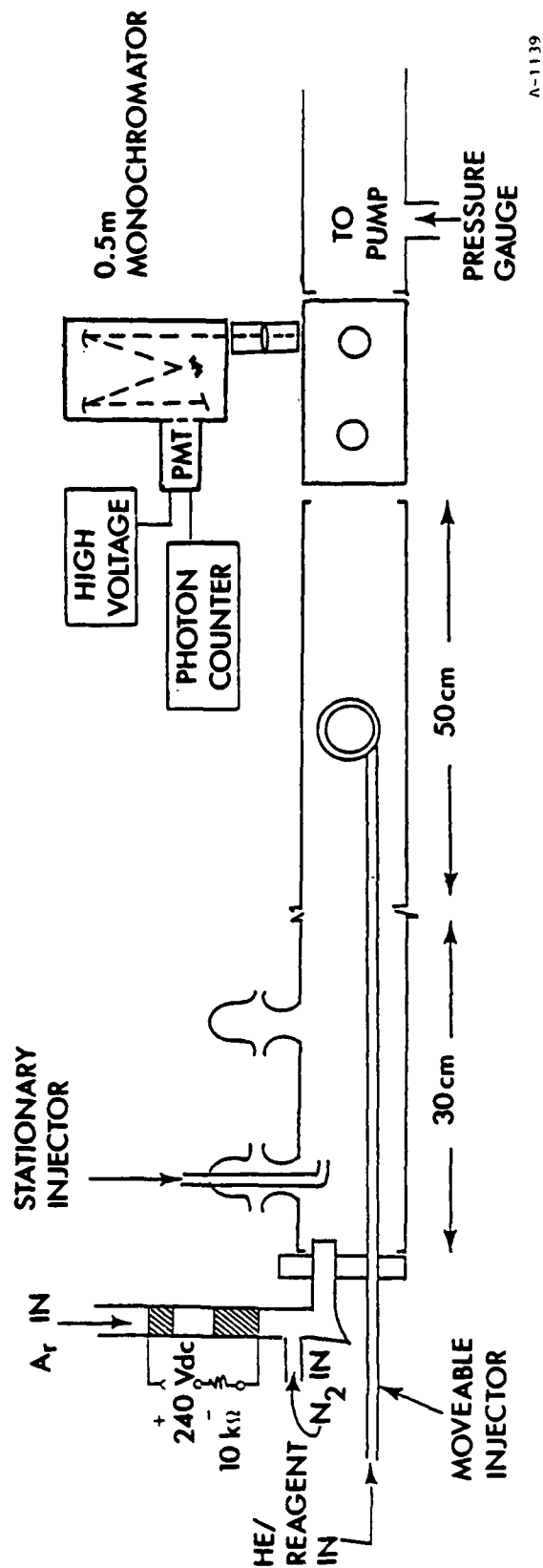


Figure 1. Flow tube apparatus configured for $N_2(A)$ decay kinetics measurements.

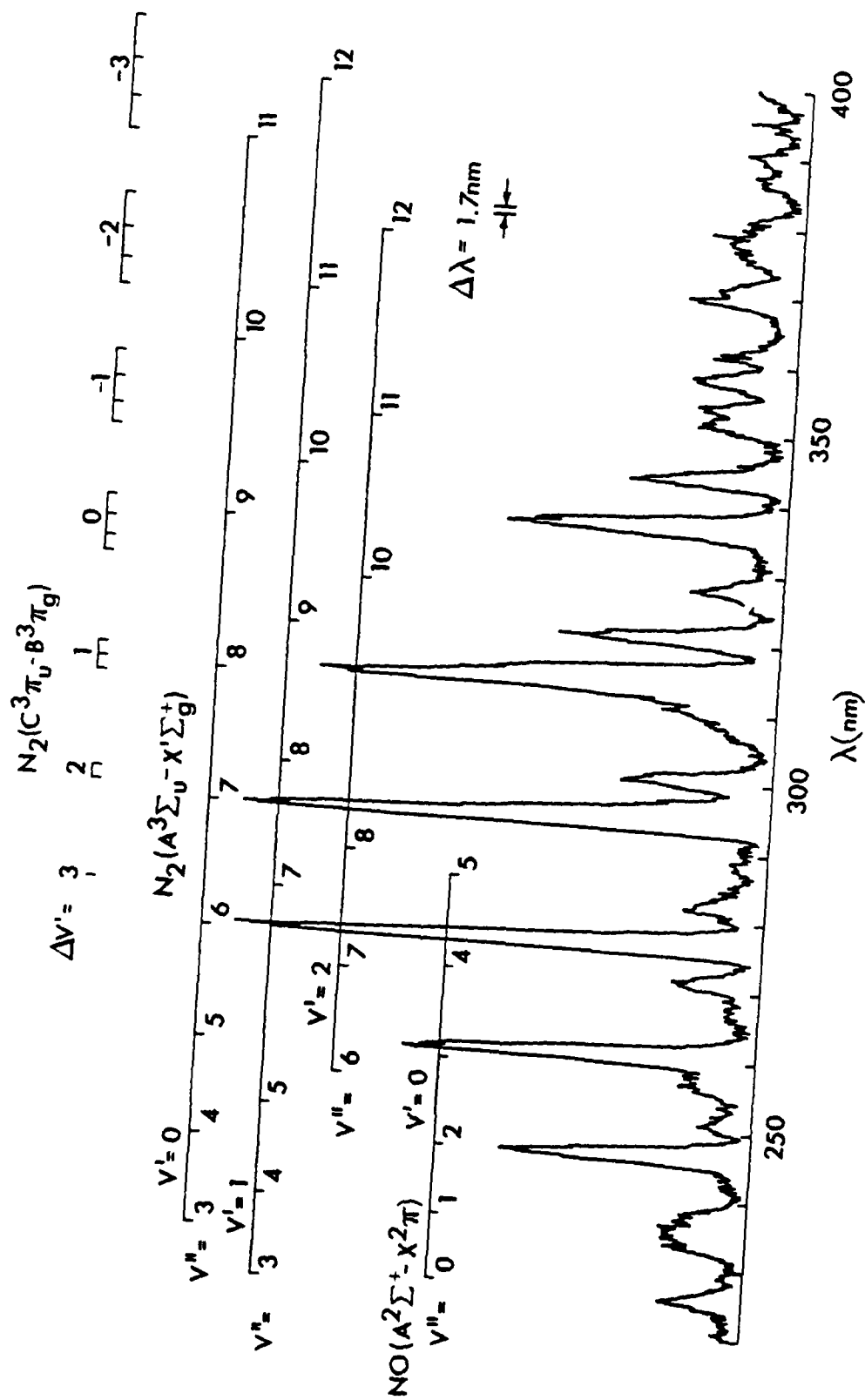
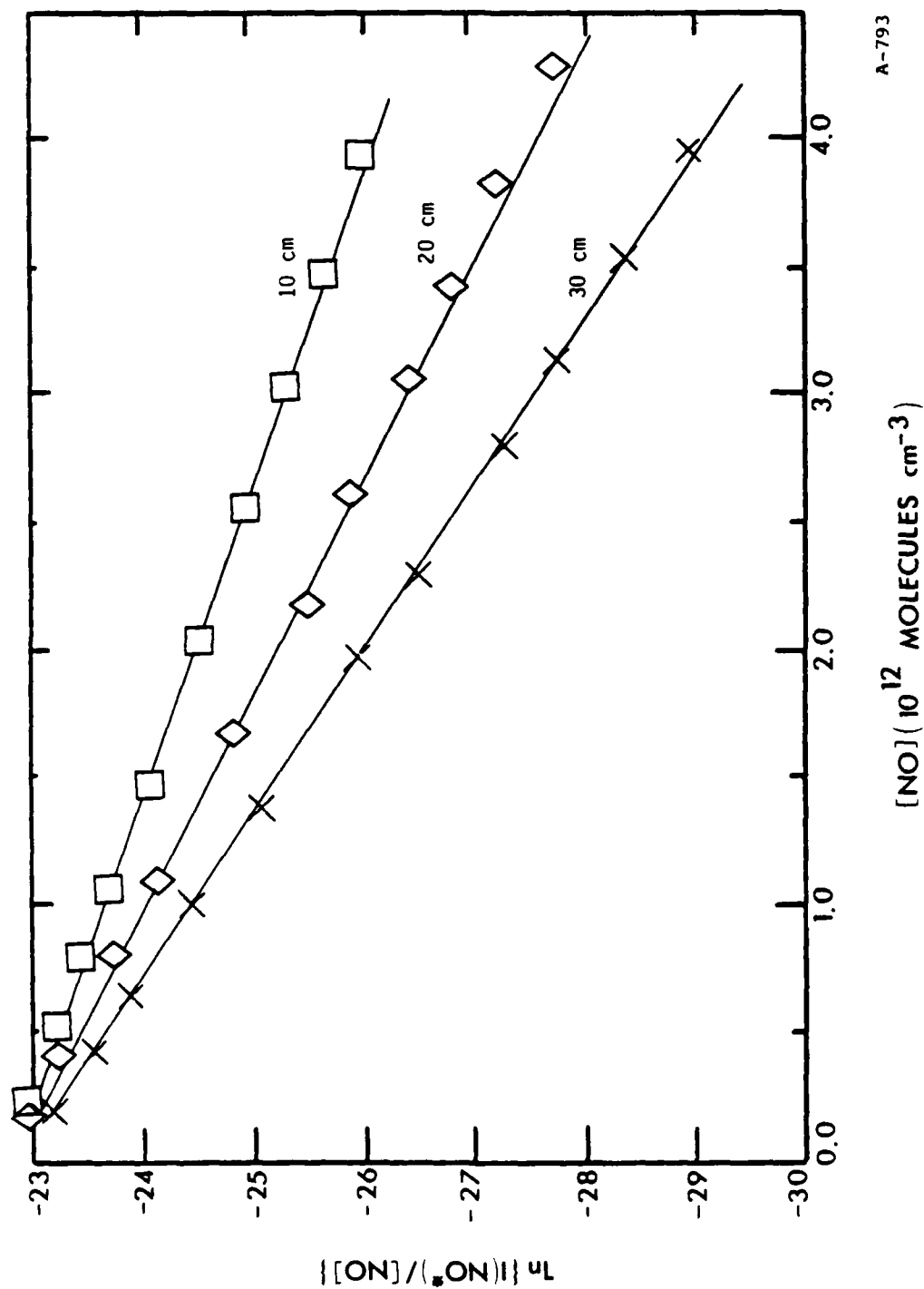


Figure 2. Vegard-Kaplan emission in flow reactor 9 ms downstream from the discharge.

A-1140



A-793

Figure 3. Decay in the natural log of the $N_2(A, v'=0)$ number density as a function of NO number density at three different reagent mixing distances.

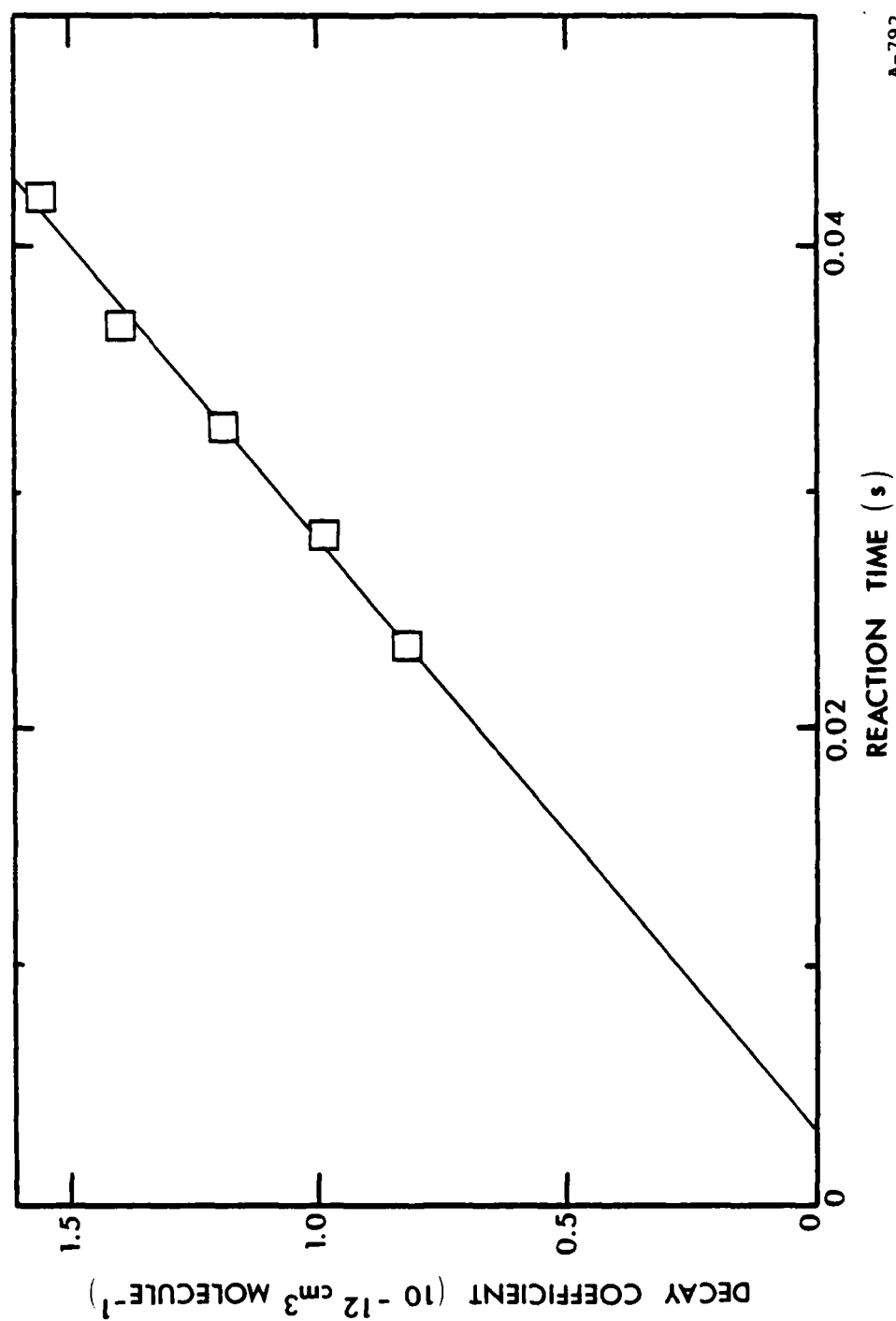
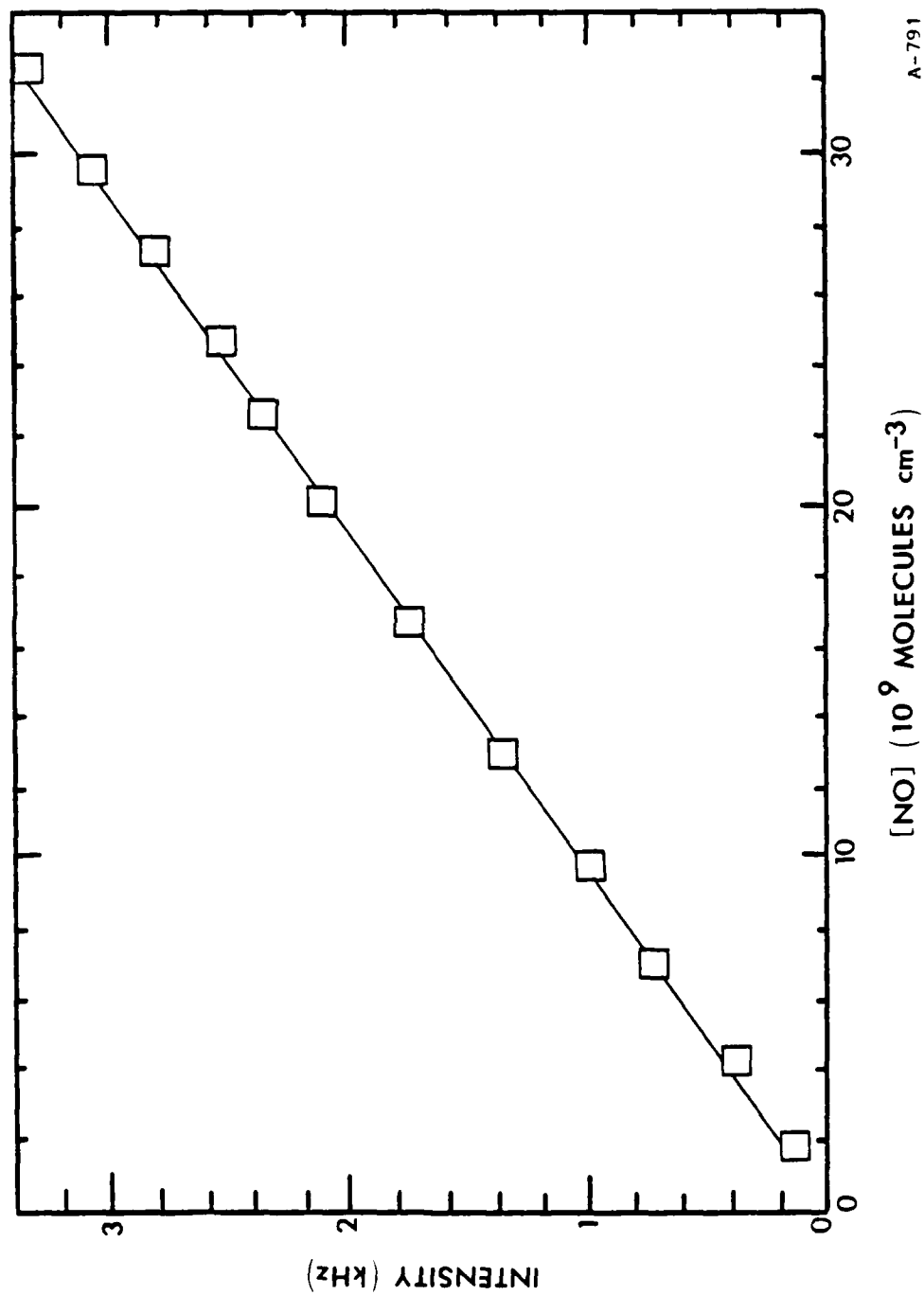


Figure 4. $\text{N}_2(\text{A}, v'=0)$ decay constants in NO as a function of reaction time.



A-791

Figure 5. Variation in the peak intensity of the NO(A-X, 0,1) band as a function of added NO number density.

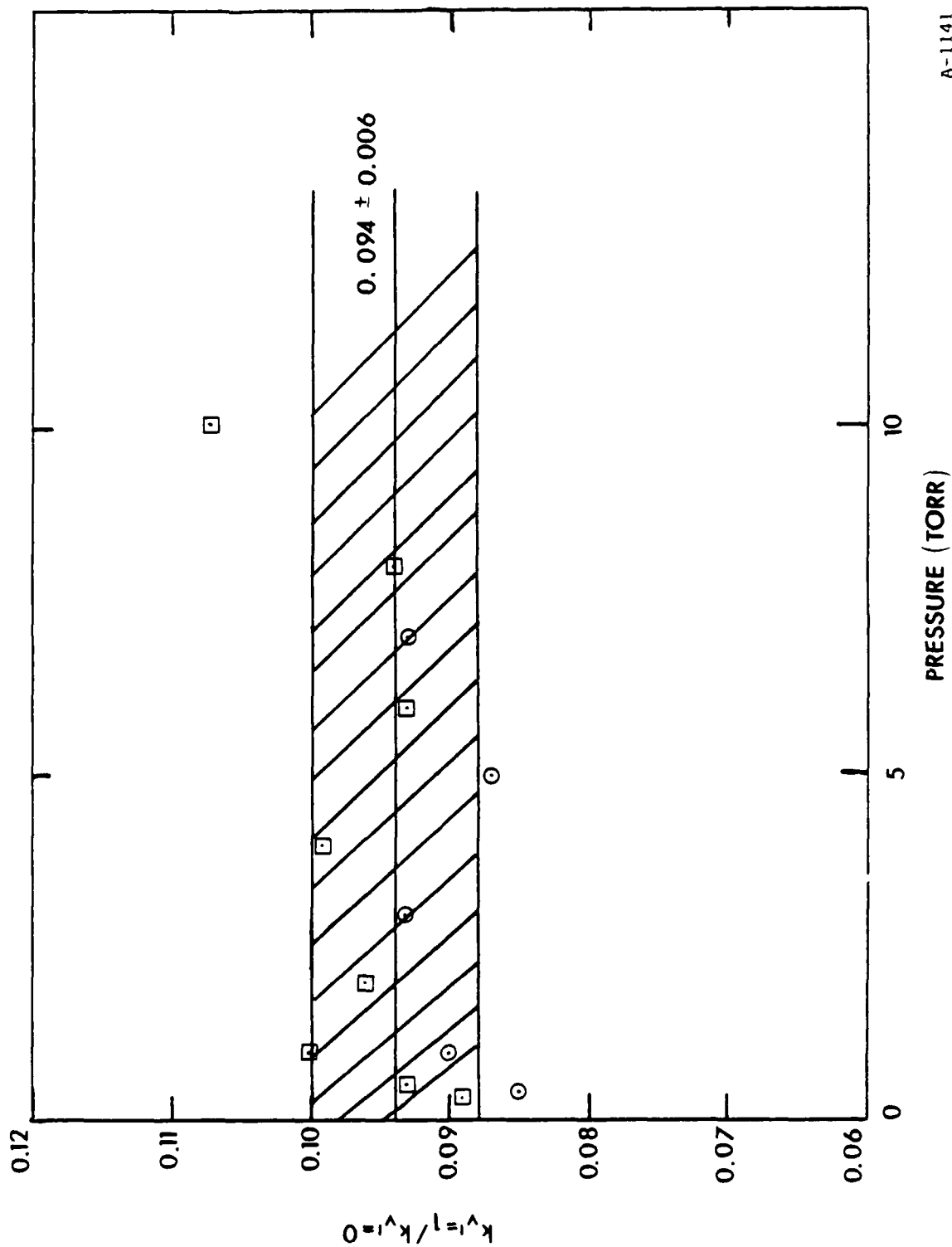


Figure 6. Ratio in the rate coefficients for exciting $\text{NO}(\text{A}, v'=1)$ to $\text{NO}(\text{A}, v'=0)$ by $\text{N}_2(\text{A}, v'=0)$ as a function of argon pressure.

A-1141

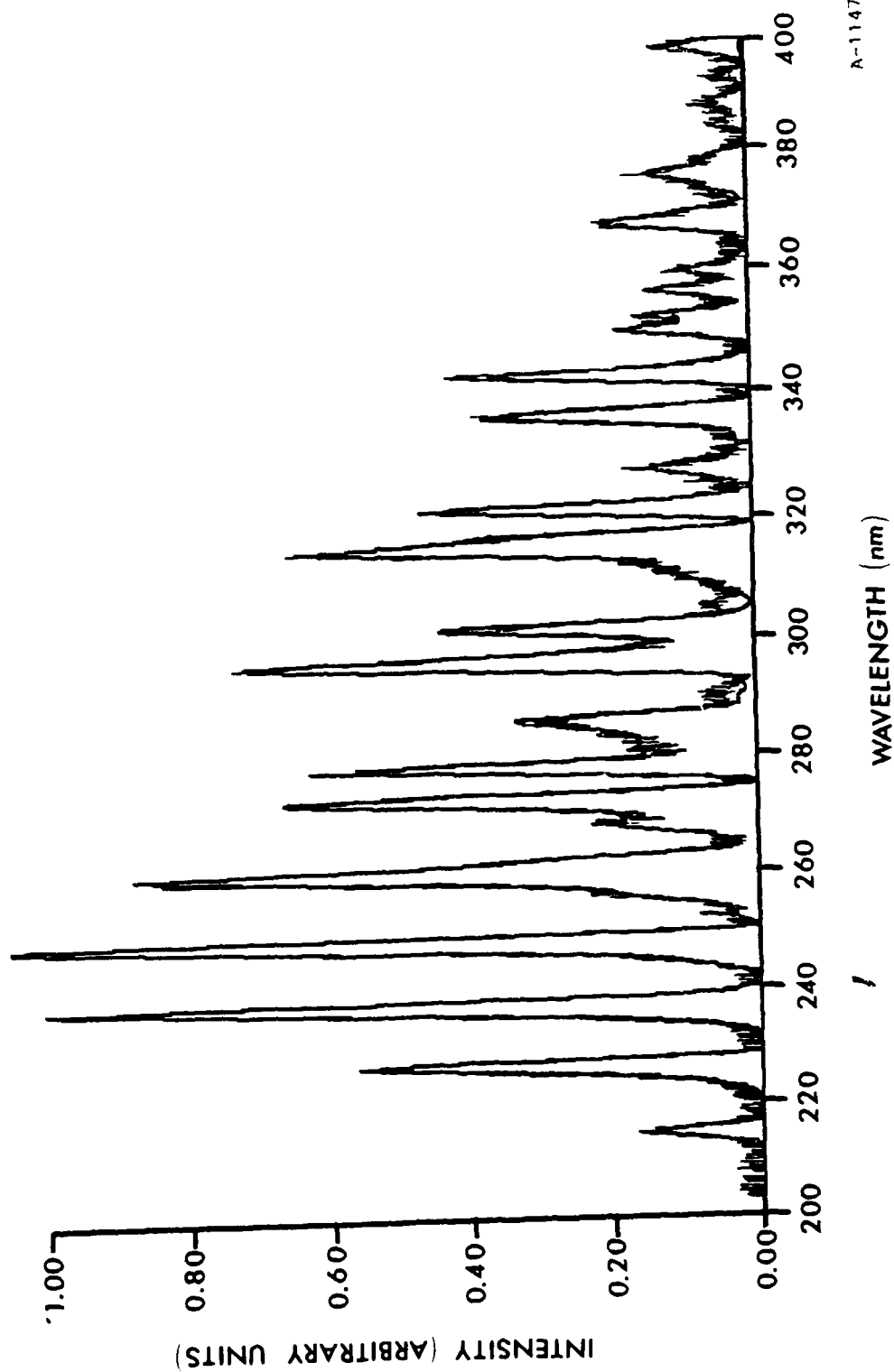


Figure 7. Spectrum of NO(A-X) in the absence of CF_4 . The light line shows the experimental data, while the heavy line shows the synthetic best fit to the data.

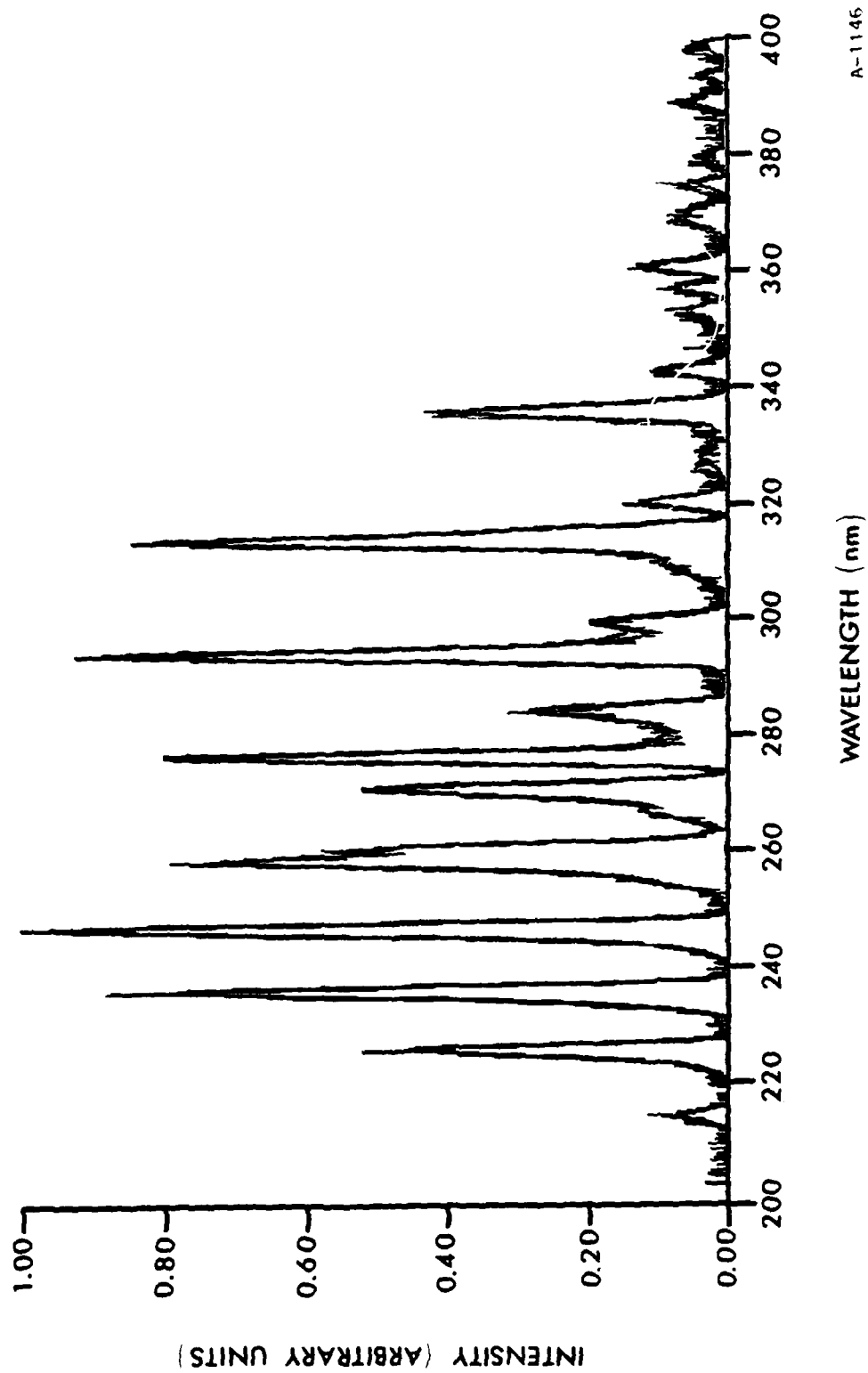


Figure 8. Spectrum of NO(A-X) and $N_2(A-X)$ in presence of CF_4 which relaxes most of the $N_2(A)$ vibrational energy. The light line is the experimental data while the heavy line shows the synthetic best fit.

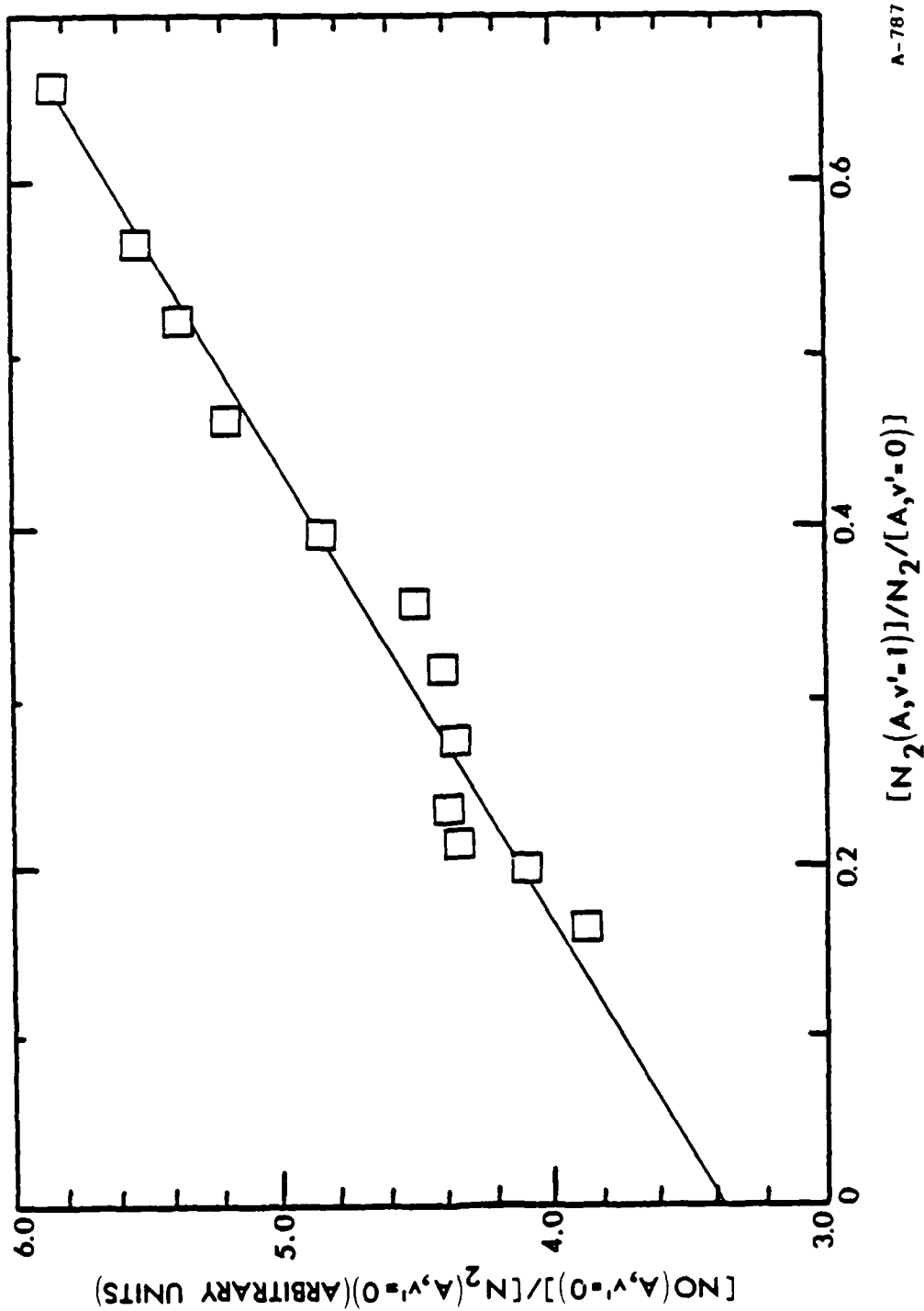
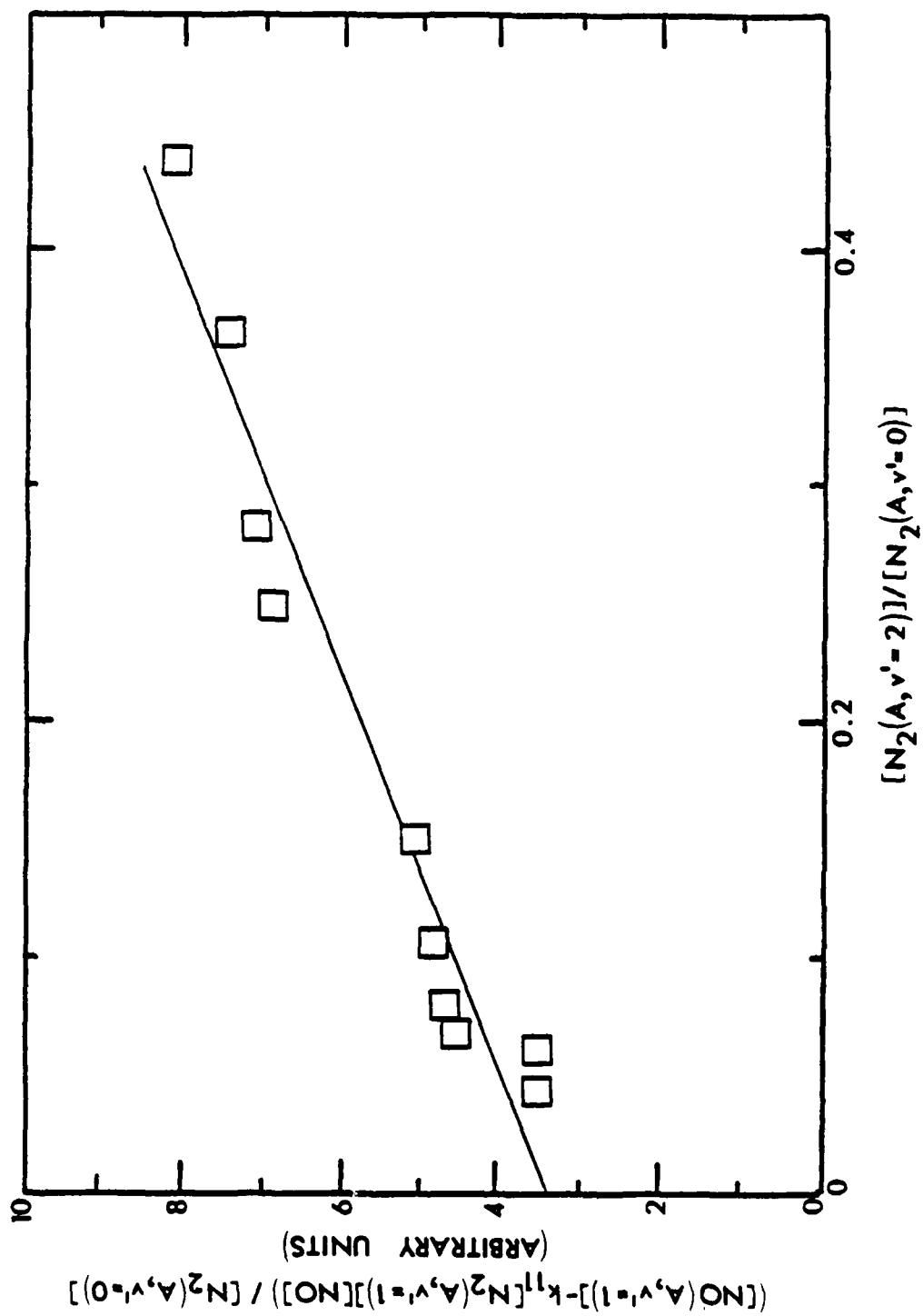


Figure 9. Excitation of $NO(A, v'=0)$ as a function of the ratio of $N_2(A, v'=1)$ to $N_2(A, v'=0)$.

A-787



Λ-789

Figure 10. Variation in the excitation of $NO(A, v'=1)$ as a function of the ratio of $N_2(a, v'=2)$ to $N_2(A, v'=0)$.

APPENDIX G

(SR-282 reproduced in its entirety)

J. Chem. Phys. 88, 231 (1988)

State-to-State $N_2(A^3\Sigma_u^+)$ Energy-Pooling Reactions: I. The Formation
of $N_2(C^3\Pi_u)$ and the Herman Infrared System

Lawrence G. Piper

J. Chem. Phys. 88, 231 (1988)

Physical Sciences Inc.
Research Park, P.O. Box 3100
Andover, MA 01810

ABSTRACT

We have studied the formation of $N_2(C^3\Pi_u, v=0-4)$ and the nitrogen Herman Infrared system, $v'=2,3$, in energy pooling reactions between $N_2(A^3\Sigma_u^+, v'=0-1)$. Our results indicate rate coefficients of (1.5 ± 0.4) and $(1.5\pm0.5) \times 10^{-10} \text{ cm}^3 \text{ molecule}^{-1} \text{ s}^{-1}$ for formation of $N_2(C^3\Pi_u, v'=0-4)$ from the energy pooling of two $N_2(A, v'=0)$ molecules and for a $v'=0$ and a $v'=1$ molecule, respectively. We did not see evidence of significant $N_2(C)$ formation in energy pooling between two $N_2(A, v'=1)$ molecules ($k < 5 \times 10^{-11} \text{ cm}^3 \text{ molecule}^{-1} \text{ s}^{-1}$).

$N_2(A, v'=0)$ energy pooling produces only $v'=3$ of the Herman Infrared system with a rate coefficient of $>(8.1\pm2.3) \times 10^{-11} \text{ cm}^3 \text{ molecule}^{-1} \text{ s}^{-1}$. Energy pooling between $N_2(A, v'=0)$ and $N_2(A, v'=1)$ produces only $v'=2$ of the Herman Infrared system with a rate coefficient $>(9.9\pm2.9) \times 10^{-11} \text{ cm}^3 \text{ molecule}^{-1} \text{ s}^{-1}$. Again, energy pooling between two $N_2(A, v'=1)$ molecules results in no significant contributions to the Herman Infrared system. The participation of $N_2(A)$ vibrational levels >2 , however, does result in excitation of the lower-lying vibrational levels of the Herman Infrared system.

I. Introduction

Stedman and Setser¹ first discovered energy pooling in triplet nitrogen when they observed that the intensity of nitrogen second-positive, $N_2(C^3\Pi_u - B^3\Pi_g)$ emission varied quadratically with the intensity of the Vegard-Kaplan, $N_2(A^3\Sigma_u^+ - X^1\Sigma_g^+)$, emission in their reactor. They estimated the rate coefficient for energy pooling to form $N_2(C^3\Pi_u)$ to be $2.1 \times 10^{-11} \text{ cm}^3 \text{ molecule}^{-1} \text{ s}^{-1}$. In a series of investigations of time-resolved emissions in the afterglow of a pulsed nitrogen discharge, Hays et al.²⁻⁴ studied $N_2(A)$ energy pooling and reported rate coefficients of 2.6×10^{-10} for formation of $N_2(C^3\Pi_u)$,⁴ $0.25 \times 10^{-10} \text{ cm}^3 \text{ molecules}^{-1} \text{ s}^{-1}$ for the formation of $N_2(C^1^3\Pi_u)$, and $1.1 \times 10^{-9} \text{ cm}^3 \text{ molecule}^{-1} \text{ s}^{-1}$ for the formation of $N_2(B^3\Pi_g)$.³ In the case of the latter state, one would have to assume that their number was a lower bound, because their detection system could see only as far as $v'=3$ of the B state. Thus, if significant energy from the pooling reaction flowed into $v'=0-2$, the rate coefficient would be somewhat larger. Subsequent work by Clark and Setser⁵ confirmed a rate coefficient of about $2 \times 10^{-10} \text{ cm}^3 \text{ molecule}^{-1} \text{ s}^{-1}$ for the production of $N_2(C^3\Pi_u)$ from $N_2(A^3\Sigma_u^+)$ energy pooling. They were unable, however, to see any evidence for formation of the $N_2(C^1^3\Pi_u)$ state. Nadler et al.⁶ discovered in 1980 that the Herman Infrared (HIR) system was populated by $N_2(A)$ energy pooling, and showed subsequently that the distribution among the vibrational levels of that state depended strongly upon the vibrational distribution of the $N_2(A)$ state.⁷ They estimated a lower limit for HIR formation⁶ of $2.5 \times 10^{-11} \text{ cm}^3 \text{ molecule}^{-1} \text{ s}^{-1}$ which they have since revised upwards to $7 \times 10^{-11} \text{ cm}^3 \text{ molecule}^{-1} \text{ s}^{-1}$.⁷ They also showed that some production of the B state did indeed occur, but were unable to estimate the rate coefficient for B-state formation because of that state's rapid quenching by nitrogen and argon. Nadler and Rosenwaks⁸ have shown recently that the vibrational distribution of $N_2(C^3\Pi_u)$ formed by energy pooling also changes as a function of the $N_2(A)$ vibrational distribution, but that the total excitation rate of the C state appears to be independent of the vibrational distribution of $N_2(A)$.

Unpublished observations at PSI in the near infrared recorded the HIR system in $N_2(A)$ energy pooling, but failed to detect significant populations of $N_2(B)$.⁹ We could not rationalize, therefore, the magnitude of the pooling rate coefficient which Hays and Oskam reported for $N_2(B)$ production. The work of Nadler et al.^{6,7} also showed convincingly that HIR production had to be similar in magnitude to the production of $N_2(B)$. Thus, the present investigations were motivated in part by our desire to reconcile the conflict between Hays and Oskam's report, and the observations of Nadler et al. and our own. We have investigated energy pooling in some detail and report here vibrational-level-specific rate coefficients for formation of $N_2(C^3\Pi_u, v'=0-4)$ and HIR $v'=2,3$ by $N_2(A^3\Sigma_u^+, v'=0-2)$. Electronic quenching plays an important role in understanding $N_2(B^3\Pi_g)$ formation. A subsequent paper covers both the excitation of $N_2(B)$ in $N_2(A)$ energy pooling as well as the electronic quenching of the B state.

II. Experimental

A. Apparatus

Previous publications have described our 2 in. discharge-flow apparatus and general operating procedures in some detail.¹⁰⁻¹⁶ Thus, we will give only a brief summary here. The studies all involved measuring spectra of the Vegard-Kaplan, first- and second-positive and HIR systems of molecular nitrogen in a flowing afterglow apparatus. The $N_2(A)$ is produced cleanly in the apparatus in the energy transfer reaction between argon or xenon metastables and molecular nitrogen.^{17,18} A hollow-cathode discharge produces the rare gas metastables. We have generally fabricated the electrode from aluminum shim, but for some of the studies here, we used 0.002 thick tantalum shim as the electrode material. The tantalum electrodes gave about 30 percent more metastables and operated better at high pressures. The energy transfer reaction between metastable xenon and nitrogen produces $N_2(B^3\Pi_g, v' < 5)$.¹⁹ This eliminates the possibility of contamination of the results for $N_2(C)$ and the higher vibrational levels of $N_2(B)$ by scattered light from the rare-gas-metastable/nitrogen mixing region which occurs when argon metastables are

used to make $N_2(A)$. The HIR system was studied at relatively high pressures (> 5 torr) with high partial pressures of nitrogen (1 to 2 torr) in the reactor. This procedure virtually eliminated overlapping of the HIR system by the first-positive system. The unfortunate consequence of this procedure, however, was that the high partial pressures of nitrogen relaxed the $N_2(A)$ vibration to > 95 percent $v'=0,1$, and thus the effects of higher vibrational levels could not be studied.

All spectra were fit by a least-squares computer program which determined the populations of all emitting states in the region of spectral coverage. This procedure eliminates the uncertainties introduced by overlapping spectral bands. Because the HIR system is unassigned, one cannot a priori generate a synthetic spectrum for this system. We therefore used experimental spectra taken at high pressures for the basis sets in our synthetic fits. Because $N_2(A, v'=0)$ energy pooling produces only $v'=3$ of the HIR system, a basis set for that state could be generated cleanly. When only $v'=0$ and 1 of $N_2(A)$ are present, only $v'=3$ and 2 of the HIR system are produced. Thus we were able to generate a fitting basis set for $v'=2$ of the HIR system by subtracting out the previously determined $v'=3$ components from a spectrum containing the two levels together. These basis sets were then used in analyzing the spectra containing $N_2(B)$ to eliminate confusion from overlap between the two states.

B. Absolute Photon Emission Rates

The data analysis requires the measurement of absolute photon-emission rates in the reactor (see below). This section details how we calibrate our system for such measurements.

The observed signal is related to the true volume emission rate through

$$I_{\text{obs}} = I_{\text{true}} \frac{\Omega}{4\pi} \eta_{\lambda} T_{\lambda} V \quad (1)$$

where $\frac{\Omega}{4\pi}$ is the effective solid angle subtended by the detection system, η_{λ} is the quantum efficiency of the photomultiplier at the wavelength of interest, T_{λ} is the transmission of the optical system (e.g. mirror reflectivities and

grating efficiency) and V is the observed volume of luminous gas in the reactor. The wavelength dependence of the product $\frac{\Omega}{4\pi} n_{\lambda} T_{\lambda} V$ is given by the relative monochromator response function R_{λ} . Absolute values of that product are obtained in a calibration experiment using the O/NO air afterglow at one or several specific wavelengths. Absolute values at wavelengths other than those chosen for calibration experiments are obtained by scaling with R_{λ} .

The relative spectral response of the monochromator was calibrated between 200 and 800 nm using standard quartz-halogen and D₂ continuum lamps (Optronic Laboratories Inc.). Additional confirmation of the calibration between 400 and 800 nm is obtained by scanning the air afterglow spectrum and comparing observed relative signal levels with the relative intensities given by Fontijn et al.²⁰ The absolute spectral response of the detection system is determined at 580 nm using the O/NO air afterglow as described previously.^{11,13}

When atomic oxygen and nitric oxide are mixed, a continuum emission extending from 375 nm to beyond 3000 nm is observed.²⁰⁻²⁸ The intensity of this emission is directly proportional to the product of the number densities of atomic oxygen and nitric oxide, and independent of pressure of bath gas, at least at pressures above about 0.2 torr.²⁸ Thus, the volume-emission rate of the air afterglow is given by

$$I_{\text{true}} = k_{\lambda} [\text{O}] [\text{NO}] \Delta\lambda \quad (2)$$

where k_{λ} is the air afterglow rate coefficient in units of cm³ molecule⁻¹ s⁻¹ nm⁻¹ and $\Delta\lambda$ is the monochromator band width. Literature values for this rate coefficient span a range of more than a factor of two,²⁰⁻²⁶ but recent studies²⁵ indicate that the original work of Fontijn et al.²⁰ is probably correct at wavelengths shorter than \approx 800 nm. We use a value of 1.25×10^{-19} cm³ molecule⁻¹ s⁻¹ nm⁻¹ at $\lambda = 580$ nm. Combining Eqs. (1) and (2) gives the observed air afterglow intensity:

$$I_{\lambda}^{O/NO} = k_{\lambda} [O][NO] \Delta \lambda \frac{\Omega}{4\pi} \eta_{\lambda} T_{\lambda} V \quad (3)$$

Air afterglow calibration experiments give a calibration factor,

$$\kappa_{\lambda} = \frac{I_{\lambda}^{O/NO}}{[O][NO]} = k_{\lambda} \Delta \lambda \frac{\Omega}{4\pi} \eta_{\lambda} T_{\lambda} V \quad (4)$$

the determination of which we described previously.^{11,13}

Absolute number densities of emitters are obtained by dividing absolute volume emission rates by known transition probabilities. The air afterglow calibration factor κ_{λ} and the moderately well established value of the air afterglow rate coefficient k_{λ} , are used to convert observed emission intensities to volume emission rates:

$$I_{\text{true}} = \frac{I_{\text{obs}} k_{\lambda_c} \Delta \lambda_c R_{\lambda_c}}{\kappa_{\lambda_c} R_{\lambda_{\text{obs}}}} \quad (5)$$

where λ_c represents the wavelength of the calibration experiments and λ_{obs} is the wavelength of the transition of interest. I_{obs} must be the total integrated band intensity. This is determined from the spectral fitting.

A series of calibration experiments taken over a period of time established the calibration factor κ_{580} to ± 10 percent. An additional uncertainty of ± 25 percent exists in the absolute value of the air-afterglow rate coefficient, k_{580} . Further uncertainties in the determination of the absolute photon-emission rates for $N_2(A)$ arise through the relative monochromator response function (10 percent) and $N_2(A)$ band transition probabilities. The uncertainty in this latter quantity is difficult to estimate. We used Shemansky's²⁹ transition probabilities to provide a ready basis for comparison with the existing literature. He estimated them to carry a 20 percent uncertainty. Our experiments on the energy transfer between $N_2(A)$ and NO^{14} , however, indicated that Shemansky's transition probabilities are likely to be 20 to 40 percent too large. We have chosen not to revise the $N_2(A-X)$ transition probabilities until this issue has been resolved definitively. Ignoring

the uncertainty in the $N_2(A-X)$ transition probabilities, the total uncertainty in each rate coefficient, systematic and statistical combined in quadrature, will be 30 percent. This large figure is determined primarily by the uncertainty in the air afterglow rate coefficient.

C. Radial Density Gradient Corrections

In the case of the energy pooling reactions, the $N_2(A)$ and the $N_2(C,B,HIR)$ have radial density gradients which are different. The $N_2(A)$ radial density gradient approximately follows the form of a Bessel function of first order,³¹

$$[N_2(A)](r) = [N_2(A)]_0 J_0\left(\lambda \frac{r}{r_0}\right) \quad (6)$$

where $[N_2(A)]_0$ is the centerline number density, r_0 is the flow tube radius, and $\lambda = 2.405$, the first zero of $J_0(x)$. The field of view of the detector is essentially a rectangular parallelepiped across the center of the tube with height, h , width, z , and length, $2r_0$ (see Fig. 1). We assume that variations down the axis of the flow tube, across the field of view, can be neglected. The average number density of $N_2(A)$ observed in the field of view is then

$$\langle [N_2(A)] \rangle = \frac{[N_2(A)]_0 \int_0^{r_0} J_0\left(\lambda \frac{r}{r_0}\right) r \theta dr}{\int_0^{r_0} r \theta dr}, \quad (7)$$

where $[N_2(A)]_0$ is the $N_2(A)$ number density in the center of the flow tube. When r is less than or equal to $h/2$, θ will equal π ; but when r becomes greater than $h/2$, θ will be given by $\sin^{-1}(h/2r)$. Thus, each integral in Eq. (7) becomes a sum of two integrals, one between the limits of 0 and $h/2$, the other running from $h/2$ to r_0 . For our conditions of $r_0 = 2.6$ cm and $h = 1$ cm, numerical integration gives

$$\langle [N_2(A)] \rangle = 0.601 [N_2(A)]_0 \quad (8)$$

As we show below, the number density of $N_2(C, B, HIR)$ is proportional to the square of the $N_2(A)$ number density. Thus

$$\langle [N_2(C, B, HIR)] \rangle = k' [N_2(A)]^2 = \frac{k' [N_2(A)]_0^2 \int_0^{r_0} J_0^2\left(\lambda \frac{r}{r_0}\right) r \theta dr}{\int_0^{r_0} r \theta dr}, \quad (9)$$

where k' is the energy pooling rate coefficient.

Integrating this expression in a similar manner to that given for $\langle [N_2A] \rangle$ gives

$$\langle [N_2(C, B, HIR)] \rangle = 0.458 k' [N_2(A)]_0^2. \quad (10)$$

Finally, using Eq. (8) above for $[N_2(A)]_0$, we find that

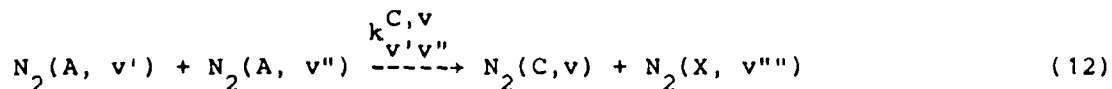
$$\langle [N_2(C, B, HIR)] \rangle = 1.267 k' \langle [N_2(A)] \rangle^2. \quad (11)$$

This correction must be made to the data on energy pooling to extract rate coefficients. This correction factor increases as the ratio h/r increases beyond unity, reaching a maximum value of 1.446 when h/r equals two (Fig. 2).

III. Results

A. $N_2(C^3\Pi_u, v'=0-4)$ Formation in $N_2(A^3\Sigma_u^+, v'=0-2)$ Energy Pooling

The processes controlling the formation and destruction of $N_2(C)$ in the energy pooling system are:



where the superscript v denotes the vibrational level of the $N_2(C)$ product molecule, the subscript v 's denote the vibrational levels of the $N_2(A)$ molecules, and k_{rad} is the radiative decay rate of $N_2(C)$.³⁰ The lifetime of $N_2(C)$ is sufficiently short (≈ 36 ns)³⁰ that we may ignore electronic quenching of that state. Because of its short radiative lifetime, $N_2(C)$ is in steady state in our reactor so that we can equate its formation and decay rates. Thus we have

$$\begin{aligned} \frac{d[N_2(C, v)]}{dt} &= 1.267 \sum_{v'} \sum_{v''} k_{v'v''}^{C,v} [N_2(A, v')] [N_2(A, v'')] \\ &\quad - k_{\text{rad}}^{C,v} [N_2(C, v)] = 0 \quad , \end{aligned} \quad (14)$$

$$[N_2(C, v)] = 1.267 \sum_{v''} \sum_{v'} \frac{k_{v'v''}^{C,v}}{k_{\text{rad}}^{C,v}} [N_2(A, v')] [N_2(A, v'')] \quad . \quad (15)$$

For the case of only one vibrational level of $N_2(A)$, Eq. (15) collapses to a single term for which the $N_2(C)$ number density varies linearly with the square of the $N_2(A)$ number density. The slope will equal the ratio of the energy-pooling rate coefficient to the radiative-decay rate of $N_2(C)$.

Figures 3 and 4 show representative spectra of the 220 to 400 nm region which encompasses most of the major emissions in the $N_2(A-X)$ and $N_2(C-B)$ systems. Comparison of the two figures shows how strongly the $N_2(C)$ intensity varies with the $N_2(A)$ intensity. Figures 5 and 6 show typical plots of the variation in the number density of $N_2(C, v')$ as a function of the square of the $N_2(A)$ number density under conditions where only $v'=0$ of the A state was in the reactor.

If only vibrational levels of 0 and 1 of $N_2(A)$ are present, Eq. (15) becomes

$$\begin{aligned}
[N_2(C, v)] &= 1.267 \frac{k_{00}^{C,v}}{k_{rad}^{C,v}} [N_2(A, v'=0)]^2 \\
&+ 2.534 \frac{k_{01}^{C,v}}{k_{rad}^{C,v}} [N_2(A, v'=0)] [N_2(A, v'=1)] \\
&+ 1.267 \frac{k_{11}^{C,v}}{k_{rad}^{C,v}} [N_2(A, v'=1)]^2 .
\end{aligned} \tag{16}$$

Dividing this equation through by $[N_2(A, v'=0)]^2$ gives a quadratic equation in the parameter $[N_2(A, v'=1)]/[N_2(A, v'=0)]$:

$$\begin{aligned}
\frac{[N_2(C, v)]}{[N_2(A, v'=0)]^2} &= 1.267 \frac{k_{00}^{C,v}}{k_{rad}^{C,v}} + 2.534 \frac{k_{01}^{C,v}}{k_{rad}^{C,v}} \frac{[N_2(A, v'=1)]}{[N_2(A, v'=0)]} \\
&+ 1.267 \frac{k_{11}^{C,v}}{k_{rad}^{C,v}} \left\{ \frac{[N_2(A, v'=1)]}{[N_2(A, v'=0)]} \right\}^2 .
\end{aligned} \tag{17}$$

Figures 7 and 8 show data plotted in this fashion for two $N_2(C)$ vibrational levels excited in the energy-pooling reaction. The most interesting thing these plots show is the absence of a significant quadratic term. The intercepts of the plots, of course, give rate coefficients that agree with those previously determined from studying just $v'=0$ pooling. Table 1 summarizes the results of $N_2(C)$ energy-pooling studies.

B. Herman Infrared Formation from $N_2(A)$ Energy Pooling

The Herman Infrared system was first observed 35 years ago by R. Herman.³² Subsequent spectroscopic work on the system has failed to

identify either the upper or lower states in the transition,³³⁻³⁵ although Nadler and Rosenwaks⁸ have been able to establish an upper limit to the upper state term energy of 12.02 eV. Nadler and Rosenwaks have discussed the identification of the two states and concluded the lower state might be the $G^3\Delta_g$, the lower state of the Gaydon-Herman Green system, and that the upper state was a $^3\Pi_u$ state which is known only through Michaels' calculations.³⁶ Gilmore³⁷ and Michaels³⁸ both dispute these identifications, however. Gilmore suggests $C''^5\Pi_u$ and $A'^5\Sigma_g^+$ as the upper and lower states, respectively.³⁷

Figures 9 and 10 show the HIR system excited in energy pooling of $N_2(A, v'=0)$ and $N_2(A, v'=0,1)$ respectively. The spectra were taken at 7.5 torr total pressure with a nitrogen partial pressure of 1.5 torr. Thus nitrogen first-positive emission is virtually absent from the spectrum. The ratio of the HIR intensity to the square of the $N_2(A)$ number density does not vary with pressure.⁶ Thus, the state is not quenched electronically under our conditions, and a steady-state analysis similar to that given above for the $N_2(C)$ state applies here. We write

$$I_{HIR} = k_{rad}^{HIR,3} [HIR, v'=3] = 1.267 k_{00}^{HIR,3} [N_2(A, v'=0)]^2. \quad (18)$$

Figure 11 shows data for $v'=3$ of the HIR system plotted this way. For these studies, CF_4 or CH_4 was added to the reactor to relax the $N_2(A)$ vibrational energy to $v'=0$. From the slope of the plot, we find that the rate coefficient for producing $v'=3$ of the HIR system in the energy pooling of two $N_2(A, v'=0)$ molecules is $8.1 \times 10^{-11} \text{ cm}^3 \text{ molecule}^{-1} \text{ s}^{-1}$. Strictly speaking, this figure is a lower limit, because other transitions of the HIR system from $v'=3$ might appear outside the bandpass of our detection system. The relative intensities of the four bands we do see, however, indicate that we have sampled both sides of the Condon parabola. Thus in all probability, we have observed the major emissions from $v'=3$. When the $N_2(A)$ was vibrationally excited, the ratio of the HIR $v'=3$ intensity to the square of the $N_2(A, v'=0)$ number density remains constant. Thus, vibrationally excited $N_2(A)$ appears not to play any role in exciting HIR, $v'=3$ from energy pooling.

Under conditions where only $v'=0$ and 1 of the $N_2(A)$ are present, we also see emission from $v'=2$ of the HIR system. The lower two vibrational levels of the HIR system appear only when the number densities of $v'=2$ and 3 of the $N_2(A)$ become important. We can analyze the HIR $v'=2$ data in a similar fashion to our analysis for vibrational effects in $N_2(C)$ production, but since we already know that two $v'=0$ molecules do not pool to make an HIR $v'=2$ molecule, we can eliminate the first term in the equation. Thus,

$$I_{\text{HIR},2}^{\text{HIR},2} = 2.534 k_{01}^{\text{HIR},2} [N_2(A, v'=0)][N_2(A, v'=1)] + 1.267 k_{11}^{\text{HIR},2} [N_2(A, v'=1)]^2, \quad (19)$$

$$\frac{I_{\text{HIR},2}^{\text{HIR},2}}{[N_2(A, v'=0)][N_2(A, v'=1)]} = 2.534 k_{01}^{\text{HIR},2} + 1.267 k_{11}^{\text{HIR},2} \frac{[N_2(A, v'=1)]}{[N_2(A, v'=0)]}. \quad (20)$$

Figure 12 shows the data for the HIR $v'=2$ system. The intercept of the plot, after application of the appropriate corrections, gives the value for the mixed $v'=0/v'=1$ pooling rate coefficient, $9.9 \times 10^{-11} \text{ cm}^3 \text{ molecule}^{-1} \text{ s}^{-1}$. Within statistical uncertainty, the linear term is not significant, again implying that energy pooling by two $v'=1$ molecules is negligible. Table 2 summarizes our results on the Herman Infrared system. Our data further show that HIR $v'=2$ is not formed by pooling of vibrational levels of $N_2(A)$ higher than $v'=1$. We have yet to collect adequate data on the formation of HIR $v'=0,1$ which is formed in pooling of $N_2(A, v' \geq 2)$.

IV. Discussion

Hays and Oskam,³ in a pulsed, static discharge, measured a rate coefficient for $N_2(C)$ formation from $N_2(A)$ energy pooling of $2.6_{-1.4}^{+2} \times 10^{-10} \text{ cm}^3 \text{ molecule}^{-1} \text{ s}^{-1}$. Within experimental error, our values agree adequately.

They reported a relative $N_2(C)$ vibrational distribution of 100:92:72:50:47 for vibrational levels 0-4, respectively. Their $N_2(A)$ vibrational distribution was 100:250:80, for vibrational levels 0-2, respectively. For an $N_2(A)$ $v'=1/v'=0$ ratio of 3/1, our results would predict an $N_2(C)$ vibrational distribution of 100:160:110:70:30, in disagreement with Hays and Oskam's result.

Applying our measured rate coefficients to Clark and Setser's⁵ 0.61/1 ratio for $N_2(A)$ $v'=1/v'=0$, gives an overall rate coefficient of $1.3 \times 10^{-10} \text{ cm}^3 \text{ molecule}^{-1} \text{ s}^{-1}$, about 60 percent of their value. Some of this discrepancy results from their not including the 27 to 45 percent correction for radial density gradient effects in their analysis. Additionally, their measurements may be contaminated by scattered second-positive emission from their discharge. They reported a $N_2(C)$ vibrational distribution of 100:89:70 for $v'=0-2$, respectively, in contrast to our measured value of 100:160:120. Scattered light will enhance $v'=0$ relative to the other vibrational levels. Subsequent measurements by Nadler et al.⁶ found a distribution of $100 \pm 4:125 \pm 6:81 \pm 4:62 \pm 12:62 \pm 25$. They used the reaction between metastable Xe atoms and nitrogen as their $N_2(A)$ source, thereby eliminating the possibility of scattered light contamination. Their $N_2(A)$ vibrational distribution was unspecified, although they did state that most of their $N_2(A)$ was in vibrational levels 0 and 1. Assuming their $N_2(A)$ vibrational distribution was similar to Clark and Setser's, then the vibrational distribution calculated from our data for comparison with that of Nadler et al. would be $100 \pm 9:157 \pm 16:119 \pm 12:81 \pm 7:32 \pm 7$, in modest accord with the results of those authors. Their distribution concurs better with what we observe when the $N_2(A)$ is somewhat hotter vibrationally. Under conditions such that only 30 to 45 percent of the $N_2(A)$ is in $v'=0$, our $N_2(C)$ vibrational distribution is $100 \pm 7:140 \pm 7:110 \pm 15:70 \pm 10:45 \pm 10$.

Nadler and Rosenwaks⁸ studied the energy pooling of $N_2(A)$ in some detail, and noted how the vibrational distribution of $N_2(A)$ affected the vibrational distribution in the product $N_2(C)$ and Herman Infrared systems. They report a vibrational distribution of $100 \pm 3:150 \pm 7:137 \pm 5:151 \pm 2:27 \pm 7$ for $N_2(C)$, $v'=0-4$ respectively, formed from energy pooling between $N_2(A)$, $v'=0$ molecules only.

This agrees moderately well with our observations which give an $N_2(C)$ vibrational distribution of $100 \pm 4:158 \pm 8:158 \pm 8:108 \pm 8:38 \pm 4$ from $N_2(A, v'=0)$ energy pooling. When the $N_2(A)$ was vibrationally excited, such that 60 percent of it was in vibrational levels 1 and above, their $N_2(C)$ distribution was $100 \pm 3:130 \pm 5:95 \pm 4:99 \pm 4:40 \pm 5$. As noted above, we observe a similar $N_2(C)$ vibrational distribution with the vibrationally hotter $N_2(A)$. In terms of distributions, our only significant disagreement with the observations of Nadler and Rosenwaks is that they report about 40 percent more excitation of $N_2(C, v'=3)$ for formation from both vibrationally excited and vibrationally cold $N_2(A)$. One intriguing finding of both studies is that the product $N_2(C)$ is more vibrationally excited when the $N_2(A)$ isn't and vice versa. Table 3 summarizes these comparisons between literature reports.

Nadler and Rosenwaks tried to rationalize their observations with a simple model which essentially is the combination of simple Franck-Condon and minimum-energy-defect models. Thus they posited that the $N_2(C)$ vibrational level populations would follow a distribution determined by the product of the Franck-Condon factors for the transitions from one of the $N_2(A)$ molecules to the C state and the other one to the X state times $\exp(-|\Delta E|/kT)$ where $|\Delta E|$ is the magnitude of the energy defect in the energy transfer reaction. Because our results are essentially state-to-state observations, we can test this model in some detail. Table 4 compares the calculated and observed state-to-state energy pooling rate coefficients for the cases of two $N_2(A, v'=0)$ molecules, $N_2(A, v'=0)$ with $N_2(A, v'=1)$ and two $N_2(A, v'=1)$ molecules. The calculated values have been normalized so that the sum of the rate coefficients for two $N_2(A, v'=0)$ molecules equals the experimentally observed rate coefficient. Clearly, the model does not do a very good job of predicting the relative vibrational distributions, how these vibrational distributions change from case to case, nor how the absolute magnitude of the vibrational distributions changes from case to case. While the model does indicate that two $N_2(A, v'=0)$ molecules excite $N_2(C, v'=2,3)$ more efficiently than is the case for vibrationally excited $N_2(A)$, it fails to predict the opposite trend for $N_2(C, v'=1,4)$. Furthermore, the model predicts very significant excitation of $N_2(C)$ in collisions with two $N_2(A, v'=1)$ molecules in disagreement with our

observations. The Franck-Condon model appears to be inadequate to describe detailed interactions in this type of energy transfer reaction. We have noted such a failure previously in our studies on the excitation of NO by $N_2(A)$.¹⁴

Nadler and Rosenwaks also investigated the excitation of the Herman Infrared system by $N_2(A)$ energy pooling. By comparing the relative intensities of the second-positive bands and the Herman Infrared bands, they estimated a lower limit to the rate coefficient for HIR formation from $N_2(A)$ energy pooling of $7 \times 10^{-11} \text{ cm}^3 \text{ molecule}^{-1} \text{ s}^{-1}$. This estimate assumes a rate coefficient for $N_2(C)$ formation of $2.5 \times 10^{-10} \text{ cm}^3 \text{ molecule}^{-1} \text{ s}^{-1}$. Reducing their HIR estimate by 40 percent to place it on the same relative basis as our $N_2(C)$ formation rate coefficients results in a value of $4 \times 10^{-11} \text{ cm}^3 \text{ molecule}^{-1} \text{ s}^{-1}$ for the Nadler and Rosenwaks estimate. This is about half of what we measure directly. Nadler and Rosenwaks' estimate is based upon a Herman infrared spectrum which is much more contaminated by first-positive emission than is our spectrum. Thus the HIR intensities would have been much more difficult for them to estimate. We also do not agree with them on some of the details of the HIR vibrational distribution produced by $N_2(A)$ energy pooling. We don't see any convincing evidence for formation of $N_2(\text{HIR}, v'=0,1)$ from the pooling of two $N_2(A, v'=0)$ molecules, whereas Nadler and Rosenwaks report that the intensities of emissions from these two levels drops by a factor of only about 2 in going from unrelaxed to vibrationally relaxed $N_2(A)$. Both studies clearly do show a strong enhancement of $N_2(\text{HIR}, v'=3)$ when only $N_2(A, v'=0)$ is present in the reactor, and both note an absence of $N_2(\text{HIR}, v'=2)$ for the case of vibrationally relaxed $N_2(A)$. In fact, we observe that the ratio of $[N_2(\text{HIR}, v'=3)]$ to $[N_2(A, v'=0)]^2$ remains constant under all conditions of vibrational excitation of the $N_2(A)$. Similarly, we find that the ratio of $[N_2(\text{HIR}, v'=2)]$ to the product $[N_2(A, v'=0)] \times [N_2(A, v'=1)]$ is invariant under all observed conditions of $N_2(A)$ vibrational excitation. This includes cases in which 70 percent of the $N_2(A)$ is vibrationally excited. Under conditions of moderate vibrational relaxation of the $N_2(A)$, however, conditions where only the two lowest vibrational levels are in the reactor, we also fail to see any evidence of $N_2(\text{HIR}, v'=0,1)$. Only under conditions such that vibrational levels 2 and above exist in the reactor do we

see any emission from the two lowest HIR vibrational levels. Under such conditions, the HIR spectra are severely overlapped by first positive emission, and difficult to analyze. Thus we have as yet made no quantitative estimates of the rate coefficients for producing these two lowest levels of the HIR system from $N_2(A)$ energy pooling.

SUMMARY AND CONCLUSIONS

We have reported state-to-state rate coefficients for excitation of $N_2(C^3\Pi_u)$ and the N_2 Herman Infrared system in $N_2(A^3\Sigma^+_u)$ energy pooling. Our results show that the energy pooling process is essentially gas kinetic, and that the final vibrational state distributions depend strongly upon the initial $N_2(A)$ vibrational distributions. This product-state selectivity is particularly striking in the case of Herman Infrared excitation where specific combinations of $N_2(A)$ states produce only one of the available HIR states. A model combining Franck-Condon overlap with minimum energy defect is inadequate to predict the observed distributions. Presumably, one must look at specific potential curve crossings in detail to understand these phenomena.

Observations of the formation of $N_2(B^3\Pi_g)$ from $N_2(A)$ energy pooling³⁹ result in rate coefficients similar in magnitude to those observed here, and also show some unusual state specificity. Taken together, our results would support a total rate coefficient for $N_2(A)$ energy pooling of $3-4 \times 10^{-10} \text{ cm}^3 \text{ molecule}^{-1} \text{ s}^{-1}$, substantially lower than some previous suggestions which have exceeded $10^{-9} \text{ cm}^3 \text{ molecule}^{-1} \text{ s}^{-1}$.^{3,7} We will discuss the $N_2(B)$ formation results and their implications regarding the total $N_2(A)$ energy pooling rate coefficient in a future publication.

ACKNOWLEDGEMENTS

We appreciate partial support for this work from the Defense Nuclear Agency (Project SA, Task SA, Work Unit 115) and the Air Force Office of Scientific Research (Task 2310G4) through Air Force Geophysics Laboratory Contract No. F19628-85-C-0032 and from the Air Force Weapons Laboratory under Contract No. F29601-84-C-0076. We enjoyed interesting discussions with Dave Green (PSI) and Terry Rawlins (PSI), Don Setser (KSU), Forrest Gilmord (RDA) and Harvey Michaels (UTRC), and appreciated Margrethe DeFaccio and Lauren Cowles' instrumental contributions to the data analysis.

References

1. D.H. Stedman and D.W. Setser, Chem. Phys. 50, 2256 (1969).
2. G.N. Hays, C.J. Tracy, A.R. Demonchy, and H.J. Oskam, Chem. Phys. Lett. 14, 352 (1972).
3. G.N. Hays and H.J. Oskam, J. Chem. Phys. 59, 1507 (1973).
4. G.N. Hays and H.J. Oskam, J. Chem. Phys. 59, 6088 (1973).
5. W.G. Clark and D.W. Setser, J. Phys. Chem. 84, 2225 (1980).
6. I. Nadler, D.W. Setser, and S. Rosenwaks, Chem. Phys. Lett. 72, 536 (1980).
7. I. Nadler, A. Rotem, and S. Rosenwaks, Chem. Phys. 69, 375 (1982).
8. I. Nadler and S. Rosenwaks, J. Chem. Phys. 83, 3932 (1985).
9. L.G. Piper, unpublished results (1980).
10. L.G. Piper, G.E. Caledonia, and J.P. Kennealy, J. Chem. Phys. 74, 2888 (1981).
11. L.G. Piper, G.E. Caledonia, and J.P. Kennealy, J. Chem. Phys. 75, 2847 (1981).
12. L.G. Piper, W.J. Marinelli, W.T. Rawlins, and B.D. Green, J. Chem. Phys. 83, 5602 (1985).
13. L.G. Piper and W.T. Rawlins, J. Phys. Chem. 90, 320 (1986).
14. L.G. Piper, L.M. Cowles, and W.T. Rawlins, J. Chem. Phys. 85, 3369 (1986).
15. L.G. Piper, M.E. Donahue, and W.T. Rawlins, J. Phys. Chem. 91, 3883 (1987).
16. L.G. Piper, J. Chem. Phys. 87, 1625 (1987).
17. D.W. Setser, D.H. Stedman, and J.A. Coxon, J. Chem. Phys. 53, 1004 (1970).
18. D.H. Stedman and D.W. Setser, Chem. Phys. Lett. 2, 542 (1968).
19. N. Sadeghi and D.W. Setser, Chem. Phys. Lett. 82, 44 (1981).
20. A. Fontijn, A., C.B. Meyer, and H.I. Schiff, J. Chem. Phys. 40, 64 (1964).
21. M. Vanpee, K.D. Hill, and W.R. Kineyko, AIAA J. 9, 135 (1971).

22. M.F. Golde, A.E. Roche, and F. Kaufman J. Chem. Phys. 59, 3953 (1973).
23. D. Golomb and J.H. Brown, J. Chem. Phys. 63, 5246 (1975).
24. G.A. Woolsey, P.H. Lee, and W.D. Slafer, J. Chem. Phys. 67, 1220 (1977).
25. M. Sutoh, Y. Morioka, and M. Nakamura, J. Chem. Phys. 72, 20 (1980).
26. A.M. Pravilov and L.G. Smirnova, Kinet. and Catal. 19 202 (1978).
27. F. Kaufman, Proc. Roy. Soc. (London) A 247, 123 (1958).
28. F. Kaufman in Chemiluminescence and Bioluminescence, M.J. Cormier, D.M. Hercules, and J. Lee, eds. pp. 83-100 (1973).
29. D.E. Shemansky, J. Chem. Phys. 51, 689 (1969).
30. A. Lofthus and P.H. Krupenie, J. Phys. Chem. Ref. Data 6, 287 (1977).
31. E.E. Ferguson, F.C. Fehsenfeld, and A.L. Schmeltpopf, Adv. Atom. Molec. Phys. V, 1 (1970).
32. R. Herman, C.R. Acad. Sci. (Paris) 233, 738 (1951).
33. P.K. Carroll and N.D. Sayers, Proc. Phys. Soc. (London) 64, 1138 (1953).
34. D. Pleiter, Can. J. Phys. 41, 1245 (1963).
35. D. Mahon-Smith and P.K. Carroll, J. Chem. Phys. 41, 1377 (1964).
36. a. H.H. Michaels, J.W. McGowan, ed., New York: Wiley, Vol. II, Ch. 3 (1981).
b. H.H. Michaels, private communication to S. Rosenwaks (1985). Cited in Ref. 8.
37. F.R. Gilmore, private communication (1986).
38. H.H. Michaels, private communication (1986).
39. L.G. Piper, manuscript in preparation.

Table 1. Rate Coefficients for $N_2(C^3\Pi_u)$ Formation from $N_2(A^3\Sigma_u^+)$ Energy Pooling.

$N_2(C, v')$	$k_{00}^{C, v'}$	$k_{01}^{C, v'}$	$k_{11}^{C, v'}$
0	2.6 ± 0.1	3.4 ± 0.7	< 1.0
1	4.1 ± 0.2	5.4 ± 1.2	< 2.0
2	4.1 ± 0.2	3.3 ± 0.8	< 1.0
3	2.8 ± 0.2	2.2 ± 0.5	< 0.7
4	1.0 ± 0.1	1.0 ± 0.6	< 0.6
Total $N_2(C)$	14.6 ± 0.8	15.3 ± 3.8	< 5.3
<p>Rate coefficients are in units of $10^{-11} \text{ cm}^3 \text{ molecules}^{-1} \text{ s}^{-1}$. Error bars represent 2σ statistical uncertainties in fits. Total uncertainties are $\approx 30\%$</p>			

Table 2. Rate Coefficients for Herman Infrared Formation from
N₂(A) Energy Pooling

HIR, v'	k ₀₀	k ₀₁	k ₁₁
3	$>8.1 \pm 0.4$	-	-
2	-	$>9.9 \pm 1.0$	-
<p>Rate coefficients are in units of $10^{-11} \text{ cm}^3 \text{ molecule}^{-1} \text{ s}^{-1}$.</p> <p>Error bars represent 2σ statistical uncertainty in fits.</p> <p>Total uncertainty is $\approx 30\%$</p>			

Table 3. Comparison Between Results of Various Groups on N₂ Excitation by N₂(A) Energy Pooling

Group	Relative N ₂ (A) Populations						Relative N ₂ (C) Populations				Total Rate ^a Coefficient
	v'= 0	1	2	3	v= 0	1	2	3	4		
Hayes and Okam ⁴	100	250	80		100	92	72	50	47	2.6 ⁺² -1.4	
Present results ^b	100	300			100	160	110	70	30		
Clark and Setser ⁵	100	61			100	89	70			1.8±0.2	
Nadler et al. ⁶	100	61	?		100±4	125±6	81±4	62±12	62±25	2.2 ^c ±0.3	
Present results ^b	100	61			100±9	157±16	119±12	81±7	32±7	1.3±0.4	
Nadler and Rosenwaks ⁸	100	-	-		100±3	150±7	137±5	151±2	27±7	1.5±0.4	
Present results ^b	100	-	-		100±4	158±8	158±8	108±8	38±4		
Nadler and Rosenwaks ⁸	100	90	60	<10	100±3	130±5	95±4	99±4	40±5		
Present results ^d	100	80	50	18	100±7	140±7	110±15	70±10	45±10		
a. Units of 10 ⁻¹⁰ cm ³ molecule ⁻¹ s ⁻¹											
b. Calculated from results in Table 1.											
c. Estimate from Ref. 5.											
d. Measured values in under conditions of high N ₂ (A) excitation.											

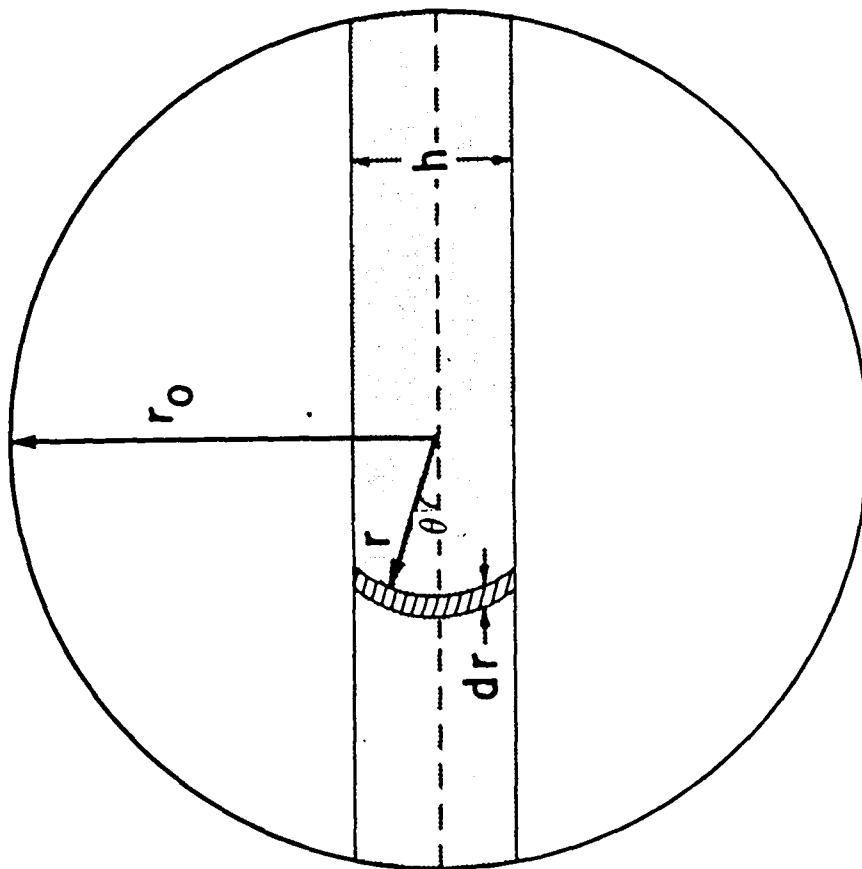
Table 4. Comparison between Observed $N_2(C^3\Pi_u)$ Vibrational Distributions Excited by $N_2(A^3\Sigma_u^+)$ Energy Pooling and those Calculated from a Franck-Condon Model

$\begin{matrix} C, v \\ k \end{matrix}$	$v'=0$		1		2		3		4		$\Sigma_k C, v$	
	Calc ^a	Obs	Calc	Obs	Calc	Obs	Calc	Obs	Calc	Obs	Calc	Obs
$2N_2(A, v'=0)$	7.14	2.6	1.3	4.1	5.7	4.1	7.3	2.8	0.10	1.0	14.5	14.6
$N_2(A, v'=0) +$ $N_2(A, v'=1)$	1.3	3.4	1.0	5.4	0.48	3.3	1.3	2.2	7.5	1.0	11.6	15.3
$2N_2(A, v'=1)$	0.0004	<1	7.3	<2	2.8	<1	0.007	<0.7	0.17	<0.6	10.3	<5

^aThe calculated values have been normalized to give the correct total rate coefficient for $2N_2(A, v'=0)$ energy pooling.

FIGURE CAPTIONS

- 1 Cross-sectional view of flow tube illustrating the geometry germane to the radial number-density gradient problem. The shaded area approximates the monochromator's field of view.
- 2 Variation in the correction factor for energy pooling measurements with the ratio h/r .
- 3 Observed (heavy line) and computed best fit (light line) to the spectral region between 250 and 400 nm. Resolution 1.0 nm. Full scale sensitivity 1 kHz.
- 4 Observed (heavy line) and computed best fit (light line) to the spectral region between 220 and 400 nm. Resolution 1.0 nm. Full scale sensitivity 3 kHz.
- 5 Variation in the number density of $N_2(C, v'=0)$ as a function of the square of the number density of $N_2(A, v'=0)$.
- 6 Variation in the number density of $N_2(C, v'=2)$ as a function of the square of the number density of $N_2(A, v'=0)$.
- 7 Variation in the ratio of the number density of $N_2(C, v'=1)$ to the square of the number density of $N_2(A, v'=0)$ as a function of the ratio of the number densities of vibrationally excited to unexcited $N_2(A)$.
- 8 Variation in the ratio of the number density of $N_2(C, v'=3)$ to the square of the number density of $N_2(A, v'=0)$ as a function of the ratio of the number densities of vibrationally excited to unexcited $N_2(A)$.
- 9 Spectrum of the Herman Infrared $v'=3$ system (light line) excited in the energy pooling of $N_2(A, v'=0)$. The heavy line is the synthetic fit to the spectrum. $P_{total} = 7.5$ torr, $X_{N_2} = 0.20$.
- 10 Spectrum of the Herman Infrared $v'=2,3$ systems (light line) excited in the energy pooling of $N_2(A, v'=0, 1)$. The heavy line is the synthetic fit to the spectrum. $P_{total} = 7.5$ torr, $X_{N_2} = 0.20$.
- 11 Variation in the number density of $N_2(HIR, v'=3)$ as a function of the square of the number density $N_2(A, v'=0)$.
- 12 Variation in the ratio of the $N_2(HIR, v'=2)$ number density to the product of the number densities of $N_2(A, v'=0)$ and $v'=1$ as a function of the ratio of the number densities of $N_2(A, v'=1)$ to $v'=0$.



A-2274L

Figure 1. Cross-sectional view of flow tube illustrating the geometry germane to the radial number-density gradient problem. The shaded area approximates the monochromator's field of view.

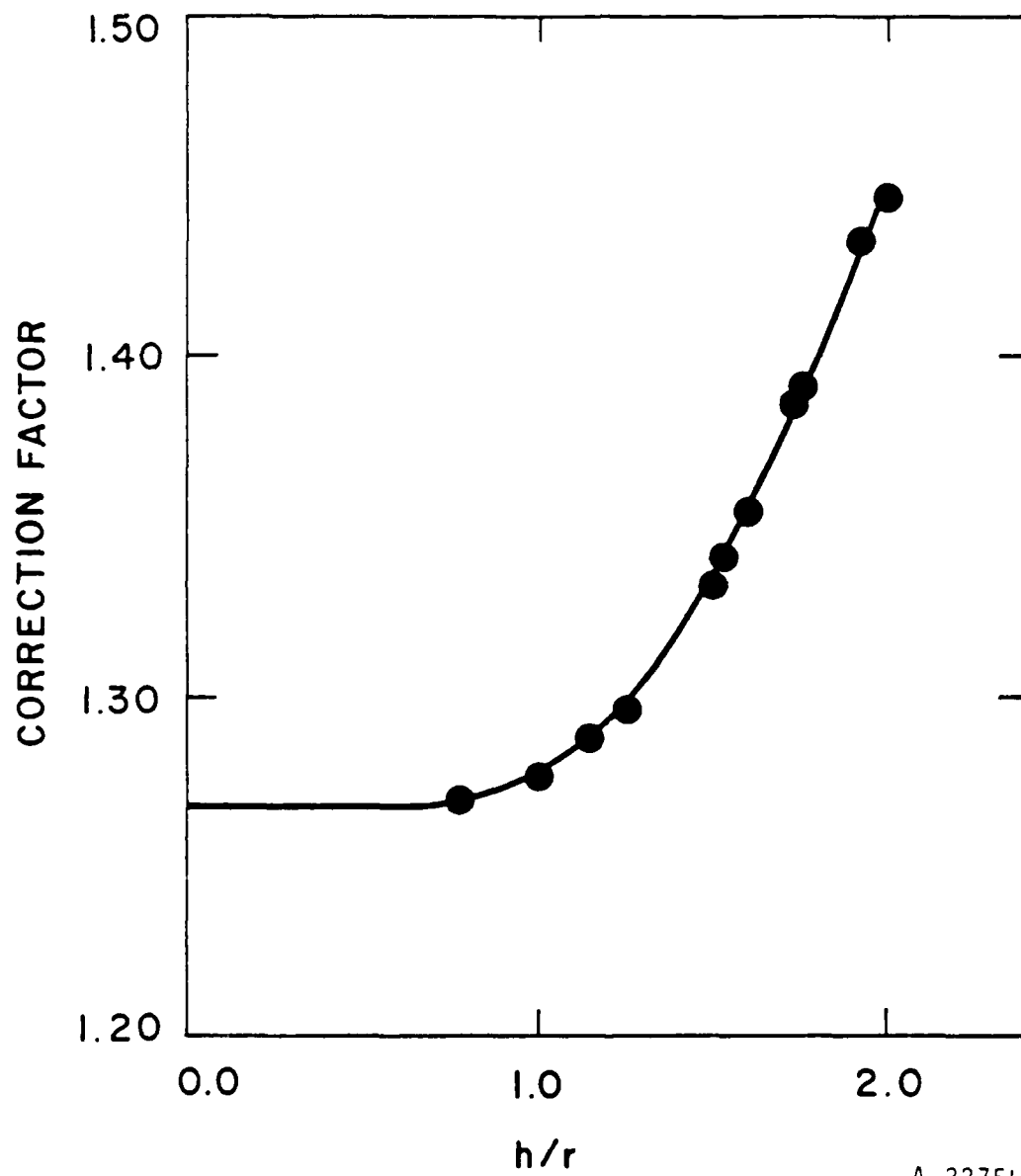
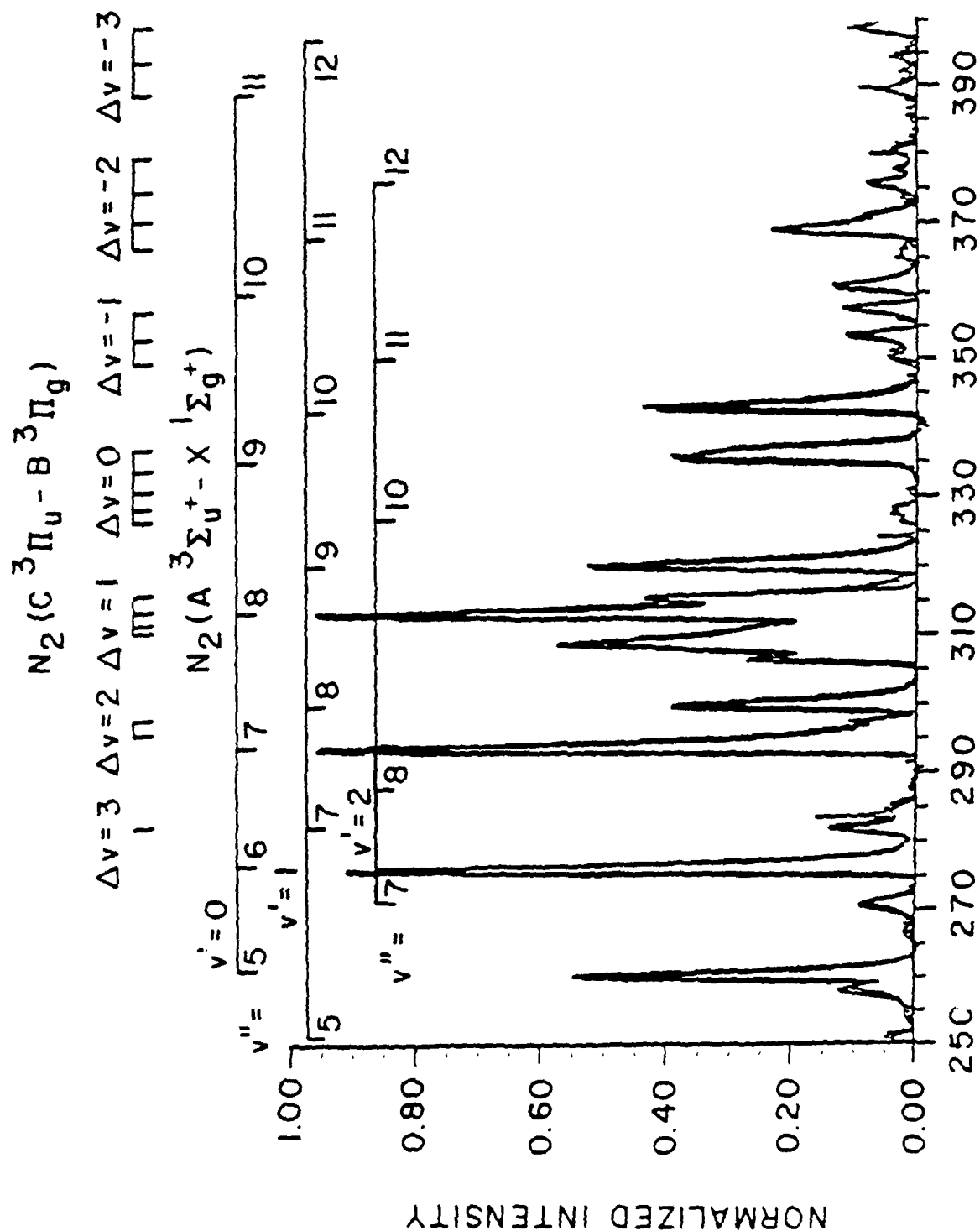
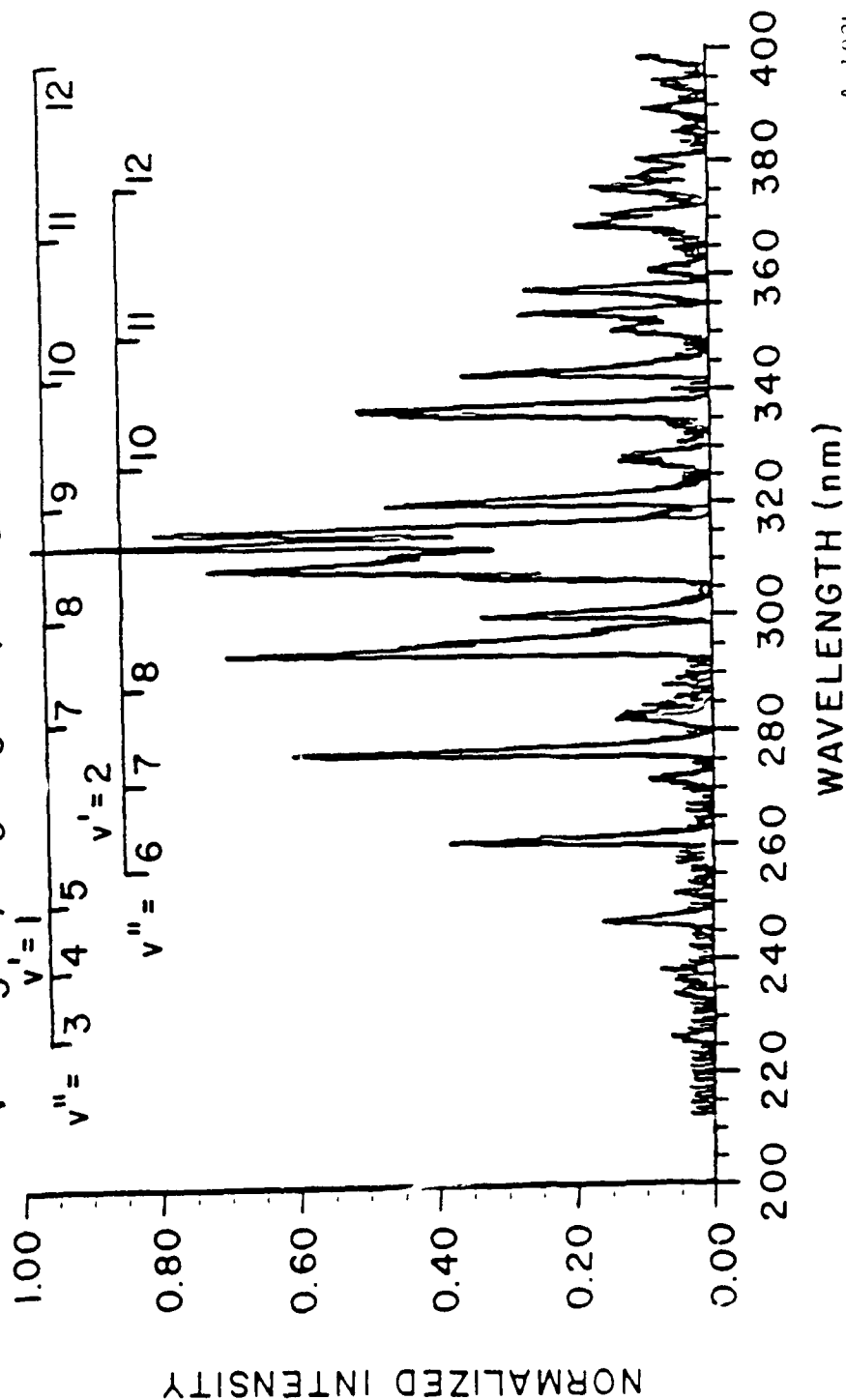
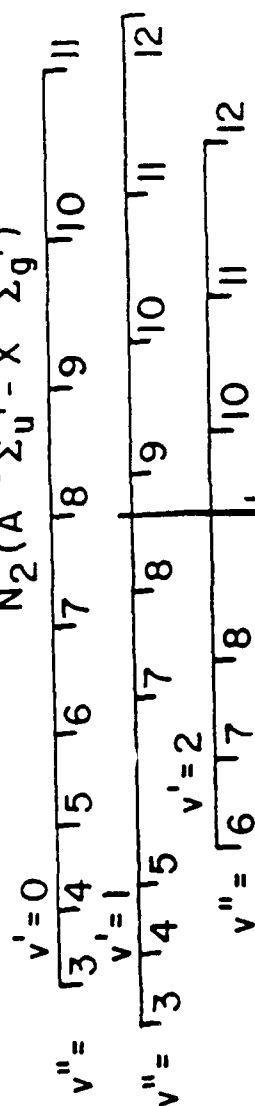
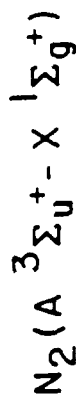
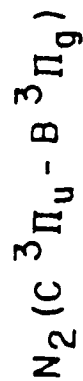


Figure 2. Variation in the correction factor for energy pooling measurements with the ratio h/r .



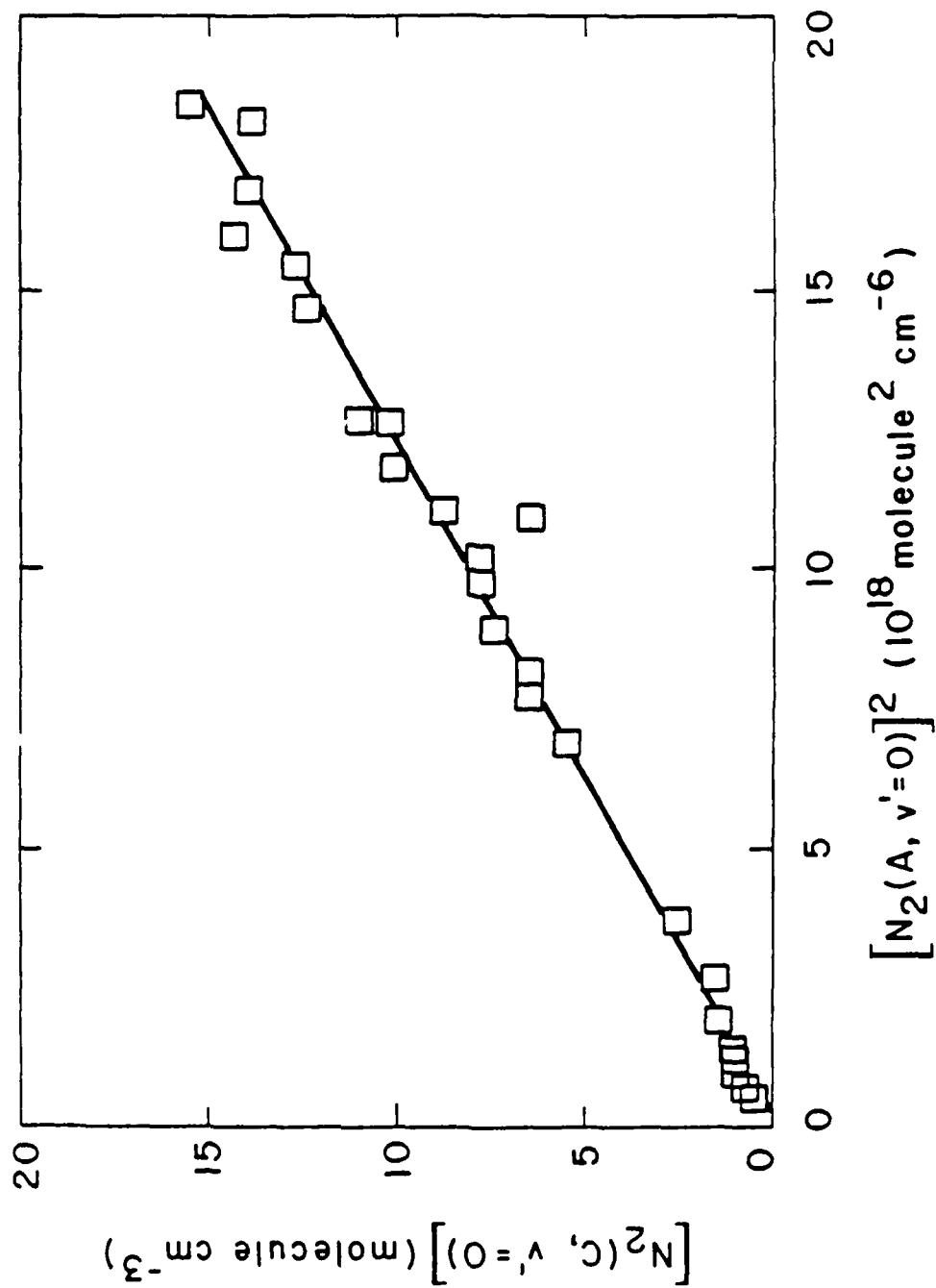
A-192L

Figure 3. Observed (heavy line) and computed best fit (light line) to the spectral region between 250 and 400 nm. Resolution 1.0 nm. Full scale sensitivity 1 kHz.



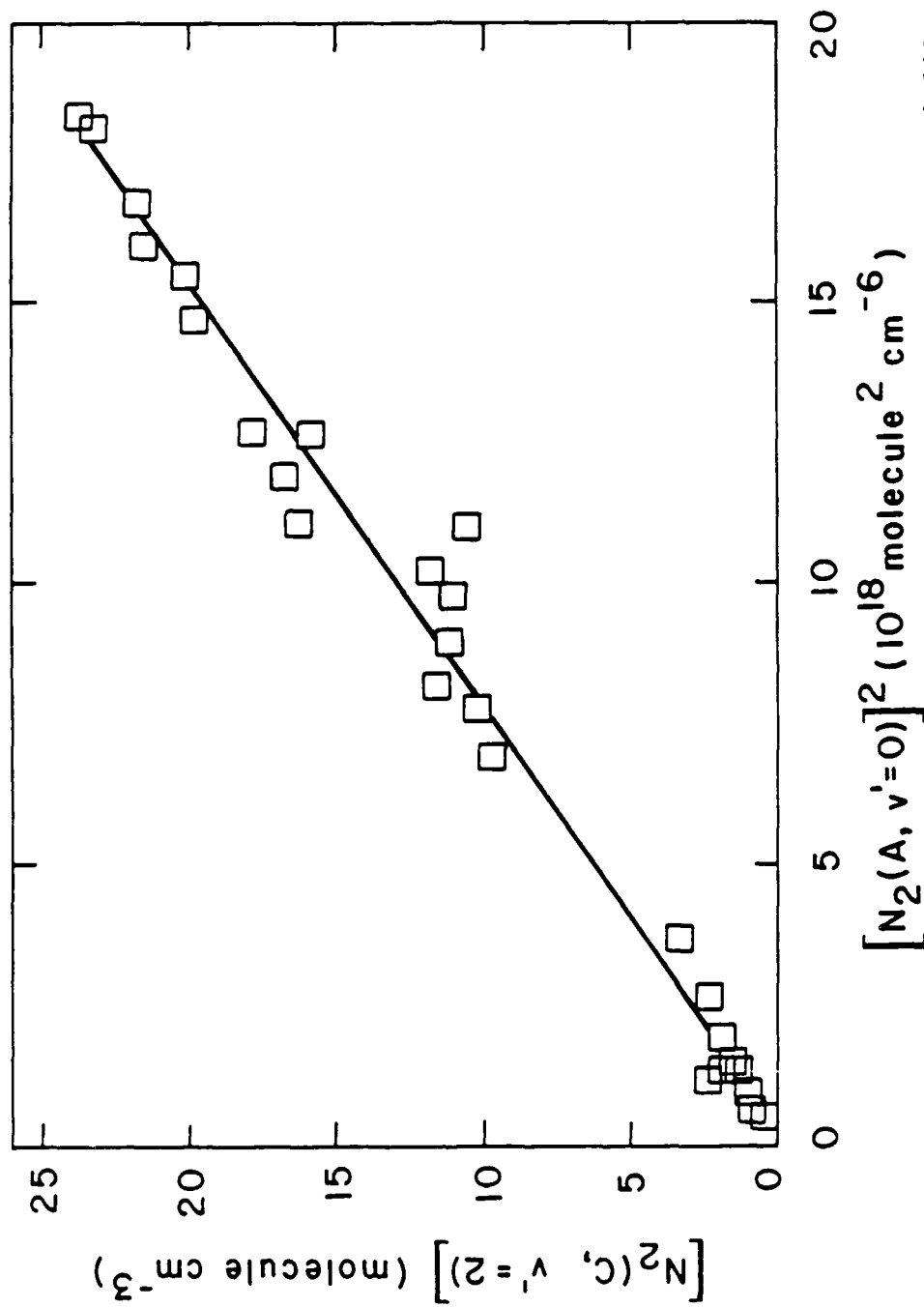
A-1931

Figure 4. Observed (heavy line) and computed best fit (light line) to the spectral region between 220 and 400 nm. Resolution 1.0 nm. Full scale sensitivity 5 kHz.



A-2140L

Figure 5. Variation in the number density of $N_2(C, v'=0)$ as a function of the square of the number density of $N_2(A, v'=0)$



A-2291L

Figure 6. Variation in the number density of $N_2(C, v'=2)$ as a function of the square of the number density of $N_2(A, v'=0)$

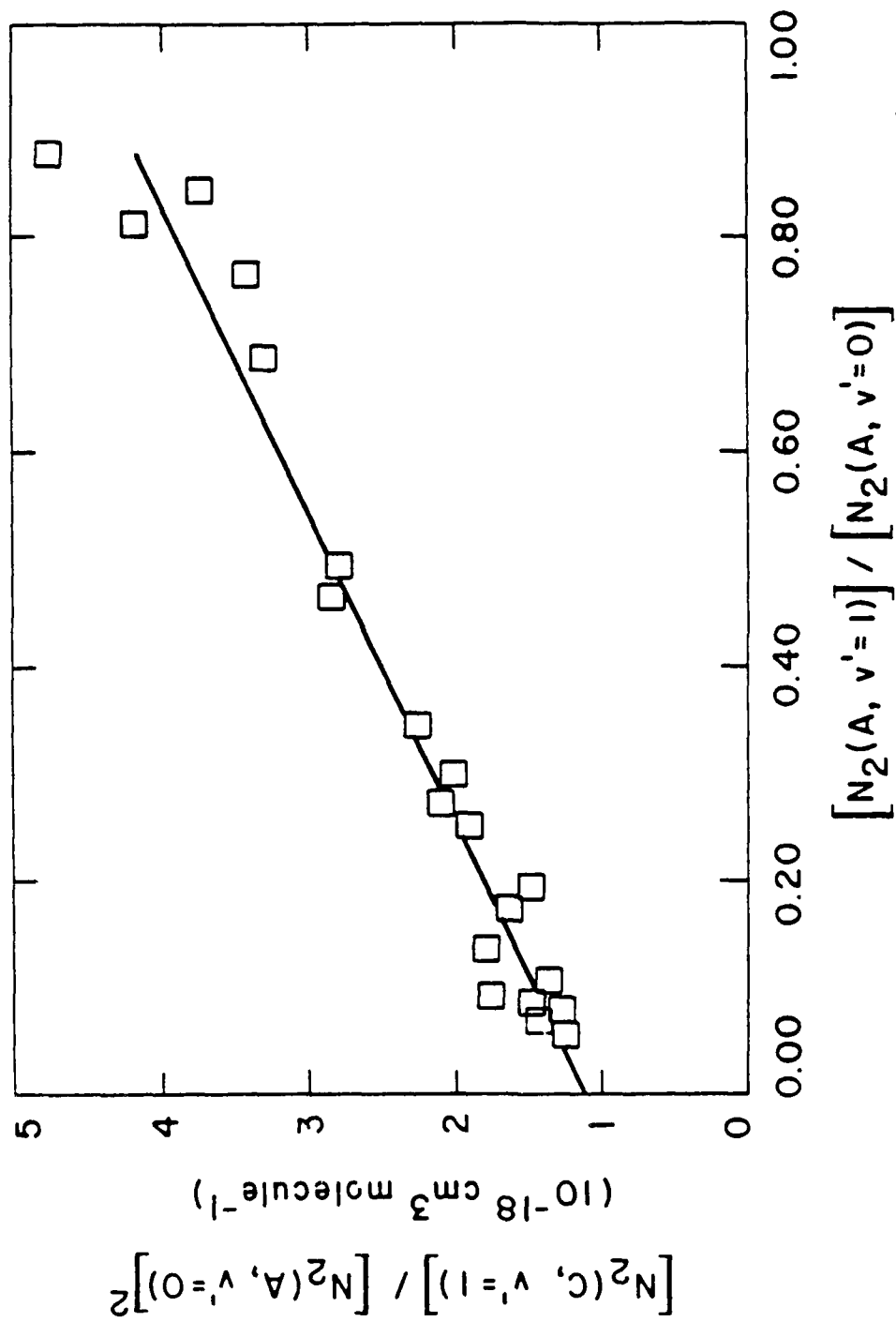
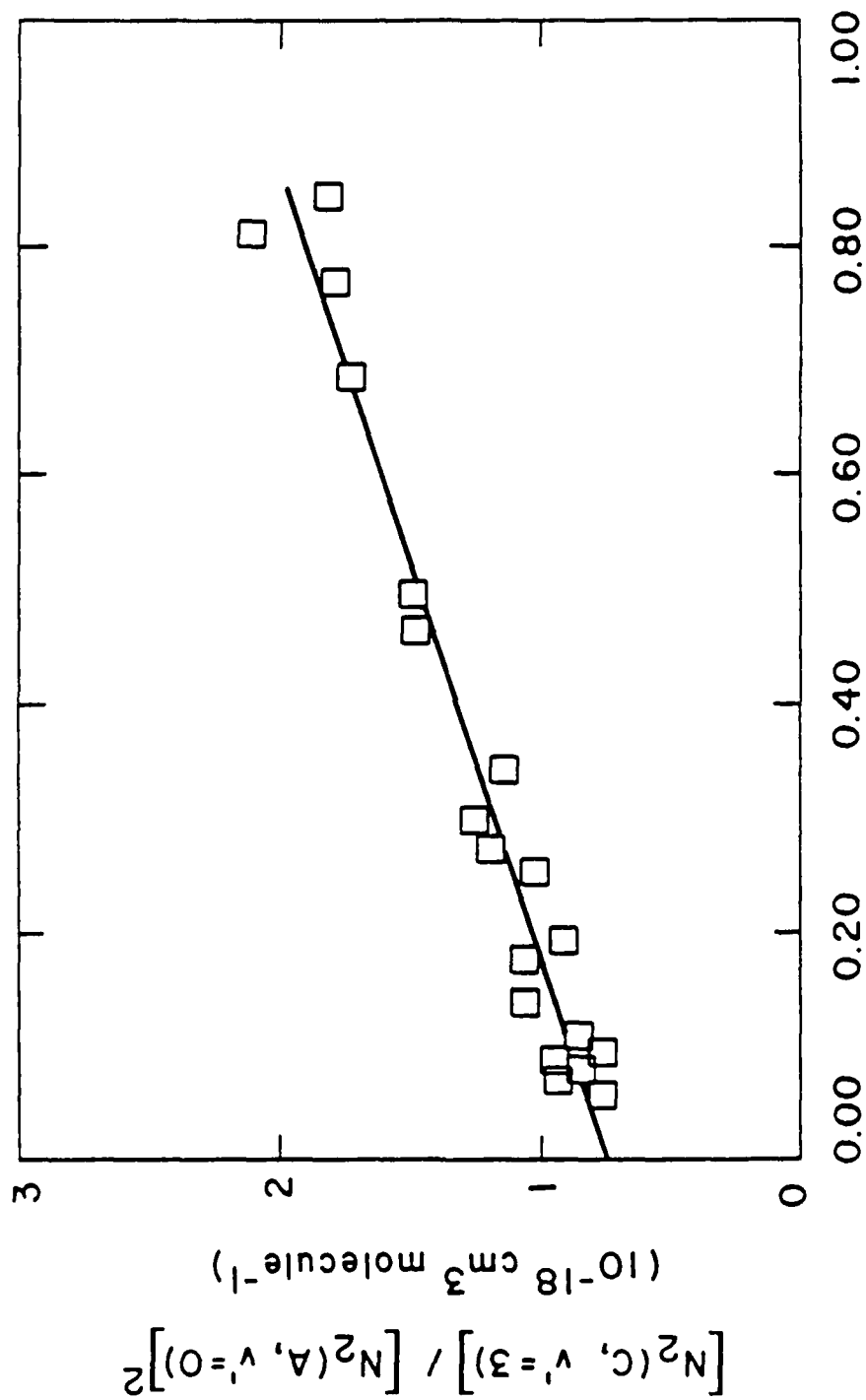


Figure 7. Variation in the ratio of the number density of $N_2(C, v'=1)$ to the square of the number density of $N_2(A, v'=0)$ as a function of the ratio of the number densities of vibrationally excited to unexcited $N_2(A)$.



A-2295aL

Figure 8. Variation in the ratio of the number density of $N_2(C, v'=3)$ to the square of the number density of $N_2(A, v'=0)$ as a function of the ratio of the number densities of vibrationally excited to unexcited $N_2(A)$.

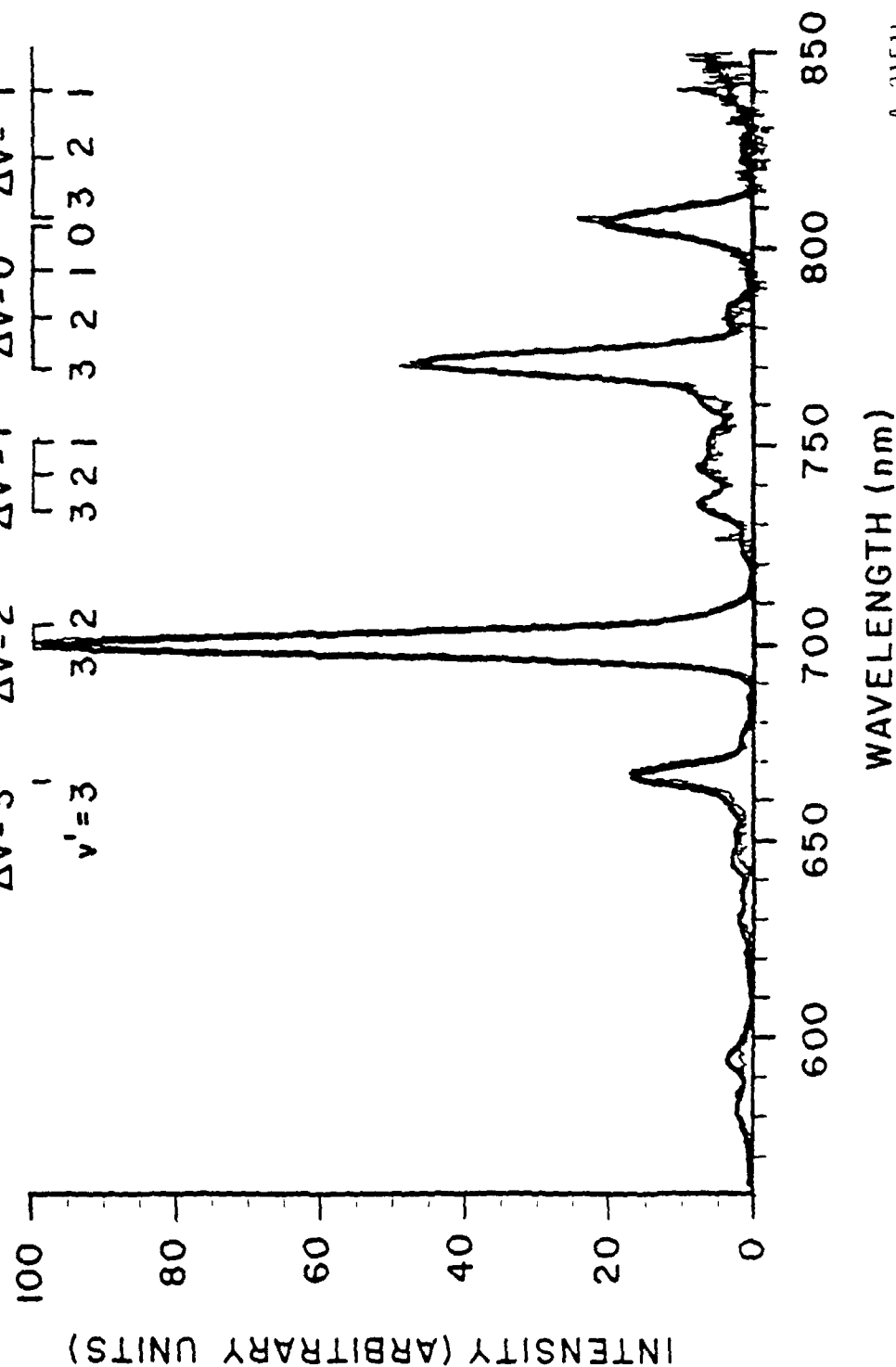
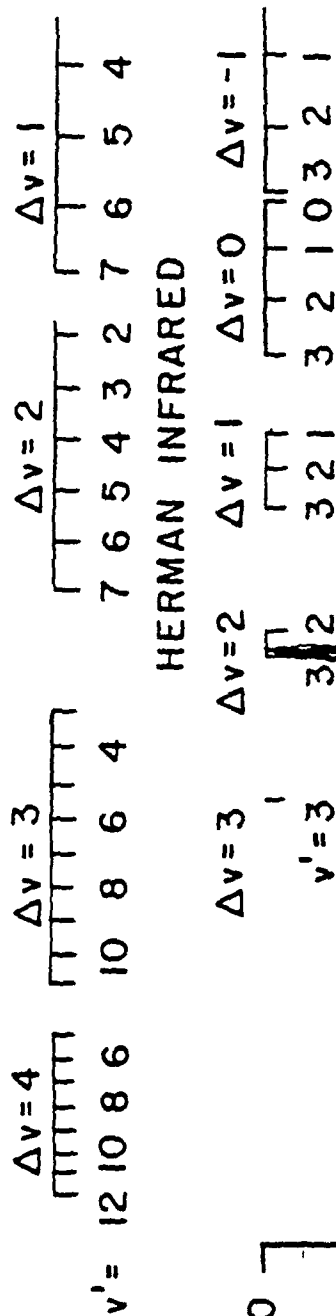


Figure 9. Spectrum of the Herman Infrared $v'=3$ system (light line) excited in the energy pooling of $\text{N}_2(\text{A}, v'=0)$. The heavy line is the synthetic fit to the spectrum. $P_{\text{total}} = 7.5$ torr, $X_{\text{N}_2} = 0.20$.

A-2151L

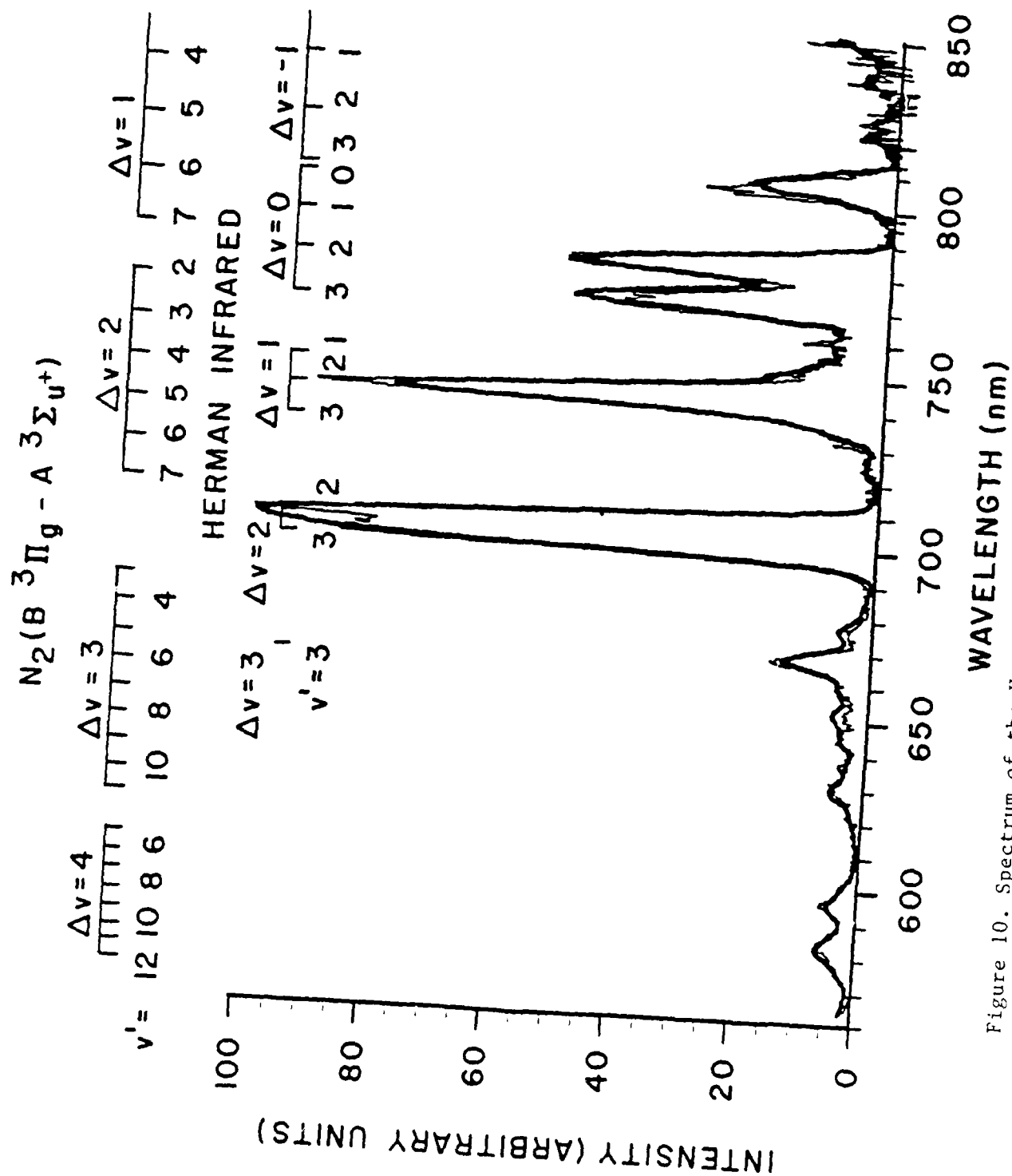


Figure 10. Spectrum of the Herman Infrared $v'-2,3$ systems (light line) excited in the energy pooling of $N_2(A, v'=0, 1)$. The heavy line is the synthetic fit to the spectrum. $P_{\text{total}} = 7.5$ torr, $X_{N_2} = 0.20$.

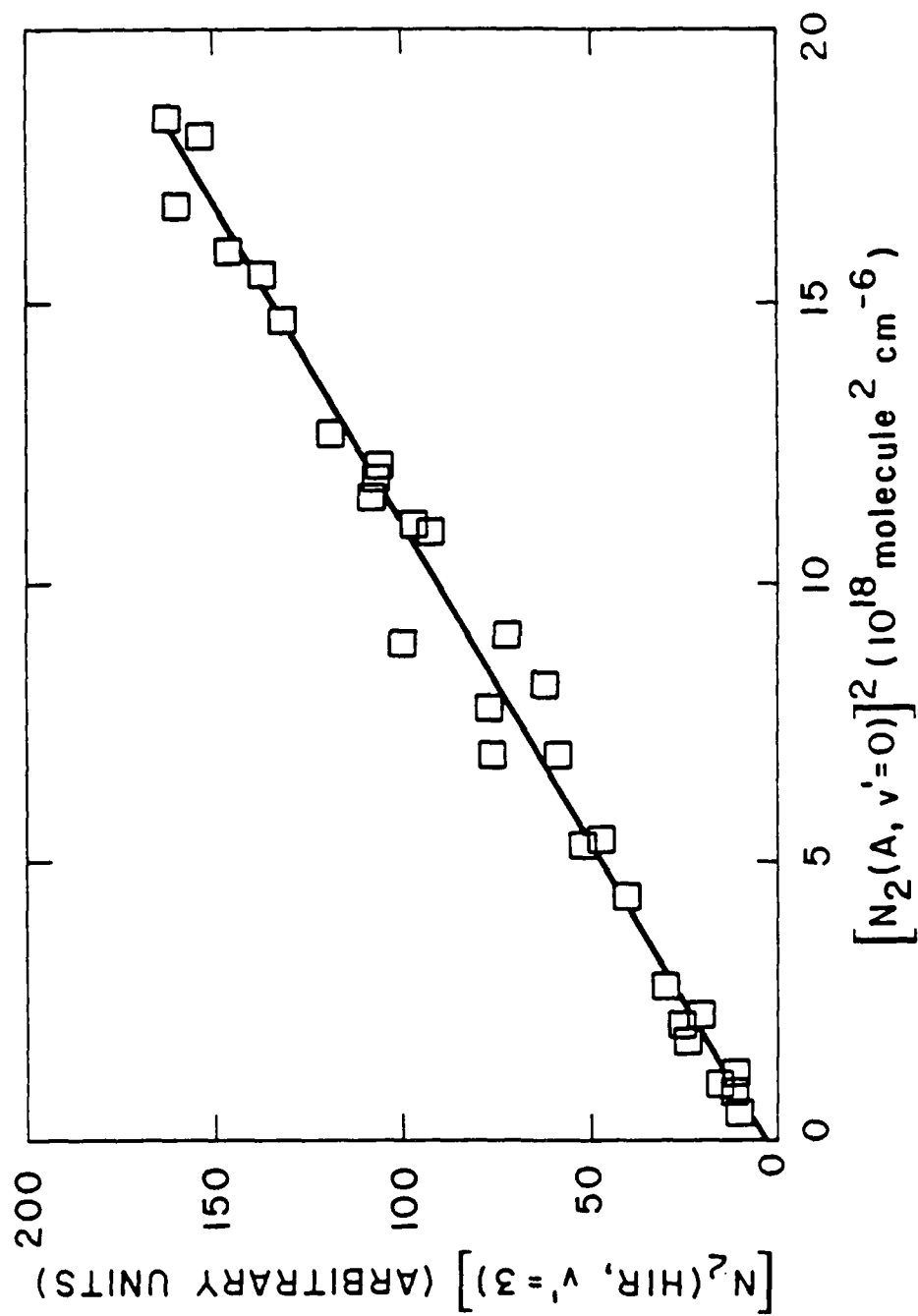


Figure 11. Variation in the number density of $N_2(\text{HIR}, v'=3)$ as a function of the square of the number density $N_2(A, v'=0)$.

A-2143L

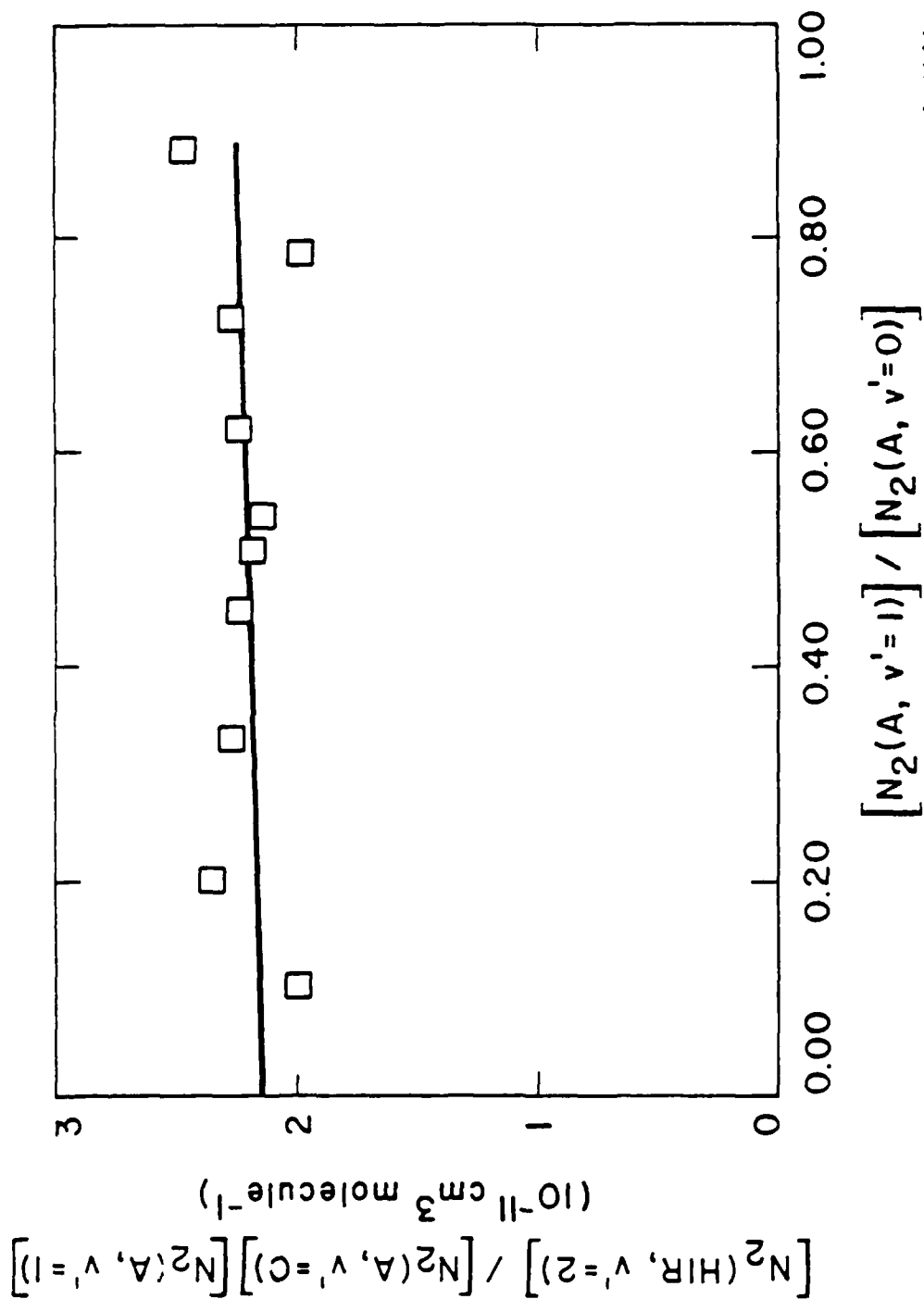


Figure 12. Variation in the ratio of the $N_2(\text{HIR}, v'=2)$ number density to the product of the number densities of $N_2(A, v'=0)$ and $v'=1$ as a function of the ratio of the number densities of $N_2(A, v'=1)$ to $v'=0$.

A-2144L

APPENDIX H

(SR-322 reproduced in its entirety)

J. Chem. Phys. 88, 6911 (1988)

State-to-State $N_2(A^3\Sigma_u^+)$ Energy Pooling Reactions: II. The Formation
and Quenching of $N_2(B^3\Pi_g, v' = 1-12)$

Lawrence G. Piper

Physical Sciences Inc.
Research Park, P.O. Box 3100
Andover, MA 01810

J. Chem. Phys. 88, 6911 (1988)

ABSTRACT

We have studied the state-to-state excitation of $N_2(B^3\Pi_g, v'=1-11)$ in energy pooling reactions between $N_2(A^3\Sigma_u^+, v'=0,1)$ molecules and subsequent quenching in collisions with molecular nitrogen. Excitation of vibrational levels 10, 2, and 3 appears to be much stronger than excitation of the other vibrational levels. In addition, we failed to observe any emission from $v'=12$ even though it is energetically accessible. The excitation rate coefficients are quite large, $7.7 \times 10^{-11} \text{ cm}^3 \text{ molecule}^{-1} \text{ s}^{-1}$ for the pooling of two $N_2(A, v'=0)$ molecules, and roughly a factor of three larger for energy pooling events involving $N_2(A, v'=1)$. The effective rate coefficients for electronic quenching of $N_2(B)$ by N_2 are also quite large, $\sim 3 \times 10^{-11} \text{ cm}^3 \text{ molecule}^{-1} \text{ s}^{-1}$. Comparison of our quenching results with the laser-excited, real-time quenching studies of Rotem and Rosenwaks indicates agreement only within factors of 2-3.

I. Introduction

Hays and Oskam¹ investigated the temporal decay of emissions from $N_2(A^3\Sigma_u^+)$ and $N_2(B^3\Pi_g)$ in the afterglow of a pulsed discharge. They noted that the intensity of the first-positive system, $N_2(B^3\Pi_g \rightarrow A^3\Sigma_u^+)$ varied quadratically with the intensity of the Vegard-Kaplan bands, $N_2(A^3\Sigma_u^+ \rightarrow X^1\Sigma_g^+)$, and interpreted this behavior as a sign that $N_2(B)$ was excited in the afterglow by energy pooling reactions involving $N_2(A)$. Their observations led them to assign a rate coefficient for the energy pooling process resulting in $N_2(B)$ formation of $1.1 \times 10^{-9} \text{ cm}^3 \text{ molecule}^{-1} \text{ s}^{-1}$. One would have to assume that this number is a lower bound because their detection system could not observe $N_2(B, v'=0-2)$. Nadler et al.² discovered in 1980 that the Herman Infrared (HIR) system, which emits over the same wavelength region as $N_2(B)$, was also populated efficiently by $N_2(A)$ energy pooling. They estimated a lower limit for HIR formation of $2.5 \times 10^{-11} \text{ cm}^3 \text{ molecule}^{-1} \text{ s}^{-1}$ which they subsequently revised upward to $7 \times 10^{-11} \text{ cm}^3 \text{ molecule}^{-1} \text{ s}^{-1}$.^{3,4} They also showed that some production of the B state did indeed occur, but they were unable to estimate the rate coefficient for B-state formation because of that state's rapid quenching by nitrogen and argon.

Unpublished observations at PSI⁵ in the near infrared recorded the HIR system in $N_2(A)$ energy pooling, but failed to detect significant populations of $N_2(B)$. We were thus skeptical of the magnitude of the pooling rate coefficient which Hays and Oskam had reported. The work of Nadler et al.²⁻⁴ also showed convincingly that HIR production had to be similar in magnitude to the production of $N_2(B)$. Thus the present investigation was motivated in part by our desire to reconcile the conflict between Hays and Oskam's report and the observations of Nadler et al. as well as our own.

In Part I of this investigation,⁶ we studied the state-to-state excitation of $N_2(C^3\Pi_u, v=0-4)$ and the Herman Infrared (HIR) system, $v=2,3$, in energy pooling reactions of $N_2(A^3\Sigma_u^+, v'=0,1)$. We showed the excitation of $N_2(C)$ to be quite efficient for energy pooling of two $N_2(A, v'=0)$ molecules or one $v'=0$ interacting with a $v'=1$ molecule, $k = 1.5 \times 10^{-10} \text{ cm}^3 \text{ molecule}^{-1} \text{ s}^{-1}$, but saw no evidence of significant formation of $N_2(C)$ when two $N_2(A, v'=1)$

molecules interacted, $k < 0.5 \times 10^{-10} \text{ cm}^3 \text{ molecule}^{-1} \text{ s}^{-1}$. The Herman Infrared system showed striking state specificity. Only HIR $v=3$ was excited by two $\text{N}_2(\text{A}, v'=0)$ molecules, $k = 8 \times 10^{-11} \text{ cm}^3 \text{ molecule}^{-1} \text{ s}^{-1}$; a $v'=0$ and a $v'=1$ molecule combined to produce only HIR $v=2$, $k = 10 \times 10^{-11} \text{ cm}^3 \text{ molecule}^{-1} \text{ s}^{-1}$; and two $\text{N}_2(\text{A}, v'=1)$ molecules appeared not to excite the Herman Infrared system at all. This paper reports the extension of these investigations to $\text{N}_2(\text{B}^3\Pi_g)$.

II. Experimental

The apparatus used for these studies has been described in detail in a number of recent publications.⁶⁻¹³ Basically the experiment involves generating $\text{N}_2(\text{A})$ metastables cleanly in a discharge-flow apparatus and then monitoring spectroscopically the Vegard-Kaplan, Herman Infrared and First-positive systems under constant conditions. The energy transfer reaction between metastable $\text{Xe}(^3\text{P}_{0,2})$ and N_2 produced the $\text{N}_2(\text{A})$ metastables.¹⁴⁻¹⁶ Introducing CH_4 downstream from the discharge allowed the vibrational distribution of the $\text{N}_2(\text{A})$ to be varied so that state-specific measurements could be made.^{8,17} The xenon metastables were produced in a hollow cathode discharge through a mixture of xenon and argon in a neon carrier gas. Typical flow rates through the discharge were 8, 150, and 3500 $\mu\text{mol s}^{-1}$ for xenon, argon, and neon, respectively. The small argon flow was crucial to produce adequate number densities of the metastable xenon atoms. The nitrogen was then added downstream from the discharge so that we could be certain that nitrogen excitation was effected only by the energy-transfer reaction. As we show later, discharging the nitrogen along with the rare gases causes direct excitation of nitrogen in the discharge which drastically alters the $\text{N}_2(\text{B})$ excitation magnitude and distribution in the afterglow. The reason for doing the experiments in neon is that, unlike argon, neon is a relatively weak quencher of $\text{N}_2(\text{B})$.^{18,19} The distributions observed in a neon buffer when the number densities of the other gases (especially nitrogen) have been reduced to a minimum, will be relatively close to nascent. This would not be the case in an argon buffer. Not only does argon quench the $\text{N}_2(\text{B})$ electronically, but it

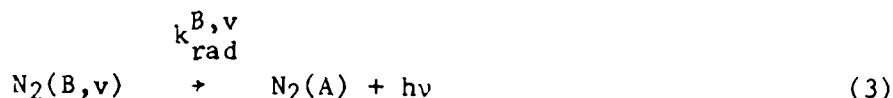
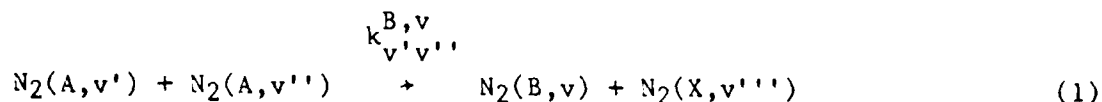
alters the $N_2(B)$ vibrational distribution drastically (see below). The procedure then was to repeat spectral scans of the various band systems as a function of nitrogen partial pressure. Analysis of the spectra gave populations of each vibrational level as a function of nitrogen partial pressure. Extrapolating the results to zero nitrogen partial pressure gave the nascent populations. Scans at several different neon partial pressures showed only small changes in total $N_2(B)$ excitation rate and in its vibrational distribution.

The spectra were analyzed by least-squares computer fitting as discussed previously.^{8,10} We used the appropriate potential constants in Lofthus and Krupenie²⁰ for the Vegard-Kaplan and First-positive systems, and used the Einstein Coefficients of Shemansky²¹ and Shemansky and Broadfoot²² to extract the $N_2(A)$ and $N_2(B)$ number densities. We treated the Herman Infrared system empirically as described previously.⁶ We also described previously our procedures for turning observed intensities into absolute photon emission rates and for correcting for the different radial density gradients of the $N_2(A)$ and the $N_2(B)$.⁶

We have expressed some concern previously that Shemansky's Einstein coefficients for $N_2(A-X)$ might be 20-40 percent too large.^{10,23} Furthermore, Shemansky and Broadfoot's Einstein coefficients for $N_2(B-A)$ transitions (which are the ones tabulated in Lofthus and Krupenie²⁰) are somewhat questionable.²³⁻²⁵ Pending resolution of these issues, however, we choose to use the commonly accepted values. We currently are investigating the $N_2(B-A)$ transition probabilities.²⁶ We have also found recently²⁶ that the potential constants of Roux et al.²⁷ fit the first-positive bands more accurately than those given in Lofthus and Krupenie.²⁰ The small differences do not affect the populations extracted from the spectral fitting, however.

III. Results

The processes controlling the formation and destruction of $N_2(B)$ in the energy pooling of $N_2(A)$ are:



where in the rate coefficients, k , the superscript v denotes the vibrational level of the $N_2(B)$ product, the subscript v denotes the vibrational level of the $N_2(A)$ molecules, and $k_{\text{rad}}^{B, v}$ is the radiative decay rate of $N_2(B, v)$. Because the $N_2(B)$ has a lifetime on the order of microseconds,^{22,25,28-30} it is in steady state within the field of view of our detector, so that we can equate its formation and destruction rates:

$$\begin{aligned} \frac{d[N_2(B, v)]}{dt} &= 1.267 \sum_{v'} \sum_{v''} k_{v', v''}^{B, v} [N_2(A, v')] [N_2(A, v'')] \\ &\quad - k_{\text{rad}}^{B, v} + k_Q^{B, v} [N_2] [N_2(B, v)] = 0 \end{aligned} \quad (4)$$

Thus we have

$$[N_2(B, v)] = \frac{1.267}{k_{\text{rad}}^{B, v} + k_Q^{B, v} [N_2]} \sum_{v'} \sum_{v''} k_{v', v''}^{B, v} [N_2(A, v')] [N_2(A, v'')] \quad (5)$$

The factor of 1.267 corrects for the differing radial density gradients of the $N_2(A)$ and $N_2(B)$.⁶ For the case of energy pooling of two $N_2(A, v'=0)$ molecules only, we have

$$[N_2(B, v)] = 1.267 \frac{k_{00}^{B, v}}{k_{\text{rad}}^{B, v}} [N_2(A, v'=0)]^2 \left\{ 1 + \frac{k_Q^{B, v}}{k_{\text{rad}}^{B, v}} [N_2] \right\}^{-1} \quad (6)$$

Rearranging this equation shows that the ratio of the square of the A state number density to the B state number density will vary linearly with the number density of the added nitrogen:

$$\frac{[N_2(A, v'=0)]^2}{[N_2(B, v)]} = 0.789 \frac{k_{\text{rad}}^{B, v}}{k_{00}^{B, v}} + 0.789 \frac{k_Q^{B, v}}{k_{00}^{B, v}} [N_2] \quad (7)$$

Figures 1 and 2 show spectra of the region between 500 and 850 nm with nitrogen partial pressures of 0.46 and 0.027 Torr respectively at a constant neon pressure of 3 Torr. Clearly, the First-positive bands increase strongly with the reduced nitrogen partial pressures. Figures 3 and 4 show representative data on the formation of the B state from the pooling of $N_2(A, v'=0)$ plotted according to Eq. (7). From these plots and similar ones for the other vibrational levels studied, we obtained both rate coefficients for B state formation from energy pooling (from the intercepts) and rate coefficients for quenching $N_2(B)$ by molecular nitrogen (from the slopes). The bulk of the experiments were at 3.0 Torr total pressure, but scans at 1.5 and 6 Torr gave similar vibrational distributions, and similar ratios of B-state number density to the square of the A-state number density as the data just discussed (see Figure 5). Thus at the lowest nitrogen partial pressures studied, $N_2(B)$ quenching by the neon, argon, xenon, and CH_4 in the reactor did not appear to be large. We therefore studied the variations in B state formation from the energy pooling of vibrationally excited $N_2(A)$ under conditions comparable to those producing the minimum B-state quenching observed in the $N_2(A, v'=0)$ studies.

For these studies, we consider the system to be essentially two vibrational levels of $N_2(A)$, i.e., $v'=0$ and $v'>0$. From Eq. (5) we derive

$$\frac{[N_2(B, v)] \left(1 + \frac{k_Q^{B, v}}{k_{\text{rad}}^{B, v}} [N_2]\right)}{[N_2(A, v'=0)]^2} = 1.267 \frac{k_{00}^{B, v}}{k_{\text{rad}}^{B, v}} + 2.534 \frac{k_{0v}^{B, v}}{k_{\text{rad}}^{B, v}} \frac{[N_2(A, v'>0)]}{[N_2(A, v'=0)]} + 1.267 \frac{k_{vv}^{B, v}}{k_{\text{rad}}^{B, v}} \left\{ \frac{[N_2(A, v'>0)]}{[N_2(A, v'=0)]} \right\}^2, \quad (8)$$

where we have corrected only for molecular-nitrogen quenching (~ 10 percent effect). Thus we can extract rates for pooling from collisions of one or both vibrationally excited $N_2(A)$ molecules from quadratic least-squares fits of the left hand side of Eq. (8) versus the ratio $[N_2(A, v' > 0)]/[N_2(A, v' = 0)]$. We used the quenching-rate coefficients determined in the $N_2(A, v' = 0)$ studies to correct the $N_2(B)$ number densities. Figures 2, 6 and 7 show how the spectrum between 550 and 720 nm changes as the degree of vibrational excitation in the $N_2(A)$ changes. Figures 8 and 9 show representative B-state vibrational levels plotted according to Eq. (8). The solid lines are calculated from the least-squares fit. The intercepts of these plots gave results within 10 percent of the $v' = 0$ results determined above. These results also show that the pooling between a $v' = 0$ and a $v' > 0$ is somewhat faster than the pooling between two $v' = 0$ molecules or between two $v' > 0$ molecules. Table 1 summarizes the rate coefficients measured, Table 2 the effective N_2 quenching rate coefficients.

In Table 1, the rate coefficients for B-state formation are corrected for formation resulting from radiative cascade from the C-state which also is formed in $N_2(A)$ energy pooling. We multiplied the rate coefficients previously determined for C-state formation⁶ by the appropriate branching ratio for radiation to the different B-state levels.²⁰ The terms with a common B-state level were then summed to derive the correction factors.

The error bars listed in Table 1 are 1σ standard deviations derived from the least squares fits. These error bars provide, in most instances, a reasonable picture of the relative uncertainties between the measurements for the various states and also the relative uncertainty between measurements made by most other groups who will have used the same lifetimes for the A and B states. One exception will be the rate coefficient for formation of $N_2(B, v' = 1)$ for which the relative uncertainty could be as much as a factor of two or three. The only emission from this level lies at the extreme edge of the monochromator's response. The response function is rather uncertain, therefore. All other observations result from a simultaneous fit of several bands with common upper states. This fitting procedure eliminates errors due to uncertainties in the response function. In absolute terms, a roughly

40 to 50 percent systematic uncertainty must be added to the statistical uncertainties to account for errors in the $N_2(A)$ and $N_2(B)$ lifetimes and in the air afterglow rate coefficient which was used to calibrate the optical system absolutely.

IV. Discussion

Examination of the data shows several interesting results. Close to half of the B state formation arises as a result of radiative cascade out of $N_2(C)$. The distribution of $N_2(B)$ vibrational levels excited by two $N_2(A, v'=0)$ is independent of vibrational level except for vibrational levels 2 and 10 which are excited two to three times more efficiently than the other levels. As the $N_2(A)$ becomes more vibrationally excited, the $N_2(B)$ vibrational distribution begins to favor the lower vibrational levels. Under no conditions did we observe any excitation of $N_2(B, v=12)$.

Clearly the Hays and Oskam result for the formation of $N_2(B)$ is incorrect. Their studies were performed in the afterglow of a pulsed discharge of nitrogen. A number of metastable species in addition to $N_2(A)$ will persist in the afterglow of a nitrogen discharge, and we expect that one of these other metastables is responsible for Hays and Oskam's observations. We tested this hypothesis briefly with experiments in an argon buffer. We compared results when the N_2 was added in the normal fashion and when it was diverted to mix with the main argon flow upstream from the discharge. Figure 10 shows our result graphically. While discharging the nitrogen with the argon increased the $N_2(A)$ number density in the observation region by about a factor of 3, the populations of the $N_2(B)$ vibrational levels grew by a factor of 70. The HIR 3,1 band, which is relatively free from first-positive overlap, and which is therefore a good monitor of the increase in A-state pooling, grew by only a factor of 9 as would be expected. The eight-fold greater increase in the B-state population than can be explained on the basis of increased A-state number densities shows clearly that discharging nitrogen directly produces metastables in addition to $N_2(A)$ which are long lived and which couple collisionally into the B state. This other state was probably responsible for

Hays and Oskam's observations. Metastable $N_2(a'^1\Sigma_u^-)$ molecules are formed in the discharge,^{12,31} and do have enough energy to excite $N_2(B)$, but we showed them not to be responsible for $N_2(B)$ formation. Adding H_2 downstream from the discharge, but upstream from the observation region, completely eliminated $N_2(a')$ emission at 171 nm but reduced the B-state emission by less than 15 percent. We are currently considering other alternatives to the precursor of the enhanced B-state emission.

Adding the rate coefficients for energy pooling into $N_2(C^3\Pi_u)$ and the Herman Infrared system reported previously⁶ to those determined here for $N_2(B^3\Pi_g)$ gives a value of 3.0 and $4.7 \times 10^{-10} \text{ cm}^3 \text{ molecule}^{-1} \text{ s}^{-1}$ for energy pooling of two $N_2(A, v'=0)$ and of $N_2(A, v'=0) + N_2(A, v'=1)$ respectively. These numbers represent a lower limit to the total energy pooling rate coefficient, because unobserved states might be involved, and also because we have not been able to evaluate the contributions of $N_2(B, v'=0)$ formation. Since vibrational levels 1 through 8 are all formed at least 50 percent by radiative cascade from the C state, we would expect $N_2(B, v'=0)$ to follow suit. This would raise the total pooling rate coefficient by less than 10 percent. The formation of unobserved states cannot readily be assessed. A number of states are available, most notably the $W^3\Delta_u$ and $B'^3\Sigma_u^-$ states. We do see the 5-1 band of the B'-B system at 825 nm, but cannot tell whether it is formed directly or by collisions between $N_2(B)$ and N_2 . In addition, we have observed a small amount of emission in the 140 to 180 nm region which is probably from the Lyman-Birge-Hopfield system, but the intensities are much too weak to resolve for an adequate identification. We would therefore not expect the singlet states to form a significant exit channel.

Various groups have used a Franck-Condon model to try to rationalize their energy transfer results.^{4,32-35} The thinking is that the energy-transfer rate coefficients should scale roughly as

$$k \sim q_1 q_2 e^{-|\Delta E|/kT} \quad (9)$$

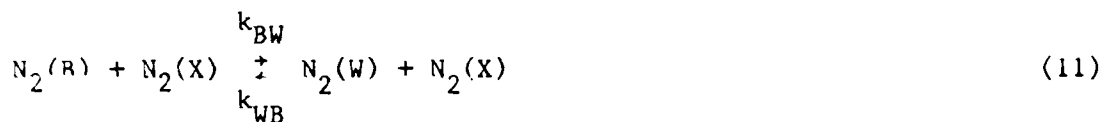
where q_1 and q_2 are the Franck-Condon factors coupling initial and final states in the energy-transfer process and ΔE is the energy defect for the transfer process. Our experimental results comprise an extensive set of state-to-state energy-transfer rate coefficients and therefore can provide an arduous test of this model. Table 3 compares experimental and model results. The model results were normalized to give the same rate coefficient as determined experimentally for the energy-pooling process involving two $N_2(A, v'=0)$ molecules. Examination of the table shows that the model fails to predict the $N_2(B, v)$ distributions from the various energy-transfer processes even qualitatively. Nor does it predict how the rate coefficient for producing a given vibrational level of $N_2(B)$ will vary as the $N_2(A)$ becomes vibrationally excited. Previously we have noted this failure of the Franck-Condon model to predict $N_2(C, v)$ distributions from $N_2(A)$ energy pooling⁶ and $NO(A, v)$ distributions excited in the energy transfer reaction between $N_2(A, v'')$ and NO .¹⁰

Table 2 lists the rate coefficients for electronic quenching of $N_2(B, v)$ determined in this study along with several other sets of values in the literature. Agreement with the measurements of Mitchell³⁶ and of Shemansky,³⁷ both of whom excited $N_2(B, v)$ by electron impact, is fair as is agreement with Gartner and Thrush's^{38,39} measurements in a recombining N-atom afterglow. Agreement with Becker et al.'s⁴⁰ afterglow observations and the kinetic absorption spectroscopy determination of Dreyer and Perner⁴¹ following excitation of nitrogen by relativistic electrons is not so good. All of these numbers are effective two-body quenching rate coefficients. The actual processes involved are much more complex. The $B^3\Pi_g$ state of nitrogen is coupled collisionally into a number of other nested electronic states including the $A^3\Sigma_u^+$, $B'^3\Sigma_u^-$, $W^3\Delta_u$, and perhaps various states of the singlet manifold including $X^1\Sigma_g^+$.^{18,19,35,42-44} Thus the quenching is actually a complex process which involves shuttling energy back and forth between the various states involved. Sadeghi and Setser^{18,42} and Rotem et al.^{19,43,44} have demonstrated this coupling between the states unequivocally. These groups have excited specific vibrational levels of the $B^3\Pi_g$ state by laser pumping $A^3\Sigma_u^+$ -state molecules. Subsequent to the laser pumping they observe emission from $B'^3\Sigma_u^-$ -state levels, and lower vibrational levels of the $B^3\Pi_g$ state, as well as pressure-dependent, multi-exponential decays of the fluorescence from the

initially populated level. In most cases the fluorescence decays can be separated into two pressure dependent components, one fairly fast, and the other quite slow. The rapidly decaying component represents coupling into a reservoir state which is in equilibrium with the initially pumped level. Generally the $W^3\Delta_u$ state is identified as the primary reservoir state.

Sadeghi and Setser¹⁸ and Rotem et al.^{19,43,44} tried to describe their observations using the two-state coupling model given by Yardley.⁴⁵ We derived a steady-state expression consistent with this model to allow comparison of our observations with those of Rotem and Rosenwaks.¹⁹

The following reactions describe the model:



where we have assumed W as the reservoir state. The B', A and perhaps even the X state could also be reservoir states. For simplicity's sake, however, we designate only one reservoir state. This set of equations defines the following rates:

$$R_f = k_{ep}[N_2(A)]^2 \quad (16)$$

$$R_1 = k_r^B + k_Q^B[N_2] \quad (17)$$

$$R_2 = k_{BW}[N_2] \quad (18)$$

$$R_{-2} = k_{WB}[N_2] \quad (19)$$

$$R_3 = k_r^W + k_Q^W[N_2] \quad (20)$$

The rate of formation of state W is

$$\frac{d[W]}{dt} = R_2[B] - (R_{-2} + R_3)[W] \quad (21)$$

Under steady-state conditions we obtain

$$[W] = \frac{R_2[B]}{R_{-2} + R_3} \quad (22)$$

The rate of formation of state B is

$$\frac{d[B]}{dt} = R_f - (R_1 + R_2)[B] + R_{-2}[W] \quad (23)$$

Under steady-state conditions, with the inclusion of Eq. (22) above, Eq. (23) becomes

$$\frac{R_f}{[B]} = \frac{(R_1 + R_2)(R_{-2} + R_3) - R_2 R_{-2}}{R_{-2} + R_3} \quad (24)$$

The two-state coupling model of Yardley explains bi-exponential decays of state B as

$$\frac{[B](t)}{[B](t=0)} = A_1 e^{-\lambda_1 t} + A_2 e^{-\lambda_2 t} \quad (25)$$

Under conditions such that $\lambda_1 \gg \lambda_2$ the following expressions apply:

$$\lambda_1 \approx R_2 + R_{-2} = k_{BW}P(1 + \chi) \quad (26)$$

$$\lambda_2 \approx \frac{(R_1 + R_2)(R_{-2} + R_3) - R_2 R_{-2}}{R_2 + R_{-2}} \quad (27)$$

$$\approx \frac{k_r^B \chi + k_r^W}{1 + \chi} + \frac{k_Q^B \chi + k_Q^W}{1 + \chi} P \quad (28)$$

$$\chi = K_{eq}^{-1} = \frac{k_{WB}}{k_{BW}} = \frac{A_2}{A_1} \quad (29)$$

Combining Eqs. (24) and (27) gives

$$\frac{R_f}{[B]} = \lambda_2 \left(\frac{R_2 + R_{-2}}{R_{-2} + R_3} \right) = \lambda_2 \left(\frac{1 + \frac{\chi}{R_3}}{\chi + \frac{R_3}{R_2}} \right) \quad (30)$$

Applying expression (28) for λ_2 gives

$$\frac{R_f}{[B]} = \frac{k_r^B \chi + k_r^W}{\chi + \frac{R_3}{R_2}} + \frac{k_Q^B \chi + k_Q^W}{\chi + \frac{R_3}{R_2}} P \quad (31)$$

This expression has a form similar to Eq. (7) which describes the quenching of $N_2(B)$. The product of the ratio of the factor multiplied by P to the constant term in Eq. (31) times k_r^B gives the effective rate coefficient for quenching, based upon rates determined experimentally from the laser-pumping experiments, i.e.,

$$k_Q^{eff} = \frac{k_Q^B \chi + k_Q^W}{k_r^B \chi + k_r^W} k_r^B \quad (32)$$

Rotem and Rosenwaks¹⁹ studied vibrational-level dependent decays as a function of nitrogen pressure. The effective rate coefficient of their slowly decaying component is

$$k_s = \frac{d\lambda_2}{dp} = \frac{k_Q^B \chi + k_Q^W}{1 + \chi} \quad (33)$$

This expression combines with Eq. (31) to give

$$k_Q^{\text{eff}} = \frac{k_s(1 + \chi)}{k_r^B \chi + k_r^W} k_r^B \quad (34)$$

We list values of k_Q^{eff} based upon their measurements of k_s and χ in Table 2. We used the radiative lifetimes of $N_2(B)$ and $N_2(W)$ calculated by Werner et al.²⁴ to derive the k_Q^{eff} values listed. The calculation assumes that the coupling is with the vibrational level of the $W^3\Delta_u$ state which is closest in energy resonance to the vibrational level of $B^3\Pi_g$ considered. Clearly this approximation is somewhat simplistic and may account for the rather mediocre agreement between our measured, effective quenching rate coefficients, and those we calculate based upon the two-state coupling model and Rotem and Rosenwaks' experimental results. Under the circumstances, perhaps a factor of two to three agreement is acceptable. The coupling is probably too complex to be explained by only a two-state model. The ultimate test of any model used to describe phenomena on a microscopic scale is that it be able to reproduce effects observed in global experiments. The two-state model achieves this goal only in part, and appears to need further development.

The microscopic details of the quenching processes depend strongly upon the quenching partner. Nitrogen appears to quench electronic energy out of all levels at roughly comparable rates, and thereby shows little evidence of effecting vibrational relaxation within the $N_2(B)$ vibrational manifold.⁴⁶ Argon, on the other hand, is much less efficient than nitrogen at quenching $B^3\Pi_g$ manifold electronically, but it rather efficiently alters the vibrational distribution.^{40,47} Figure 11 demonstrates this point dramatically. The spectrum in Figure 11a for which the nitrogen partial pressure is 0.21 torr, shows fairly strong first-positive band attenuation relative to the unquenched Herman Infrared band at 703 nm. The vibrational distribution, however, is quite similar to that in Figure 6 which was taken under conditions of

sufficiently low nitrogen partial pressure that electronic quenching is minimal. Figure 11b shows that reducing the nitrogen partial pressure, so as to eliminate N_2 quenching effects, results in a much stronger first-positive system intensity. In argon, however, the vibrational-level distribution is drastically altered. Raising the argon pressure further, as shown in Figures 11c and d, does result in some reduction in the first-positive system intensity, but more noticeable is the continual shifting of the vibrational distribution. Especially interesting in Figure 11d, which is with 10 torr of argon, is that the vibrational distribution appears to hang up in $v'=8$. The apparent electronic quenching by argon in Figure 11c and d compared to Figure 11b might result only from shifting the $B^3\Pi_g$ population into vibrational levels $v'=0-2$ which do not emit in the spectral region observed. The observations would have to be extended into the infrared to clarify this point. Clearly $N_2(B^3\Pi_g)$ quenching is an extremely complex process, and simple models such as implied by Eq. (7) or even Eq. (31) are not completely adequate.

V. Summary and Conclusions

While our results indicate clearly that the formation of $N_2(B^3\Pi_g)$ in $N_2(A^3\Sigma_u^+)$ energy-pooling reactions is efficient, $k \sim 10^{-10} \text{ cm}^3 \text{ molecule}^{-1} \text{ s}^{-1}$, it is an order of magnitude less efficient than previous reports.¹ Our investigations indicate that the earlier measurements were made in the presence of additional N_2 metastables which also are collisionally coupled to $N_2(B)$. The sum of the rate coefficients for $N_2(B)$ excitation reported here and those for $N_2(C)$ and $N_2(HIR)$ reported previously⁶ give a lower limit to the total $N_2(A)$ energy-pooling rate coefficient of $3 \text{ to } 5 \times 10^{-10} \text{ cm}^3 \text{ molecule}^{-1} \text{ s}^{-1}$ depending on the $N_2(A)$ vibrational level distribution. This figure is substantially below the previously reported values of $1 \text{ to } 3 \times 10^{-9} \text{ cm}^3 \text{ molecule}^{-1} \text{ s}^{-1}$. This discrepancy could be reduced somewhat by including unobserved nitrogen states such as $B'^3\Sigma_u^-$ and $W^3\Delta_u$. Including these states will require spectral observations well out into the infrared. The 0,0 transitions of $B'^3\Sigma_u^- - B^3\Pi_g$ lies at 1528 nm while the 2,0 and 1,0 transitions of $W^3\Delta_u - B^3\Pi_g$ are at 3320 and 6430 nm respectively. The 0,0 transition of the W-B system is too far

into the infrared for conventional detectors. Nevertheless, a search in the infrared for B'-B transitions as well as transitions from the higher vibrational levels of the W state appears to be the next important step in unravelling N₂(A) energy pooling.

Our observations of state-to-state transfer rates provide an important test for the Franck-Condon model which has been invoked so enthusiastically in recent years. We have been unable to find even qualitative agreement between this model and our observations on N₂(A) energy pooling, both in this work and in our experiments reported in Ref. 6. Neither did our state-to-state measurements on the excitation of NO(A²Σ⁺) by N₂(A)¹⁰ provide any support for this model. The failure of the Franck-Condon model to describe these systems is especially intriguing because it apparently describes reasonably well some aspects of the excitation of sulfur-containing molecules by N₂(A).^{48,49}

ACKNOWLEDGEMENTS

This work was supported partially by contract F19628-85-C-0032 with the Air Force Geophysics Laboratory, who are sponsored by the Defense Nuclear Agency under Project 5A, Task 5A, work unit 00115 and by the Air Force Office of Scientific Research under Task 2310G4, and also partially by contract F19628-85-C-0076 with the Air Force Weapons Laboratory. We appreciate illuminating discussions with Prof. Donald W. Setser of Kansas State University and Dave Green and Terry Rawlins of PSI and the invaluable data analysis capabilities of Margrethe DeFaccio.

REFERENCES

1. G.N. Hays and H.J. Oskam, J. Chem. Phys. 59, 1507 (1973).
2. I. Nadler, D.W. Setser, and S. Rosenwaks, Chem. Phys. Lett. 72, 536 (1980).
3. I. Nadler, A. Rotem, and S. Rosenwaks, Chem. Phys. 69, 375 (1982).
4. I. Nadler and S. Rosenwaks, J. Chem. Phys. 83, 3932 (1985).
5. L.G. Piper, unpublished results (1980).
6. L.G. Piper, J. Chem. Phys. 88, 321 (1988), part 1.
7. L.G. Piper, G.E. Caledonia, and J.P. Kennealy, J. Chem. Phys. 75, 2847 (1981).
8. L.G. Piper, W.J. Marinelli, W.T. Rawlins, and B.D. Green, J. Chem. Phys. 83, 5602 (1985).
9. L.G. Piper and W.T. Rawlins, J. Phys. Chem. 90, 320 (1986).
10. L.G. Piper, L.M. Cowles, and W.T. Rawlins, J. Chem. Phys. 85, 3369 (1986).
11. L.G. Piper, M.E. Donahue, and W.T. Rawlins, J. Phys. Chem. 91, 3883 (1987).
12. L.G. Piper, J. Chem. Phys. 87, 1625 (1987).
13. L.G. Piper, G.E. Caledonia, and J.P. Kennealy, J. Chem. Phys. 74, 2888 (1981).
14. D.W. Setser, D.H. Stedman, and J.A. Coxon, J. Chem. Phys. 53, 1004 (1970).
15. D.H. Stedman and D.W. Setser, Chem. Phys. Lett. 2, 542 (1968).
16. N. Sadeghi and D.W. Setser, Chem. Phys. Lett. 82, 44 (1981).
17. J.M. Thomas, J.B. Jeffries, and F. Kaufman, Chem. Phys. Lett. 102, 50 (1983).
18. N. Sadeghi and D.W. Setser, J. Chem. Phys. 79, 2710 (1983).
19. A. Rotem and S. Rosenwaks, Optical Engineering 22, 564 (1983).
20. A. Lofthus and P.H. Krupenie, J. Phys. Chem. Ref. Data 6, 287 (1977).

21. D.E. Shemansky, J. Chem. Phys. 51, 689 (1969).
22. D.E. Shemansky and A.L. Broadfoot, J. Quant. Spectrosc. Radiat. Transfer 11, 1385 (1971).
23. L.G. Piper, S.J. Davis, H.C. Murphy, W.P. Cummings, L.P. Walkauskas, M.A. DeFaccio, L.M. Cowles, W.T. Rawlins, W.J. Marinelli, and B.D. Green, PSI-076/TR-593 under Air Force Weapons Laboratory contract no. F29601-84-C-0076 (1987).
24. H.W. Werner, J. Kalcher, and E.A. Reinsch, J. Chem. Phys. 81, 2420 (1984).
25. E.E. Eyler and F.M. Pipkin, J. Chem. Phys. 79, 3654 (1983).
26. L.G. Piper, K.W. Holtzclaw, B.D. Green, and W.A.M. Blumberg, Bull. APS 33, XXX (1988) and manuscript in preparation.
27. F. Roux, F. Michaud, and J. Verges, J. Mol. Spectrosc. 97, 253 (1983).
28. M. Jeunehomme, J. Chem. Phys. 45, 1805 (1966).
29. T.A. Carlson, N. Duric, P. Erman, and M. Larsson, Physica Scripta 19, 25 (1979).
30. R.F. Heidner III, D.G. Sutton, and S.N. Suchard, Chem. Phys. Lett. 37, 243 (1976).
31. M.F. Golde, Chem. Phys. Lett. 31, 348 (1975).
32. F. Deperesinka, J.A. Beswick, and A. Tramer, J. Chem. Phys. 71, 2477 (1979).
33. D.H. Katayama, T.A. Miller, and V.E. Bondybey, J. Chem. Phys. 69, 3602 (1978).
34. R.D. Coombe and C.H.-T. Lam, J. Chem. Phys. 80, 3106 (1984).
35. D.S. Richards and D.W. Setser, Chem. Phys. Lett. 136, 215 (1987).
36. K.B. Mitchell, J. Chem. Phys. 53, 1957 (1970).
37. D.E. Shemansky, J. Chem. Phys. 64, 565 (1976).
38. E.M. Gartner and B.A. Thrush, Proc. R. Soc. Lond. A. 346, 103 (1975).
39. E.M. Gartner and B.A. Thrush, Proc. R. Soc. Lond. A. 346, 121 (1975).
40. K.H. Becker, E.H. Fink, W. Groth, W. Jud, and D. Kley, Discuss. Faraday Soc. 53, 35 (1972).
41. J.W. Dreyer and D. Perner, Chem. Phys. Lett. 16, 169 (1972).

42. N. Sadeghi and D.W. Setser, Chem. Phys. Lett. 77, 304 (1981).
43. A. Rotem, I. Nadler, and S. Rosenwaks, J. Chem. Phys. 76, 2109 (1982).
44. A. Rotem, I. Nadler, and S. Rosenwaks, Chem. Phys. Lett. 83, 281 (1981).
45. J.T. Yardley, Introduction to Molecular Energy Transfer, Academic Press, New York, 1980.
46. B.D. Green, W.J. Marinelli, L.G. Piper, and W. Blumberg, manuscript in preparation.
47. R.L. Brown, J. Chem. Phys. 52, 4604 (1970).
48. D.S. Richards and D.W. Setser, Chem. Phys. Lett. 136, 215 (1987).
49. D.Z. Cao and D.W. Setser, J. Phys. Chem. 92, XXXX (1988).

TABLE 1. Rate Coefficients for $N_2(B^3\Pi_g)$ Formation from $N_2(A^3\Sigma_u^+)$ Energy Pooling.

$N_2(B, v')$	$k_{00}^{B,v}$ ^a			$k_{01}^{B,v}$			$k_{11}^{B,v}$		
	Observed	Cascade ^{b,c}	Direct	Observed	Cascade	Direct	Observed	Cascade	Direct
1	2.4±0.6	3.6±0.1	---	6.6±1.0	3.3±0.4	3.3±1.4	---		
2	3.9±0.2	2.3±0.1	1.6±0.3	5.6±1.8	2.6±0.4	3.0±2.2	14.7±4.3		
3	1.9±0.1	1.5	0.4±0.1	5.8±0.3	1.6±0.2	4.2±0.5	---		
4	1.6±0.1	1.1	0.5±0.1	2.7±1.0	1.1±0.2	1.6±1.2	3.8±2.5		
5	1.5±0.1	0.8	0.7±0.1	2.2±0.6	0.6±0.1	1.6±0.7	4.5±1.3		
6	1.1±0.1	0.5	0.6±0.1	1.7±0.2	0.4±0.1	1.3±0.3	1.5±0.5		
7	0.9±0.1	0.3	0.6±0.1	1.6±0.1	0.3	1.3±0.1	---		
8	0.6±0.1	0.2	0.4±0.1	1.3±0.1	0.2	1.1±0.1	---		
9	0.9±0.1	0.1	0.8±0.1	1.0±0.4	0.1	0.9±0.4	1.6±1.0		
10	1.8±0.1		1.8±0.1	2.8±0.5		2.8±0.5	1.3±1.1		
11	0.32±0.04		0.32±0.04	0.4±0.2		0.4±0.2	1.0±0.5		
$N_2(B)$ TOTAL			7.7±1.1			21.5±7.6	28±11		

a. Rate coefficients are in units of $10^{-11} \text{ cm}^3 \text{ molecules}^{-1} \text{ s}^{-1}$

b. Cascade corrections are based upon the results of Ref. 6

c. If no cascade error bar is listed, it is less than ±0.05

TABLE 2. Rate Coefficients^a for N₂(B) Quenching by N₂.

N ₂ B, v	This Work	Mitchell ³⁶	Shemansky ³⁷	Becker et al. ⁴⁰	Rotem ^b and Rosenwaks ¹⁹	Gartner and Thrush ^{38,39}	Dreyer and Perner ⁴¹
1	1.0±0.8	0.8	~1		1.2	>0.77	0.22±0.02
2	0.8±0.1	1.2	1.9±0.2		3.6	>0.89	0.32±0.02
3	3.0±0.2	2.1	1.7±0.2		9.0		
4	2.4±0.1	1.9	1.8±0.2		4.3		
5	2.6±0.1	1.8	2.3±0.2		6.8		
6	2.1±0.3	1.8	4.1±0.4		-		
7	6.4±0.3	2.4	6.6±0.4		-		
8	8.0±2.4		7.2±0.4		7.5		
9	7.0±1.2		9.8±1.0	0.9	2.8		
10	2.3±0.2		6.3±0.8	2.8	5.3	4.4±0.9	
11	2.8±0.2		2.0±0.3	7.2	-		

a. Units 10⁻¹¹ cm³ molecule⁻¹ s⁻¹.

b. Based on two-state coupling model.

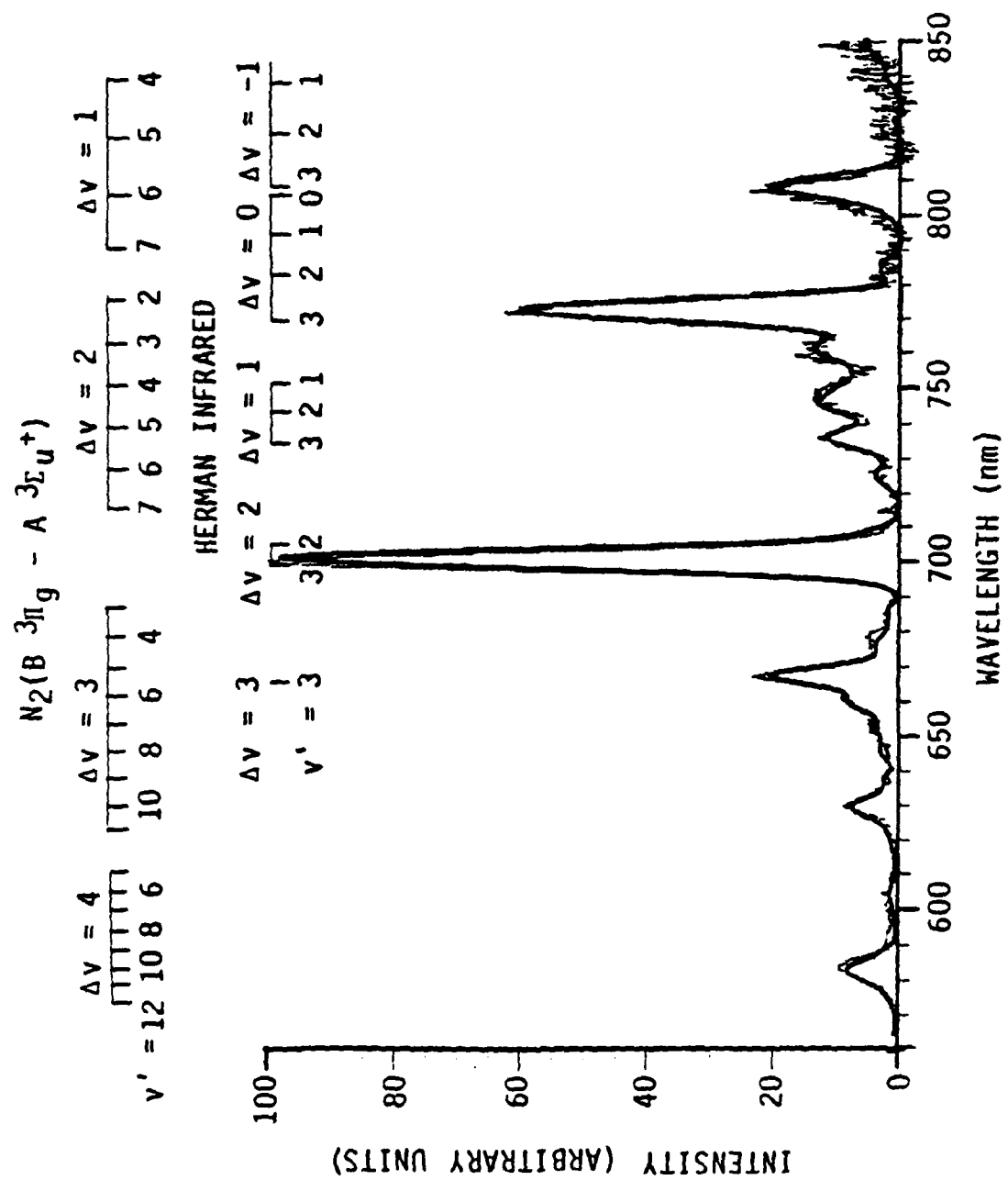
TABLE 3. Comparison Between Observed Energy Pooling Rate Coefficients and Those Predicted by a Franck-Condon Model.

$N_2(B, v')$	k_{00}^{B, v^a}		k_{01}^{B, v^a}		k_{11}^{B, v^a}	
	Model ^b	Observed	Model ^b	Observed	Model ^b	Observed
1	0.03	-	12.4	3.3	0.06	-
2	0.3	1.6	16.3	3.0	27.2	14.7
3	1.0	0.4	10.6	4.2	82.1	-
4	2.9	0.5	3.7	1.6	73.2	3.8
5	3.0	0.7	5.2	1.6	24.4	4.5
6	0.14	0.6	5.5	1.3	14.1	1.5
7	0.003	0.6	0.24	1.3	15.3	-
8	0.004	0.4	0.05	1.1	6.5	-
9	0.06	0.8	0.025	0.9	0.6	1.6
10	0.06	1.8	0.8	2.8	-	1.3
11	0.02	0.3	2.9	0.4	0.2	1.0
12	0.14	-	0.044	-	0.02	-
$N_2(B)$ TOTAL	7.7	7.7	58.1	21.5	243.1	28.0
<p>a. Units are $10^{-11} \text{ cm}^3 \text{ molecule}^{-1} \text{ s}^{-1}$</p> <p>b. The model calculations have been normalized to give the same total rate coefficient for two $N_2(A, v'=0)$ molecules as was observed experimentally.</p>						

LIST OF FIGURES

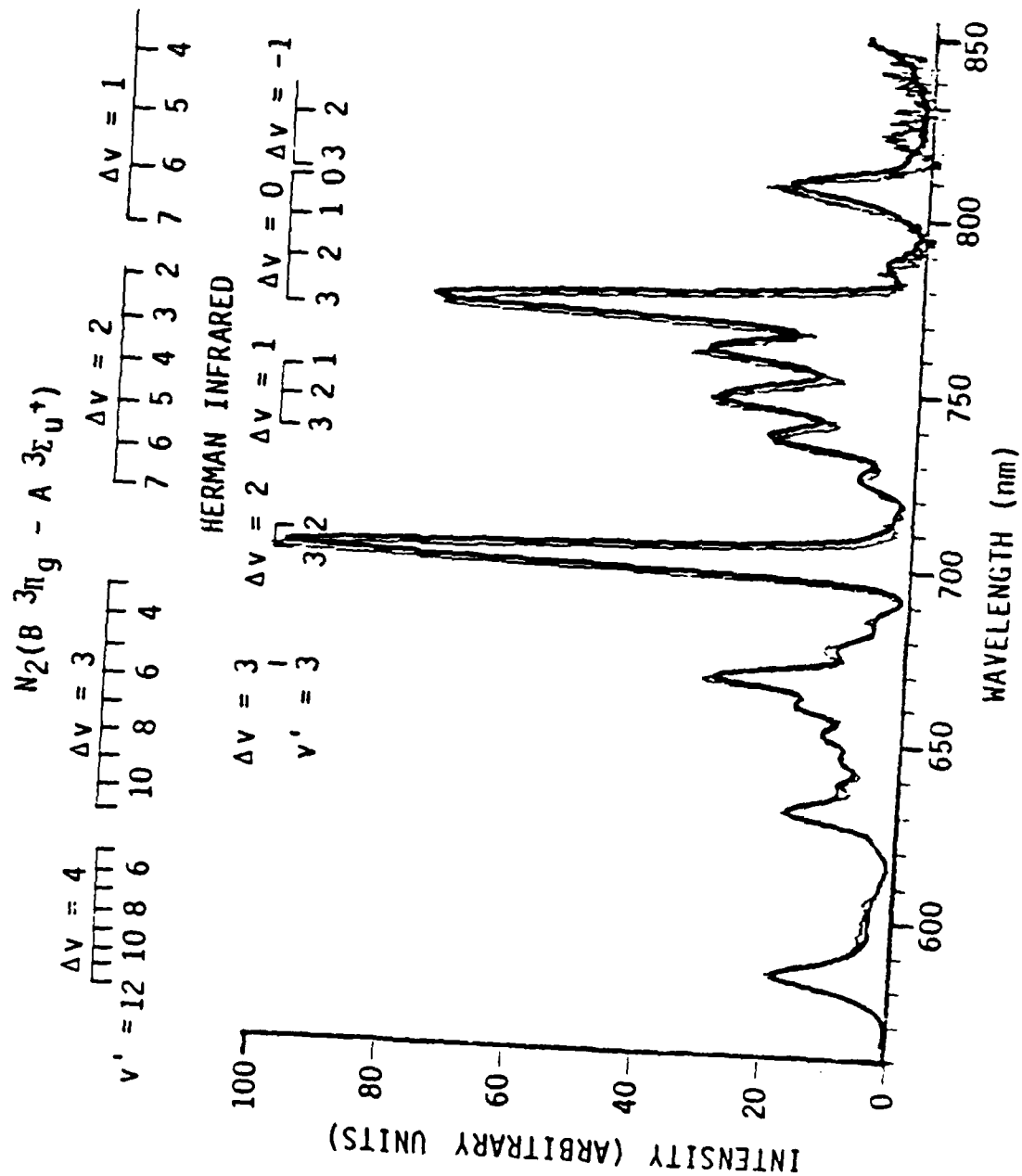
Figure

- 1 Spectrum of the nitrogen Herman Infrared $v'=3$ and first-positive systems excited in the energy pooling of $N_2(A, v'=0)$ for a nitrogen partial pressure of 0.46 Torr and a Ne pressure of 3 Torr. The experimental spectrum is the light line while the heavy line shows the synthetic best fit to the spectrum.
- 2 Spectrum of the nitrogen Herman Infrared $v'=3$ and first-positive systems excited in the energy pooling of $N_2(A, v'=0)$ for a nitrogen partial pressure of 0.027 Torr.
- 3 Variation in the ratio of the square of the number density of $N_2(A, v'=0)$ to that for $N_2(B, v'=4)$ as a function of the molecular nitrogen number density.
- 4 Variation in the ratio of the square of the number density of $N_2(A, v'=0)$ to that for $N_2(B, v'=10)$ as a function of the molecular nitrogen number density.
- 5 Variation in $N_2(B, v)$ excited from energy pooling of $N_2(A, v'=0)$ with neon pressure.
- 6 Spectrum of the nitrogen Herman Infrared $v'=2,3$ and first-positive systems excited in the energy pooling of $N_2(A, v'=0,1)$ for a nitrogen partial pressure of 38 mTorr and no added methane.
- 7 Spectrum of the nitrogen Herman Infrared $v'=2,3$ and first-positive systems excited in the energy pooling of $N_2(A, v'=0,1)$ for a nitrogen partial pressure of 38 mTorr and a methane partial pressure of 1.4 mTorr.
- 8 Variation in the ratio of the number density of $N_2(B, v'=2)$ to the square of the number density of $N_2(A, v'=0)$ as a function of the ratio of $N_2(A) v'>0$ to $v'=0$. The solid line shows the results of a quadratic least square fit to Eq. 8.
- 9 Variation in the ratio of the number density of $N_2(B, v'=10)$ to the square of the number density of $N_2(A, v'=0)$ as a function of the ratio of $N_2(A) v'>0$ to $v'=0$.
- 10 Spectra of HIR $v'=3$ and N_2 first-positive systems when the $N_2(A)$ is formed by direct discharge of the N_2 with the argon and when it is formed in the conventional manner by adding the N_2 downstream from the discharge. The two spectra were normalized so that the Herman Infrared 3,1 bands at 703 nm would coincide.
- 11 Variation in the $N_2(B,A)$ spectrum produced in $N_2(A)$ energy pooling with changes in nitrogen and argon partial pressures. The solid line is the best fit synthetic spectrum.



A-2153

Figure 1



A-2152

Figure 2

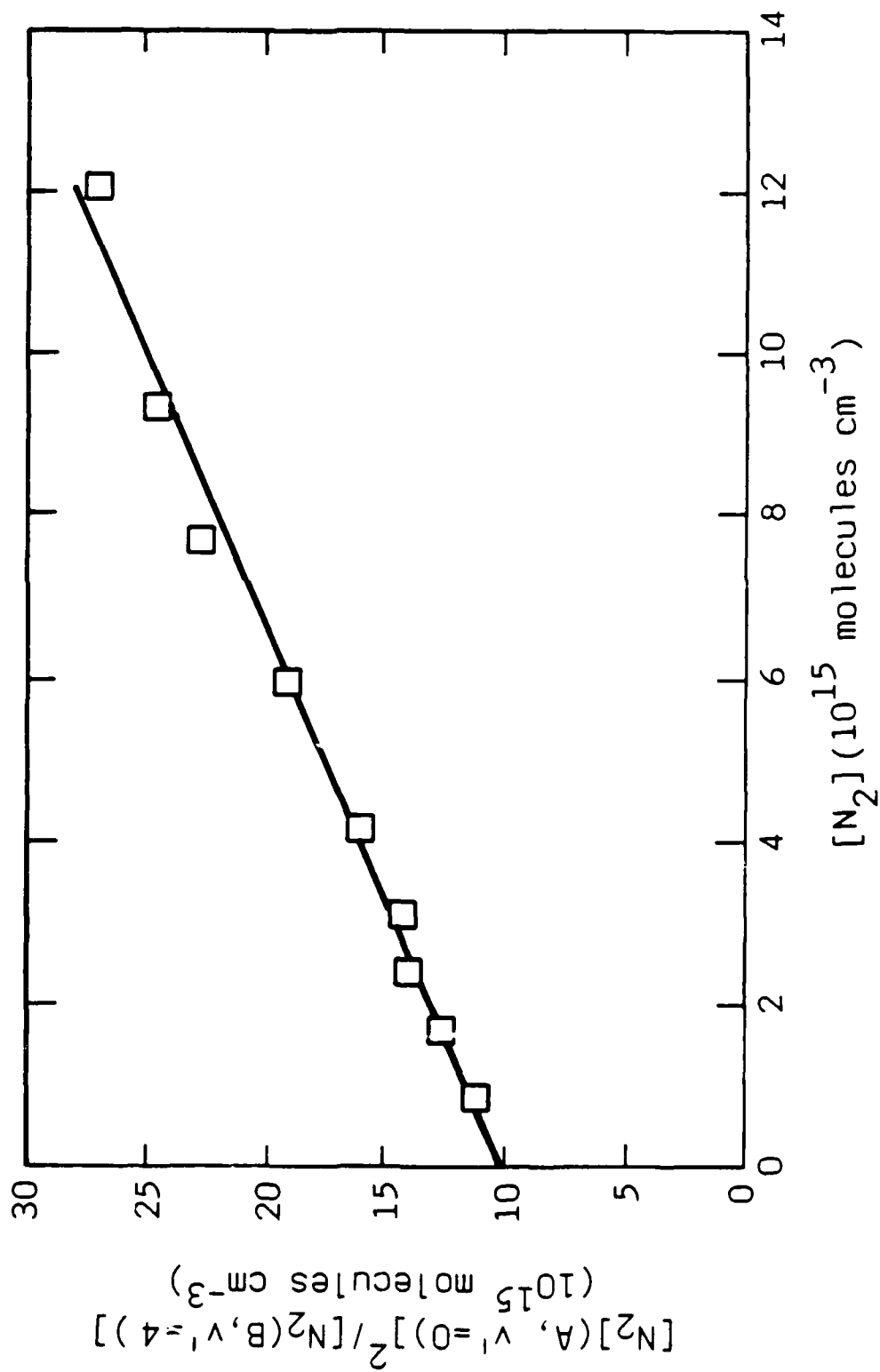


Figure 3

A-2145

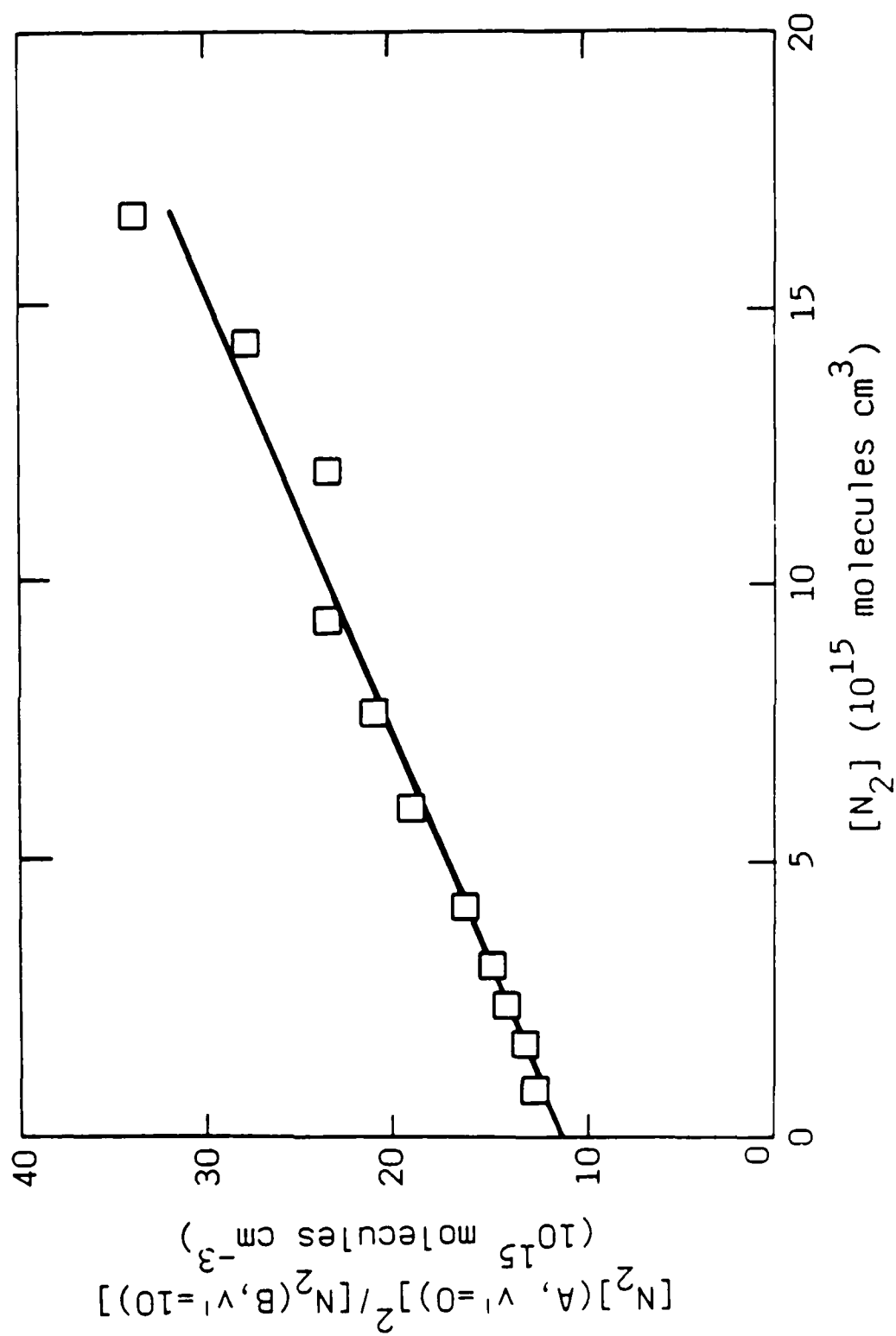
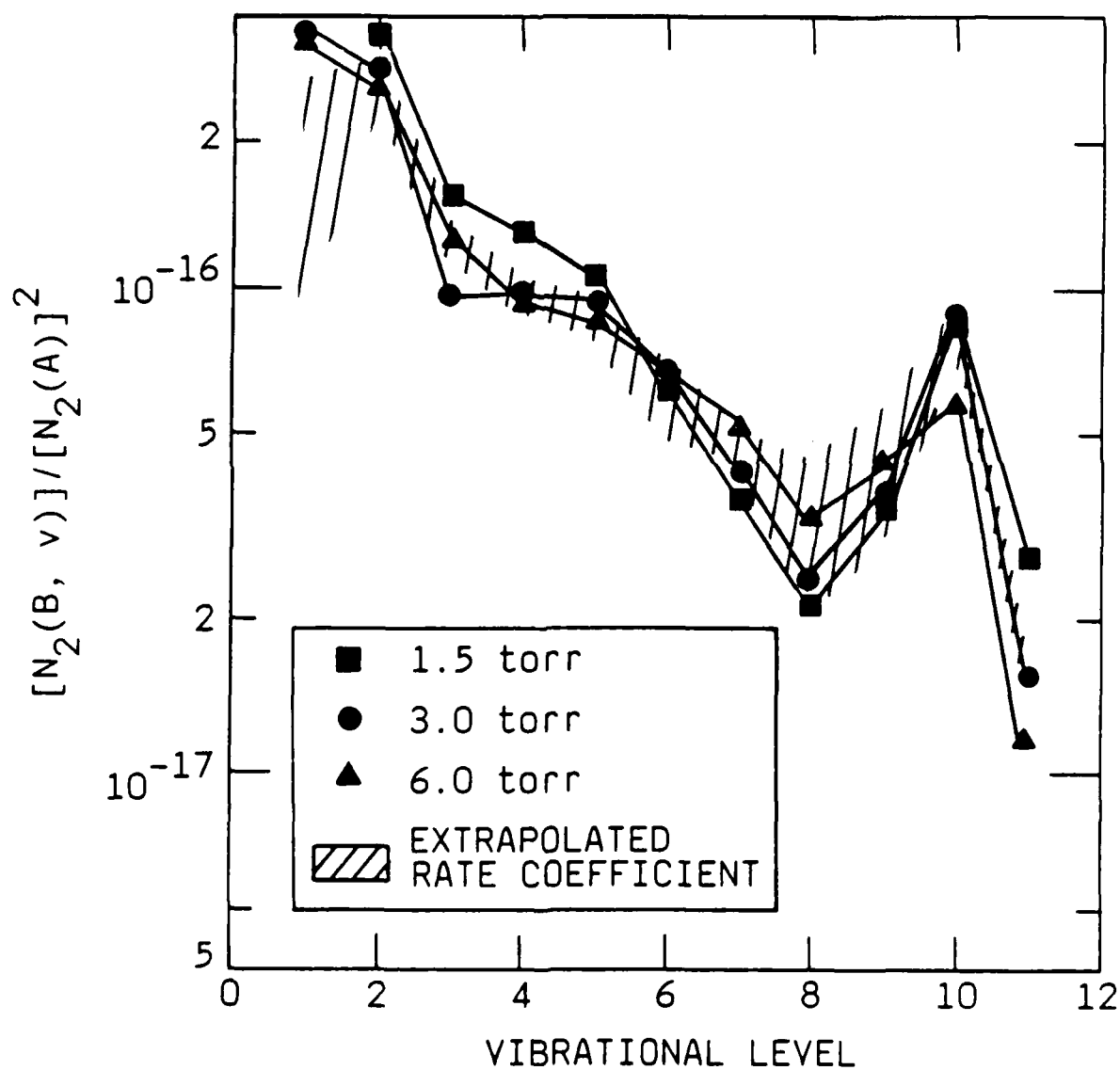
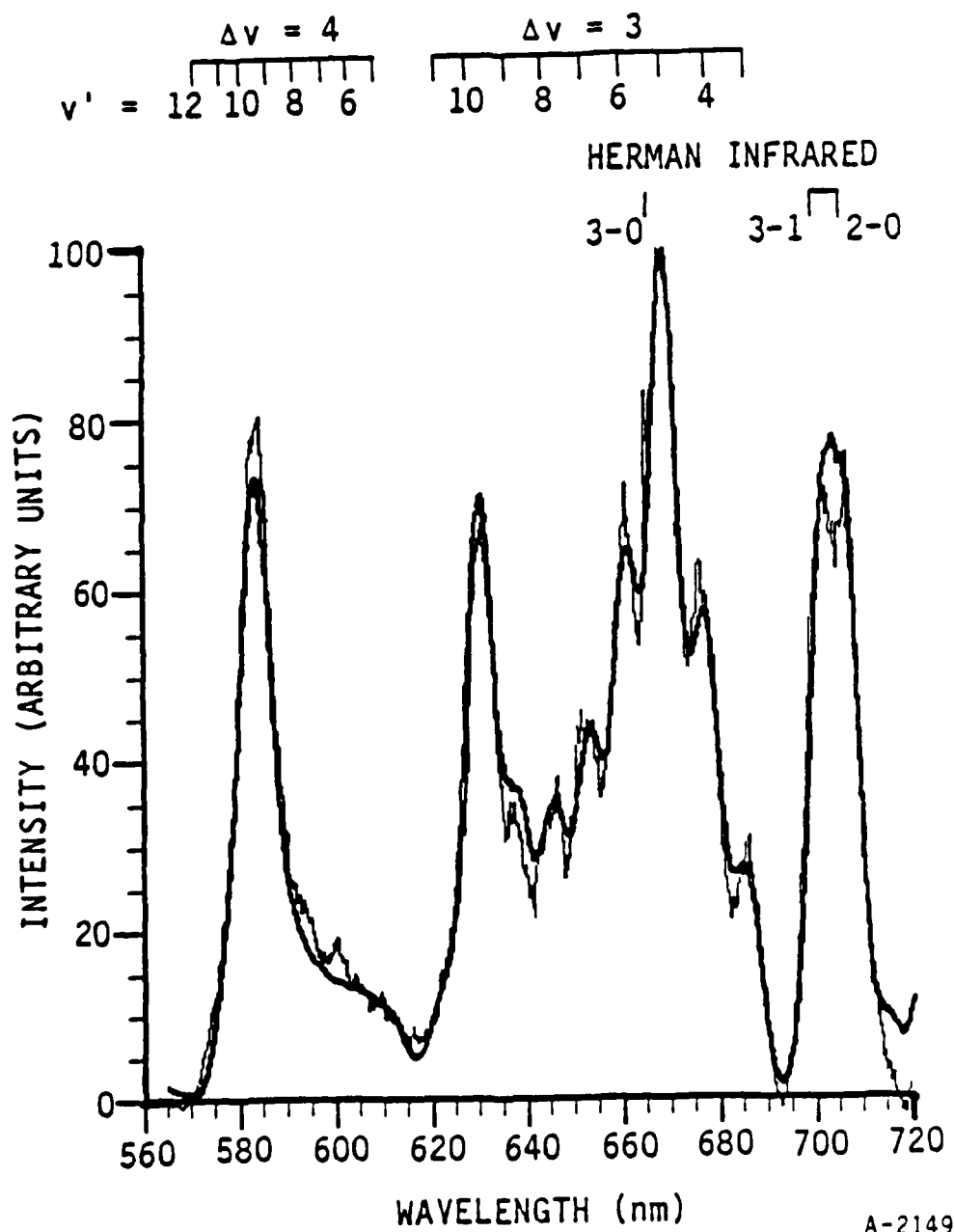
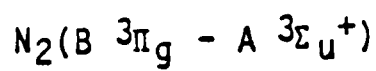


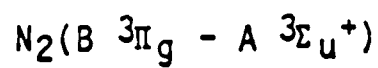
Figure 4



A-3027

Figure 5

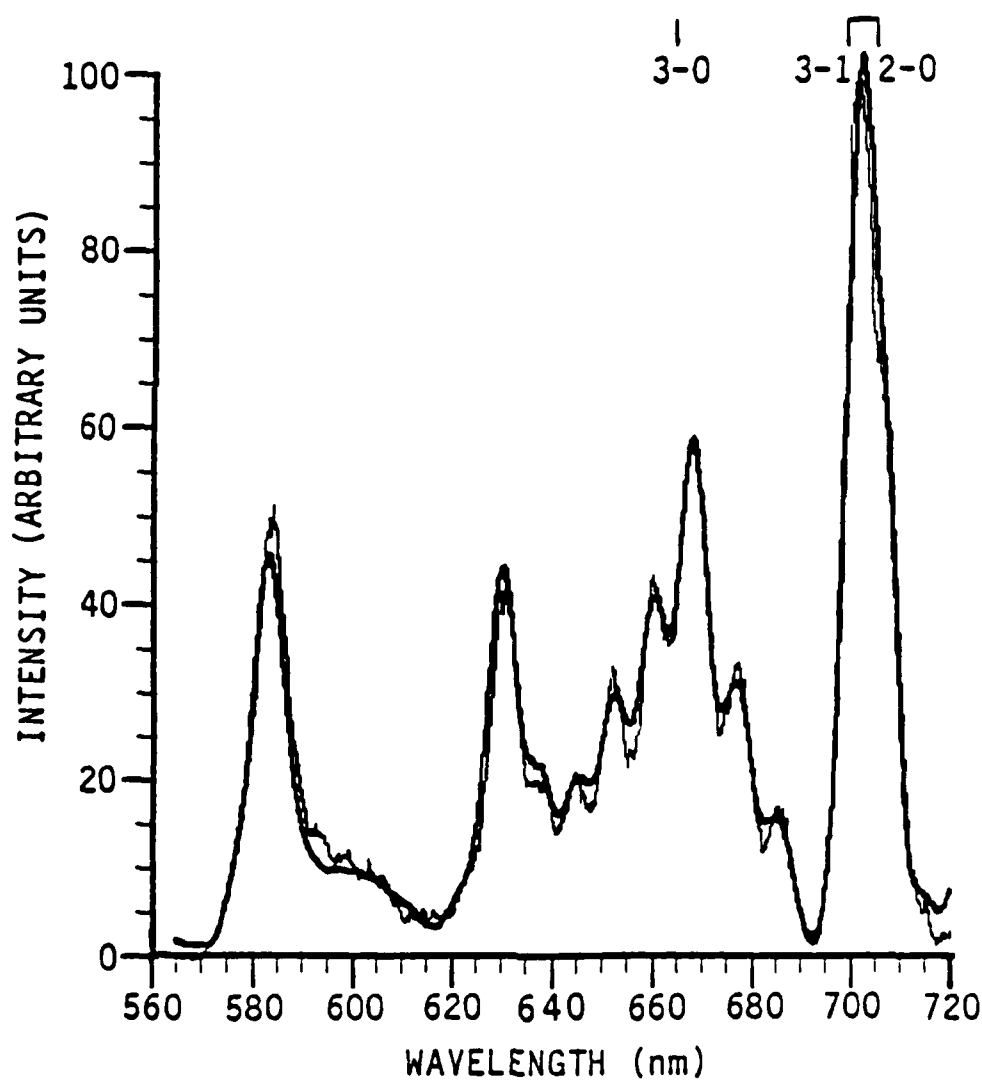




$\Delta v = 4$
12 10 8 6

$\Delta v = 3$
10 8 6 4

HERMAN INFRARED



A-2150

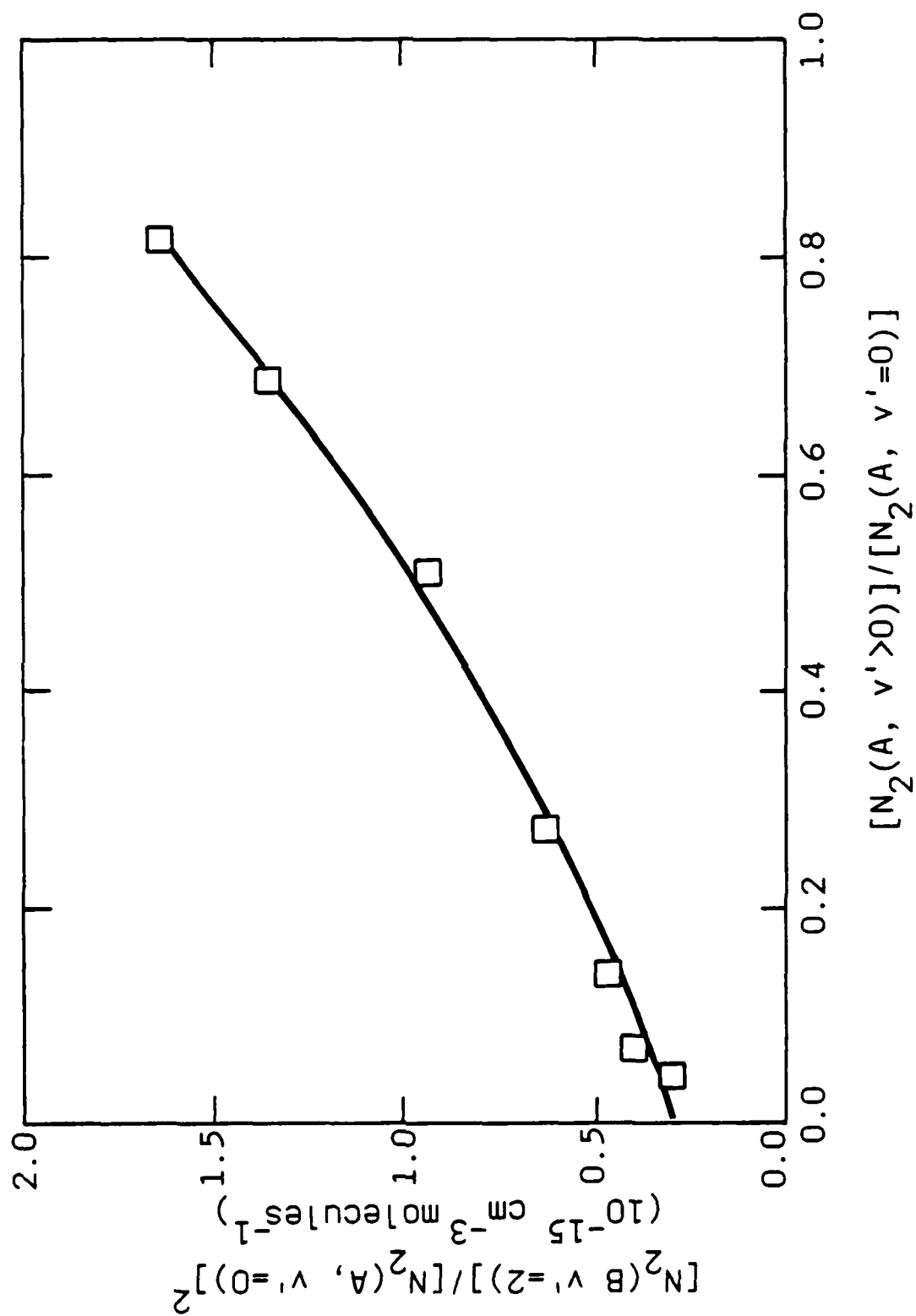
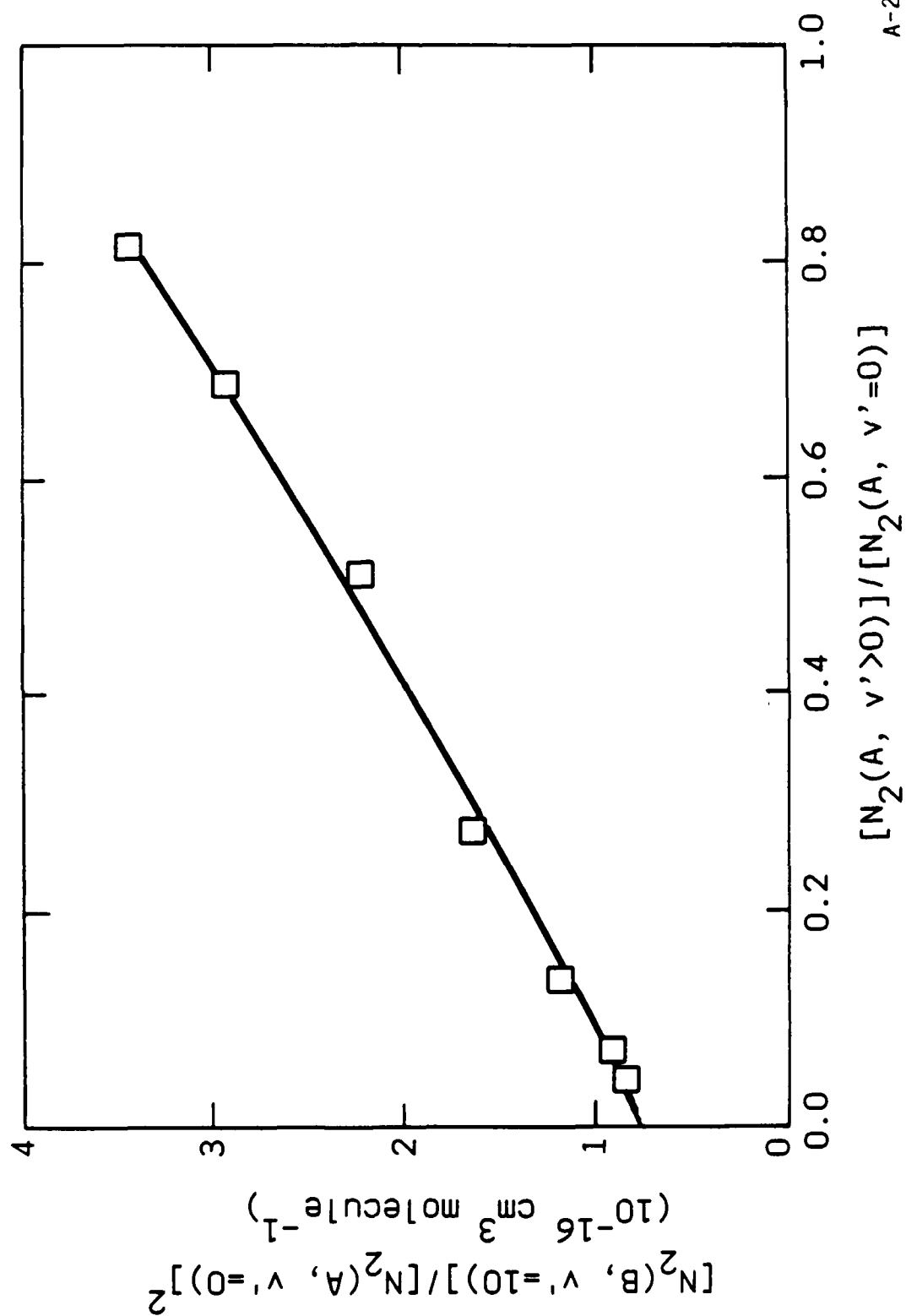


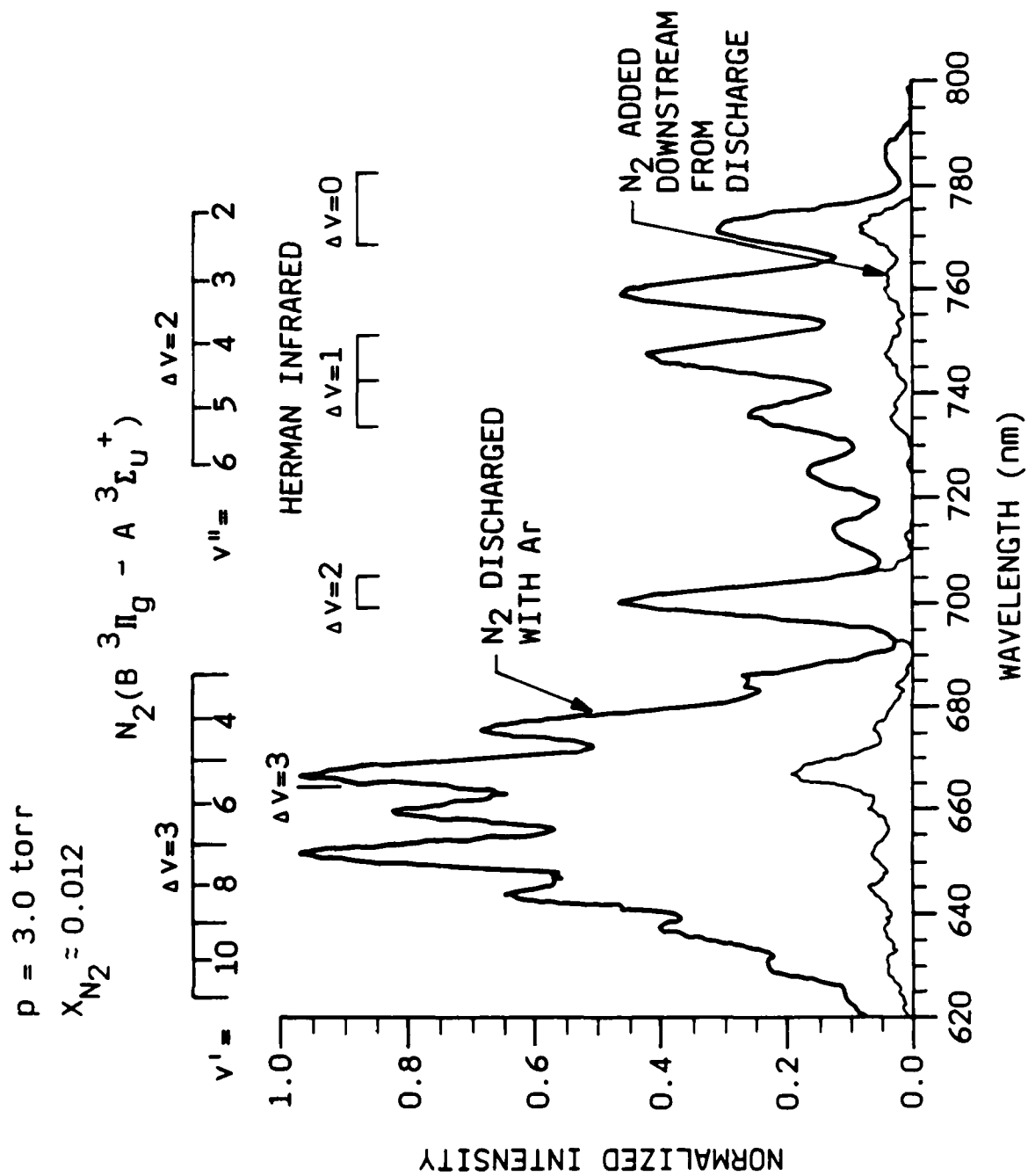
Figure 8

A-2147

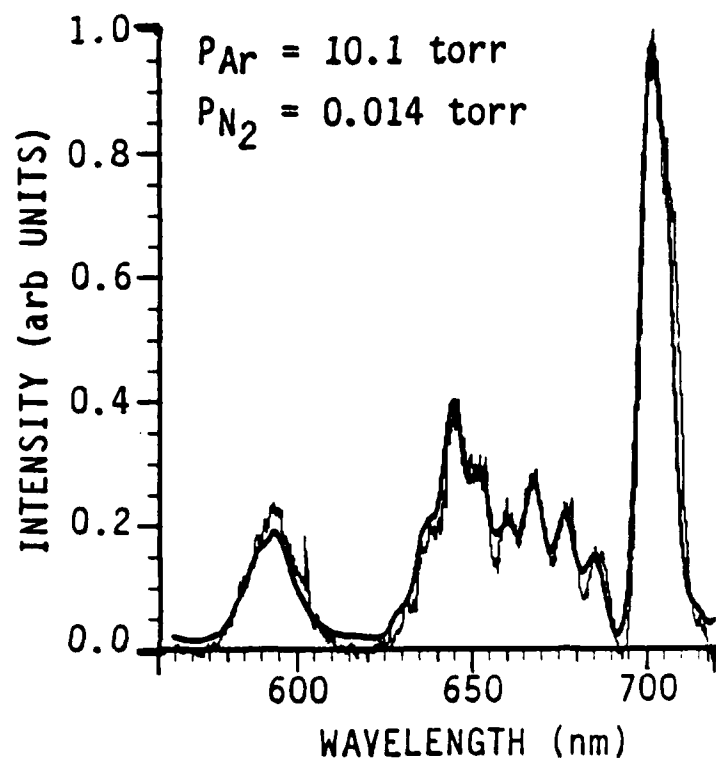
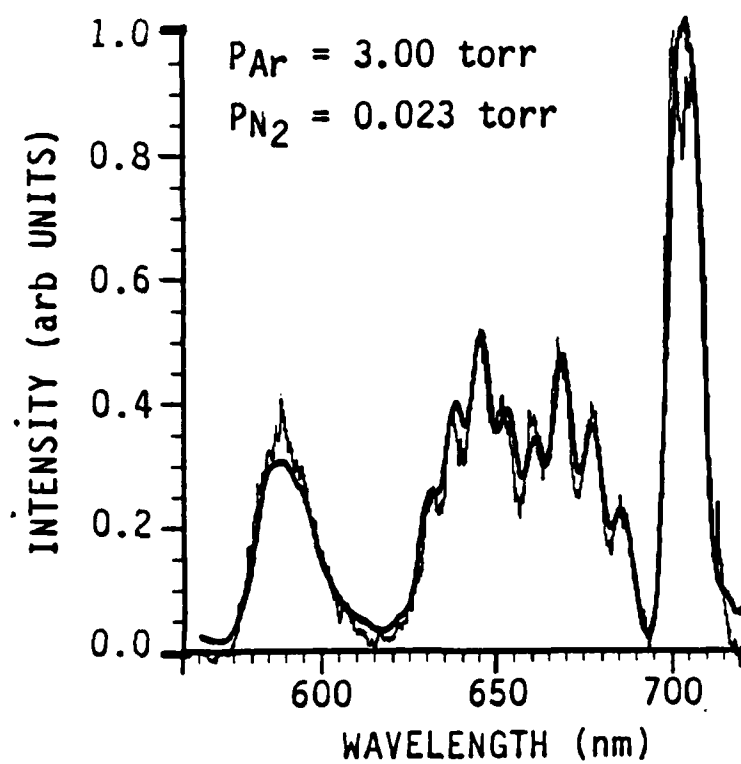
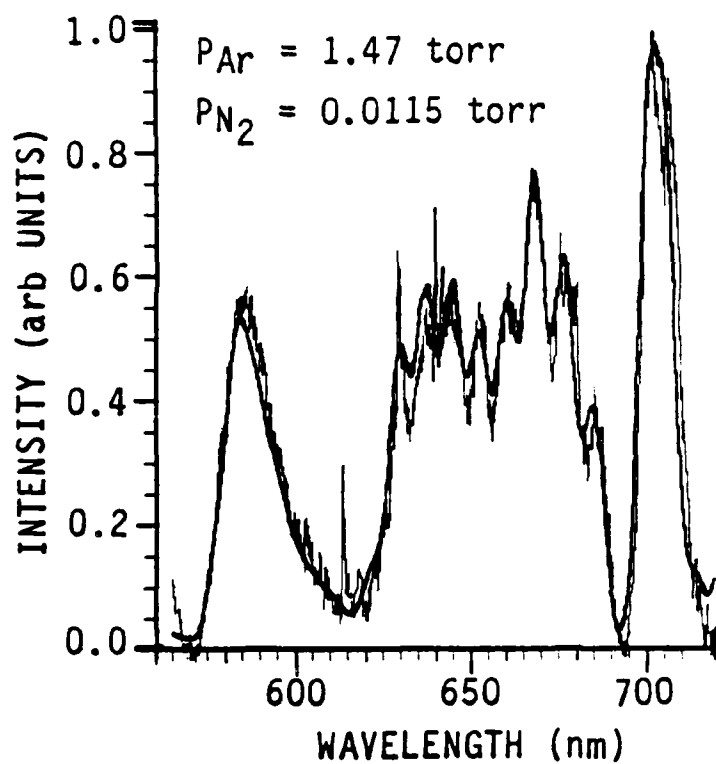
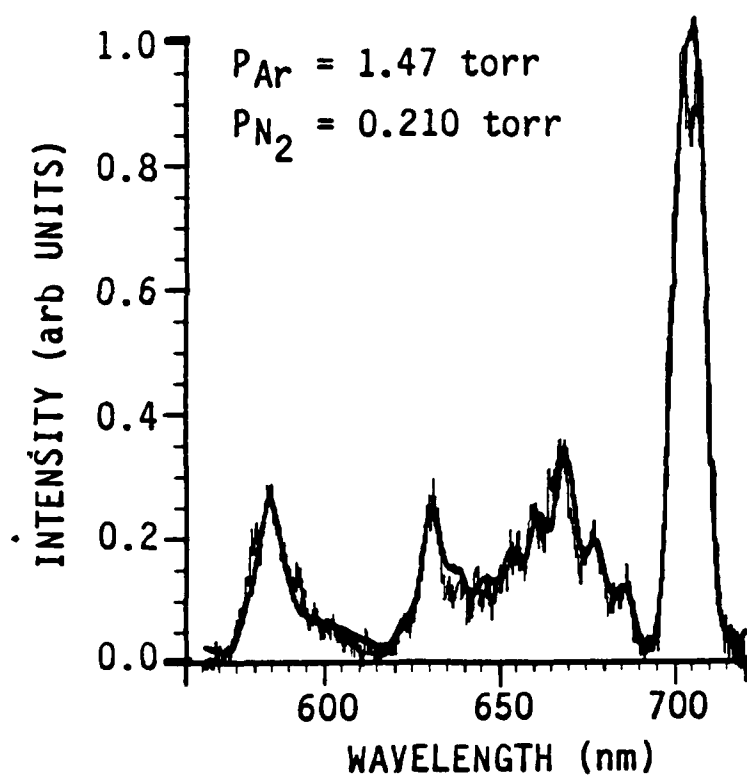


A-2139

Figure 9



A-670



A-3028

APPENDIX I

(SR-359 reproduced in its entirety)

J. Chem. Phys. 90, XXXX (1989)

THE EXCITATION OF $N(^2P)$ BY $N_2(A^3\Sigma_u^+, v'=0,1)$

BY

Lawrence G. Piper

Physical Sciences Inc.
Dascomb Research Park, P.O. Box 3100
Andover, MA 01810-7100

J. Chem. Phys. 91, XXXX (1989)

ABSTRACT

We have studied the electronic energy transfer reaction between $N_2(A^3\Sigma_u^+, v'=0,1)$ and $N(^4S)$ in a discharge-flow reactor. Monitoring the decay of the forbidden Vegard-Kaplan emission, $N_2(A^3\Sigma_u^+ - X^1\Sigma_g^+)$, as a function of time and of atomic nitrogen number density allows determination of the total reaction rate coefficients for removal of vibrational levels 0 and 1 by $N(^4S)$. Simultaneously observing the temporal profiles of the Vegard-Kaplan bands and of the forbidden $N(^2P-^4S)$ line at 346.6 nm allows the branching fraction into atomic nitrogen excitation to be determined. The total quenching rate coefficient for both $v'=0$ and 1 is $(4.0 \pm 0.5) \times 10^{-11} \text{ cm}^3 \text{ molecule}^{-1} \text{ s}^{-1}$ at 300 K. The apparent rate coefficient for exciting $N(^2P)$ by $N_2(A, v'=0)$ is $(19 \pm 3) \times 10^{-11} \text{ cm}^3 \text{ molecule}^{-1} \text{ s}^{-1}$, at 300 K, while that for excitation by $N_2(A, v=1)$ is $(5 \pm 1) \times 10^{-11} \text{ cm}^3 \text{ molecules}^{-1} \text{ s}^{-1}$. We interpret the large discrepancy between the $N(^2P)$ excitation and $N_2(A)$ destruction rate coefficients as evidence that the currently accepted value for the $N(^2P-^4S)$ transition probability is a factor of four to five too small, or else that our source of $N_2(A)$ metastables, energy transfer from metastable argon atoms to molecular nitrogen, is contaminated by the presence of a second nitrogen metastable species with an energy in excess of 3.6 eV.

1. INTRODUCTION

Metastable $N(^2P)$ atoms are commonly observed constituents in nitrogen discharge afterglows¹⁻³ and in the aurorally disturbed upper atmosphere.⁴⁻⁶ In spite of this, its chemistry has been little studied, probably because $N(^2P)$ reacts slowly with most molecules.^{7,8} The reaction of $N(^2P)$ with O_2 has been invoked as a source of vibrationally excited nitric oxide with accompanying hot-rotational band heads ($T_{rot} \sim 10^4$ K).⁹ In addition, the ratio of the intensity of the $N(^2P-^2D)$ transition at 1040 nm to the $N_2^+(A^2\Pi_u, v'=0 - ^1\Sigma_g^+, v''=0)$ transition at 1109 nm has been used to monitor the depth of penetration of auroral electrons.¹⁰ The intensity ratio becomes smaller for deeper auroral penetration because $N(^2P)$ is quenched by O-atoms efficiently.⁸

Several years ago we attempted to measure rate coefficients for quenching $N(^2P)$ by a variety of atmospheric constituents. We used a microwave discharge through a mixture of nitrogen dilute in argon or helium as our $N(^2P)$ source, and monitored $N(^2P)$ unequivocally by vacuum ultraviolet resonance fluorescence. In most instances we observed multiexponential quenching behavior. This behavior suggested that we were observing not only quenching of $N(^2P)$ generated in the discharge, but also quenching of discharge-produced precursors which were coupled kinetically to $N(^2P)$ along the length of the flow reactor. We concluded that a nitrogen/argon discharge didn't provide a clean source of $N(^2P)$ and that reliable kinetic studies could not be pursued using such a source.

The interaction between $N_2(A)$ and N excites $N(^2P)$.^{11,12} Because $N(^2P)$ is inefficiently quenched by atomic nitrogen,¹ this reaction might provide a relatively clean source of $N(^2P)$ for kinetic studies in a flow system. Before such studies can be pursued, the $N_2(A) + N$ reaction must be characterized. This report details such a quantitative characterization.

The rate coefficient for quenching $N_2(A^3\Sigma_u^+)$ by N was first estimated by Wray¹³ to be about $5 \times 10^{-11} \text{ cm}^3 \text{ molecule}^{-1} \text{ s}^{-1}$. Subsequent work by Young and St. John,¹⁴ Meyer et al.,¹¹ Vidaud et al.,¹⁵ and Young and Dunn¹² all have concurred with Wray's estimate, obtaining values between 3 and $5 \times 10^{-11} \text{ cm}^3 \text{ molecule}^{-1} \text{ s}^{-1}$. Meyer et al. and Young and Dunn both showed that $N(^2P)$ was a product from this quenching reaction but neither group made any quantitative estimates of the efficiency of the energy transfer.

2. EXPERIMENTAL

The experiments were carried out in a 2-in. diameter discharge flow apparatus which is shown schematically in Figure 1. The apparatus is in two parts. The upstream section is where the $N_2(A)$ and N are produced and subsequently mixed. Observations occur in the downstream section. It has been manufactured from quartz so as to transmit ultraviolet radiation.

The interaction between metastable argon atoms, produced in a dc discharge, and molecular nitrogen^{16,17} generates the metastable nitrogen. For some experiments, adding CF_4 just downstream from where the $N_2(A)$ enters the flow reactor^{18,19} relaxes vibrationally excited metastable nitrogen to $v'=0$.

Further downstream the atomic nitrogen enters the main flow tube through a 10-mm diameter hook-shaped injector. A microwave discharge through a mixture of Ar and N_2 produces the N-atoms in a side arm of the flow reactor. The atoms subsequently flow through a glass wool plug to deactivate electronically and vibrationally excited nitrogen metastables.²⁰

All relevant species are detected spectroscopically. Radiation from the Vegard-Kaplan bands, $N_2(A^3\Sigma_u^+, - X^1\Sigma_g^+)$, between 250 and 370 nm, reveals the presence of $N_2(A)$ while emission from the $N(2P-4S)$ transition at 346.6 nm shows the presence of the atomic metastable. A 0.5 m monochromator, mounted on rails and equipped with a thermoelectrically cooled photomultiplier and photon-counting rate meter, detected the light in the flow reactor. A lab computer digitized the analog signals from the rate meter and stored them on a floppy diskette for subsequent processing.

Only the relative number densities of the atomic and molecular metastables are important, so the spectroscopic system needs to be calibrated in a relative sense only. Scanning the spectrum of a standard D_2 lamp provided this calibration.

Observing the N-atom recombination afterglow with a 580 ± 5 nm photometer indicates the ground-state atom number densities. The intensity of this afterglow is proportional to the square of the N-atom number density.²¹ Measurements of the square root of this intensity as a function of [N] calibrated the photometer. The well known $N + NO \rightarrow N_2 + O$ titration established [N] absolutely.²²

At fairly low atomic nitrogen number densities, titrating N-atoms to the extinction of the N-atom afterglow can result in errors due to the slowness of the $N + NO$ reaction. We therefore overtitrated the N-atoms to convert them to atomic oxygen. The excess NO then combines with the O to produce the O/NO air afterglow which also is detected by the photometer. Observing this signal as a function of added nitric oxide indicated the number density of atomic oxygen produced in the N-atom titration. Since the reaction between N and NO is stoichiometric, the amount of O produced equals the amount of N titrated.²² We have discussed in some detail our techniques for calibrating air afterglow observations to detect atomic oxygen quantitatively.^{23,24}

For the experiment we wish to observe changes in the number densities of $N_2(A)$ and $N(^2P)$ as a function of reaction time and of atomic-nitrogen number density. The procedure, therefore, involved scanning the spectral region between 250 and 370 nm at five different positions along the length of the flow reactor while holding the N-atom number density constant. This process was repeated numerous times for differing number densities of atomic nitrogen both in the presence and the absence of CF_4 . The number densities of $N_2(A)$ and $N(^2P)$ in each spectral scan were then determined from a least-squares fit of a synthetic spectrum to the response-corrected experimental spectrum. This fitting procedure accounts for overlap with other radiating systems in the spectral region.

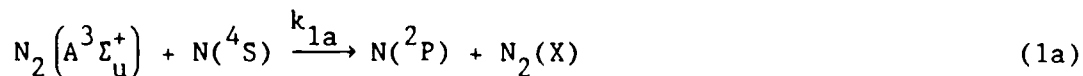
Some of these interfering radiators included the nitrogen second-positive bands, $N_2(C^3\Pi_u - B^3\Pi_g)$, which result from $N_2(A)$ energy pooling;²⁵ the NO γ -bands, $NO(A^2\Sigma^+ - X^2\Pi)$, which result from the excitation of NO (produced in small quantities in the Ar and N_2 discharges) by $N_2(A)$;²⁶ the NO β -bands, $NO(B^2\Pi - X^2\Pi)$, which result from the three-body recombination of N- and O-atoms;²⁷ and the CN blue system, $CN(B^2\Sigma^+ - X^2\Sigma^+)$, which results from the excitation of impurity-generated CN by $N_2(A)$. Figure 2 shows some typical spectral scans at 17 ms reaction time in the presence of varying amounts of atomic nitrogen. The heavy line over the experimental spectrum is the synthetic best fit to that spectrum.

We used Shemansky's Einstein coefficients²⁸ to determine the $N_2(A)$ number densities and the $N(2P-4S)$ transition probability calculated by Garstang²⁹ for $N(2P)$. We have recently presented data indicating that Shemansky's Einstein coefficients are 20 to 40 percent too large,^{26,30} but until this issue is settled unequivocally, we prefer to use his values to facilitate comparison with the rest of the literature. Godefroid and Froese Fischer³¹ recently computed the $N(2P-4S)$ transition probability using modern computational facilities and techniques. Their value is only 11 percent smaller than that calculated by Garstang. To our knowledge, no one has attempted an experimental verification of this important transition probability. Experimental measurements of the $O(1S-1D)$ ³² and $I(2P_{1/2}-2P_{3/2})$ ^{33,34} transition probabilities, however, have shown Garstang's calculations on these transitions to be quite good.

Typical conditions in the flow reactor included flows of argon buffer and primary nitrogen of 1800 and 300 $\mu\text{moles s}^{-1}$, respectively, the N-atom discharge flows of argon and nitrogen were 500 and 0 to 10 $\mu\text{moles s}^{-1}$, respectively, while the CF_4 flow rate of 0 or 120 $\mu\text{moles s}^{-1}$. The total pressure generally was 1.8 torr, the bulk flow velocity 1300 cm s^{-1} , and reaction times varied between 10 and 30 ms.

3. RESULTS

The following reactions describe the important kinetic processes occurring in the reactor:



The removal of $\text{N}_2(\text{A})$ by radiation or by collisions with nitrogen or argon is negligible compared to wall removal. This is also the case for removal of $\text{N}(\text{P}^2)$ by radiation or quenching by N_2 . All of these potential loss terms, therefore, were ignored. $\text{N}(\text{P}^2)$ is quenched slowly by argon.^{35,36} In our analysis we treated this process as a slight enhancement to the wall removal rate (vide infra). While CF_4 removes vibrational energy from $\text{N}_2(\text{A})$ moderately efficiently,^{18,19} it quenches the electronic energy of neither $\text{N}_2(\text{A})$ nor $\text{N}(\text{P}^2)$.

A. The Quenching of N₂(A) by N

Equation (5) describes the rate of change in the N₂(A) number density with time in the reactor:

$$\frac{d[N_2(A)]}{dt} = - \left\{ k_W^A + k_1 [N] \right\} [N_2(A)] \quad (5)$$

Because the N-atom number density is typically three or more orders of magnitude greater than that of N₂(A), and because under our conditions wall removal of N(⁴S) is negligible, Eq. (5) can be solved by separation of variables, giving,

$$\ln \left\{ \frac{[N_2(A)]}{[N_2(A)]_{t=0}} \right\} = - 0.62 \left(k_W^A + k_1 [N] \right) z / \bar{v} \quad , \quad (6)$$

where we have replaced the time, t, by its equivalent under our experimental conditions: 0.62 times the experimentally measured ratio of the reaction distance, z, to the bulk flow velocity, \bar{v} .

The factor of 0.62 corrects for the coupling of the N₂(A) radial density gradient with the parabolic velocity profile in the reactor. This correction, the reasons for it, and the conditions under which it becomes important have been well documented in the literature.³⁷⁻³⁹ The purpose of our having a relatively long flow distance between the entrance of our reactor and our observation region is to ensure that laminar flow is fully developed in the reactor so that this correction can be made unambiguously.⁴⁰

By fixing the N-atom number density and varying the reaction distance, we determine the pseudo first-order decay rate of N₂(A), viz.,

$$-\bar{v} \frac{d \ln [N_2(A)]}{dz} = 0.62 \left(k_W^A + k_1 [N] \right) = K_A \quad (7)$$

The rate coefficient for the removal of $N_2(A)$ by N then results from measurements of pseudo first-order decay rates, K_A , as a function of the atomic-nitrogen number density:

$$k_1 = \frac{1}{0.62} \frac{d K_A}{d [N]} \quad (8)$$

Figures 3 and 4 show the variations in the natural log of the number densities of $N_2(A)$ $v'=0$ and $v'=1$ as a function of reaction time for various N-atom number densities. The slopes of the lines in these plots are the pseudo first-order decay rates. Figures 5 and 6 show how the pseudo first-order decay rates for $N_2(A)$ $v'=0$ and 1, respectively, vary as a function of N-atom number density. The slopes of the lines in Figures 5 and 6, after division by 0.62, give the rate coefficients for $N_2(A)$ removal by N.

We find the rate coefficients for $N_2(A)$ removal by N of $(3.8 \pm 0.3) \times 10^{-11} \text{ cm}^3 \text{ molecule}^{-1} \text{ s}^{-1}$ for $v'=0$ in the runs in the presence of CF_4 and (4.1 ± 0.1) and $(3.9 \pm 0.2) \times 10^{-11} \text{ cm}^3 \text{ molecule}^{-1} \text{ s}^{-1}$ for $v'=0$ and 1 respectively, in the runs without CF_4 added. These values are identical within experimental error.

The error limits given are standard deviations from the least-squares fits to the data. Considering all sources of statistical and systematic error results in an overall $\pm 1\sigma$ uncertainty of about 12 percent. We therefore quote a rate coefficient for $N_2(A, v'=0,1)$ removal by N of $(4.0 \pm 0.5) \times 10^{-11} \text{ cm}^3 \text{ molecule}^{-1} \text{ s}^{-1}$.

The number densities of $N_2(A, v'=2)$ were so small as to limit decay measurements to a range of less than a factor of three to five. This small range is insufficient for measuring reliable rate coefficients. In general, $v'=2$ disappeared at about the same rate as the other vibrational levels, indicating that the rate coefficient for its removal is of similar magnitude.

B. The Excitation of $N(^2P)$ by $N_2(A)$

The rate equation for the formation and removal of $N(^2P)$ in our reactor is

$$\frac{d [N(^2P)]}{dt} = k_{1a} [N_2(A)][N] - (k_W^P + k_3 [N])[N(^2P)] \quad (9)$$

Using the exponential form of Eq. (6) above for the number density of $N_2(A)$, allows Eq. (9) to be solved, giving

$$[N(^2P)] = \frac{0.62 k_{1a} [N][N_2(A)]_0}{K_P - K_A} \left\{ e^{-K_A z/\bar{v}} - e^{-K_P z/\bar{v}} \right\} \quad (10)$$

Equation (10) has the visually simplifying substitutions

$$K_A = 0.62 (k_W^A + k_1 [N]) \quad (11)$$

and

$$K_P = 0.62 (k_W^P + k_3 [N]) \quad (12)$$

The terms K_A and K_P are the pseudo first-order decay rates for $N_2(A)$ and $N(^2P)$ respectively. The factors of 0.62 are included to account for the fluid mechanical affects. The corrections have been derived in detail by Shaw and Stock⁴¹ and by DeSouza et al.⁴² and their derivation need not be repeated here.

Rearranging Eq. (10) leads to the result

$$\frac{[N(^2P)]}{[N_2(A)]} = \frac{0.62 k_{1a} [N]}{K_P - K_A} \left\{ 1 - e^{-(K_P - K_A) z/\bar{v}} \right\} \quad (13)$$

By knowing K_A and K_P , we can extract the desired rate coefficient k_{1a} from least squares fits to the ratio $[N(^2P)]/[N_2(A)]$ as a function of $[N]$ and of time. The values of K_A result directly from the measurements described in the previous section. K_P is determined by using k_3 values from the literature^{1,8} and k_W^P values determined from the least-squares fits. We can check the reasonableness of the resulting k_W^P by comparing with data already in the literature.

The result of the fit to data taken in the presence of CF_4 , i.e., only $\text{N}_2(\text{A}, v'=0)$, is $k_{1a} = (1.9 \pm 0.3) \times 10^{-10} \text{ cm}^3 \text{ molecule}^{-1} \text{ s}^{-1}$ and $k_w^P = (75 \pm 10) \text{ s}^{-1}$. The uncertainty in the fit reflects sensitivity to variations in the value determined for k_w^P and for the effective mixing length. This latter quantity is a correction to the distance between the injector and the detection region needed to account for imperfect mixing at the injector. Analysis of the decay plots of $\ln[\text{N}_2(\text{A})]$ versus reaction distance indicated that the lines intersected at a common value of $4 \pm 2 \text{ cm}$. This value was used to correct for mixing effects.

Equation (13) was also used to analyze the data taken in the absence of CF_4 . As in the previous case, the data were fit to the ratio of $[\text{N}(^2\text{P})]/[\text{N}_2(\text{A}, v'=0)]$. The effective excitation rate coefficient determined from this fit is

$$k_{1a}^{\text{eff}} = k_{1a}^{v'=0} + k_{1a}^{v'>0} \frac{[\text{N}_2(\text{A}, v'>0)]}{[\text{N}_2(\text{A}, v'=0)]} \quad (14)$$

The number density ratio, which comes from the spectral fits, is 0.78 ± 0.08 . The effective k_{1a} from the fits without CF_4 is $(2.3 \pm 0.3) \times 10^{-10} \text{ cm}^3 \text{ molecule}^{-1} \text{ s}^{-1}$ from which we derive that $k_{1a}^{v'>0} = (0.5 \pm 0.1) \times 10^{-10} \text{ cm}^3 \text{ molecule}^{-1} \text{ s}^{-1}$.

Table 1 summarizes our experimental results.

4. DISCUSSION

A. N₂(A) + N Removal

Our determination of the total rate coefficient for quenching N₂(A) by N, $(4.0 \pm 0.5) \times 10^{-11} \text{ cm}^3 \text{ molecule}^{-1} \text{ s}^{-1}$, agrees well with most other determinations. In some instances, the agreement can be considered fortuitous. Neither Wray¹³ nor Vidaud et al.¹⁵ observed N₂(A) directly, but had to make inferences based upon indirect measurements. In particular, agreement with Vidaud et al.'s¹⁵ experiment is somewhat puzzling. They used both photoionization and isothermal calorimetry as their metastable-nitrogen diagnostics. Neither of these diagnostics is specific to N₂(A). In addition to obtaining an N-atom quenching-rate measurement, they determined a wall-quenching probability for their metastable of 10^{-5} . Flow tube measurements both in our laboratory as well as others⁴³ show conclusively that N₂(A) is deactivated with essentially unit probability in wall collisions. Thus Vidaud et al. must have been observing some other metastable in their experiment. One possibility is vibrationally excited nitrogen which is known to deactivate somewhat more slowly than N₂(A) in wall collisions.²⁰

Meyer et al.¹¹ reported two separate determinations of the rate coefficient for N₂(A) quenching by N. One measurement was made relative to the quenching rate of N₂(A) by O₂. Using an assumed value for this latter quenching rate coefficient of $6.0 \times 10^{-12} \text{ cm}^3 \text{ molecule}^{-1} \text{ s}^{-1}$, they reported a value for k_1 of $5.1 \times 10^{-11} \text{ cm}^3 \text{ molecule}^{-1} \text{ s}^{-1}$. Since the O₂ quenching rate coefficient is now known to be about half of the value chosen by Meyer et al. (assuming a typical distribution of N₂(A) vibrational levels in their discharge flow system),⁴⁴⁻⁴⁶ their reported value for k_1 must be reduced accordingly. A second determination by them resulted from observing the quenching of Hg 253.7 nm emission in their reactor as a function of added

atomic nitrogen number density. The mercury emission was excited by transfer from $N_2(A)$ and thereby served as a tracer of the $N_2(A)$ number density. The result from that study gave a value for k_1 of $4.3 \times 10^{-11} \text{ cm}^3 \text{ molecule}^{-1} \text{ s}^{-1}$. They made no corrections for imperfect mixing or for fluid dynamical effects.

Young and St. John¹⁴ and Dunn and Young¹² excited $N_2(A)$ in a Tesla discharge. While this type of discharge tends to dissociate nitrogen inefficiently, it is a source of other nitrogen metastables which could be kinetically coupled to $N_2(A)$. Young and St. John reported a 30 percent increase for quenching $N_2(A, v'=1)$ compared to the rate coefficient for quenching $N_2(A, v'=0)$ whereas Dunn and Young reported no difference between the two vibrational levels.

B. $N(^2P)$ Product Formation

Our measurements result in an excitation rate coefficient for $N(^2P)$ by $N_2(A, v'=0)$ which is five times greater than the total quenching rate coefficient. Part of this discrepancy may result from errors in the published values for the transition probabilities of $N_2(A)$ and $N(^2P)$. A 30 to 40 percent decrease in the Einstein coefficient for $N_2(A)$ ²⁹ would reduce this discrepancy somewhat, but even so would require that the Einstein coefficient for the $N(^2P-4S)$ transition calculated by Garstang could be as much as a factor to four too small. If the excitation probability were significantly less than unity, then this transition probability would be even larger. Godefroid and Froese Fischer's³¹ calculation appears to confirm Garstang's result. We think this aeronomically important transition probability merits an experimental confirmation.

An alternative explanation would be that $N_2(A)$ isn't the only molecular-nitrogen metastable present in our flow reactor. Energy transfer from metastable argon to molecular nitrogen might also produce a companion

metastable to $N_2(A)$ which we can't observe in radiation between 200 and 900 nm. This companion metastable would have to have number density much greater than that of the $N_2(A)$ to explain our results.

Our recent study on the various products resulting from the $N_2(A)$ interaction with molecular oxygen⁴⁷ provided evidence for such a companion metastable. One aspect of those studies was the determination of the amount of atomic oxygen that was produced in the reaction. Our observations indicated that the O-atom yield was a factor of three greater than could be accounted for even if every $N_2(A)$ molecule dissociated O_2 . Dreiling and Setser also have reported evidence of a companion metastable to $N_2(A)$,⁴⁸ which carried at least 6.5 eV internal energy, in their studies on the excitation of mercuric halides by $N_2(A)$. The energy of the companion metastable reported in both studies is more than sufficient to excite $N(^2P)$ in an energy-transfer reaction with $N(^4S)$.

In the present study as in the earlier study we were careful to add the nitrogen to the flow of argon metastables downstream from the dc discharge which produced the metastable argon. This ensures that the nitrogen metastables only can be produced in the energy-transfer reaction and not by direct electron impact as could be the case were the nitrogen co-discharged with the argon. This latter configuration generates more $N_2(A)$, but we have observed previously that it also generates other nitrogen metastables which enhance $N_2(B-A)$ emission in the afterglow far in excess of what would be generated from $N_2(A)$ energy pooling.⁴⁹ Dreiling and Setser also were careful to add their nitrogen downstream from the metastable-argon discharge.

We cannot find a satisfactory explanation as to the identity of this companion metastable. Known metastable states of molecular nitrogen below 11.6 eV, which have radiative lifetimes in excess of a millisecond, include

$a'^1\Sigma_u^-$, $w^1\Delta_u$, $A^3\Sigma_u^+$, $W^3\Delta_u$, $A'^5\Sigma_u^+$, and $N_2(X^1\Sigma_g^+, v)$. Some of these states undoubtedly can persist for long times in the afterglow.

Sadeghi and Setser¹⁷ have shown that essentially all of the quenching events between metastable argon and molecular nitrogen result in $N_2(C^3\Pi_u)$ excitation. A minor fraction of the reaction results in dissociation,^{50,51} but $N_2(C)$ clearly is the dominant channel. The radiative lifetime of $N_2(C)$ is so short, 36 ns,⁵² that molecules in this state will undergo only one collision prior to radiation at a pressure of 2 Torr. Thus electronic quenching of this state should be unimportant, and all of the molecules initially in this state will cascade radiatively to the $B^3\Pi_g$ state. Given the vibrational distribution of $N_2(C)$ excited by $Ar^*(^3P_{2,0})$ ¹⁷ and the $N_2(C \rightarrow B)$ Einstein coefficients tabulated in Lofthus and Krupenie,⁵² we calculate that about 97 percent of the radiative cascade from $N_2(C)$ will populate $N_2(B)$ in vibrational levels 4 and below. Under the conditions of our experiment, some of the molecules in the B-state will radiate to the lower vibrational levels of the $A^3\Sigma_u^+$ state. Many of them, however, will be transferred collisionally into lower B-state levels,⁵³ to other levels of the triplet manifold, principally the A, $B'^3\Sigma_u^-$, and W-states,⁵⁴⁻⁵⁸ or perhaps directly into high vibrational levels of the $X^1\Sigma_g^+$, ground-electronic state. The best available evidence suggests that much of the quenching of the B-state is effectively a vibrational relaxation process. Ultimately, $v'=0$ of the B- and W-states and $v'=7$ of the A-state are the primary end products of B-state quenching.

Heidner et al.⁵⁹ have shown that $N_2(B, v=0)$ and $N_2(W, v=0)$ rapidly establish an equilibrium between themselves, and then, somewhat more slowly, collisions with ground-state nitrogen quench the coupled complex. Under our conditions ($[N_2] = 8 \times 10^{15}$ molecules cm^{-3}), the quenching time of the coupled complex will be 60 μs given Heidner et al.'s quenching rate coefficient of

$2 \times 10^{-12} \text{ cm}^3 \text{ molecule}^{-1} \text{ s}^{-1}$. The most likely product of this quenching is $v'=7$ of the A-state. Dreyer and Perner⁶⁰ have shown, however, that this level is relaxed vibrationally by collisions with ground-state nitrogen. Their rate coefficient of $2.4 \times 10^{-12} \text{ cm}^3 \text{ molecule}^{-1} \text{ s}^{-1}$ implies a relaxation time of 50 μs under our conditions. Thus the evidence suggests that, even if the B-state levels initially populated in the radiative cascade from the C-state are quenched before they radiate, $\text{N}_2(\text{A})$ still is the ultimate product from the $\text{Ar}^* + \text{N}_2$ energy-transfer reaction.

Were the C-state coupled collisionally to the nearby $\text{C}''^5\Pi_u$ state, the $\text{A}'^5\Sigma_g^+$ state could be populated by radiative cascade on the Herman infrared system.^{61,62} In this event, one would be able to observe Herman infrared emission in the Ar^*/N_2 flame. One does not observe such emission, however. Direct excitation of either the C'' or A' states is precluded by spin conservation.

Spin-conservation rules also proscribe excitation of the singlet nitrogen metastables. These rules again are supported by direct observations in the vacuum ultraviolet which do not find significant emission in the Lyman-Birge-Hopfield bands, $\text{N}_2(\text{a}^1\Pi_g \rightarrow \text{X}^1\Sigma_g^+)$.^{50,63} Were the singlet excitation into the a' - or w -states, one would still expect to see LBH emission because the three singlet states are efficiently coupled collisionally.⁶⁴

In summary, the available evidence suggests that the quenching of metastable argon by nitrogen ultimately should result in $\text{N}_2(\text{A})$ production. The only alternative possibility for a long-lived metastable would appear to be $\text{N}_2(\text{X},v)$. To explain our results, however, would require efficient spin-changing collisions to convert triplet nitrogen into singlet nitrogen in high vibrational levels. Golde and Thrush⁶⁵ suggest that efficient manifold switching can result from collisions with nitrogen atoms. In the upstream end

of our reactor, however, our atom number density can at most be 10^{10} atoms cm^{-3} . Such low number densities cannot generate sufficient collisions on the required time scale of tens of microseconds to effect triplet-to-singlet manifold switching. Spin changing in collisions with molecular nitrogen or argon should be inefficient. We have failed to find evidence that this $\text{N}_2(\text{A})$ source produces $\text{N}_2(\text{X}, \text{v})$ in low vibrational levels.⁶⁶ This observation doesn't preclude the possibility of anomalous $\text{N}_2(\text{X}, \text{v})$ distributions consisting of molecules containing either 6 eV of vibrational energy or none. It just doesn't seem particularly likely.

C. Other Products

Some fraction of the interactions between $\text{N}_2(\text{A})$ and N probably also results in $\text{N}(^2\text{D})$ formation. The low-temperature matrix measurements from Dressler's group⁶⁷⁻⁷⁰ show that both $\text{N}(^2\text{P})$ and $\text{N}(^2\text{D})$ are excited in the reaction between $\text{N}_2(\text{A})$ and N. They also observe the vibrational levels of the ground electronic state which are excited in the $\text{N}_2(\text{A})$ deactivation. When $\text{N}(^2\text{P})$ is the excited product, $\text{v}''=6-9$ primarily are populated with roughly equal probability. The thermochemical limit for the ground-state N_2 is $\text{v}''=9$. When $\text{N}(^2\text{D})$ is the atomic product, most of the ground-state population resides in $\text{v}'=7-10$, although excitation up to $\text{v}''=13$ was observed. In this case the thermochemical limit would give $\text{N}_2(\text{X}, \text{v}''=14)$. They assumed that the excitation of both states is a direct process.

We see no reason, based upon the evidence reported by Dressler's group, why much of the $\text{N}(^2\text{D})$ excitation might not result from lattice-induced radiative cascade from initially excited $\text{N}(^2\text{P})$. The $\text{N}(^2\text{P})$ radiates in the matrix with a 1 ms lifetime, whereas the effective radiative lifetime of the $\text{N}(^2\text{D})$ in the lattice is 37 seconds. Clearly, some of the $\text{N}(^2\text{D})$ excitation must be direct because several vibrational levels of $\text{N}_2(\text{X})$ are populated above

the $N(^2P)$ thermochemical limit. Kunsch⁶⁹ states that unpublished results from the group indicate a somewhat greater intensity from $N(^2D)$ than from $N(^2P)$. This observation argues for direct $N(^2D)$ formation.

We looked briefly for $N(^2D)$ using a resonance-fluorescence diagnostic.⁴⁰ We observed $N(^2D)$ in our reactor only when both the $N_2(A)$ and the N were present together. The $N(^2D)$ number densities were of the same order of magnitude as those for $N(^2P)$. Because the observations were made after a fairly long reaction time, the $N(^2D)$ could have resulted from $N(^2P)$ quenching by argon rather than from direct excitation by $N_2(A)$. Unravelling this issue will require lengthy and detailed measurements.

Superficially, our data indicate that the excitation rate of $N(^2P)$ by vibrationally excited $N_2(A)$ is reduced by a factor of four in spite of the fact that the total quenching rates are the same for vibrationally excited and relaxed $N_2(A)$. Certainly, if the discrepancy between the rate coefficients for $N(^2P)$ excitation by $N_2(A, v'=0)$ and for $N_2(A)$ quenching by N is caused by inaccuracies in the Einstein coefficients, this would be the surprising result. If the discrepancy is caused by a companion metastable, however, then the data indicate that the branching ratio for $N(^2P)$ excitation by $N_2(A, v>0)$ is unity and, furthermore, that CF_4 doesn't quench the companion metastable.

If the apparent difference in $N(^2P)$ excitation rates between vibrationally excited and unexcited $N_2(A)$ is real, it might be because the branch to form $N(^2P)$ decreases with increasing vibrational level. Kunsch⁷⁰ performed some trajectory calculations on this system. He found that whereas 95 percent of his trajectories starting with $N_2(A, v'=0)$ were effective in exciting $N(^2P)$, only 70 percent of the trajectories starting from $v'=1$ succeeded. Trajectories involving $N_2(A, v'=3)$ resulted in $N(^2P)$ excitation less than 50 percent of the time. Kunsch's calculations involving $N(^2D)$ as a product

product did not address the issue of vibrational excitation in the $N_2(A)$. Clearly, additional gas-phase experiments designed to observe both excited-atom products are warranted.

D. $N(^2P)$ Quenching

$N(^2P)$ wall loss is diffusion controlled.^{37,38} The wall-loss rate, therefore, is

$$k_w^P = \frac{0.62 D_0}{\Lambda^2 P}, \quad (15)$$

where D_0 is the diffusion coefficient at 1 torr, and Λ is the characteristic diffusion length. This value is the ratio of the radius of the flow reactor to the first root of the zeroth-order Bessel function:

$$\Lambda = \frac{r_0}{2.405}. \quad (16)$$

Ianuzzi and Kaufman³⁵ obtained a value of $230 \text{ cm}^2 \text{ s}^{-1}$ at 1 torr for $N(^2P)$ diffusing in argon. Other values reported in the literature are $214 \text{ cm}^2 \text{ s}^{-1}$ by Lin and Kaufman³⁶ (corrected from 400 K) and $160 \pm 20 \text{ cm}^2 \text{ s}^{-1}$ by Cernogora and Sadeghi.⁷¹

In addition to diffusion to the walls, a small loss of $N(^2P)$ results from quenching by the argon bath gas. Ianuzzi and Kaufman³⁵ reported a rate coefficient for this process of $4 \times 10^{-16} \text{ cm}^3 \text{ molecule}^{-1} \text{ s}^{-1}$. Lin and Kaufman³⁶ proposed a similar value, $7 \times 10^{-16} \text{ cm}^3 \text{ molecule}^{-1} \text{ s}^{-1}$. Rather than include this quenching term explicitly, we compensated for it implicitly by including it with the effective wall quenching rate. Our effective wall quenching rate, 75 s^{-1} , is compatible with a diffusion coefficient of $210 \text{ cm}^2 \text{ s}^{-1}$ at 1 Torr and an argon quenching rate of $4 \times 10^{-16} \text{ cm}^3 \text{ molecule}^{-1} \text{ s}^{-1}$. These values agree quite well with the more direct measurements of Ianuzzi and Kaufman.

Taghipour and Brennan¹ have estimated a rate coefficient for reaction (3) of $6 \times 10^{-13} \text{ cm}^3 \text{ molecule}^{-1} \text{ s}^{-1}$. Young and Dunn⁸ obtained a similar value, but Golde and Thrush²² estimated a value considerably larger, $1 \times 10^{-11} \text{ cm}^3 \text{ molecule}^{-1} \text{ s}^{-1}$. For additions of large number densities of atomic nitrogen, such that the conversion from $\text{N}_2(\text{A})$ to $\text{N}(^2\text{P})$ is essentially complete in the vicinity of the injector, we see only a small decrease in $[\text{N}(^2\text{P})]$ as $[\text{N}(^4\text{S})]$ is further increased. The magnitude of this decrease is consistent with the smaller N-atom quenching rate coefficients of $\text{N}(^2\text{P})$ given by Taghipour and Brennan and Young and Dunn rather than that estimated by Golde and Thrush.

5. SUMMARY AND CONCLUSIONS

We have shown that the total rate coefficient for quenching $N_2(A^3\Sigma_u^+)$ by N-atoms is $(4.0 \pm 0.5) \times 10^{-11} \text{ cm}^3 \text{ molecule}^{-1} \text{ s}^{-1}$ at room temperature. We saw no obvious variation in this value with $N_2(A)$ vibrational level. $N(^2P)$ is excited quite efficiently in this reaction, but $N_2(A, v'=0)$ appears to be a factor of four more efficient in the excitation than is $N_2(A, v'>0)$.

The rate coefficient determined for $N(^2P)$ excitation by $N_2(A, v'=0)$, based upon currently accepted Einstein coefficients for $N_2(A)$ and $N(^2P)$, is five times the total quenching rate coefficient. This indicates that either the accepted value for the $N(^2P-4S)$ Einstein coefficient is seriously in error, or else that the interaction between metastable argon and molecular nitrogen generates another nitrogen metastable in addition to $N_2(A)$. Either possibility could indicate serious misunderstandings of processes important in disturbed atmospheres or nitrogen discharges. Clearly both issues require further investigation.

In spite of the somewhat unsatisfactory situation regarding the discrepancies between $N(^2P)$ excitation and $N_2(A)$ destruction rate coefficients, our study shows that our experimental configuration provides a straight forward source of $N(^2P)$ suitable for kinetic studies. Some preliminary investigations of $N(^2P)$ kinetics using this source indicate a freedom from the kinetic complications observed using a microwave discharge in N_2/Ar mixtures to generate $N(^2P)$. These studies currently are underway, and will be detailed in a future publication.

ACKNOWLEDGMENTS

This work was performed under Contract No. F19628-85-C-0032 with the Air Force Geophysics Laboratory, and was sponsored by the Defense Nuclear Agency (Project SA, Task SA/SDI, Work Unit 00175) and the U.S. Air Force Office of Scientific Research (Task 2310G4). We appreciate comments and criticism of PSI colleagues Terry Rawlins, Steve Davis, Mark Fraser, and Dave Green. We also acknowledge Kristina Cairns' efforts in support of the data analysis.

REFERENCES

1. A. Taghipour and W. Brennen, Chem. Phys. 37, 363 (1979).
2. J.F. Noxon, J. Chem. Phys. 36, 926 (1962).
3. G.J. Diebold, I.V. Rivas, S. Shafeizad, and D.L. McFadden, Chem. Phys. 52, 453 (1980).
4. E.C. Zipf, P.J. Espy, and C.F. Boyle, J. Geophys. Res. 85, 687 (1980).
5. J.C. Gerard and O.E. Harang, J. Geophys. Res. 85, 1757 (1980).
6. G.G. Sivjee and R.A. Marshall, J. Geophys. Res. 88, 3153 (1983).
7. D. Husain, S.K. Mitra, and A.N. Young, J.C.S. Faraday II 70, 1721 (1974).
8. R.A. Young and O.J. Dunn, J. Chem. Phys. 63, 1150 (1975).
9. W.T. Rawlins, M.E. Fraser, and S.M. Miller, J. Phys. Chem. 93, XXXX (1989).
10. J.K. Hartman, P.J. Espy, W.R. Pendleton, Jr., and G.G. Sivjee, EOS 67, 321 (1986).
11. J.A. Meyer, D.W. Setser, and D.H. Stedman, J. Phys. Chem. 74, 2238 (1970).
12. O.J. Dunn and R.A. Young, Int. J. Chem. Kinet. 8, 161 (1976).
13. K.L. Wray, J. Chem. Phys. 44, 623 (1966).
14. R.A. Young and G.A. St. John, J. Chem. Phys. 48, 895 (1968).
15. P.H. Vidaud, R.P. Wayne, M. Yaron, and A. von Engel, J. Chem. Soc. Faraday Trans. 2 72, 1185 (1976).
16. D.H. Stedman and D.W. Setser, Chem. Phys. Lett. 2, 542 (1968).
17. N. Sadeghi and D.W. Setser, Chem. Phys. Lett. 82, 44 (1981).
18. L.G. Piper, W.J. Marinelli, W.T. Rawlins, and B.D. Green, J. Chem. Phys. 83, 5602 (1985).
19. J.M. Thomas, J.B. Jeffries, and F. Kaufman, Chem. Phys. Lett. 102, 50 (1983).
20. J.E. Morgan and H.I. Schiff, Can. J. Chem. 41, 993 (1963).
21. I.M. Campbell and B.A. Thrush, Proc. Roy. Soc. (London) A296, 201 (1967).
22. B. Brocklehurst and K.R. Jennings, Prog. React. Kin. 4, 3 (1967).

23. L.G. Piper and G.E. Caledonia, J. Chem. Phys. 75, 2847 (1981).
24. L.G. Piper and W.T. Rawlins, J. Phys. Chem. 90, 320 (1986).
24. L.G. Piper, J. Chem. Phys. 88, 231 (1988).
26. L.G. Piper, L.M. Cowles, and W.T. Rawlins, J. Chem. Phys. 85, 3369 (1986).
27. R.D. Kenner and E.A. Ogryzlo, in Chemil- and Bio-luminescence, John G. Burr, ed., New York: Marcel Dekker, Inc., 45 (1985).
28. D.E. Shemansky, J. Chem. Phys. 51, 689 (1969).
29. R.H. Garstang, The Airglow and the Aurora, Armstrong and Dalgarno, ed., New York: Pergamon Press (1956).
30. L.G. Piper, K.W. Holtzclaw, B.D. Green, and W.A.M. Blumberg, EOS 69, 419 (1988), and manuscript in preparation.
31. M. Godefroid and C. Froese Fischer, J. Phys. B 17, 681 (1984).
32. A.C. Corney and J. Williams, J. Phys. B 5, 686 (1971).
33. H.V. Lilenfeld, R.J. Richardson, and F.E. Hovis, J. Chem. Phys. 74, 2129 (1981).
34. R. Engleman, Jr., B.A. Palmer, and S.J. Davis, J. Opt. Soc. Amer. 73, 1585 (1983).
35. M.P. Iannuzzi and F. Kaufman, J. Chem. Phys. 73, 9 (1980).
36. C.-L. Lin and F. Kaufman, J. Chem. Phys. 55, 3760 (1971).
37. E.E. Ferguson, F.C. Fehsenfeld, and A.L. Schmeltekopf, in Advances in Atomic and Molecular Physics V, D.R. Bates, ed., New York: Academic (1970).
38. R.C. Bolden, R.S. Hemsworth, M.J. Shaw, and N.D. Twiddy, J. Phys. B3, 45 (1970).
39. J.H. Kolts and D.W. Setser, J. Chem. Phys. 68, 4848 (1978).
40. L.G. Piper, M.E. Donahue, and W.T. Rawlins, J. Phys. Chem. 91, 3883 (1987).
41. M.J. Shaw and H.M.P. Stock, J. Phys. B: Atom Molec. Phys. 8, 2752 (1975).
42. A.R. DeSouza, G. Gousset, M. Touzeau, and Tu Khiet, J. Phys. B: At. Mol. Phys. 18, L661 (1985).
43. J.A. Meyer, D.H. Klosterboer, and D.W. Setser, J. Chem. Phys. 55, 2084 (1971).

44. L.G. Piper, G.E. Caledonia, and J.P. Kennealy, J. Chem. Phys. 74, 2888 (1981).
45. A.R. DeSousa, M. Touzeau, and M. Petitdidier, Chem. Phys. Lett. 121, 423 (1985).
46. J.M. Thomas, F.Kaufman, and M.F. Golde, J. Chem. Phys. 86, 6885 (1987).
47. M.E. Fraser and L.G. Piper, J. Phys. Chem. 93, XXXX (1989).
48. T.D. Dreiling and D.W. Setser, Chem. Phys. Lett. 74, 211 (1980).
49. L.G. Piper, J. Chem. Phys. 88, 6911 (1988).
50. L.G. Piper, unpublished results (1974).
51. J. Balamuta and M.F. Golde, J. Chem. Phys. 76, 2430 (1982).
52. A. Lofthus and P.H. Krupenie, J. Phys. Chem. Ref. Data 6, 113 (1977).
53. A.M. Pravilov, L.G. Smirnova, and A.F. Vilesov, Chem. Phys. Lett. 144, 469 (1988).
54. A. Rotem, I. Nadler, and S. Rosenwaks, Chem. Phys. Lett. 83, 281 (1981).
55. A. Rotem, I. Nadler, and S. Rosenwaks, J. Chem. Phys. 76, 2109 (1982).
56. N. Sadeghi and D.W. Setser, Chem. Phys. Lett. 77, 304 (1981).
57. N. Sadeghi and D.W. Setser, J. Chem. Phys. 79, 2710 (1983).
58. A. Rotem and S. Rosenwaks, Opt. Engn. 22, 564 (1983).
59. R.F. Heidner III, D.G. Sutton, and S.N. Suchard, Chem. Phys. Lett. 37, 243 (1976).
60. J.W. Dreyer and D. Perner, J. Chem. Phys. 58, 1195 (1973).
61. H. Partridge, S.R. Langhoff, C.W. Bauschlicher, Jr., and D.W. Schwenke, J. Chem. Phys. 88, 3174 (1988).
62. A.F. Vilesov, A.M., Pravilov, and L.G. Smirnova, Opt. Spectrosc. 62, 297 (1987).
63. L.A. Gundel, D.W. Setser, M.A.A. Clyne, J.A. Coxon, and W. Nip, J. Chem. Phys. 64, 4390 (1976).
64. W.J. Marinelli, B.D. Green, M.A. DeFaccio, and W.A.M. Blumberg, J. Phys. Chem. 92, 3429 (1988).
65. M.F. Golde and B.A. Thrush, Proc. Roy. Soc. (London) A 330, 79 (1972).
66. L.G. Piper and W.J. Marinelli, J. Chem. Phys. 89, 2918 (1988).

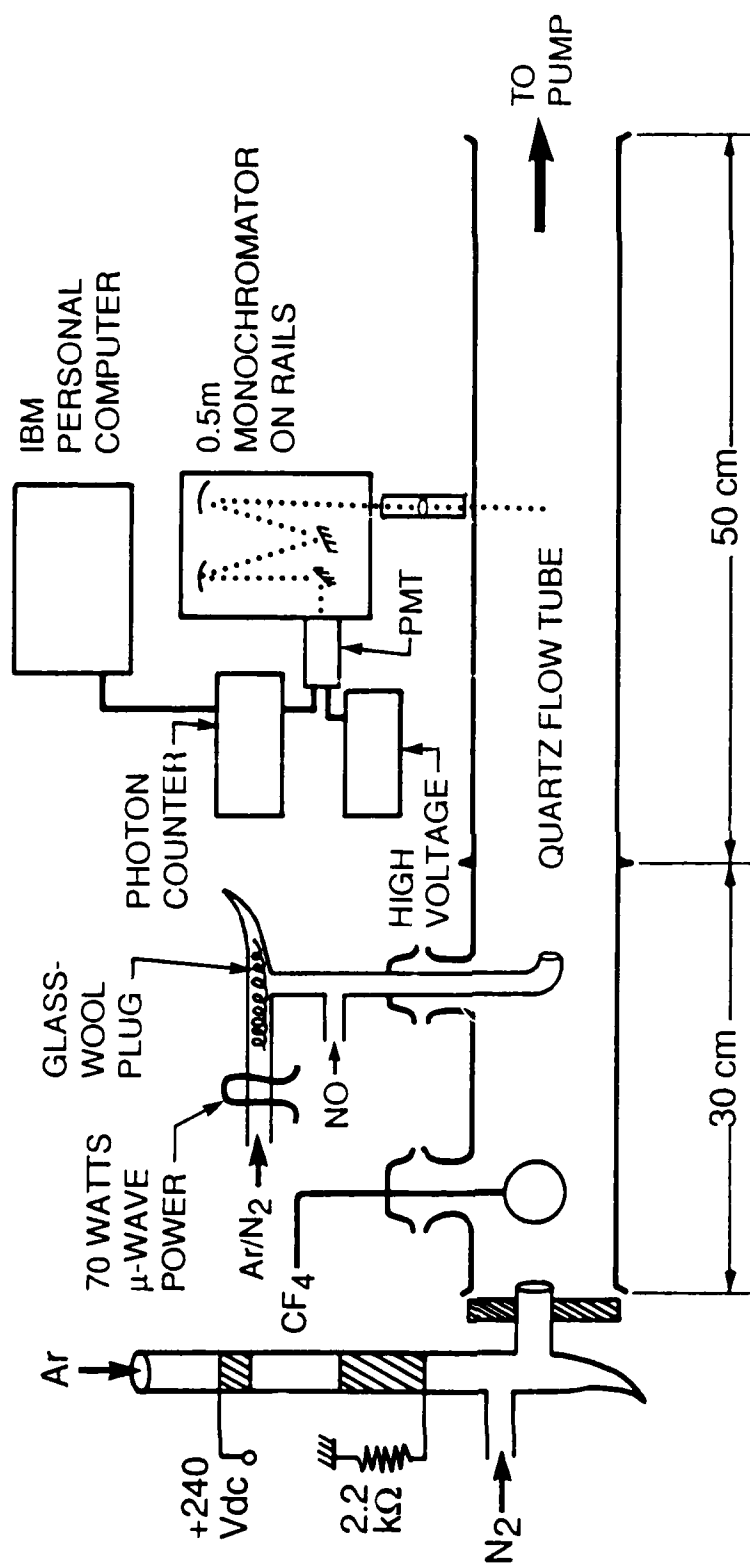
67. K. Dressler, O. Oehler, and D.A. Smith, Phys. Rev. Lett. 34, 1364 (1975).
68. O. Oehler, D.A. Smith, and K. Dressler, J. Chem. Phys. 66, 2097 (1977).
69. P.L. Kunsch and K. Dressler, J. Chem. Phys. 68, 2550 (1978).
70. P.L. Kunsch, J. Chem. Phys. 68, 4564 (1978).
71. G. Cernogora and N. Sadeghi, Chem. Phys. Lett. 74, 417 (1980).
72. M.F. Golde and B.A. Thrush, Faraday Disc. Chem. Soc. 53, 233 (1972).

Table 1. Rate Coefficients for $N_2(A) + N$ Interaction

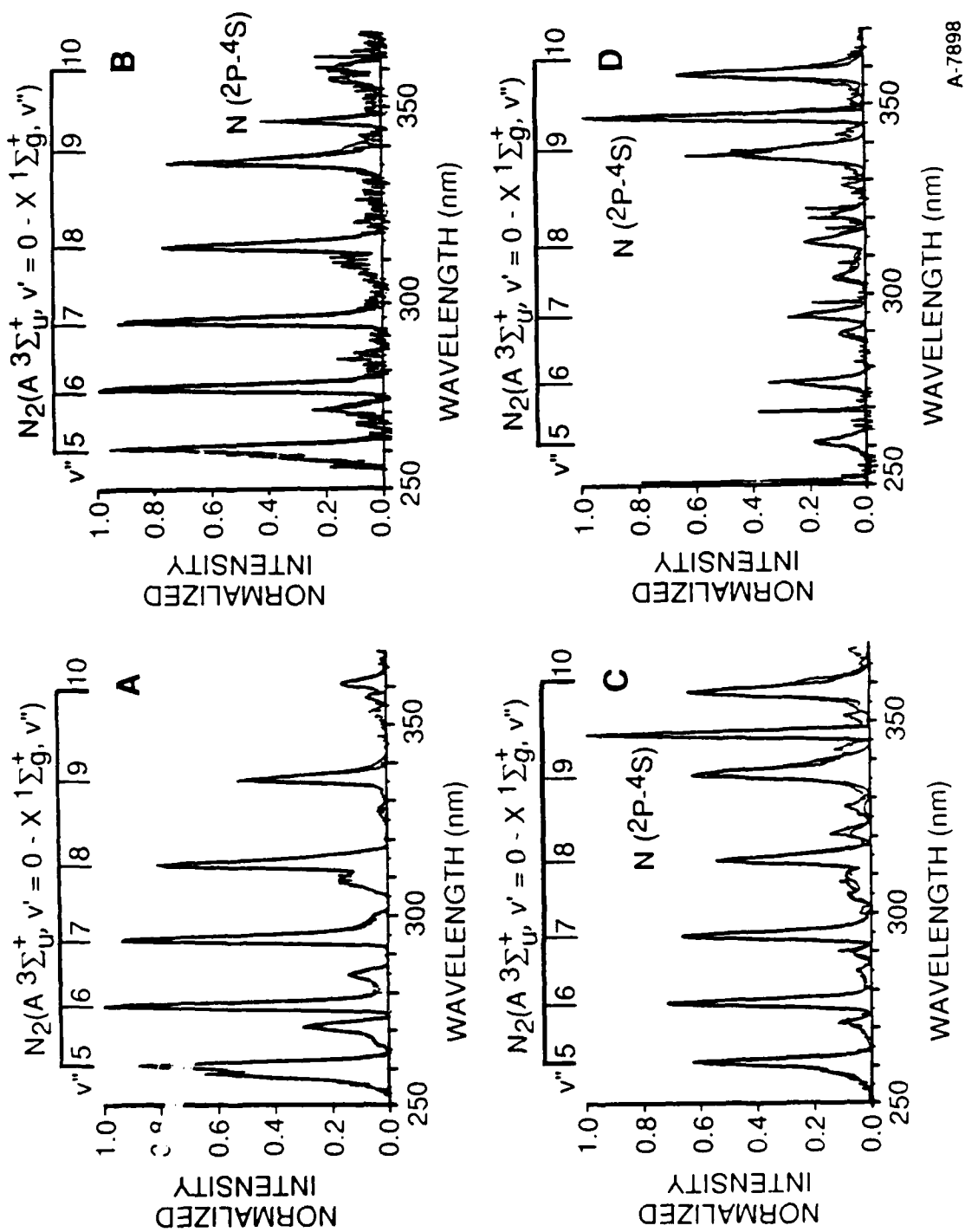
Process	Rate Coefficient ($10^{-11} \text{ cm}^3 \text{ molecule}^{-1} \text{ s}^{-1}$)
$N_2(A, v'=0) + N \rightarrow \text{products}$	3.8 ± 0.3 with CF_4 4.1 ± 0.2 no CF_4
$N_2(A, v'=1) + N \rightarrow \text{products}$	3.9 ± 0.2 no CF_4
Average	4.0 ± 0.5
$N_2(A, v'=0) + N \rightarrow N(^2P) + N_2(X)$	19 ± 3
$N_2(A, v'>0) + N \rightarrow N(^2P) + N_2(X)$	5 ± 1

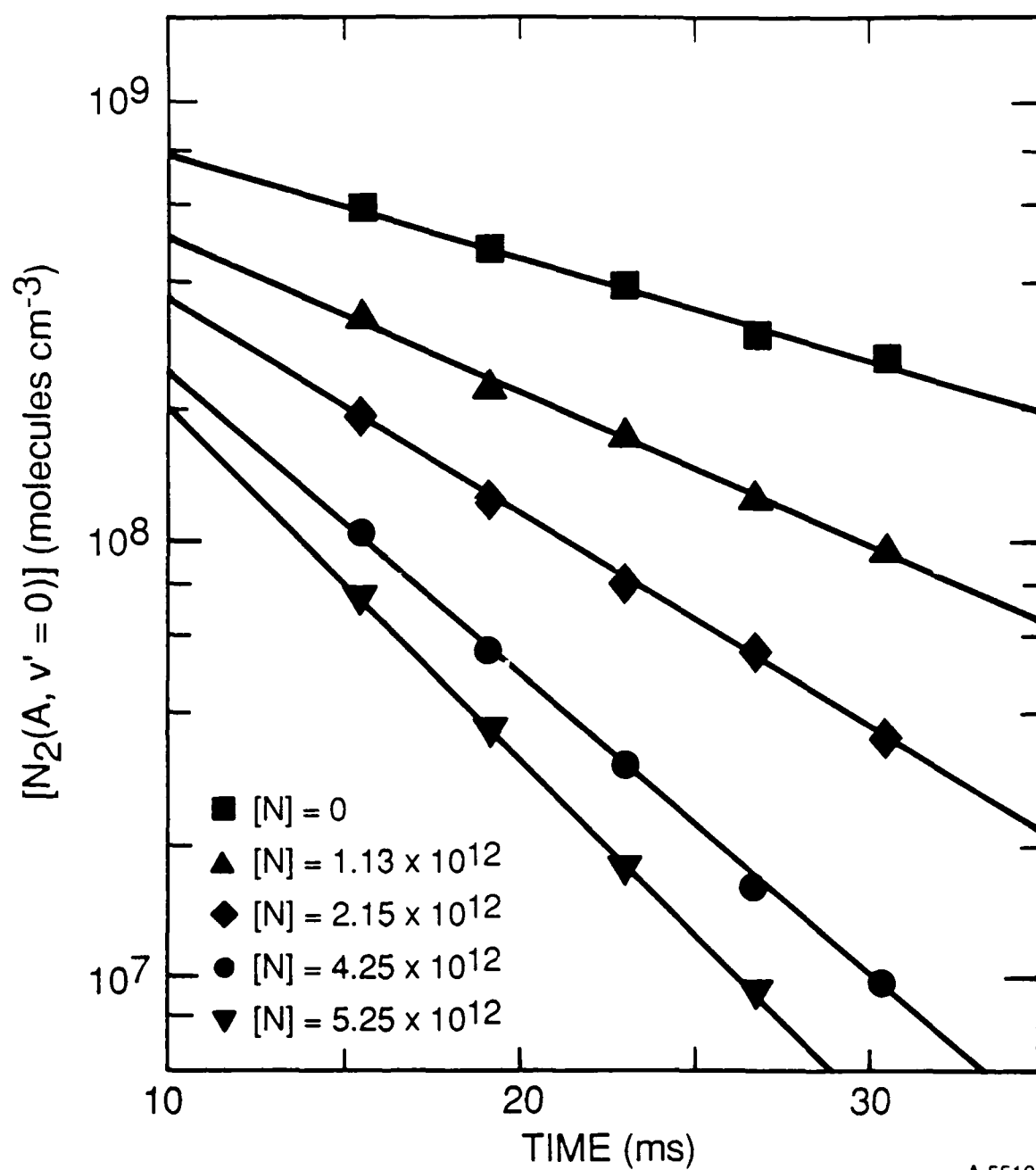
LIST OF CAPTIONS

- Figure 1. Schematic of discharge flow-reactor
- Figure 2. $N_2(A^3\Sigma_u^+, v=0 - X^1\Sigma_g^+)$ and $N(^2P-^4S)$ emission 17 ms downstream from N injector. The light line shows the experimental spectra while the heavy line shows the synthetic fit to the data. The important spectral features are marked on the figure. Unmarked spectral features include NO γ bands at low [N], NO β bands at high [N], and bands of the CN(B-X) system, ~358 nm, and NH(A-X) system, ~336 nm, at high [N]. (a) [N] = 0; (b) [N] = 0.8×10^{12} atoms cm^{-3} ; (c) [N] = 2.0×10^{12} atoms cm^{-3} ; (d) [N] = 3.6×10^{12} atoms cm^{-3}
- Figure 3. Decay of $N_2(A^3\Sigma_u^+, v'=0)$ as a function of time and of $N(^4S)$ number density
- Figure 4. Decay of $N_2(A^3\Sigma_u^+, v'=1)$ as a function of time and of $N(^4S)$ number density
- Figure 5. $N_2(A, v'=0)$ decay rates as a function of [N]
- Figure 6. $N_2(A, v'=1)$ decay rates as a function of [N]
- Figure 7. $N(^2P)$ excitation by $N_2(A^3\Sigma_u^+, v'=0)$. The curves through the data points show the results of the fit of Eq. (13) to the data
- Figure 8. $N(^2P)$ excitation by $N_2(A, v'=0,1,2)$. The curves through the data points show the results of the fit of Eq. (13) to the data

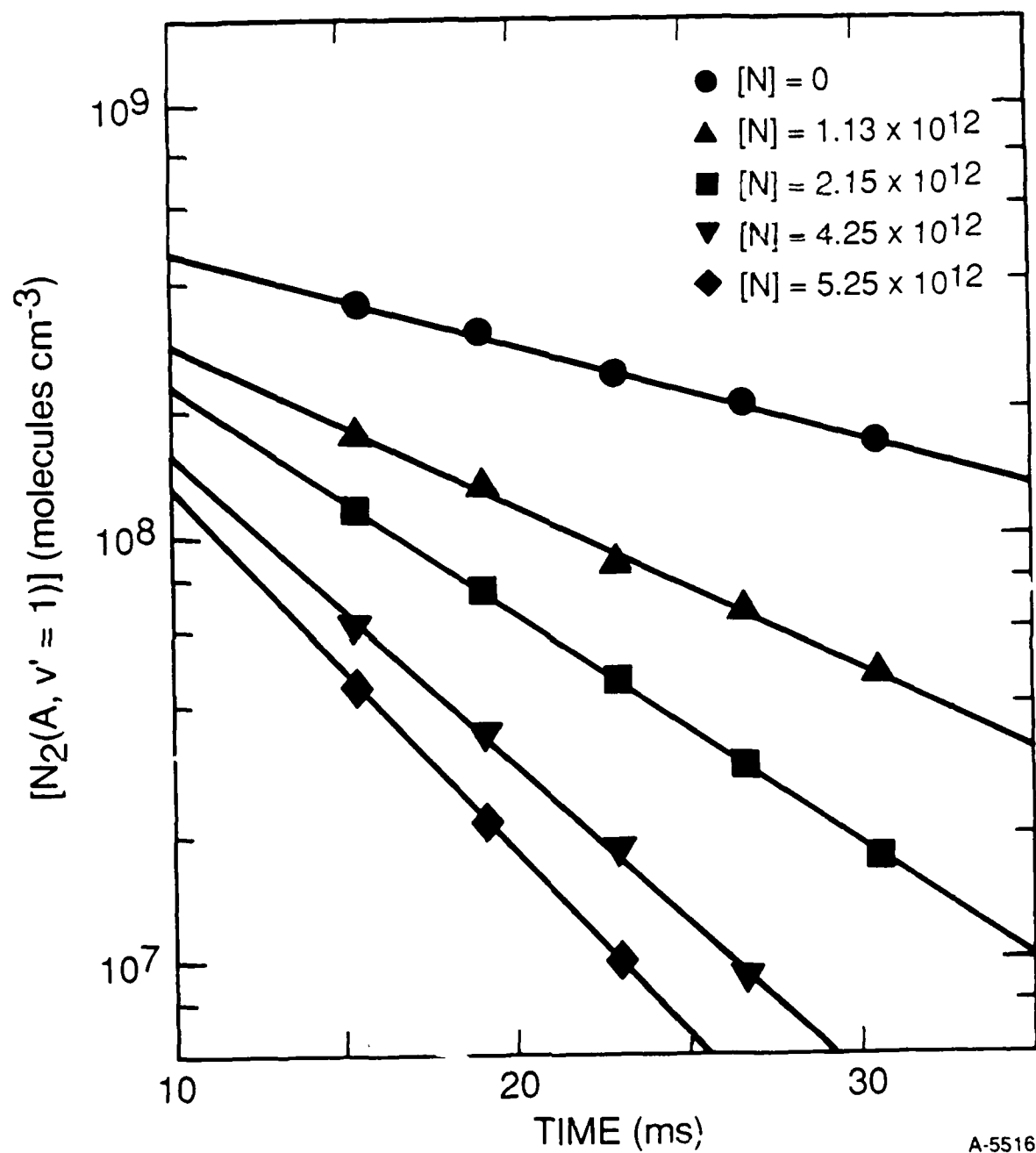


A-5520

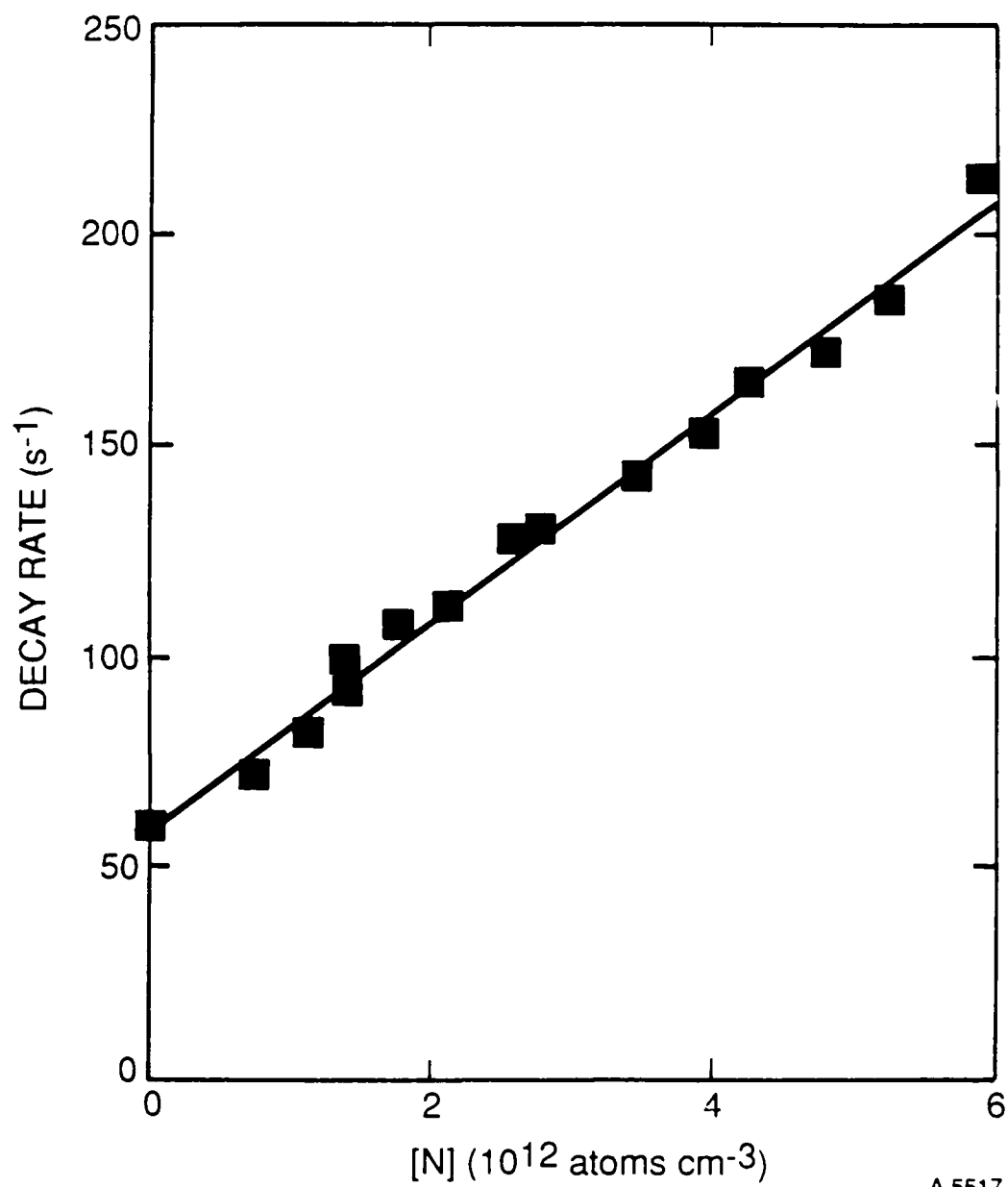




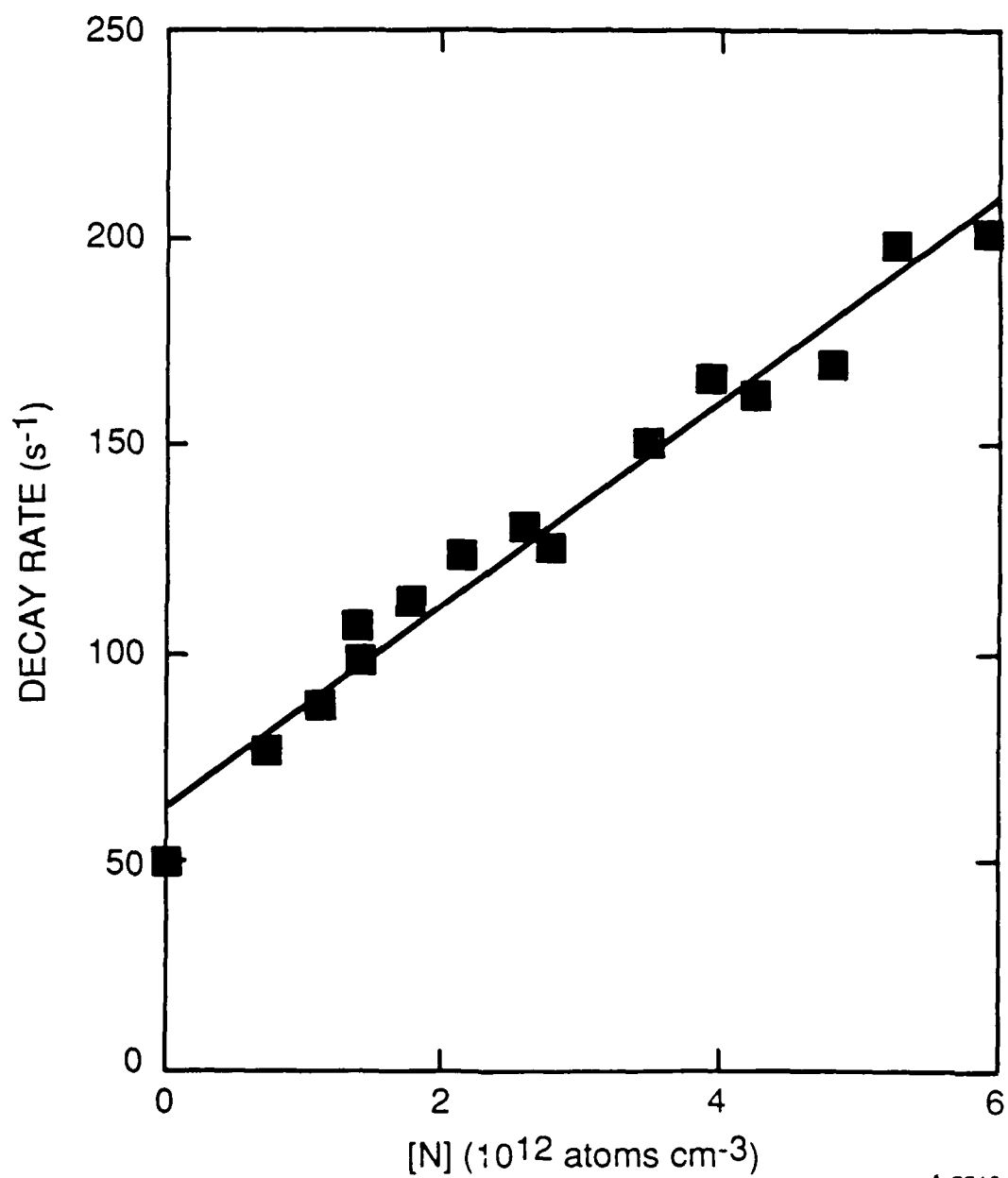
A-5519



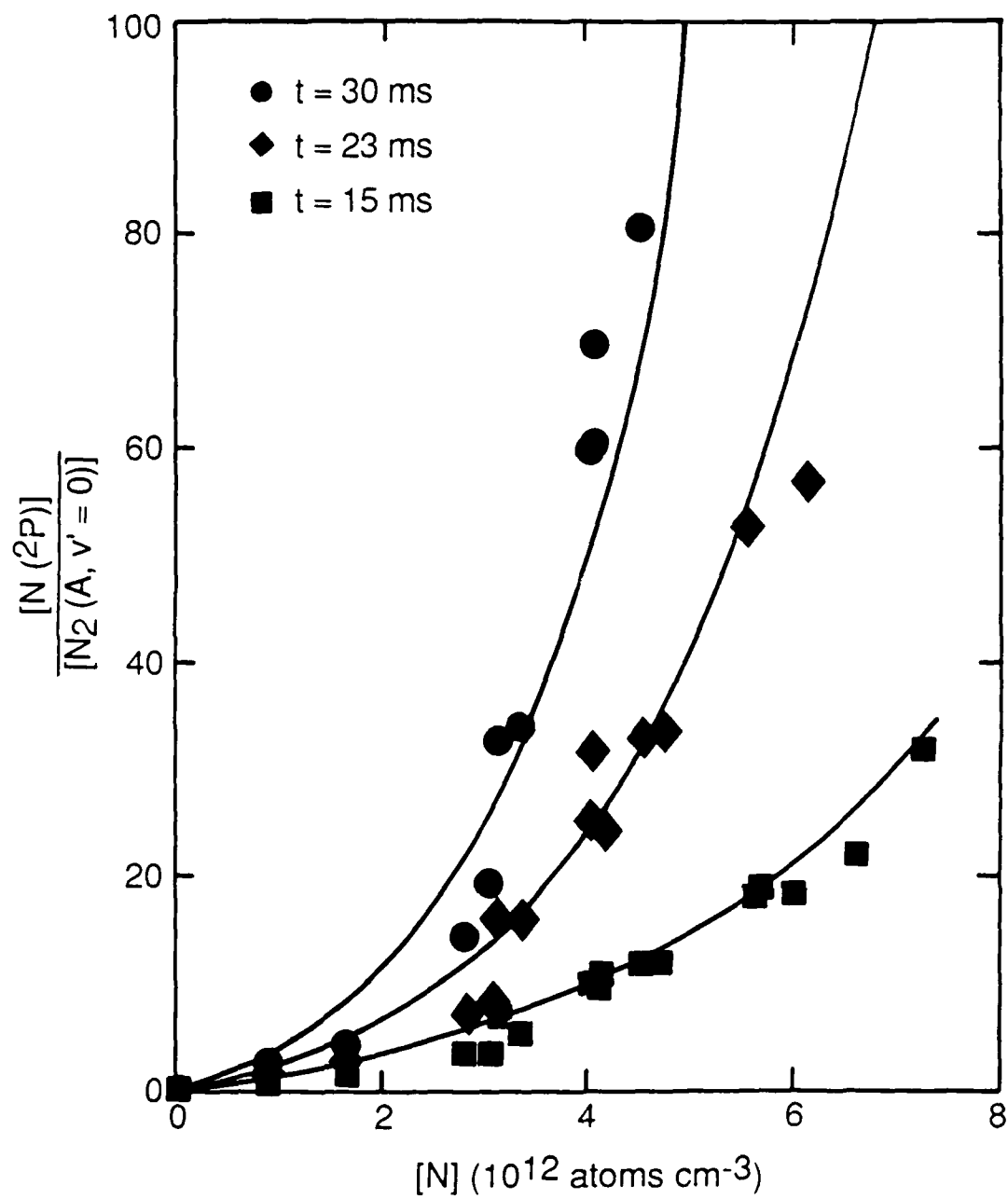
A-5516



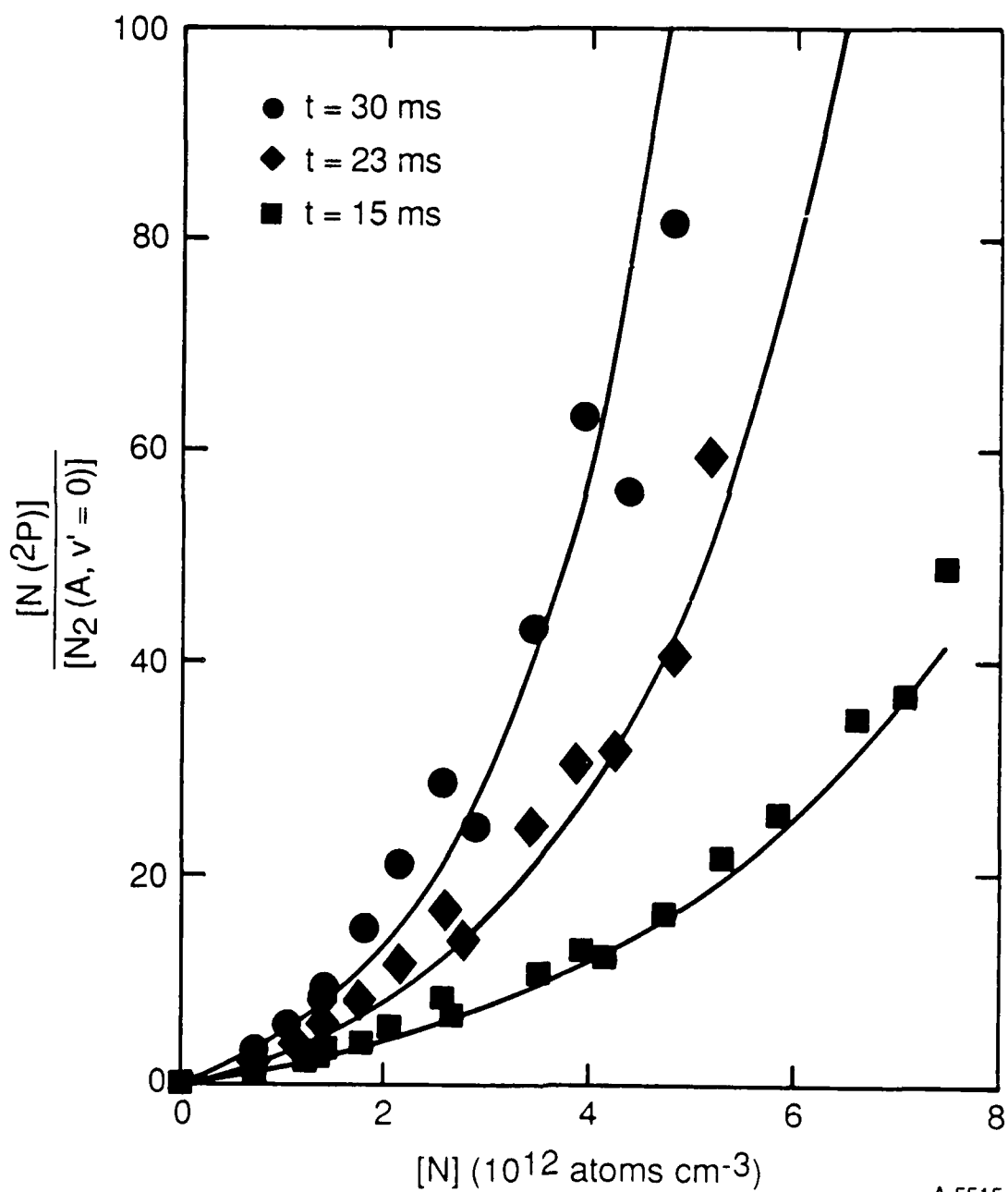
A-5517



A-5518



A-5514



A-5515

U.S. GOVERNMENT PRINTING OFFICE